



INTERNATIONAL ATOMIC ENERGY AGENCY
UNITED NATIONS EDUCATIONAL, SCIENTIFIC AND CULTURAL ORGANIZATION



INTERNATIONAL CENTRE FOR THEORETICAL PHYSICS
34100 TRIESTE (ITALY) - P.O.B. 586 - MIRAMARE - STRADA COSTIERA 11 - TELEPHONES: 224281/2/3/4/5/6
CABLE: CENTRATOM - TELEX 460392-1

SMR/111 - 8

SECOND SUMMER COLLEGE IN BIOPHYSICS

30 July - 7 September 1984

Photoacoustic Spectroscopy and Applications to Biological Systems

B.S.H. ROYCE
Department of Mechanical and Aerospace Engineering
School of Engineering and Applied Science
Princeton University
Princeton, N.J. 08540
U.S.A.

These are preliminary lecture notes, intended only for distribution to participants.
Missing or extra copies are available from Room 230.

PHOTOACOUSTIC SPECTROSCOPY
AND APPLICATIONS TO BIOLOGICAL SYSTEMS

BARRIE S. H. ROYCE
Applied Physics and Materials Laboratory
PRINCETON UNIVERSITY
Princeton, New Jersey, USA 08544

1

A. Bocarsly	J. Benziger	F. Sanchez-Sinencio
A. Mandelis	Y. C. Teng	R. Muratore
	S. McGovern	

OUTLINE OF LECTURE SEQUENCE

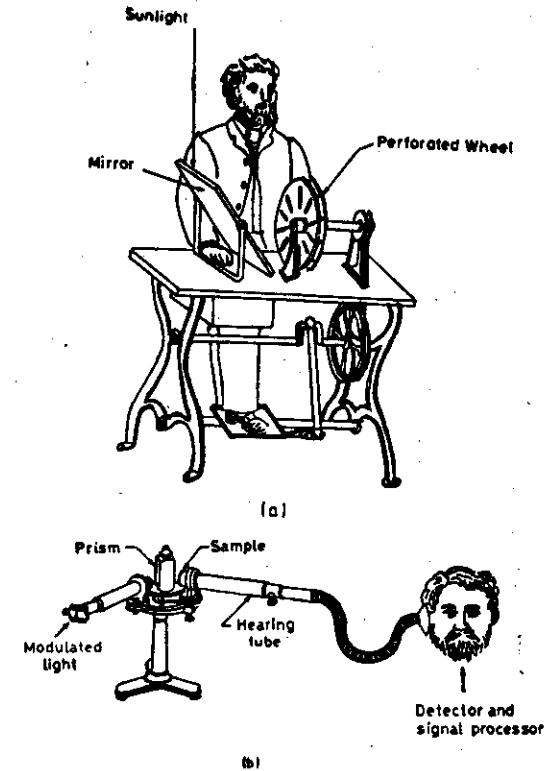
- A. Physical Discussion of Photoacoustic Spectroscopy and the Signal Detection Modes
- B. Models for Photoacoustic Signal Generation
- C. Experimental Methods in Photoacoustic Spectroscopy
- D. Photoacoustic Measurements on Biological Systems

2

A. Physical Discussion of Photoacoustic Spectroscopy and the Signal Detection Modes

1. Historical Introduction
2. Generic Photoacoustic Configuration
3. Radiation Absorption by the Sample
4. Types of Signal Path
5. Signal Detection Methods
6. Photoacoustic Configurations for Various Sample Types
7. Conclusions

A. G. Bell "The Production of Sound by Radiant Energy,"
Phil. Mag. 11 (1881) 510.



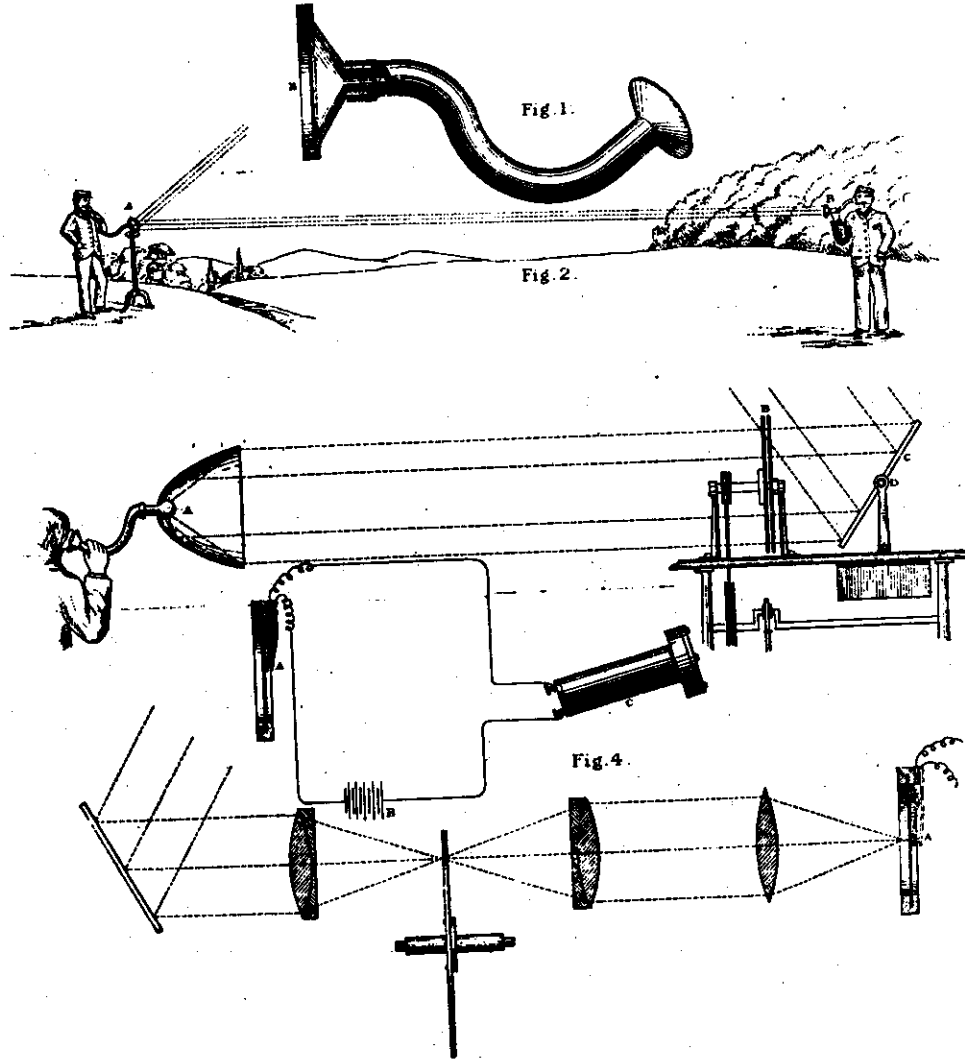
Bell's spectrophone: (a) chopper (b) spectrophone. (from Bell 1881).

Identified the signal sources for powdered samples:

- 1) Heat Transfer to Gas in Hearing Tube
- 2) Thermal Expansion of Sample
- 3) Thermal Expansion of Interstitial Gas.

Resulting from the Absorption of Light.

Technique was an outgrowth of applied research into optical communications and a technical problem with the selenium photoresistors.



others involved in the phenomenon were also well known in Physics:

Roentgen

Tyndall



WILHELM CONRAD ROENTGEN
German physicist
March 27, 1845 - Feb. 10, 1923

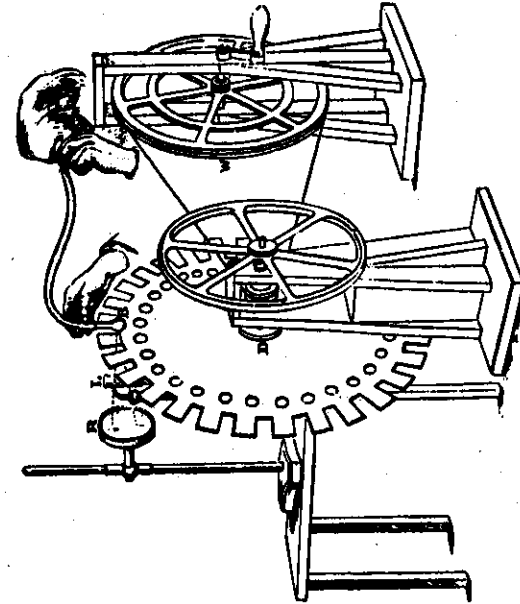
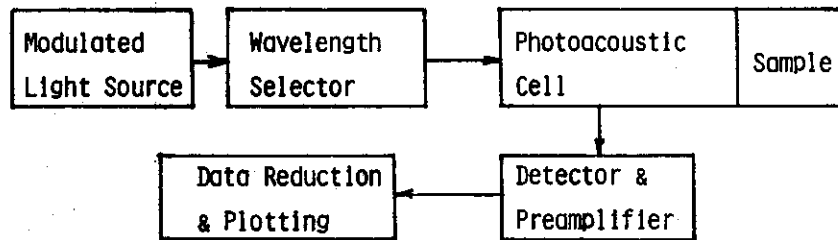


FIGURE 1. Tyndall's apparatus for demonstrating the optoacoustic effect. (From Tyndall, J., *Sound*, 6th ed., Longmans, Green, London, 1896.)

Signal Path for Photoacoustic Spectroscopy

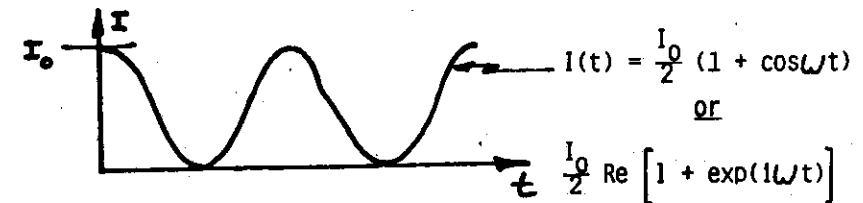


- 1) Modulated Light → Periodic; Pulse; Random.
- 2) Wavelength Selection → Dispersive System
 { U.V. to Infrared } Tuned Light Source
 and Microwave Interferometer
- 3) Absorption of Radiation by Sample in Photoacoustic Cell → Various De-excitation Paths Possible
- 4) Absorbed Radiation Degraded to Heat with Some Efficiency. Other Competing Processes may Contribute to Signal.
- 5) Detection → Gas Microphone
 Laser Beam
 Radiation Detector
 Piezoelectric Detector
- 6) Normalization and Reduction of Spectral Data.

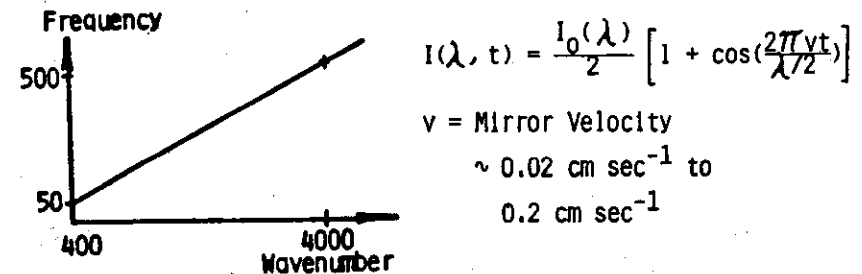
LIGHT MODULATION METHODS

A) Periodic

- 1) Use Mechanical Chopper to Produce Intensity Modulation of Light. Single Frequency, 20 Hz to 1 KHz.



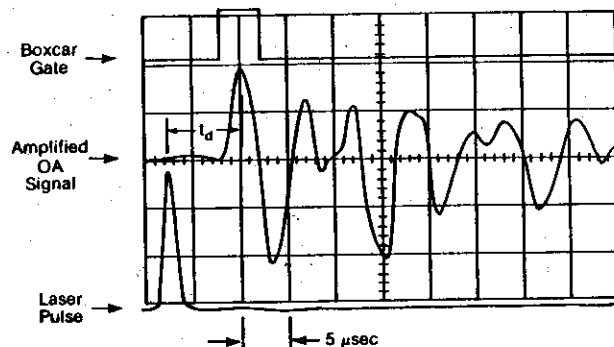
- ii) Interferometer. Each wavenumber (wavelength) has a different modulation frequency that depends upon the mirror velocity → wide range of acoustic modulation frequencies



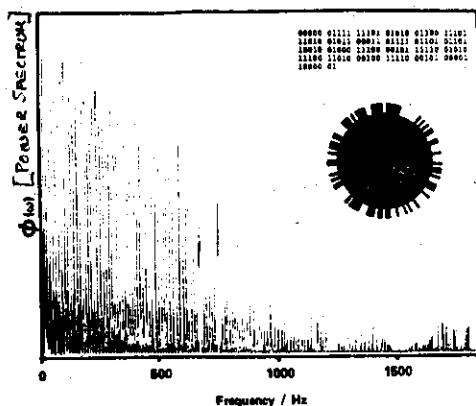
- iii) Polarization Modulation: Intensity Constant periodic change of direction of linear polarization of the light

B) Pulse Light Source

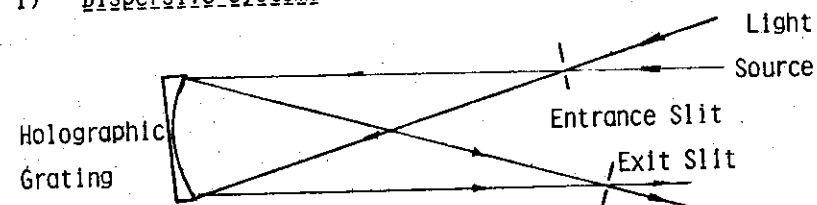
Nd:YAG Pumped Dye Laser
Flashlamp Pumped Dye Laser



Detect the Signal in the Time Domain

C. Pseudo Random Modulation

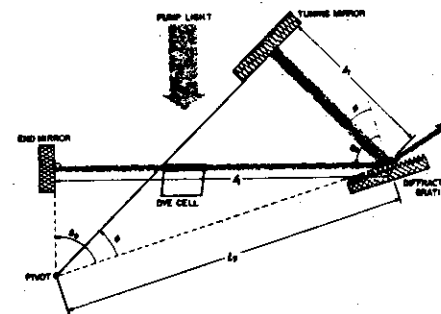
Use Correction techniques to Recover the Signal

1) Dispersive Systems

Wide Spectral Range UV \rightarrow IR. Good for Survey Spectra. Low Spectral Resolution ~ 4 nm.

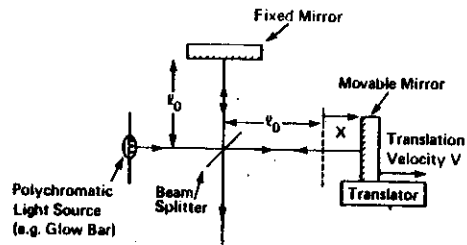
2) Tuned Light Sources

Dye Lasers for CW or Pulsed Radiation.



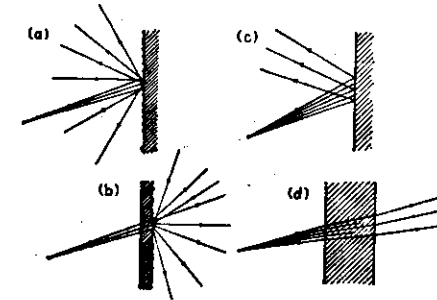
Narrow Tuning Range with a Single Dye. High Spectral Resolution.

3) Interferometers



High Optical Throughput. Wide Spectral Range. Spectral Selection Using Modulation Frequency Discrimination.

ABSORPTION OF RADIATION BY THE SAMPLE

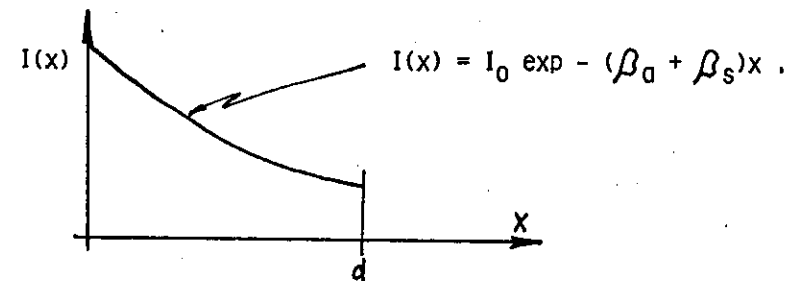
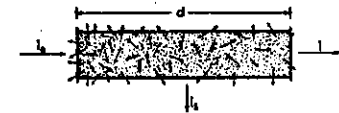


Schematic representation of (a) diffuse reflection; (b) diffuse transmission; (c) absorption upon reflection; (d) absorption upon transmission.

Absorbed Radiation is Responsible for PAS Signal. The Energy Distribution Within the Sample is also Important. Both Absorption and Scattering of the Radiation will Influence this Profile.

β_a = Absorption Coefficient

β_s = Scattering Contribution



13

Absorbed Radiation May Create Electronically Excited States or Interact with Infrared Modes of the Material Under Study.

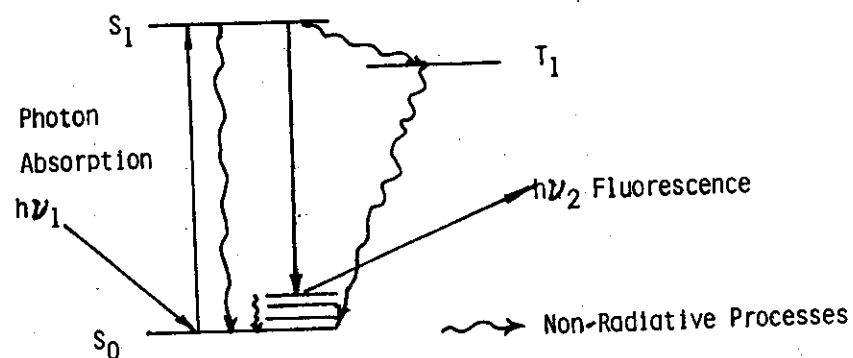
De-excitation Paths which Product Heat or Photochemistry may Contribute to the PAS Signal.

$$\phi_{NR} + \phi_{PC} + \phi_F = 1$$

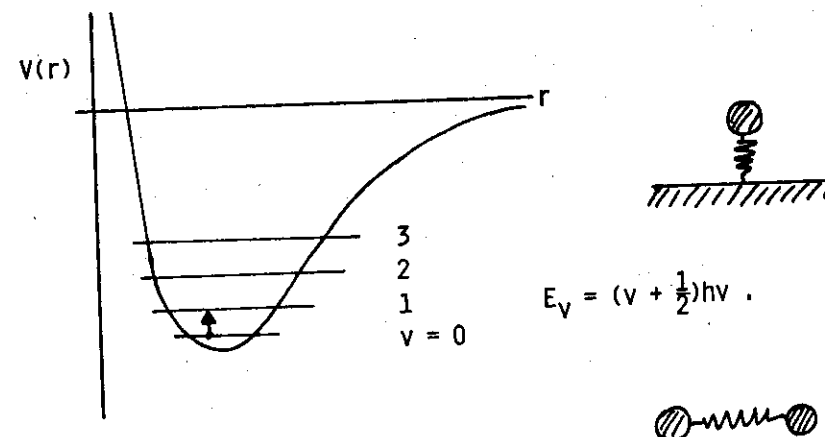
ϕ_{NR} = Quantum Efficiency for Heat Generation by Non Radiative Decay

ϕ_{PC} = Quantum Efficiency for Photochemical Processes $\rightarrow \Delta P ?$

ϕ_F = Quantum Efficiency for Fluorescence Decay



14



Photons Increase Energy Associated with One of the Modes of Motion are the Surface Atom or a Gas Phase Atom.

The Surface Atom Couples to the Bulk Solid and the Energy Degrades as Heat.

The Gas Phase Atom Suffers Collisions with Other Gas Phase Atoms and Vibrational \rightarrow Translational Energy Transfer Occurs Increasing the Gas Temperature.

The Heat Generated by the Non Radiative Decay Processes Produces a Space and Time Dependent Heat Source Within the Sample that Produces the PAS Signal.

The Spatial Extent is Characterized by the Optical Absorption Length.

$$\mu_{\beta}(\lambda) \equiv \left\{ \frac{1}{\beta(\lambda)} \right\}$$

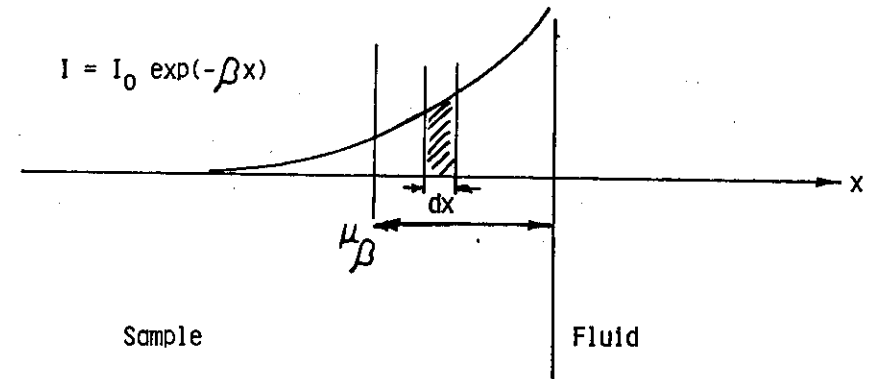
The Temporal Behavior is Determined by the Modulation Mode Employed.

For Light Scattering Samples it is Convenient to Separate the Two Contributions to α viz Absorption and Scattering $\alpha \equiv (\alpha_a + \alpha_s)$ and Define Two Characteristic Lengths for the Sample:

Absorption Length $\mu_a(\lambda) \equiv \left\{ \frac{1}{\beta_a(\lambda)} \right\}$

Scattering Length $\mu_s(\lambda) \equiv \left\{ \frac{1}{\beta_s(\lambda)} \right\}$

For a One Dimensional Non-Scattering Sample Exposed to Harmonically Modulated Radiation Heat Transfer from the Sample to the Fluid in Contact with it is One Source of the PAS Signal.



The Heat Deposited in dx at x is:

$$dQ(x) \propto I_0(t) \exp(-\beta x) \beta dx .$$

This Heat Diffuses in the Sample and into the Contacting Fluid. The Periodic Component Gives Rise to a Periodic Temperature Change in the Near Surface Fluid. This May be Detected as a Pressure or Refractive Index Change of the Fluid. It is also Possible to Detect the Temperature Change of the Surface Directly.

Both the Amplitude and Phase of the Signal Depend Upon the Deposition Profile.

Thermal Diffusion can be Characterized by a Thermal Diffusivity, α_1 , which is Related to the Thermal Diffusion Coefficient of the Material, a_1 , by

$$a_1 \equiv \left(\frac{\omega}{2\alpha_1} \right)^{1/2} \equiv \frac{1}{\mu_1}$$

Where μ_1 is the Thermal Diffusion Length in the Material and ω the Modulation Frequency of the Periodic Heat Source.

The Energy Deposition Profile can be Characterized by the Location of its Centroid which is the Weighted Average of the Heat Contribution at the Interface from each Absorbing Layer dx .

$$\langle x \rangle \equiv \left[\frac{\int_0^e I_0 \beta x \exp [-(a_s + \beta) x] dx}{\int_0^e I_0 \beta \exp [-(a_s + \beta) x] dx} \right]$$

For a Material for which the Optical Absorption Length is Short Compared to the Sample Thickness i.e. $\mu_\beta \ll l$ the Position of the Centroid can be Approximated as

$$\frac{1}{\langle x \rangle} = \frac{1}{\mu_s} + \frac{1}{\mu_\beta}$$

For an
Optically Thick
Sample

For a High Optical Absorption Coefficient

$$\mu_\beta \ll \mu_s \quad \text{and} \quad \langle x \rangle_s \approx \mu_\beta$$

The Phase of the Photoacoustic Response then Contains a Contribution due to the Thermal Diffusion Time from a Depth Equal to the Optical Absorption Depth. As β Increases this time Decreases.

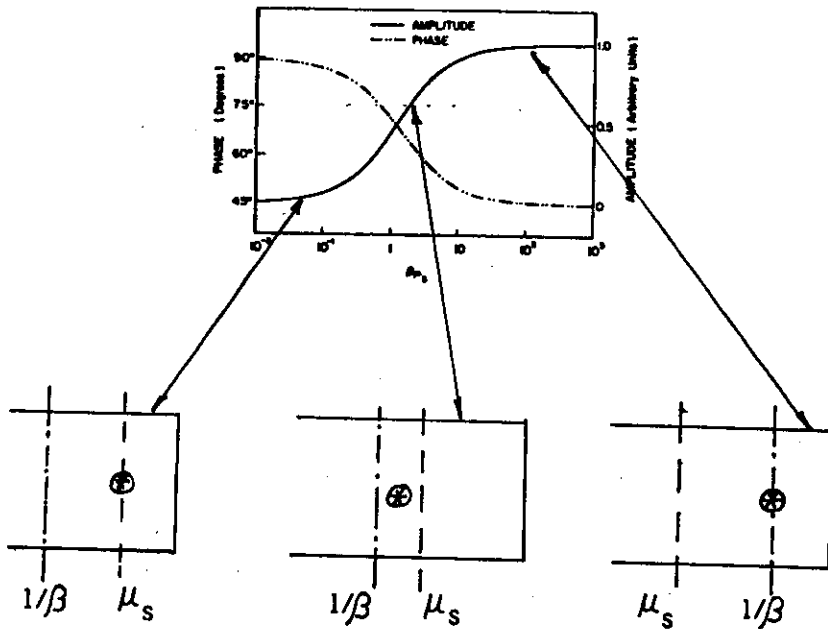
For a Low Optical Absorption Coefficient

$$\mu_\beta \gg \mu_s \quad \text{and} \quad \langle x \rangle_s \approx \mu_s$$

The Phase of the Photoacoustic Response is then Dominated by the Thermal Diffusion Time from a Depth

$$\mu_s \propto \sqrt{1/\omega}$$

The Amplitude of the Surface Temperature Excursion Determines the Amplitude of the PAS Signal. The Approximate Volume Heated by the Radiation Scales as μ_B . Once $\mu_B \ll \mu_s$ the Surface Temperature is Independent of μ_B and the Signal is Constant in Amplitude.



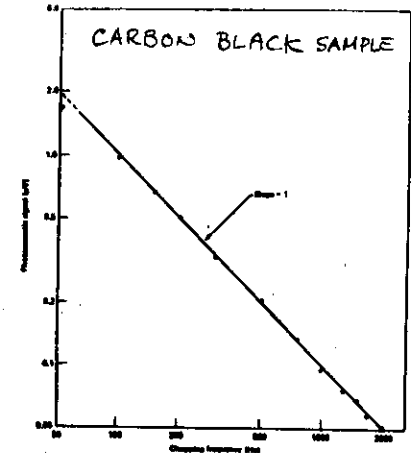
The Surface Temperature is also Frequency Dependent. Both the Exposure Period and the Thermal Diffusion Length Depend on the Modulation Frequency.

For a sample in Photoacoustic Saturation $\mu_s \gg \mu_B$

Amplitude $\neq f(\beta)$

Exposure $\propto (1/\omega)$

PAS Signal $\propto \omega^{-1}$.

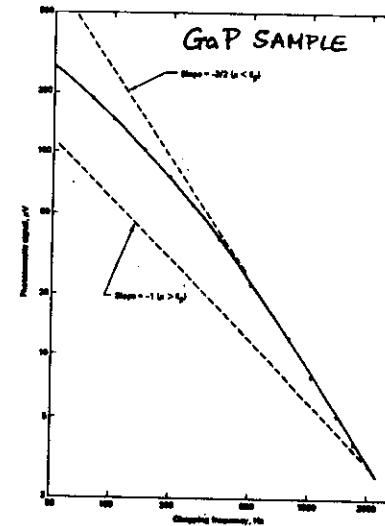


For a non-Saturated Sample $\mu_B > \mu_s$.

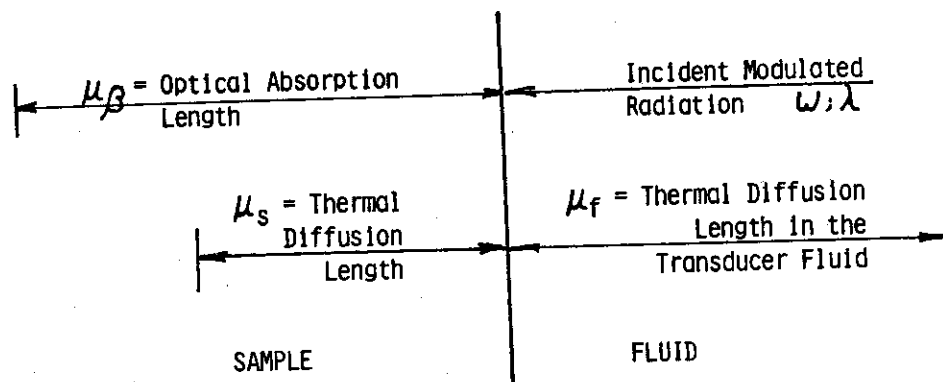
$\mu_s \propto (1/\sqrt{\omega})$

Exposure $\propto (1/\omega)$

PAS Signal $\propto \omega^{-3/2}$.



LENGTH SCALES IN PHOTOACOUSTIC SPECTROSCOPY



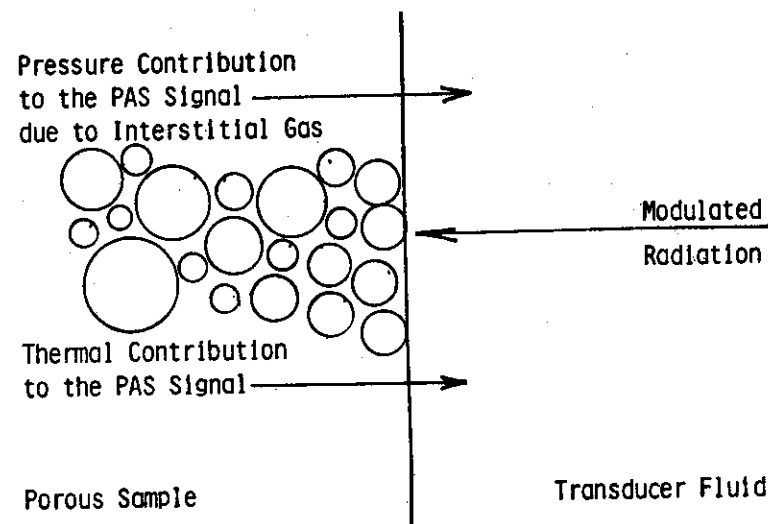
For $\mu_s < \mu_\beta$ Have a Spectroscopic Tool.

VALUES OF THERMAL PARAMETERS FOR VARIOUS MATERIALS

Substance	Density ρ (g/cm ³)	Specific heat C (cal/g·°C)	Thermal Conductivity κ (cal/cm·sec·°C)	Thermal Diffusivity $\alpha = \kappa/\rho C$ (cm ² /sec)	Thermal diffusion Length at 100 Hz $\mu = (2\alpha/\omega)^{1/2}$ (cm)
Aluminum	2.7	0.216	4.8×10^{-1}	0.82	5.1×10^{-2}
Stainless steel	7.5	0.12	3.3×10^{-2}	3.7×10^{-3}	1.1×10^{-1}
Brass	8.5	0.089	2.6×10^{-1}	0.34	3.3×10^{-2}
KCl crystal	2.0	0.21	2.2×10^{-2}	5.2×10^{-3}	1.3×10^{-2}
Crown glass	2.6	0.16	2.5×10^{-3}	6.0×10^{-3}	4.4×10^{-3}
Quartz	2.66	0.188	2.2×10^{-3}	4.4×10^{-3}	3.7×10^{-3}
Rubber	1.12	0.35	3.7×10^{-4}	9.4×10^{-4}	1.7×10^{-3}
Polyethylene	0.92	0.55	5×10^{-4}	9.9×10^{-4}	1.8×10^{-3}
Water	1.00	1.00	1.4×10^{-3}	1.4×10^{-3}	2.1×10^{-3}
Ethyl alcohol	0.79	0.60	4.2×10^{-4}	8.9×10^{-4}	1.7×10^{-3}
Chloroform	1.53	0.23	2.9×10^{-4}	8.4×10^{-4}	1.6×10^{-3}
Air	1.29×10^{-3}	0.24	5.7×10^{-5}	0.19	2.5×10^{-2}
Helium	1.80×10^{-4}	1.25	3.4×10^{-4}	1.52	7.0×10^{-2}

Source: Rosemwaig, 1978.

Many Samples are in Powder or Fiber Form. New Signal Paths Occur. Thermal Properties are Changed. Optical Properties are Changed.



The Sample can be Characterized by its Porosity, ϵ ,
 $0 \leq \epsilon \leq 1$.

The Energy Deposition Profile is Changed by Both Absorption and Light Scattering Changes

$$\beta \rightarrow \beta(1 - \epsilon).$$

Diffuse Light Scattering Doubles the Effective Optical Path Length in the Powder as Compared to a Non-Scattering Material.

The Thermal Conductivity of the Sample is Dominated by Gas Phase Heat Transport.

The Heat Capacity of the Sample is Dominated by the Solid Phase Heat Capacity.

For SiO_2 Powder or Fiber in Air

$$\rho = \rho_{\text{SiO}_2}(1 - \epsilon) = 2.66(1 - \epsilon) \text{ g cm}^{-3}$$

$$C = C_{\text{SiO}_2} = 1.88 \times 10^{-1} \text{ cal (g } ^\circ\text{C)}^{-1}$$

$$K = K_{\text{Air}} = 5.7 \times 10^{-5} \text{ cal (cm sec } ^\circ\text{C)}^{-1}$$

For a Powder with 50% Porosity

$$\alpha = 2.28 \times 10^{-4} \text{ cm}^2 \text{ sec} \quad \mu = 8.5 \times 10^{-4} \text{ cm}$$

For a Fiber Sample with a 95% Porosity

$$\alpha = 2.28 \times 10^{-3} \text{ cm}^2 \text{ sec} \quad \mu = 2.69 \times 10^{-3} \text{ cm}$$

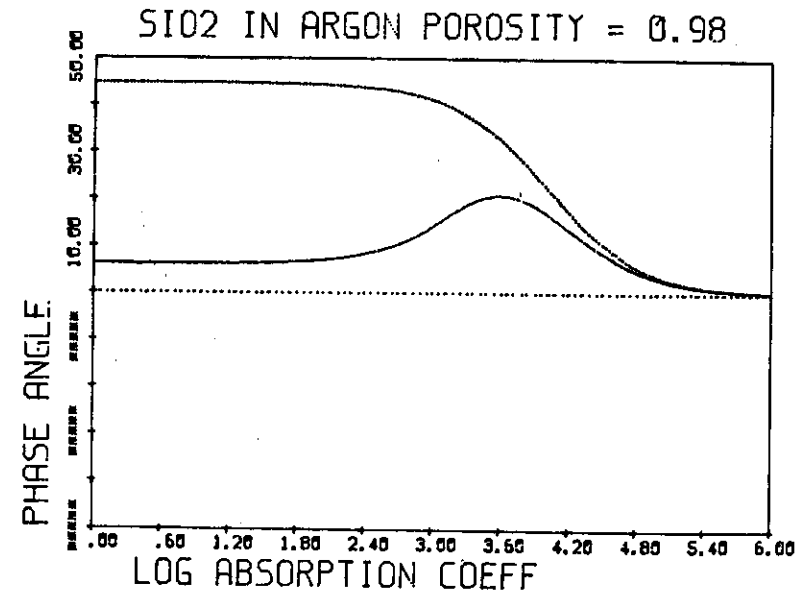
For Single Crystal Quartz

$$\alpha = 4.4 \times 10^{-3} \text{ cm}^2 \text{ sec} \quad \mu = 3.7 \times 10^{-3} \text{ cm}$$

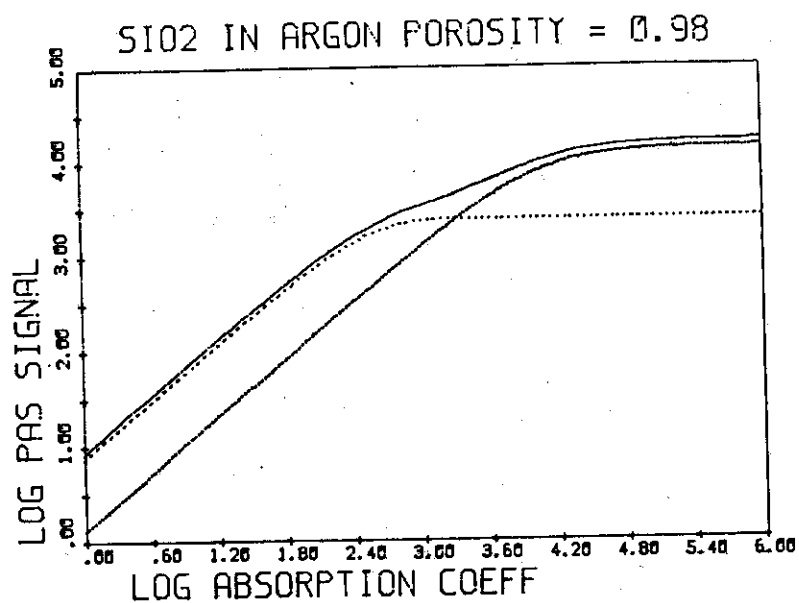
Another Signal Path due to the Thermal Expansion of the Interstitial Gas is also Possible. This Gives Rise to a "Pressure Term" in the PAS Signal which Depends on the Volume of Interstitial Gas Heated.

Important at Low Absorption Coefficients.

No Phase Lag at Normal Frequencies Since Information is Transferred with the Velocity of Sound.



Pressure Contribution from the Expansion of the Interstitial Gas adds to the Thermally Induced Pressure and Dominates at Low Optical Absorption Coefficients.



SAMPLE THERMAL EXPANSION

Periodic or Pulse Heating of a Condensed Phase Generates Thermo-elastic Waves which can be Detected by Piezoelectric Transducers.

For Cylindrical Geometry of Energy Absorption the Fractional Change in Radius Produced in an Adiabatic, Isobaric Expansion is:

$$\frac{\Delta R}{R} = \frac{\alpha_t \Delta T}{2}$$

This Expansion Generates a Radial Pressure Wave that Interacts with the Piezoelectric Transducer to Generate the Photoacoustic Signal. ΔT Depends upon the Optical Absorption, β , in the Sample so that the Signal has the Form:

$$\left\{ \begin{array}{l} \text{Signal Per} \\ \text{Unit Energy} \end{array} \right\} = K \frac{\alpha_t \beta c}{c_p}$$

K is a Geometry Dependent Constant, C the Sound Velocity and c_p the Specific Heat of the Medium.

Thermoelastic Parameters for Various Substances

Substance	Density (g/cm ³)	Coefficient of Linear Thermal Expansion $\alpha_l (\times 10^{-4})$	Bulk Modulus $B (\times 10^{10})$ (dynes/cm ²)	Sound Velocity (25° C) $c_0 (\times 10^3)$ (cm/sec) ^a
<i>Liquids</i>				
Acetone	0.790	4.8	0.79	1.20
Carbon disulfide	1.292	4.1	1.08	1.14
Carbon tetrachloride	1.263	4.0	0.94	0.93
Chloroform	1.527	4.2	0.99	1.00
Ethyl alcohol	0.792	3.7	0.90	1.16
Glycerin	1.26	1.7	4.76	1.90
Methyl alcohol	0.791	3.8	0.81	1.12
Water	1.00	0.67	1.89	1.48
<i>Solids</i>				
Aluminum	2.70	0.23	77	6.42
Brass	8.2-8.8	0.18	105	4.70
Copper	8.96	0.17	135	5.01
Glass (crown)	2.5-2.7	0.09	50	5.10
Gold	19.3	0.14	185	3.24
Lead	11.34	0.29	43	1.96
Silver	10.5	0.19	100	3.65
Steel	7.8	0.25	175	5.94

^aThe sound velocities given for solids represent longitudinal velocities.

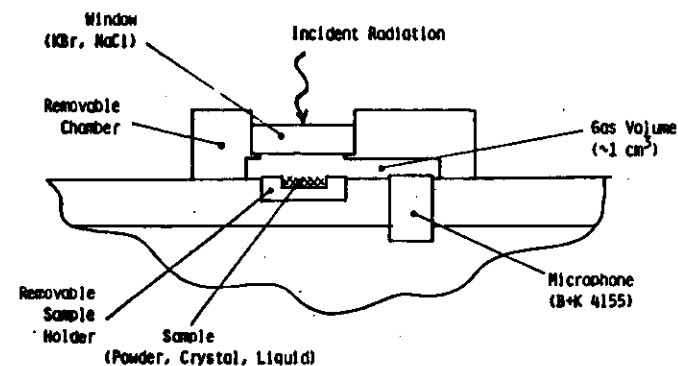
Piezoelectric Detection is not good for Detecting Pressure Signals in Gases because of the Acoustic Impedence Mismatch Between the Gas and the Transducer.

The Method is good for Direct Coupling to Liquid and Solid Samples which have a Similar Acoustic Impedence to the Transducer.

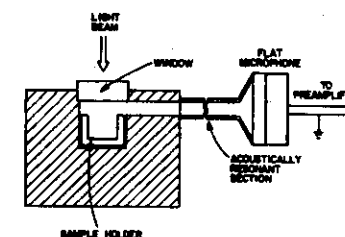
SIGNAL DETECTION CONFIGURATIONS

a) Gas-Microphone Cells

1) Non-Resonant Cell with Flat Frequency Response



2) Resonant Cell with Signal Enhancement

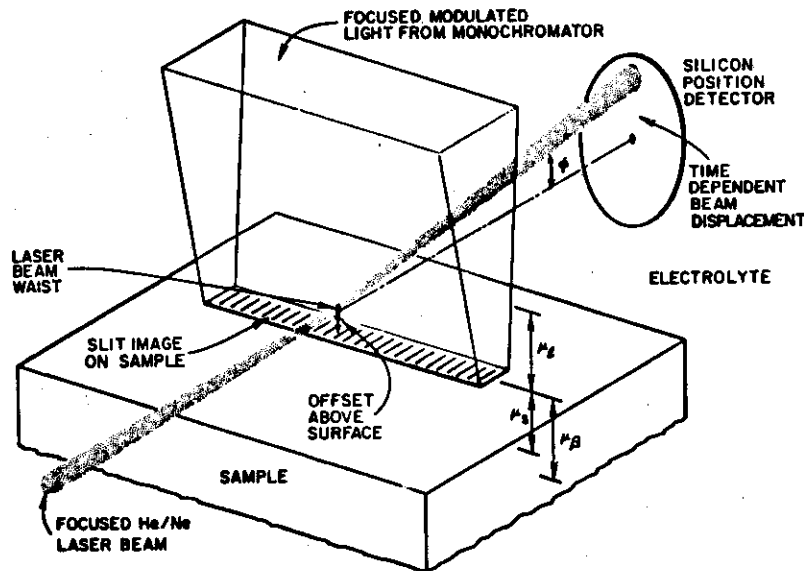


Separation of Microphone and Sample Permits Sample Temperature to be varied over a wide range.

Gas Flow Capability Permits in cell Reactions to be Employed.

b) Laser Probe...Mirage Effect Cells

Detects the Near Surface Temperature Gradient through its Effect on the Refractive Index of the Fluid. Good for either a Gas or Liquid in contact with the Sample.

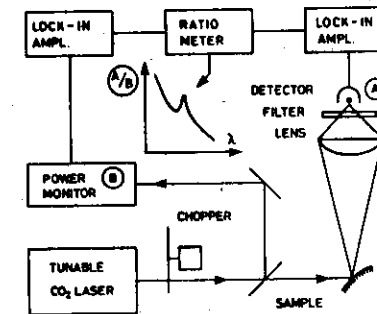


Periodic Component of the Beam Deflection Scales as the Excess Surface Temperature.

$$\phi \propto \left(\frac{dn}{dT}\right) \left(\frac{\Delta T}{\mu_e}\right).$$

c) Photothermal Radiometry

Detects Change Infra-red Emission by the Sample as a Result of Optical Absorption Processes



Radiant Energy Emitted by the Sample Depends on Stefan-Boltzman Law

$$W = \epsilon \sigma T^4$$

Temperature Change ΔT due to Photothermal Process Causes a Signal Change

$$W = 4\epsilon\sigma T^3 \Delta T(E(\lambda), \beta).$$

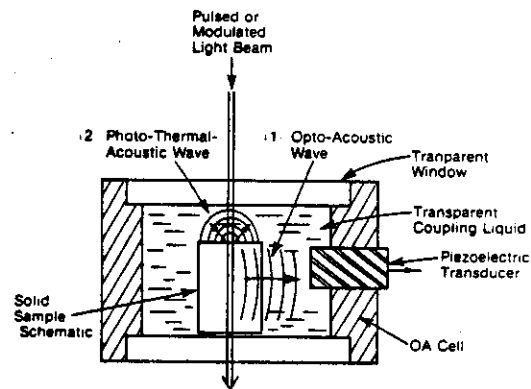
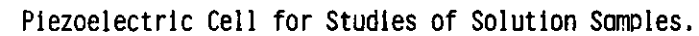
$$\left(\frac{\Delta W}{W}\right) = \left\{ \frac{4 \Delta T(E(\lambda), \beta)}{T} \right\}$$

Can be Used without a Cell. An Advantage for Some In Situ Studies.

Piezoelectric Cell Configuration for Powder Samples

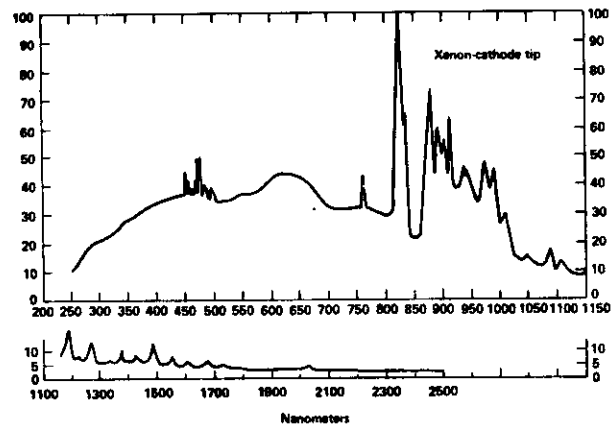
The diagram illustrates the experimental setup for measuring the acoustic velocity of a thin layer of grease. The setup includes the following components and connections:

- Pulsed Dye Layer** and **Scanning Drive** are connected to a **BS** (Beam Splitter).
- The **BS** directs light through a lens and a **2-METER SPECTROMETER** to the **PZT TRANSDUCER**.
- The **PZT TRANSDUCER** is coupled to a **THIN LAYER OF GREASE**, which is sandwiched between **FUSED QUARTZ PLATES**.
- An **ACOUSTIC WAVE** is generated in the grease layer, causing **SCATTERED LIGHT**.
- The **SCATTERED LIGHT** is collected by the **2-METER SPECTROMETER** and detected by the **PZT TRANSDUCER**.
- The output of the **PZT TRANSDUCER** is amplified by an **AMPLIFIER** and then processed by **BOXCAR A** and **BOXCAR B**.
- BOXCAR A** and **BOXCAR B** are connected to the **COMPUTER**.
- The **COMPUTER** also receives input from the **Scanning Drive** and the **Pulsed Dye Layer**.
- The **COMPUTER** outputs a signal to the **PLOTTER**, which displays a graph of A/B versus V .

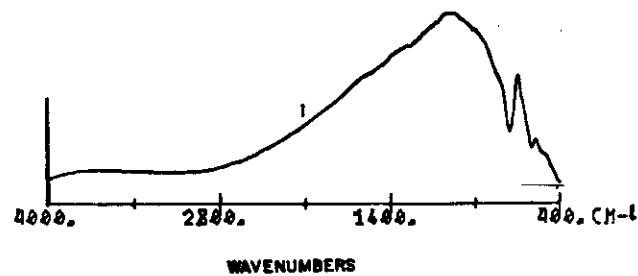


Photoacoustic Signal is Proportional to the Incident Radiation Intensity. The Signal must be Corrected for the Spectral Dependence of this Quantity. A Black Absorber in Photoacoustic Saturation gives a Signal that Depends on $I(\lambda)$. Graphite Powder is a good Black Absorber.

1) Spectral Output of a Xenon Arc Source.



11) Spectral Throughput of Fourier Transform Interferometer.

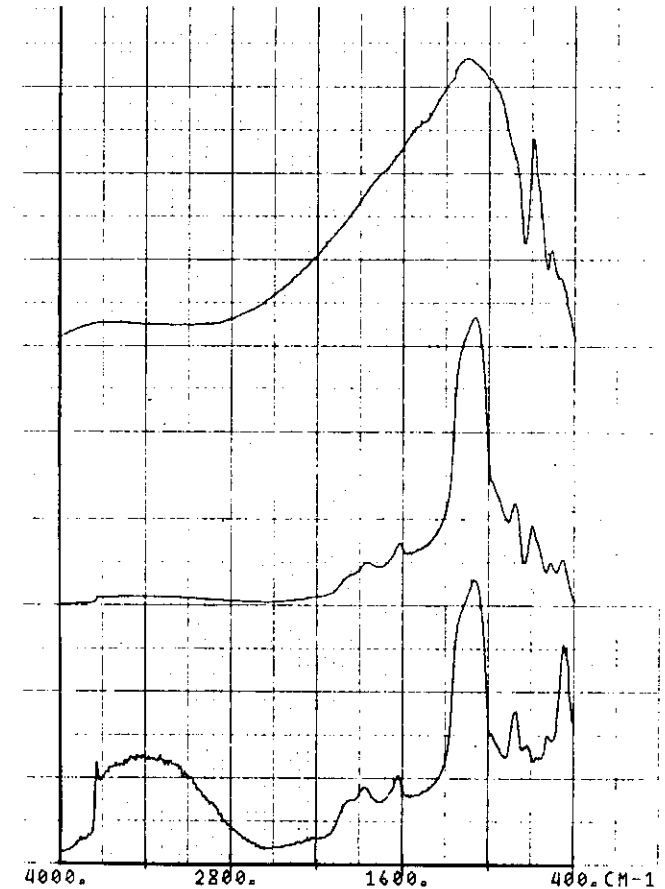


EFFECT OF NORMALIZATION

Black Body

Raw FTIR PAS Data

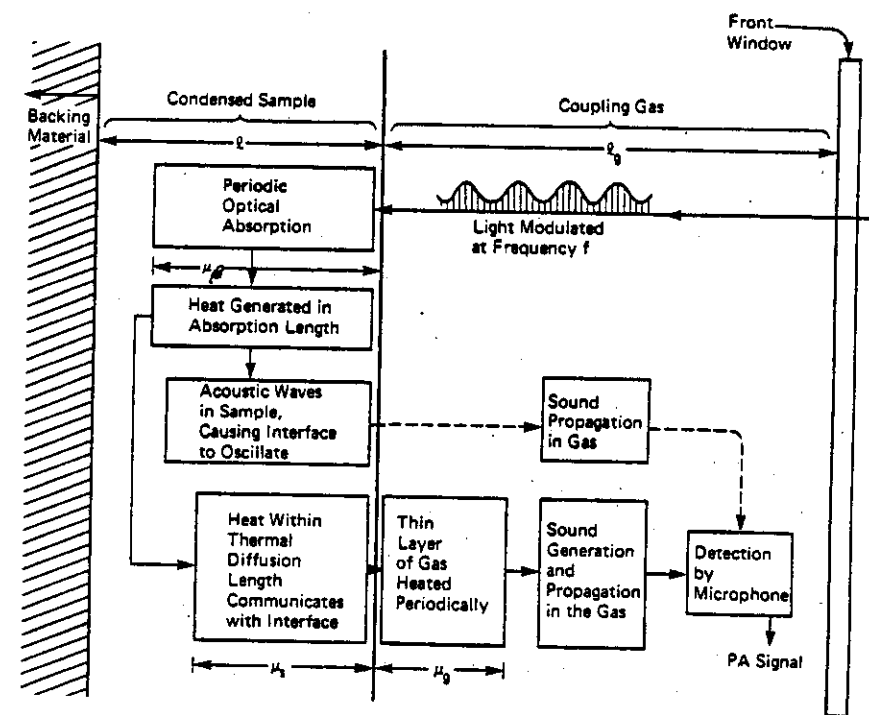
Normalized Data



B) MODELS FOR PHOTOACOUSTIC SIGNAL GENERATION

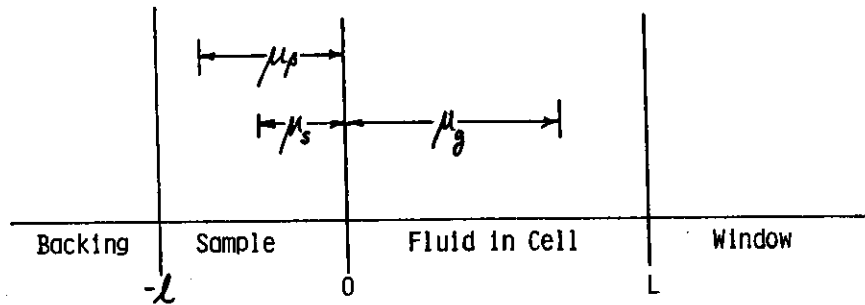
- 1) Thermal Transport in a One Dimensional Model
- 2) Thermal Expansion Contributions to the PAS Signal: Powder or Fiber Samples
- 3) Light Scattering Effects
- 4) Photothermal Deflection Spectroscopy, The Mirage Effect.
- 5) Concentration Gradient Effects

For a Homogeneous Sample the Photoacoustic Signal Path has the Form Shown Below. This is the Problem to be Modeled in terms of One Dimensional Heat and Pressure Transport.



For Powder or Fiber Samples the Thermal Expansion of the Interstitial Gas Contributes to the Pressure Term in the Model.

ONE-DIMENSIONAL PHOTOACOUSTIC MODEL

Assume

- 1) Photons Deposit Energy only in the Sample which has an Absorption Coefficient $\beta(\lambda)$. $\mu_\beta \equiv (1/\beta)$.

- 2) Incident Radiation is Modulated Periodically

$$I(t) = \frac{I_0}{2} [1 + \cos \omega t] \quad , \quad \omega = 2\pi f$$

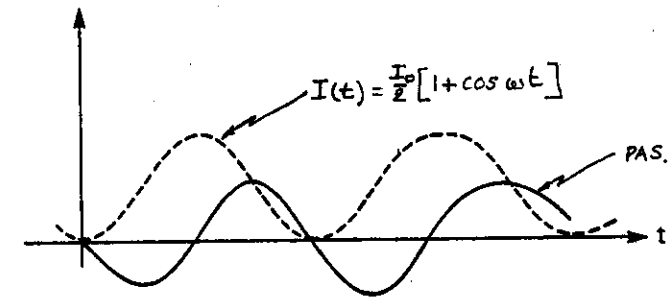
$f \sim 20 \text{ Hz} \rightarrow 1 \text{ kHz.}$

- 3) No Light Scattering occurs so that Energy Deposition Profile has the form

$$I(x) = I_0 \exp(-\beta|x|).$$

- 4) All Components of the System are in Good Thermal Contact.
- 5) The Outer Walls of the Cell Remain at a Constant Temperature T_0 .

The Photoacoustic Response of the System is Measured by the Pressure Fluctuations in the Cell Fluid. In the Steady State these will be Periodic with the Same Frequency, ω , as the Incident Radiation and with a Phase Shift, ϕ , with Respect to the Radiation.



The Pressure and Temperature are Coupled and Described in One Dimension By

$$\frac{\partial^2 p}{\partial x^2} - \frac{\rho_0}{B} \frac{\partial^2 p}{\partial t^2} = -\rho_0 \beta_t \frac{\partial^2 T}{\partial t^2}$$

$$K \frac{d^2 T}{dx^2} - \frac{K}{\alpha} \frac{\partial T}{\partial t} + S = -T_0 \beta_t \frac{\partial p}{\partial t}.$$

S = Thermal Energy Source due to Optical Absorption;
 K = Thermal Conductivity; α = Thermal Diffusivity;
 B = Isothermal Bulk Modulus; β_t = Thermal Expansion Coefficient; ρ_0, T_0 = Ambient Density and Temperature.

Provided the Radiation Modulation Frequency

$$\omega \ll (c_0^2/\alpha_g) \simeq 10^9 \text{ Hz For Air}$$

The Time Required for Sound Propagation in the Gas is Much Shorter than a Modulation Period and the Pressure in the Cell is not Spatially Varying. $p = p(T)$ Only Provided the Volume Change of the Solid is Small so that the Gas Velocity at All of its Boundaries is Zero.

Under These Conditions the Coupled Pressure and Temperature Equations can be Replaced by Thermal Diffusion Equations for the Various Regions of the Cell. This Approach was first followed by Rosencwaig and Gersho and will be Adopted Below.

Three Dimensional Effects may also be Neglected Provided the Lateral Distance Between the Optically Heated Sample and the Cell Walls is Greater than a Thermal Diffusion Length. For Typical Cell Dimensions this is True Above about 5 Hz.

COUPLED THERMAL DIFFUSION EQUATIONS

For the Solid: $0 \leq x \leq -l$

$$\frac{\partial^2 T_s(x,t)}{\partial x^2} - \frac{1}{\alpha_s} \frac{\partial T_s(x,t)}{\partial t} = - \frac{\dot{H}(x,t)}{K_s}$$

For the Gas, Window and Backing:

$$\frac{\partial^2 T_i(x,t)}{\partial x^2} - \frac{1}{\alpha_i} \frac{\partial T_i(x,t)}{\partial t} = 0$$

$i = g, w, b$

$\alpha_i = \text{Thermal Diffusivities}$

The Boundary Conditions require Heat Flux and Temperature Continuity at the Junctions between the Regions.

$$T_i(\text{boundary}, t) = T_j(\text{boundary}, t)$$

$$K_i \frac{\partial}{\partial x} T_i(\text{boundary}, t) = K_j \frac{\partial}{\partial x} T_j(\text{boundary}, t)$$

Only the Solid Phase has a Heat Source Term

$$\dot{H}(x,t) = \frac{1}{2} \eta I_0 \beta \exp(-\beta |x|) \cos \omega t$$

or

$$\dot{H}(x,t) = \frac{1}{2} \eta I_0 \beta \exp(-\beta |x|) \operatorname{Re}[\exp i \omega t]$$

The Time Dependent Gas Pressure $\langle \Delta p_g(t) \rangle$ constitutes the Photoacoustic Signal and is Related to $T_g(x,t)$ which is found from the above equations

$$p(x,t) = R \rho(x,t) T(x,t)$$

R = Gas Constant, $\rho(x,t)$ = Gas Density

$$\int_0^L \frac{p(x,t)}{T(x,t)} dx = R \int_0^L \rho(x,t) dx = RM_0$$

M_0 = Total Mass of Gas in Cell = Constant

$$T(x,t) = T_0 + T_g(x,t) \quad ; \quad p(x,t) dx = p_0 + \langle p_g(t) \rangle$$

$$\langle p_g(t) \rangle = \frac{p_0}{T_0 L} \int_0^L T_g(x,t) dx$$

This relationships holds for all values of L including those for which $L < \mu_g$. The Rosencwaig-Gersho acoustic piston model breaks down in this limit due to heat losses to the Window.

$T_g(x,t)$ is a complex quantity (i.e. amplitude and phase) which is found by solving the four coupled Thermal Diffusion equations subject to the Boundary Conditions of Temperature and Heat Flux Continuity.

Mandellis et al used Fourier Transform Methods to Evaluate $T_g(x,t)$ which has the form:

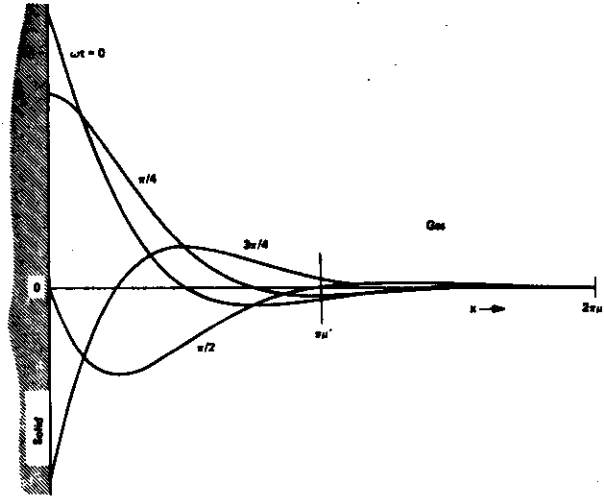
$$T_g(x,t) = \frac{A \exp(-\sigma_g x + i\omega t)}{(\beta^2 - \sigma_s^2)} \left\{ \frac{(r-1)(b+1) \exp(\sigma_s L) - (r+1)(b-1) \exp(-\sigma_s L) + 2(b-r) \exp(-\beta L)}{(g+1)(b+1) \exp(\sigma_s L) - (g-1)(b-1) \exp(-\sigma_s L)} \right\} \quad (2)$$

$$r = (1-i) \left(\frac{\beta}{2a_s} \right) ; \quad b = \left(\frac{a_b K_b}{a_s K_s} \right) ; \quad g = \left(\frac{a_g K_g}{a_s K_s} \right) ; \quad \sigma_1 = (1+i)a_1 \quad \text{and} \quad A = \left(\frac{I_0 \beta \eta}{2K_s} \right)$$

Substituting this value in the expression for $\langle p_g(t) \rangle$ gives:

$$\langle p_g(t) \rangle = \left(\frac{p_0 I_0 \eta \beta}{2K_s T_0 L} \right) \operatorname{Re} \left[\frac{\exp(i\omega t - \frac{\pi}{4})}{\sqrt{2} a_g (\beta^2 - \sigma_s^2)} \left\{ \frac{(r-1)(b+1) \exp(\sigma_s L) - (r+1)(b-1) \exp(-\sigma_s L) + 2(b-r) \exp(-\beta L)}{(g+1)(b+1) \exp(\sigma_s L) - (g-1)(b-1) \exp(-\sigma_s L)} \right\} \right]$$

The Temperature Profile in the Gas as a function of Time in the Period and Distance from the Surface has the form shown Below.



The Thermal Wave Decays in a Distance of Approximately $2\pi\mu_g$ away from the Heated Sample Surface. This has a value of about 1 mm for air with $\omega = 100$ Hz.

$$T_s(\text{surface}) = T_g(0, t) = \theta \cos \omega t$$

$$T_g(x, t) = \theta \exp(-a_g x) \cos(\omega t - a_g x)$$

$\langle p_g(t) \rangle$ is a complex quantity and the Amplitude and Phase of the Pressure with respect to the Modulated Light Stimulus may be Obtained from its Real and Imaginary Components

$$\langle p_g(t) \rangle \equiv \text{Re} \left[Q \exp(i \{ \omega t - \frac{\pi}{4} \}) \right] \equiv \text{Re} \left[a \exp(i \{ \omega t - \frac{\pi}{4} \} - \psi) \right]$$

$$Q = Q_1 + i Q_2 = a \exp(-i\psi) .$$

The Amplitude of the Signal

$$|\langle p_g(t) \rangle| = |Q| = a = (Q_1^2 + Q_2^2)^{1/2}$$

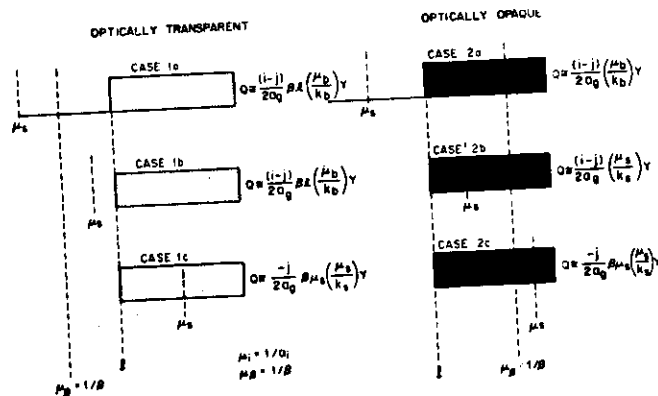
The Phase Lag with respect to the Light Source

$$\Phi = (\frac{\pi}{4} + \psi) = \left\{ \frac{\pi}{4} + \tan^{-1}(\frac{-Q_2}{Q_1}) \right\}$$

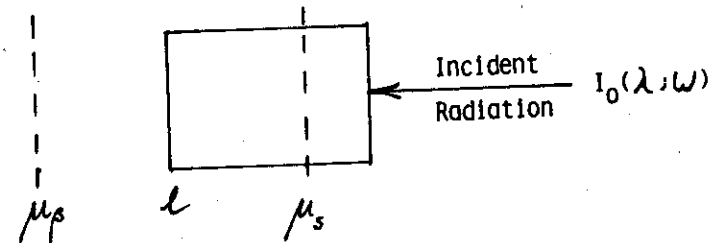
Both these Expressions are Algebraically Complicated and Simplification by Suitable Choice of Experimental Conditions is Needed.

Physically Distinct and Interesting Cases were first discussed by Rosencwaig based on the Relationship between Various Characteristic Lengths for the problem, viz:

Thickness of the Sample	l
Thermal Diffusion Length	μ_s
Optical Energy Deposition Length	$\mu_\beta \equiv \frac{1}{\beta}$



- 1) Optically Transparent, Thermally Thick Sample
 $2\pi\mu_s \leq l$ $\mu_\beta > l$

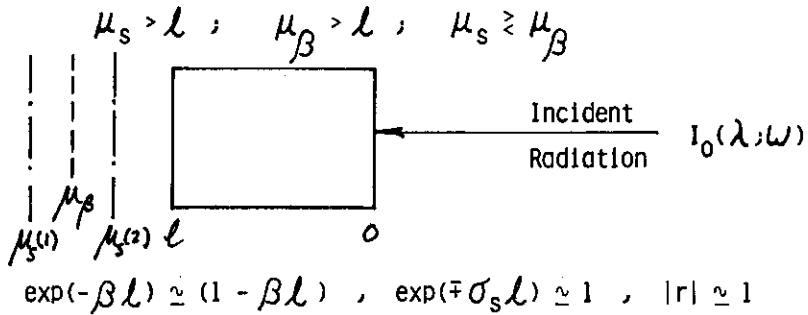


The Radiation Absorbed in the Thermal Diffusion Length μ_s is the Main Source of the Signal
 $\exp(-\beta l) \simeq (1 - \beta l)$; $\exp(-\sigma_s l) \simeq 0$; $|r| \ll 1$.

$$Q \simeq \frac{-j}{2\alpha_0} \left(\frac{\mu_s}{k_s}\right) \gamma (\beta \mu_s).$$

- a) Signal Depends on the Product of an Optical and a Thermal Property of the Material
 $\langle p(t) \rangle \propto (\beta \mu_s).$
- b) Both energy per cycle and μ_s depend on the Modulation Frequency
 $\langle p(t) \rangle \propto (\omega)^{-3/2}$
- c) The Sample is Thermally thick so backing Properties do not enter the Signal Expression.

- 2) Optically Transparent, Thermally Thin.

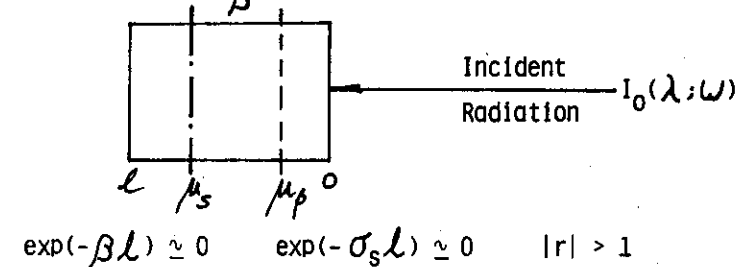


$$Q = \frac{(1 - 1)}{2a_g} \left(\frac{\mu_b}{k_b} \right) Y(\beta l) .$$

- a) Signal depends on the Product of an Optical and a Physical Property (βl). No energy is deposited in the Transparent Backing and so l replaces μ_s for this case.
- b) Since μ_β and μ_s are both larger than l and the Backing is Transparent their Relative Values are not important.
- c) Heat is Lost to the Backing and this influences the Surface Temperature of the Sample and Hence the PAS Signal.
- d) $(\mu_b/a_g) = (1/a_b a_g) \propto (\omega^{-1})$

- 3) Optically Opaque, Thermally Thick

$\mu_s < l ; \mu_\beta \ll \mu_s .$

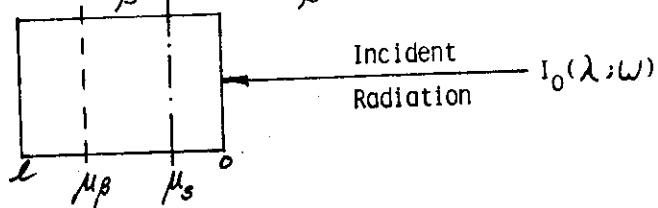


$$Q = \frac{(1 - 1)}{2a_g} \left(\frac{\mu_s}{k_s} \right) Y ; Y \propto I_0$$

- a) Signal Contains only Thermal Properties of the Sample. Since $\mu_\beta \ll \mu_s$ the Details of the Energy Distribution Profile are not important.
- b) Since Y scales as I_0 the PAS Signal varies as I_0 . This is a Direct Measure of $I_0(\lambda)$.
- c) μ_s, a_g depend on $\sqrt{\omega}$ so that $(\mu_s/a_g) = (1/a_s a_g) \propto (\omega^{-1})$. Signal has an inverse dependence on frequency.
- d) Photoacoustic Saturation.

4) Thermally Thick, Optically Thick

$$\mu_s < l; \quad \mu_\beta < l; \quad \mu_\beta > \mu_s$$



$$\exp(-\beta l) \approx 0, \quad \exp(-\sigma_s l) \approx 0, \quad |r| < 1.$$

$$Q = \frac{-1}{2a_g} \left(\frac{\mu_s}{k_s} \right) \gamma (\beta \mu_s)$$

- a) Signal Again depends on Product of a Thermal and an Optical Property of the Material $(\beta \mu_s)$.
- b) $\left(\frac{\mu_s}{a_g} \right) \propto \frac{1}{\omega}$; $\mu_s \propto \frac{1}{\sqrt{\omega}}$, and the Signal Therefore varies as $\omega^{-3/2}$.
- c) This is a Common Condition for PAS Measurements of Bulk Samples and the Amplitude and Phase Expressions are Rather Simple for this Case.

For this Case the Signal Amplitude is given by:

$$q = \frac{p_0 I_0}{4K_s a_g T_0 L} \left\{ \frac{\beta \mu_s^2}{\sqrt{(\beta \mu_s)^2 + 2(\beta \mu_s) + 2}} \right\}$$

And the Variable Component of the Phase by:

$$\tan \psi = \left\{ 1 + \frac{2}{(\beta \mu_s)} \right\}$$

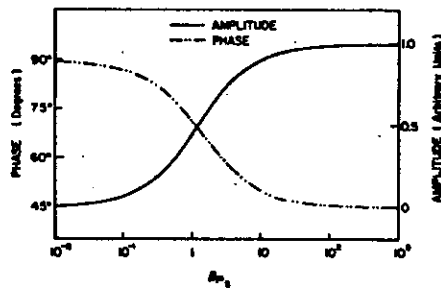
The Amplitude can then be written in terms of the Phase:

$$q = \frac{1}{f} \left[\frac{p_0 I_0 \sqrt{\alpha_g \alpha_s}}{2 \sqrt{2} K_s T_0 L} \right] \cos \psi$$

where f is the Modulation Frequency.

At a constant Modulation Frequency μ_s is a constant and both the Amplitude and the Phase of the Photoacoustic Response depend on β .

Photoacoustic Amplitude and Phase for a Thermally Thick Sample.



At Low Optical Absorption Coefficients $(\beta\mu_s) \ll 1$

$$\tan \psi \rightarrow \infty, \quad \psi \rightarrow 90^\circ, \quad \cos \psi \rightarrow 0, \quad a \rightarrow 0$$

At Large Optical Absorption Coefficients $(\beta\mu_s) \gg 1$

$$\tan \psi \rightarrow 1, \quad \psi \rightarrow 45^\circ, \quad \cos \psi \rightarrow \text{constant}, \quad a \neq f(\beta).$$

This Behavior is illustrated above and corresponds to the situation considered previously in terms of the Centroid of the Energy Deposition Profile.

2) Thermal Expansion Contributions to the PAS Signal

a) Homogeneous Sample. Liquid or Solid.

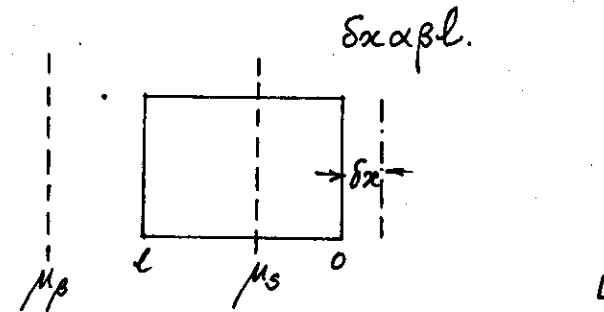
If the material under study has a High Thermal Expansion Coefficient Absorption of Radiation which causes Periodic Heating will produce a displacement of the Sample-Gas Interface. This now gives rise to new Boundary Conditions:

$$v_g = v_s \quad \text{at } v = 0 \quad \text{and} \quad p_g = p_s$$

The Motion of the Sample Surface Contributes a Periodic Pressure Signal that must be added to the Pressure Signal discussed above that arises from the Heat Transfer to the Gas.

The Actual Length of the Sample heated determines the Surface Displacement rather than the Thermal Diffusion Length. For a Wavelength dependent contribution to the PAS Signal from this Source the Sample must be Transparent viz.

$$\mu_\beta > l \quad \text{and} \quad (1 - \exp(-\beta l)) \rightarrow \beta l$$



$\delta x(t)$ can be evaluated for a Thermally Thick, Acoustically Thin Sample and has the form:

$$\delta x(t) \approx \frac{-i\alpha_t I_0}{2\omega(\rho c_p)_s} \left\{ 1 - \exp(-\beta l) \right\} \exp(i\omega t)$$

when $\mu_s \ll l$ and $K_s l_s \ll 1$.

This Surface Displacement gives rise to a Pressure Contribution in the Gas

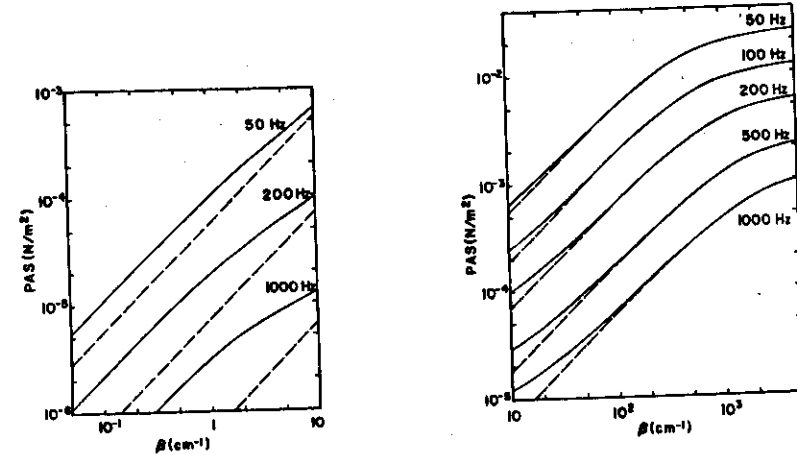
$$p_g = \frac{\gamma p_0}{L} \delta x(t)$$

which may be added to the Thermal Pressure to obtain the complete Photoacoustic Signal

$$\langle p(t) \rangle = - \frac{i\gamma p_0 I_0}{2\omega(\rho c_p)_s L} \left[\frac{\beta}{\sigma_g T_0 (g+1)(r+1)} + \alpha_t (1 - \exp(-\beta l)) \right]$$

Both the Amplitude and Phase of this Signal differ from their values for the Thermal Pressure Term alone.

The Dependence of the Total Pressure upon the value of the Optical Absorption Coefficient for a Dye-Water Sample has the Form shown below



The dashed lines are the contributions from the Thermal Term alone. As expected the additional contribution due to Expansion is greatest at Low Optical Absorption Coefficients. At High Optical Absorption Coefficients the Expansion Term saturates and is Absorption Coefficient Independent. Only the Thermal Term Contributes to the Signal in this Range.

b) Heterogeneous Samples -- Powders and Fibers

These samples are considered to be Composite Materials with the Interstitial Gas being the Component that exhibits Thermal Expansion and contributes a Term to the PAS Signal.

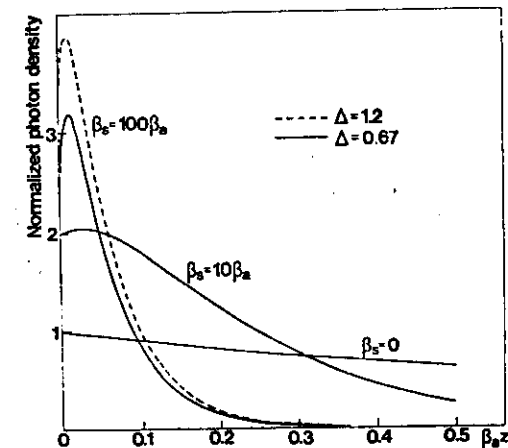
The Composite Nature of the Sample introduces two additional Factors:

- 1) The Thermal and Optical Properties involve combinations of Gas and Solid Values.
- 2) Light Scattering will alter the Photon Distribution in the Sample at High Scattering Coefficients.

The Light Scattering Contribution depends on the Size of the Particle compared to the Wavelength of the Probe Light. With Realistic Particle Sizes Scattering tends to be important in the visible spectral region and less important in the Infrared ($4000 \rightarrow 400 \text{ cm}^{-1}$).

Light Scattering by the Sample Produces two Competing Effects on the Signal:

- 1) Diffuse Reflection at the Sample Surface reduces the Total Energy deposited in the Sample and tends to reduce the PAS Signal.
- 2) Redistribution of the Photon Deposition Profile by Scattering moves the Distributed Heat Source Closer to the Sample Surface and tends to Increase the "Thermal" PAS Signal Component.

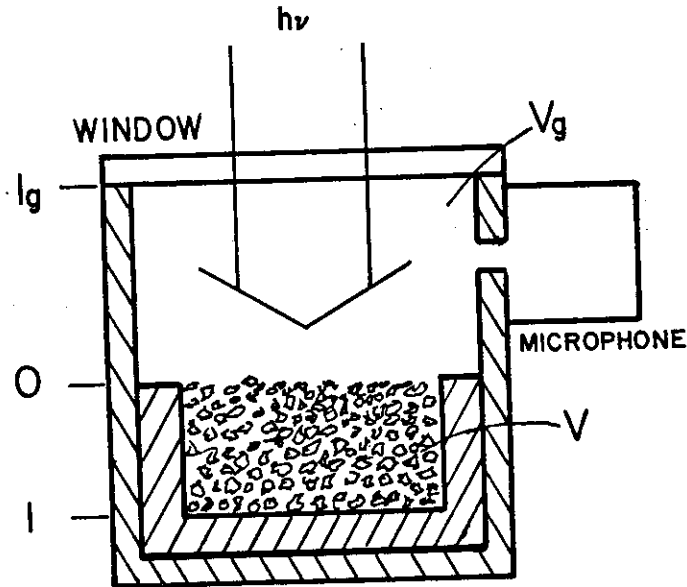


$$I = I_0 \exp(-\{\beta_a + \beta_s\}x) \quad ; \quad \beta_s = \text{Scattering Coefficient}$$

$$\Delta = \frac{2}{3}(1 + 2R) \quad ; \quad R = \text{Reflection at Boundary}$$

$$R = 0 \quad , \quad \Delta = 0.67 \quad ; \quad R = 0.40 \quad , \quad \Delta = 1.2$$

The Photoacoustic Configuration for the Porous Sample is Illustrated Below.



The Sample has a Total Volume V and a Porosity ϵ so that the Total Gas Volume in the Cell is

$$V_e = V_g + \epsilon V$$

The Volume ϵV is heated by interaction with the absorbing Solid of Volume $(1 - \epsilon)V$ and the Solid and Gas Phase of the Composite Sample are always in Thermal Equilibrium. Expansion of the Interstitial Gas Increases the Cell Pressure.

Heat is also Transferred by Conduction from the Composite Sample to the Gas above the Sample. This heat transfer causes a Pressure increase as was discussed above.

These Two Pressure Contributions add and the Total (Complex) Pressure in the Cell is given by the following expression due to Yassa, Jackson and Amer.

$$PA(\text{Total}) = PA(\text{Thermal}) + PA(\text{Pressure})$$

$$= \frac{\alpha_g}{V_e K_g} \left\{ \frac{\tau(0)}{\sigma_g} + \frac{\alpha}{\alpha_g} \int_0^l \tau(z) dz \right\}$$

α_g = Thermal Expansion Coefficient of the Gas

$\alpha = \epsilon \alpha_g$ = Thermal Expansion Coefficient of the Composite Sample ($\alpha_g \gg \alpha_s$)

$\tau(0)$ = Temperature Distribution within μ_s of Surface

$\tau(z)$ = Complete Temperature Profile in Sample.

The First Term is the "Thermal Signal". The Second Term is the "Pressure Signal".

The Form of the Signal may be seen by Considering the Thermally Thick, Optically Thick Limit in the absence of Light Scattering.

In this Limit:

$$PA(\text{Thermal}) = \frac{p_0(1+\gamma)}{2v_e T_0 \sigma_g} \left[\frac{I_0}{K\sigma} \left(\frac{\beta}{\beta + \sigma} \right) \right]$$

$$PA(\text{Pressure}) = \frac{p_0 I_0}{v_e T_0 K \sigma^2} \epsilon \left[1 - \exp(-\beta l) \right]$$

In the Low Absorption Coefficient Region where the Pressure Contribution is most Important:

$$\exp(-\beta l) \sim 1 - \beta l$$

$$\beta \ll \sigma_g \quad \text{so that} \quad \left(\frac{\beta}{\beta + \sigma} \right) \sim \frac{\beta}{\sigma}$$

and the Total Photoacoustic Response is:

$$PA(\text{Total}) \approx \frac{p_0 I_0 \beta}{v_e T_0 K \sigma^2} \left[\frac{(1+\gamma)}{2\sigma_g} + \epsilon l \right]$$

For Materials of High Porosity for which

$$\epsilon l \gg (1+\gamma)/2\sigma_g$$

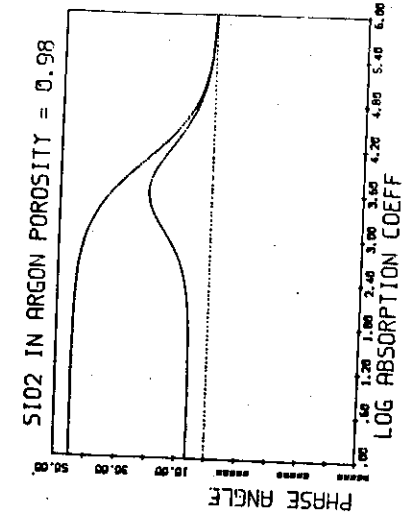
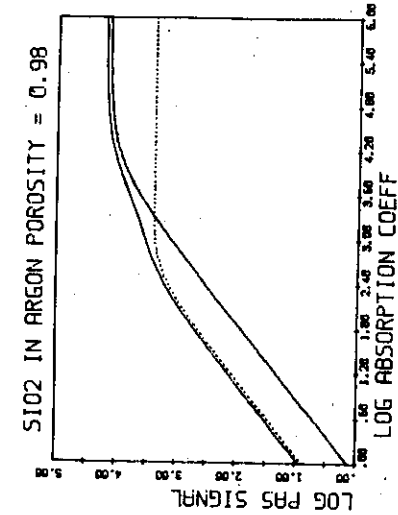
$$PA(\text{Total}) \approx \frac{I_0 p_0 \epsilon \beta l}{v_e T_0 K \sigma^2}$$

This is: Linearly Dependent on the Absorption Coefficient, Increases with Increasing Sample Thickness, Independent of the Gas Properties, Varies Inversely with Frequency and has a Constant Phase Lag of $\pi/2$.

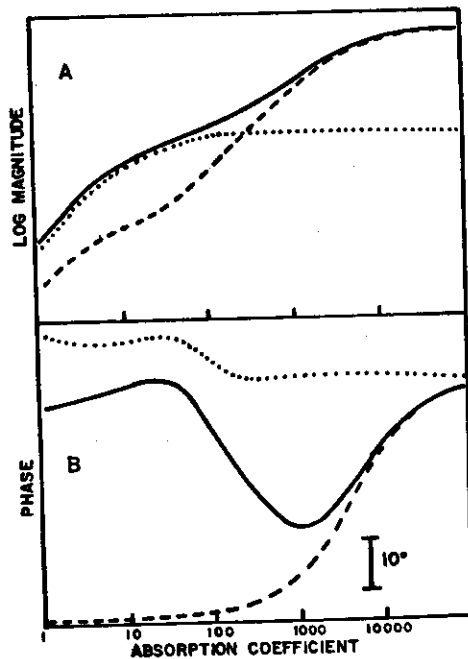
In the General Case the Complex Signal can be Written in Terms of the Properties of the Solid and Gas Phases to Give:

$$PA(\text{Total}) = \frac{-i I_0 p_0 \beta_s}{v_e T_0 \omega (\rho c_p)_s} \left[\frac{(1-\epsilon)(1+\gamma)}{2\sqrt{2}} \left(\frac{K}{\omega \rho c_p g} \right)^{1/2} + \frac{\epsilon}{(1-\epsilon)\beta_s} (1 - \exp\{(\epsilon-1)\beta_s l\}) \right]$$

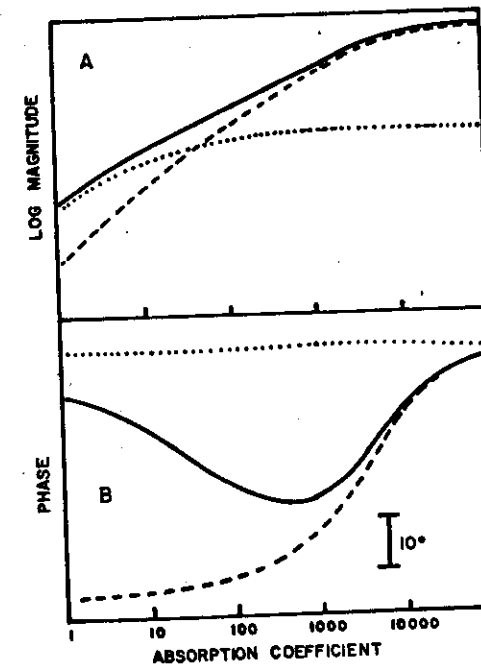
The Amplitude and Phase Spectra for this Case are shown below.



In Many Real Situations the Sample Backing is not Transparent but has a High Reflectivity. This Alters the Energy Distribution in the Sample and the Coupling between the Sample and the Backing Alters the Phase of the Pressure Signal. Since the Sample is Thermally Thick the Phase of the Thermal Signal does not Change.



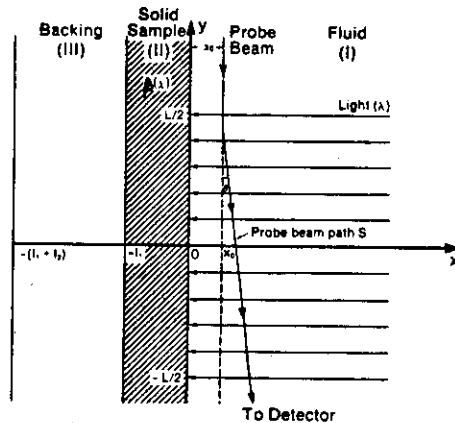
When Light Scattering is taken into Account the Photon Penetration into the Sample is Reduced. The Optical Energy is Deposited Closer to the Sample Surface and Reflection from the Sample Holder becomes Unimportant. When this is the case the Pressure Contribution to the Phase does Contain Effects due to the Backing and is Approximately Independent of the Absorption Coefficient.



PHOTOTHERMAL DEFLECTION SPECTROSCOPY

THE MIRAGE EFFECT

In the Mirage Effect the Temperature Gradient near the Sample Surface in the Fluid in Contact with the Absorbing Sample is Detected through its Effect on the Refractive Index. A Laser Beam is used to Probe this Local Refractive Index and the Beam Deflection is the Source of the Photoacoustic Signal.



The Laser Probe Passes a distance x_0 away from the Illuminated Region of the Surface. In General $x_0 \approx \mu_f$. The Sample is the Only Region that has Optical Absorption $\beta(\lambda)$ and it is Assumed to be Homogeneous and non-Light Scattering.

The Incident Radiation is Periodically Modulated and is Converted to Heat in the Sample with an Efficiency so that the Distributed Heating Rate has the Form:

$$\dot{H}(x,t) = \frac{\eta I_0}{2} \beta \exp(-\beta|x|) \operatorname{Re}[1 + \exp(i\omega t)]$$

The Temperature Distribution in the near Surface Fluid is again found by solving the Coupled Thermal Diffusion Equations for the System in one dimension using Boundary Conditions of Temperature and Heat Flux Continuity at each Interface.

$$T_f(x,t)_{\text{Total}} = \operatorname{Re}[T_f(x,t)] + T_0$$

Where T_0 is the Ambient Temperature of the Fluid and $\operatorname{Re}[T_f(x,t)]$ is the solution to the Thermal Diffusion Equations which contains both a Periodic, $T_{AC}(x,t)$, and Steady State, $T_{DC}(x)$, Component. It is these Departures from the Ambient Temperature that Cause the Deflection of the Laser Beam through the Refractive Index Gradients they Produce.

The Total Deflection, θ , will have a periodic, $\theta_{AC}(x)$, and a Steady State, $\theta_{DC}(x)$, Component.

The Two Temperature Profiles have the form:

$$T_{DC}(x) = \frac{-I_0 \beta \eta}{2K_s \beta^2} \left[\frac{(1 - \exp\{-\beta L_1\})(1 - F_{sb} \beta L_2) - \beta L_1'}{1 + F_{ff} \beta L_1 + F_{fb} \beta L_2} \right] \exp(-6x)$$

and

$$T_{AC}(x, t) = \frac{I_0 \beta \eta}{2K_s (\beta^2 - \sigma_s^2)} \left[\frac{(r-1)(b+1) \exp(\sigma_s L_1) - (r+1)(b-1) \exp(-\sigma_s L_1) + 2(b-r) \exp(-\beta L_1')}{(f+1)(b+1) \exp(\sigma_s L_1) - (f-1)(b-1) \exp(-\sigma_s L_1)} \right] \times \exp(-\sigma_f x + i\omega t)$$

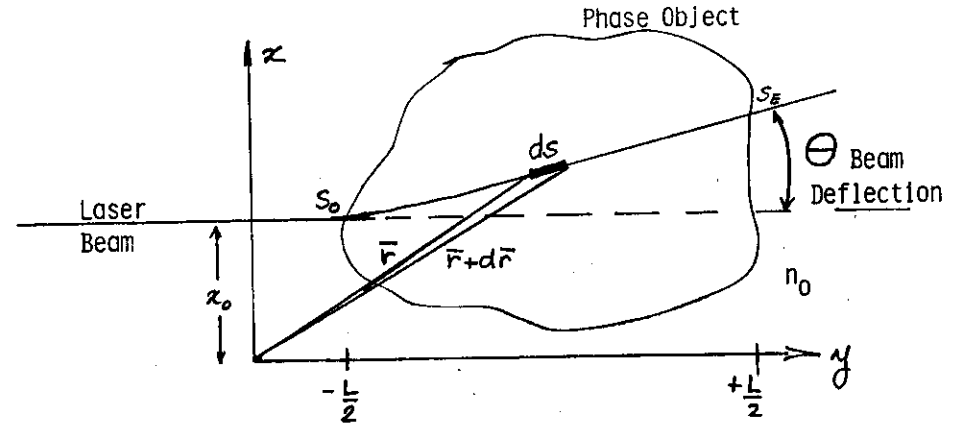
87

Where $F_{1j} = K_1/K_j$ and G is the Reciprocal of the Distance Above the Sample Surface at which the DC Temperature Profile has Decreased to $(1/e)$ of its Surface Value.

The Second Term is just that derived for the Photoacoustic Case and gives rise to the Periodic Laser Beam Deflection that is used for Spectroscopy.

66

When a Laser Beam Passes through a Phase Object the Beam Trajectory has the form shown below and may be described by a Ray Propagation Equation



$$\frac{d}{ds} \left[n(\vec{r}, t) \frac{d\vec{r}}{ds} \right] = \nabla n(\vec{r}, t)$$

s = distance along the ray measured from s_0

\vec{r} = vector position of the point s .

In the Paraxial Ray Approximation for small changes in Refractive Index from its ambient value, n_0 , and with $n(\vec{r}, t)$ a Function of x only the equation becomes:

$$n_0 = \frac{\partial^2 x}{\partial y^2} = \frac{\partial}{\partial x} n(x, t)$$

The Beam Deflection is obtained by Integrating this expression over the limits of the Phase Object: $-(L/2) \leq y \leq (L/2)$.

$$\theta(x_0, t) = -\left(\frac{dn}{dT}\right) \frac{L}{n_0} \left[\left. \frac{\partial}{\partial x} \left\{ T_{AC}(x, t) + T_{DC}(x) \right\} \right| \right]_{x=x_0}$$

The AC and DC Components of the Total Deflection obtained from this expression are:

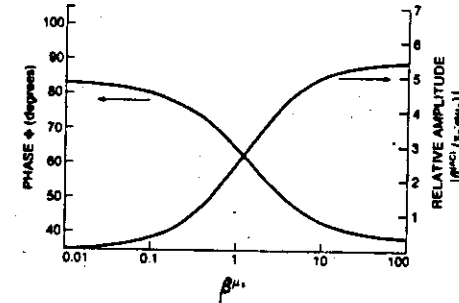
$$\theta_{DC}(x_0) = \left\{ \frac{-LGI_0}{2K_S \beta n_0} \left(\frac{dn}{dT} \right) \right\} \left[\frac{\beta L_1 - (1 - \exp(-\beta L_1)) (1 - F_{SB} \beta L_2)}{1 + F_{fS} \beta L_1 + F_{fD} \beta L_2} \right] \exp(-\alpha x_0)$$

and

$$\theta_{AC}(x_0, t) = \left\{ \frac{-LI_0 \beta}{2K_S n_0} \left(\frac{dn}{dT} \right) \right\} \operatorname{Re} \left\{ \left[\frac{\sigma_f}{(\beta^2 + \sigma^2)} \right] \left[\frac{(r-1)}{(f+1)} \right] \exp(-\sigma_f x_0 + i\omega t) \right\}$$

The form of $\theta_{AC}(x_0, t)$ indicates that the Mirage Signal has both a Magnitude and a Phase with respect to the Modulated Light.

In the Thermally Thick, Optically Thick Limit for the Sample and with the Fluid Thickness also Greater than $2\pi\mu_f$ the AC Component of the Deflection Signal for a fixed x_0 and ω behaves in a manner similar to the Photoacoustic Response Discussed Previously.



Comparison between TPDS amplitude and phase as functions of the product $(\beta\mu_s)$ in the thermally thick limit ($\nu = 50$ Hz, $x_0 = 5 \times 10^{-2}$ cm).

In this Limit the Signal Amplitude is:

$$\left| \theta_{AC}(x_0, \beta\mu_s) \right| = -\frac{LI_0}{n_0 K_S} \left(\frac{dn}{dT} \right) \left(\frac{\alpha_s}{\alpha_f} \right)^{1/2} \left[\frac{\frac{1}{2}(\beta\mu_s)^2 - (\beta\mu_s) + 1}{(\beta\mu_s)^2 + 4/(\beta\mu_s)^2} \right]^{1/2} \exp(-\alpha_f x_0)$$

and the Variable Component of the Phase is:

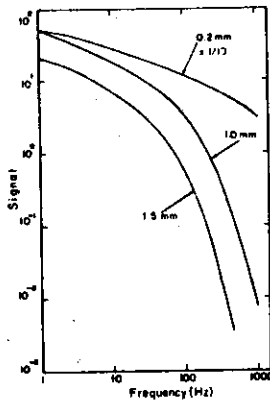
$$\psi(x_0, \beta\mu_s) \simeq \alpha_f x_0 - \tan^{-1} \left[\frac{2}{(\beta\mu_s)^2} \right] - \tan^{-1} \left[\frac{\beta\mu_s}{2 - \beta\mu_s} \right]$$

In the Thermally Thick Optically Opaque Limit $\beta\mu_s \gg 1$
and the Amplitude and Phase Become

$$\psi(x_0, \beta\mu_s) \approx \frac{x_0}{\mu_f} - \tan^{-1} \left[\frac{2}{(\beta\mu_s)^2} \right]$$

$$\theta_{AC}(x, \beta\mu_s) \approx \frac{LI_0}{2n_0K_s} \left(\frac{\alpha_s}{\alpha_f} \right)^{1/2} \left(\frac{dn}{dT} \right) \left(\frac{1}{2} - \frac{1}{\beta\mu_s} \right)^{1/2} \exp\left(-\frac{x_0}{\mu_f}\right)$$

In the Limit of Photothermal Deflection Saturation the
Frequency Dependence of the Deflection Signal Arises from
the $\exp(-x_0/\mu_f)$ Term and the Signal Decreases Exponentially
with the Square Root of the Modulation Frequency.



Curves shown are
for Different Values
of x_0 .

$$L = 140 \mu$$

CONCENTRATION GRADIENT EFFECTS

The Preceding Discussion of Mirage Effect Spectroscopy has
assumed that the Refractive Index Gradient causing the Beam
Deflection arises from a Temperature Gradient.

The Expression for the Deflection in terms of the Refractive
Index Gradient has the form:

$$\theta = A \int_{y=y_0}^{y_1} \left(\frac{dn}{dx} \right) dy \quad \text{For Paraxial Rays}$$

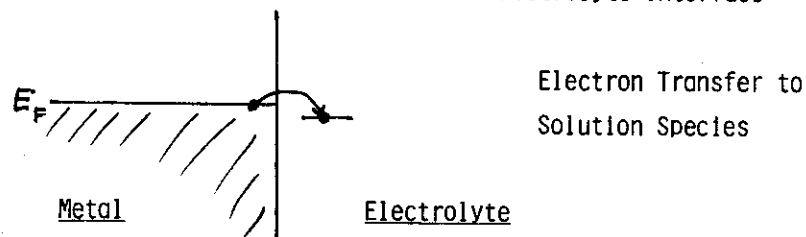
A Refractive Index Gradient can also be produced by a
Concentration Gradient in the Near Surface Fluid so that

$$\left(\frac{dn}{dx} \right) = \left(\frac{dn}{dc} \right) \left(\frac{dc}{dx} \right)$$

$\left(\frac{dc}{dx} \right)$ may be Time Dependent as a Result of Photochemical
Reactions in the Aoid and so $\theta = \theta(t)$. This Signal may
therefore be used to Probe $C(x,t)$.

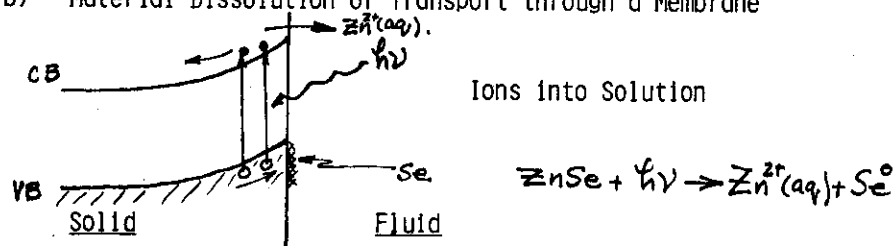
The Time Dependence of θ has a simple form when $C(x,t)$ is Controlled by Diffusion Processes in the Fluid. Two Examples of Experimental Situations where this may occur are illustrated below.

a) Charge Exchange at an Electrode-Electrolyte Interface



Electron exchange between the electrode and ionic species in the electrolyte may be caused by the application of an electric field. The process creates a new species at the surface which will diffuse into the bulk electrolyte, and

b) Material Dissolution or Transport through a Membrane

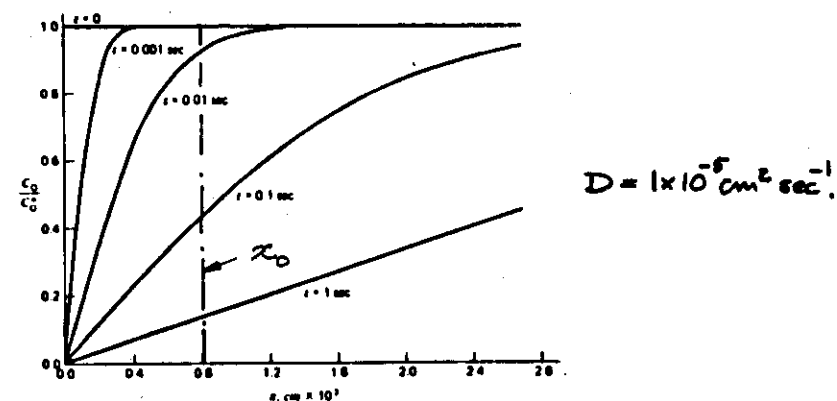


Photocorrosion of Semiconductors is an example of this type of Reaction.

When the Process Generating New Species for the Fluid is Such that the Surface Concentration can be maintained Constant and the Transport Process is Diffusion Limited then the Concentration Profile has the Simple form shown below

$$C(x,t) = C_s(1 - \text{erf}\{x/\sqrt{4Dt}\})$$

C_s = Surface Concentration, D = Diffusion Coefficient



The Laser Probe Beam is in a Fixed Location x_0 above the Surface and the Local Concentration Gradient is Time Dependent as Illustrated in the Diagram.

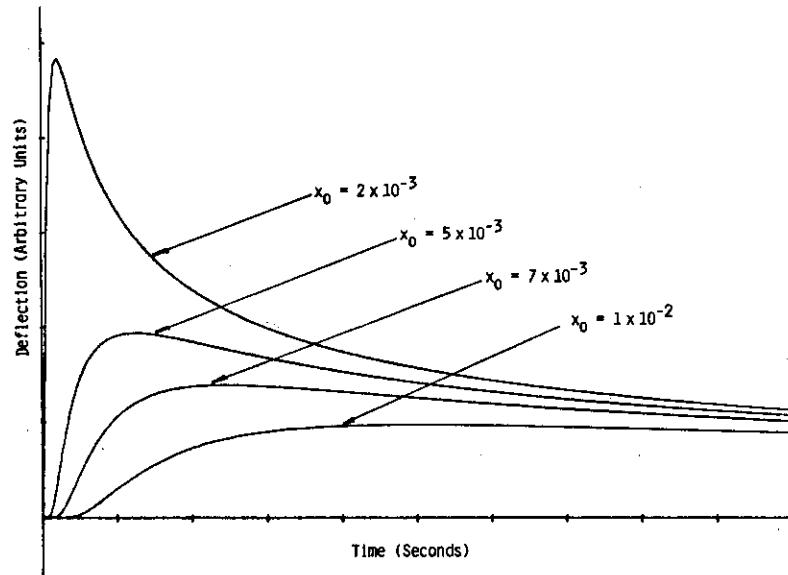
$$\theta(t, x_0) = \frac{d}{dt} \left[C_s(1 - \text{erf}\{x/\sqrt{4Dt}\}) \right]_{x=x_0}$$

$$\theta(t, x_0) = \frac{d}{dt} \left[c_s (1 - \operatorname{erf} \{x / \sqrt{4Dt}\}) \right]_{x=x_0}$$

$$= \frac{d}{dt} \left[\int_0^{x/\sqrt{4Dt}} \frac{2}{\sqrt{\pi}} \exp(-x^2/4Dt) \frac{dx}{\sqrt{4Dt}} \right]_{x=x_0}$$

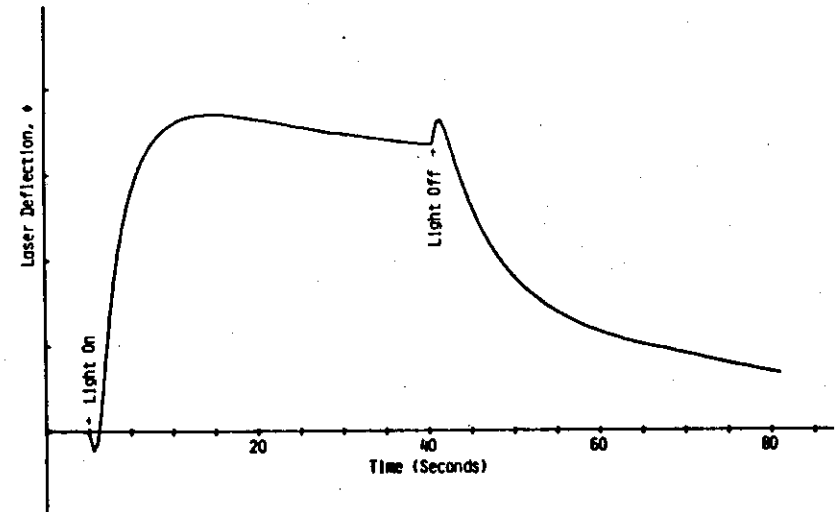
$$\theta(t, x_0) = \frac{B}{\sqrt{\pi Dt}} \exp\left(-\frac{x^2}{4Dt}\right)$$

The Diagram Below shows the Time Dependence of θ for Various Values of x_0 for the case $\{B/\sqrt{\pi Dt}\} = 1 \times 10^{-1}$ and $D = 1 \times 10^{-5}$.



The Times Associated with Processes of this Type are Long (~ 100 secs) and it is essentially "DC" compared to the Spectroscopic Modulation Period (~ 0.01 secs). The Two Effects are therefore easily Separable.

The Thermal Diffusion Process that gave rise to θ_{DC} discussed with respect to Spectroscopy has a Time Constant that is similar to this Matter Diffusion Process. The Combined effects of Thermal and Matter Diffusion are shown below for a Photodecomposition reaction in ZnSe.



$\left(\frac{dn}{dc}\right)$ and $\left(\frac{dn}{dT}\right)$ have Opposite Signs.

EXPERIMENTAL METHODS IN PHOTOACOUSTIC SPECTROSCOPY

- 1) Considerations in the Choice of Components
- 2) Design of a Practical Gas-Microphone Photoacoustic Cell
- 3) Dispersive Spectrometers
- 4) Fourier Transform Spectrometers
 - a) Continuous Scan
 - b) Step and Integrate
- 5) Mirage Effect Detectors
- 6) Discussion

CONSIDERATION IN THE CHOICE OF COMPONENTS

Photoacoustic Spectroscopy is Normally a Detector Noise Limited Technique. It is therefore important to obtain the Largest Signal possible from the Photoacoustic Cell, to Minimize Preamplifier Electrical Noise and to Minimize External Acoustic Noise Reaching the Cell.

To do this:

- 1) Maximize the Light Reaching the Sample Since the Signal Scales as $I_0(\lambda)$.
- 2) Reduce Scattered Light and Absorption by Other Components of the Cell.
- 3) Minimize the Cell Volume since for a given Energy Input the Signal is proportional to $(1/V)$.
- 4) Use a Microphone with a High Sensitivity. A Value of about 50 mV/Pa is desirable.
- 5) Keep the Distance Between the Microphone and the Preamplifier to a Minimum. Electrically and Acoustically shield both components
- 6) Filter and Stabilize Power Supply Voltages to the Microphone and Pre-Amplifier. Avoid Ground Loops in the Signal Path.
- 7) Make the Cell Walls thick to act as good Acoustic Shields and Support the Cell-Preamplifier System on Acoustically Isolating Platforms.

LIGHT SOURCES - INCOHERENT

These are necessary for a wide spectral range capability.

<u>Spectral Range</u>	<u>Light Source</u>
UV → Visible 200 nm → 800 nm	Xenon Arc Source 150 W → 500 W [10 mW/mm ² -sr-nm]
Near Infrared 800 nm → 5 μm	Quartz Halogen Tungsten Filament [1 mW/mm ² -sr-nm]
Far Infrared 2.5 μm → 25 μm	Globar Nernst Glower

The Collection Optics for the Light Source Should Match the Requirements of the Monochrometer or Interferometer.

Higher Wattage Lamps are not always an Advantage since the Source Size may Increase. The Collection Optics may be unable to Send the Extra Radiation into the Dispersion Element.

Source Stability is important since the PAS Signal will Fluctuate with the Output of the Source. Feedback Control of the Lamp Power Supply is an Advantage for Precision Measurements.

COHERENT LIGHT SOURCES

Limited Spectral Range but High Brightness. Continuous or Pulsed. High Spectral Resolution

UV → Visible	Dye Lasers Particular Laser Lines
Infra Red	CO, CO ₂ Laser Lines Raman Shifted Dye Laser Color Center Lasers Diode Lasers

Because of the Collimated Nature of the Laser Output and its Narrow Spectral Range the Spectral Radiance is Higher than that of an Incoherent Source. (Rosencwaig: 20 mW dye laser, Spectral radiance up to 10¹⁰ mW/mm²-sr-nm.)

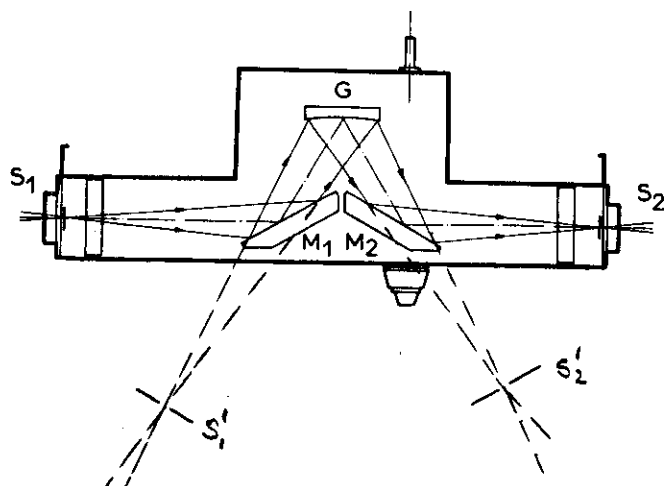
Tuning Range is normally Narrow so these Sources Need to Match a Particular Absorption Feature of Interest.

WAVELENGTH SELECTION SYSTEMS

Grating Monochrometers

Holographic Gratings have the Advantage of a Wide Spectral Range, Low Scattered Light and Focussing Capability. A Typical Optical Configuration is shown below for a Jobin-Yvon H2O Monochromator

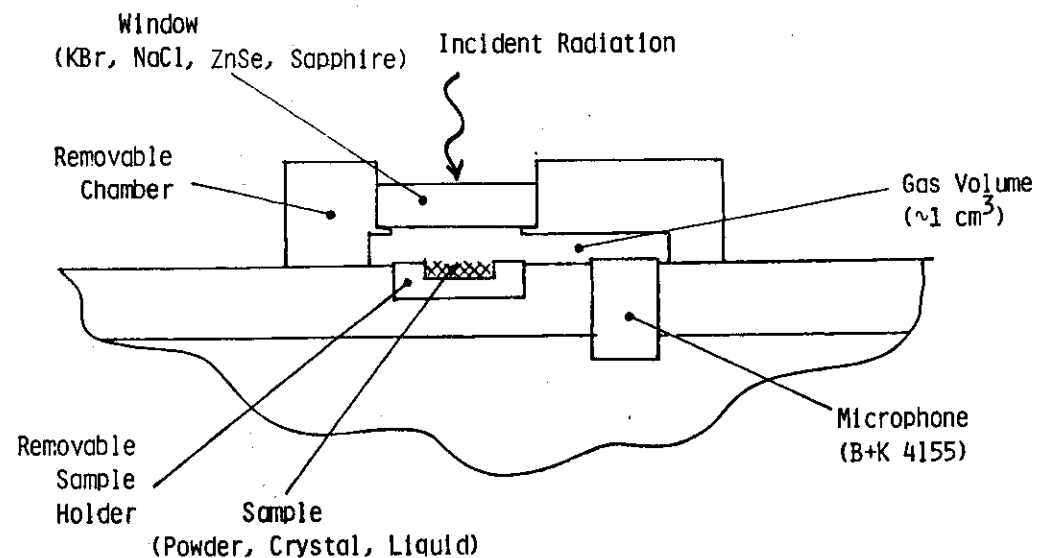
200 → 800 nm F4.2 40 x 45 mm Concave Grating



A Three Grating Version (HT20) is Available and was Developed for PAS. In this the Mirrors M_1 and M_2 are Absent and the Optical Configuration S_1^1 , S_2^1 is used. 200 → 3200 nm. F4.2 Three 40 x 45 mm Concave Gratings. Dispersion ~ 2 nm/mm.

DESIGN OF A PHOTOACOUSTIC CELL

The General Configuration of a Cell with a Resonant Frequency above 1 kHz is Shown Below. This has been used with Visible and FTIR Optical Sources.



The Cell is Fabricated from Aluminum and Stainless Steel and all Internal Surfaces are Polished Metal to Minimize Stray Light Absorption.

The Sample Holder is Polished Stainless Steel of about 2.5 cm dia. with a 1 cm dia. sample well about 1 mm deep. The Window Diameter is also 2.5 cm dia. and Scattered Light from the Sample Tends to Exit from the Cell through the Window.

The Cel' Windows are Chosen for the Wavelength Range to be Studied.

<u>Window Material</u>	<u>Approximate Spectral Range</u>	<u>Comments</u>
Sapphire	200 nm \rightarrow 6 μ m	Good General Window
KBr, NaCl	200 nm \rightarrow 25 μ m	Hygroscopic. Good for IR.
ZnSe	600 nm \rightarrow 25 μ m	Good General IR Window.

Sapphire is a Good Window for the UV \rightarrow IR Range and is Durable. KBr is used to get FTIR Data in the 25 μ m Region but is Easily Damaged by Water. ZnSe is a Durable Window for the IR Region.

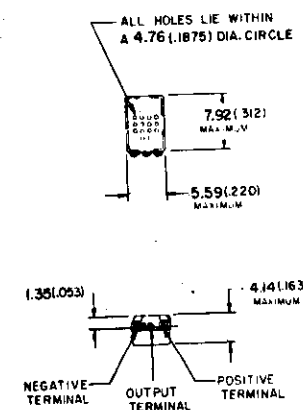
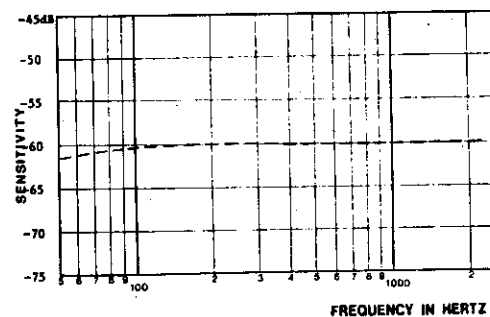
All these Materials can be Obtained in the 2.5 cm dia. size and about 4 mm thickness from Infrared Spectroscopic Supply Houses.

In Some Cell Designs Double Windows Separated by an Air Space are used to Reduce Acoustic Transmission into the Cell.

The Microphone is in the Same Compartment as the Sample. The Model used is Manufactured by Bruel and Kjaer and has a Sensitivity of 50 mv/Pa. The Frequency Response is Flat Between 4.0 Hz and 16 kHz \pm 2 dB. The Microphone is Self Polarized and about 1.3 cm diameter.

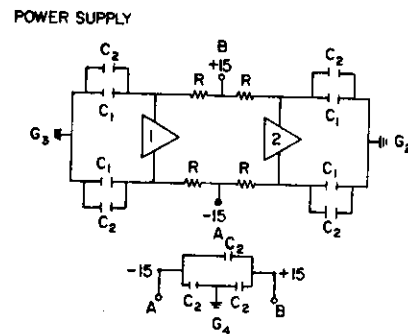
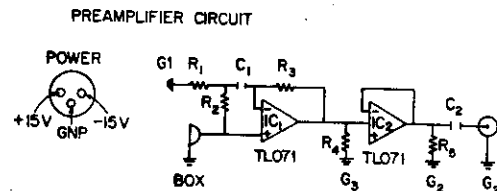
An Alternate Microphone of Higher Sensitivity is the B+K 4179. This has a Diameter of 2.5 cm and a Sensitivity of 100 mV/Pa. This Microphone is specially developed for low signal strengths and may be used with a B+K Type 2660 Preamplifier for Maximum Signal to Noise Ratio.

Knowles (or other) Electret Hearing Aid Microphones may also be used. These microphones are compact and easily fit in the PAS Cell.



KNOWLES 1685 WITH 2.6 V BIAS: 4 mV/PA AT 100 Hz.

The Preamplifier is Closely Coupled to the Microphone with Short Leads so as to Reduce Mechanical and Electrical Noise. A Circuit with reasonable performance used with the B+K 4155 Microphone is shown below. Components should be selected for Low Noise if possible.



Component Values

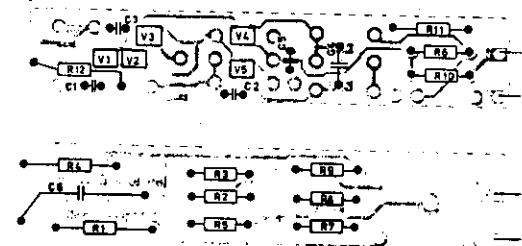
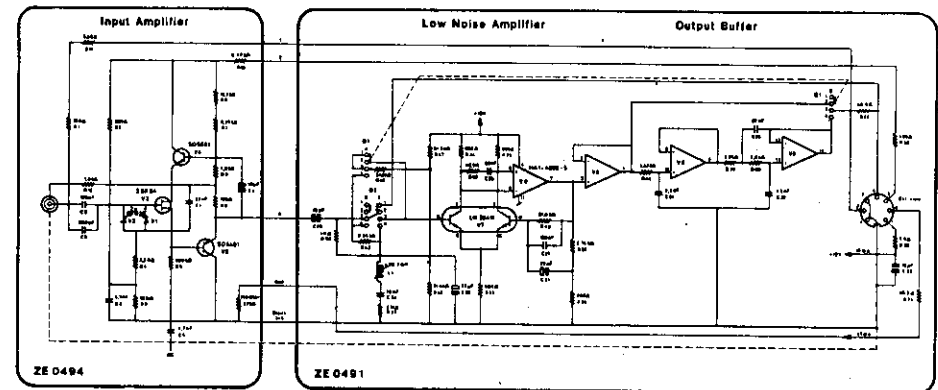
a) Preamplifier

$R1 = 1 \text{ M}\Omega$, $R2 = R3 = 10 \text{ M}\Omega$, $R4 = R5 = 100\text{k}\Omega$,
 $C1 = 1 \text{ }\mu\text{F} = C2$. All resistors are carbon or metal film.

b) Power Supply

$R = 120\Omega$, $C1 = 50 \text{ }\mu\text{F}$, $C2 = 0.01 \text{ }\mu\text{F}$.

The Circuit Diagram and Component Layout of a High Quality Commercial Preamplifier (B&K 2660) are shown below. This yields a Signal to Noise Ratio about a Factor of 5 \rightarrow 10 Better than the Previous Design. This Improvement can reduce data taking time by a Factor of 25 \rightarrow 100.

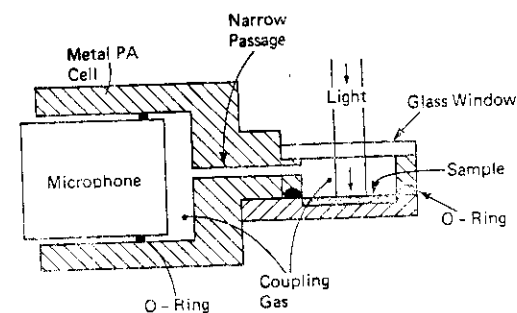


ZE 0494 Input Circuit

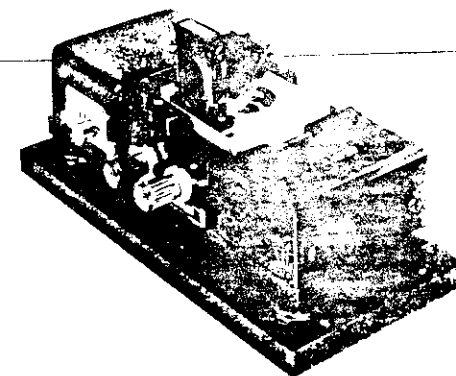
Close Coupling of the Input Circuit to the Microphone is Essential for a High Signal to Noise Ratio. High Quality Selected Components are Used.



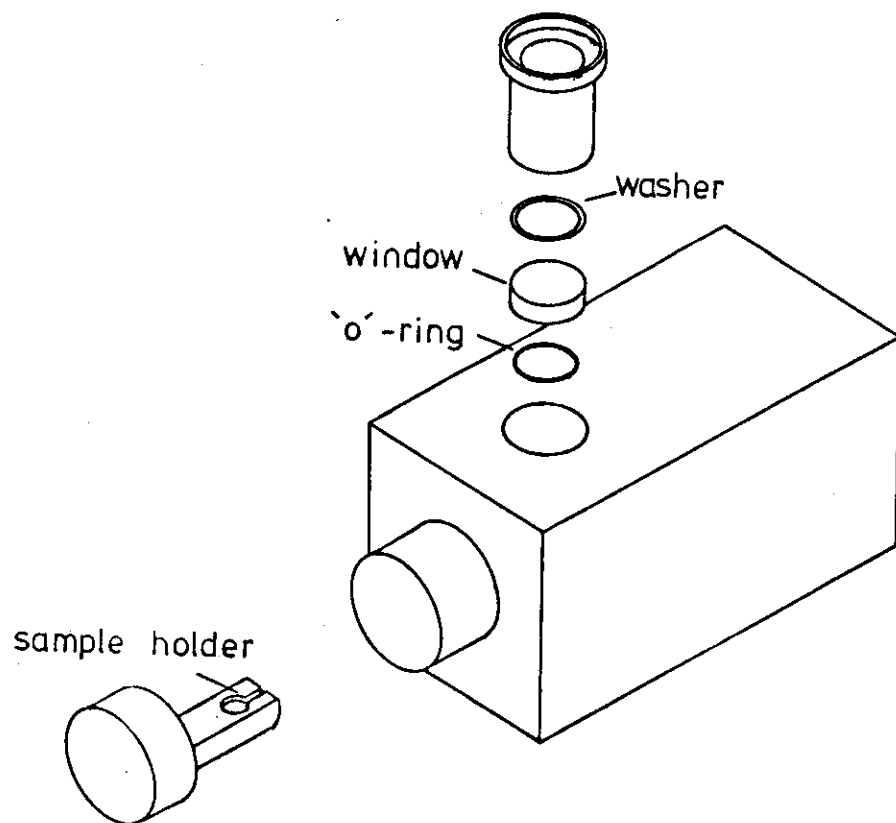
An Alternate Cell Configuration that can couple well to a Cylindrical Microphone and Preamplifier is sketched below. The Coupling Gas Volume should be kept to a Minimum and the connecting tube should have as Large a diameter as possible. Light should not hit the Microphone. The Preamplifier should be directly behind the Microphone and sealed against external pressure fluctuations.



A Commercial cell suitable for both Single Frequency and FTIR use is shown below. EG+G: PAR 6003 Cell.

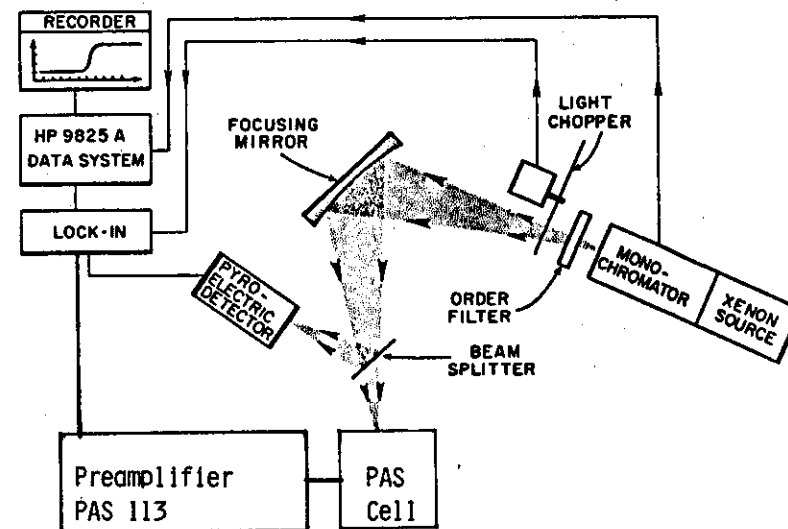


A Diagram of the Commercial EDT401.10 PAS Cell is Shown Below. Again the Microphone is Closely Coupled to the Preamplifier. The Sample Cell Volume is Small with 'O' rings providing Acoustic Isolation.



DISPERSIVE SPECTROMETERS

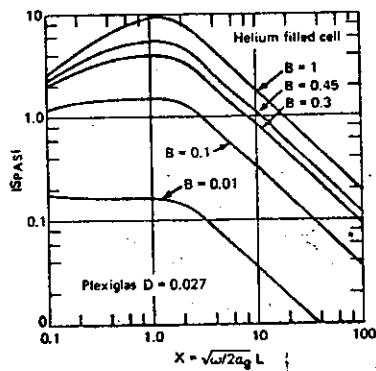
The Optical and Electronic Configuration of a Typical Gas Microphone PAS Cell Spectrometer is shown below.



The Optical System is put together on an Optical Breadboard for Ease of Adjustment of the Components. To Reduce Vibrations Transmitted to the System the Breadboard is Supported on Antivibration Mounts. The Photoacoustic cell is Isolated from it with Antivibration Mounts. The Light Chopper is also Antivibration mounted and separated from the Cell to reduce Acoustic Transmission through the Air. The Pyroelectric Detector is used to Monitor Variations in $I_0(\lambda)$.

The Light Chopper can Produce Radiation with an Amplitude Modulation Frequency in the Range 20 Hz \rightarrow 1 kHz. Choice of the Actual Frequency is made on a Signal/Noise Basis.

Because the Thermal Diffusion Length of the Solid and the Gas are Frequency Dependent Amplitude and Phase Contributions from the Backing and the Window may Arise at Low Modulation Frequencies.



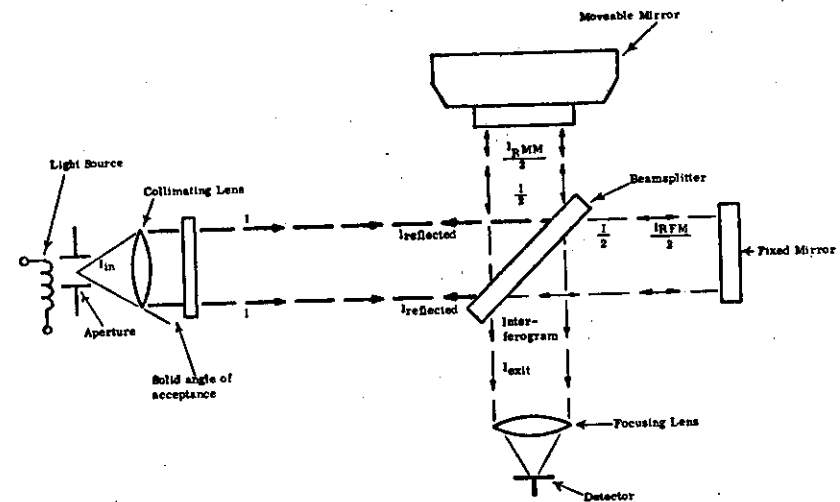
Room Noise has a $(1/f)$ Amplitude Behavior and Damping of Low Frequency Vibrations is More Difficult.

Modulation Frequencies Between 70 Hz and 200 Hz are often a Good Choice.

Lock in Detection Provides a High Rejection of Frequencies that are not at the Signal Modulation Frequency.

FOURIER TRANSFORM SPECTROMETERS

The Optical Layout of a Fourier Transform Spectrometer is Illustrated below. The Movable Mirror can be driven at speeds from 0.02 cm sec^{-1} to about 0.2 cm sec^{-1} for PAS Data Collection. When used for Photoacoustic Measurements the Gas-Microphone Cell is Placed at the Focus of the Exit Mirror.



Light of a Given Wavenumber is Modulated by Interference of the Beams that Take the Two Paths in the Michelson Interferometer. The Modulation Occurs at an Acoustic Frequency that Depends Upon the Mirror Velocity.



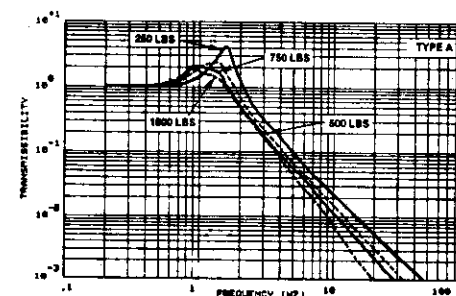
For Typical FTIR-PAS Spectroscopy the Wavenumber Range Studied is 400 cm^{-1} to 4000 cm^{-1} ($25\mu\text{m}$ to $2.5\mu\text{m}$) with a Mirror Velocity of $V\text{ cm sec}^{-1}$ the Acoustic Modulation Frequency is $f = 2 V\nu$ at the Wavenumber ν .

For the Above Wavenumber Range the Acoustic Modulation Frequencies with a Mirror Velocity of 0.02 cm sec^{-1} lie Between 16 Hz and 160 Hz.

These relatively Low Frequencies are an Advantage for PAS Since the Signal Magnitude has a Reciprocal Dependence on the Modulation Frequency.

Building Noise also has a High Amplitude in this Range. The Spectrometer and Cell must therefore be well isolated in order to obtain an acceptable Signal to Noise Ratio. A Satisfactory Method is to Support the Interferometer on an Isolated Table and to Further Isolate the PAS Cell within the Spectrometer using suitable Antivibration Mounts.

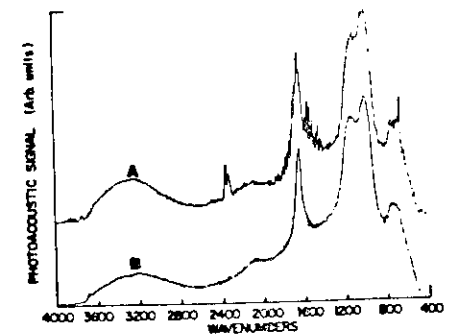
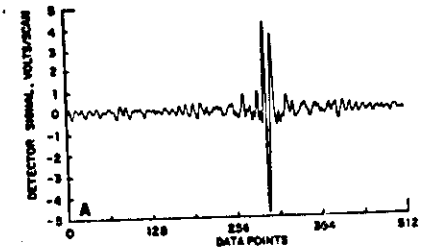
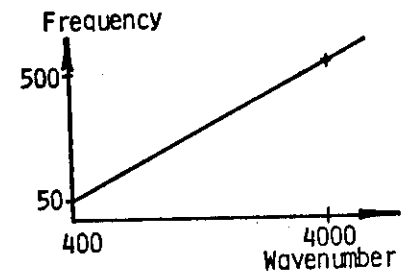
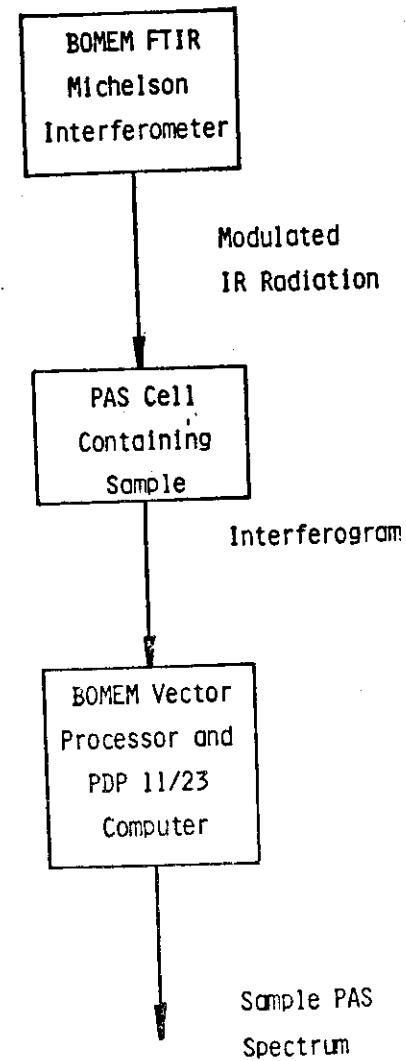
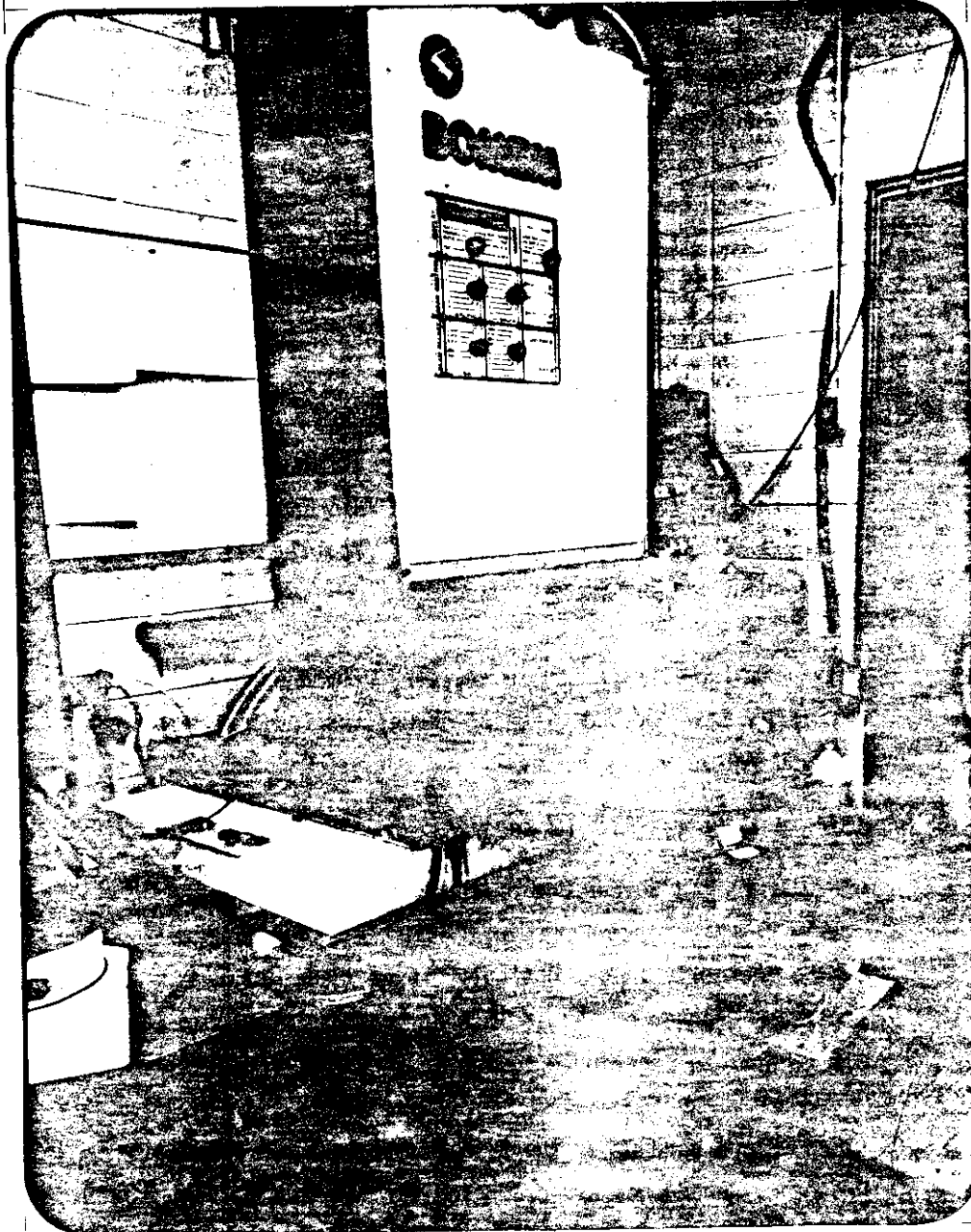
To Isolate the Interferometer at Low Frequencies some form of Air Suspension is desirable. Laser Table Legs are good in this Application and have a Transmission Behavior of the form shown below.



Above 10 Hz the Building Noise is Attenuated by Two to Three Orders of Magnitude by this Method.

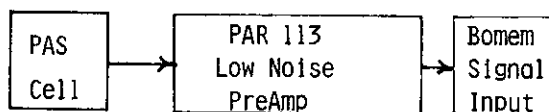
The Photoacoustic Cell can be Mounted in the Interferometer Cell Compartment on Small Air Balloons or Soft Rubber Isolation Mounts. These Support a Heavy Well Damped Table on which the Cell is placed.

Noise Transmission reduction can greatly reduce Data Acquisition Time. Noise Reduction by Signal Averaging n Interferograms only improves the Signal to Noise Ratio by \sqrt{n} . A Direct Noise Reduction by a Factor of 10 is Equivalent to Increasing the Number of Scans by Two Orders of Magnitude.



The Signal Path Shown Above should be Free of Ground Loops to Minimize Electrical Noise in the Signal to the FTIR.

Some Variable Amplification is desirable so that the Analog to Digital Converter in the FTIR can be used Properly (i.e. ~75% of Max. Range). This Reduces the Digital Noise in the Signal.



The PAR 113 Low Noise Preamplifier Permits the Signal Band Width to be Controlled. This is Adjusted so that the High Pass Filter is at Approximately 0.5xLowest Modulation Frequency and the Low Pass Filter at 2.0xHighest Modulation Frequency. The Gain Range of this Amplifier is between 10 and 10,000. For Typical Samples gains in the Range 200 to 2,000 are Needed with the Cell Having an Electronic Gain of about 40.

The Modulation Frequency Range Associated with the Spectral Bandwidth Studied in an FTIR also has an Effect on the PAS Signal.

At any Given Wavenumber the Number of Photons Arriving at the Sample, $I_0(\lambda)$, Depends upon the Exposure Time per Period and is Therefore Inversely Dependent on the Mirror Velocity.

At a given Mirror Velocity the Modulation Frequency varies Inversely with the Wave Number BUT the Photon Energy Varies Directly with the Wave Number. The Energy Deposited in the Sample if these Photons are Completely Absorbed is Therefore Independent of Wave Number.

The Thermal Diffusion Length μ_s does Depend upon the Modulation Frequency and Hence Varies Across the Spectral Range at a Given Velocity.

$$\mu_s = \sqrt{2\alpha/\omega} \quad ; \quad \omega \propto 1/\nu \quad ; \quad \mu_s \propto \sqrt{2\alpha\nu}$$

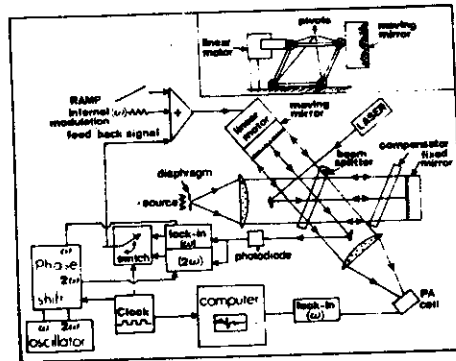
where ν is the Wavenumber of the Radiation.

In the Thermally Thick, Optically Thick limit the PAS Amplitude Depends on $\beta\mu_s$. This Wavenumber Dependence of μ_s will Therefore Contribute to the Measured Peak Height.

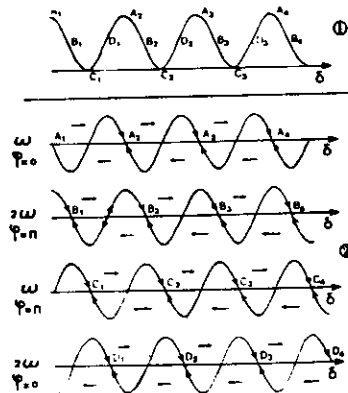
At any Given Wavenumber the Signal will have the Modulation Frequency Dependence expected from the PAS Theory. The Signal will therefore vary inversely with Mirror Velocity. Low Velocities are therefore an Advantage.

STEP AND INTEGRATE FOURIER TRANSFORM METHODS

An Alternate Approach to Fourier Transform Spectroscopy is to construct the interferogram step by step. The Moving Mirror is displaced to some Path Difference, the Radiation through the Interferometer is modulated and lock-in detection methods are applied to recover the signal. An Experimental Apparatus of this type developed by Debarre et al is shown below. Similar equipment was also developed by Farrow et al.



Laser Fringes from a Coaxial He/Ne Reference Laser are used to Measure and Control the Moving Mirror position. A sinusoidal motion is added to this Mirror to Provide Modulation of the Incident Light at a Measuring Frequency ω .



This Method for Fourier Transform Spectroscopy has the Following Advantages:

- Spectral Range between 360 nm and $3\mu\text{m}$.
- High Light Throughput due to Large Input Aperture; 0.6 W; High PAS Signal.
- Single Modulation Frequency so no wave number dependence of μ_s .
- Internal Modulation of the Optical Path Difference avoids Noise due to a Mechanical Chopper.
- This mode of Modulation Produces an Interferogram that looks like the derivative of the DC Interferogram and therefore has a Zero Mean Value. This makes it less Sensitive to Long Term Lamp Power Fluctuations.
- Spectral Resolution on the Order of 1 cm^{-1} can be obtained.
- Both the Amplitude and the Phase of the PAS Signal may be obtained.
- Rapid Production of Spectral Data with a PC Type Computer doing the Data Reduction.

Because of the High Light Throughput of the Spectrometer care must be taken with the Radiation Incident on the Samples. This could Damage Biological Materials.

Heating of the Sample near the Zero Path Difference setting of the Mirrors causes a DC Component of the Signal that has a Finite Relaxation Time. This may limit the rate at which data may be taken in this region.

Photochemical Reactions that are sensitive to the DC Light Intensity (e.g. photosynthesis) will contribute to the Signal.

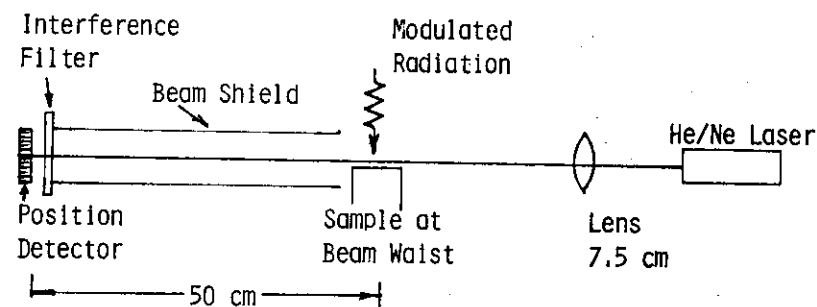
The Analog to Digital Converter used to input the data to the Computer may introduce a Digital Quantization Error and Limit the Dynamic Range that can be Recorded.

Computation Time and Precision of the Fast Fourier Transform by the Small Computer may also restrict the Dynamic Range and Spectral Resolution.

MIRAGE EFFECT DETECTORS

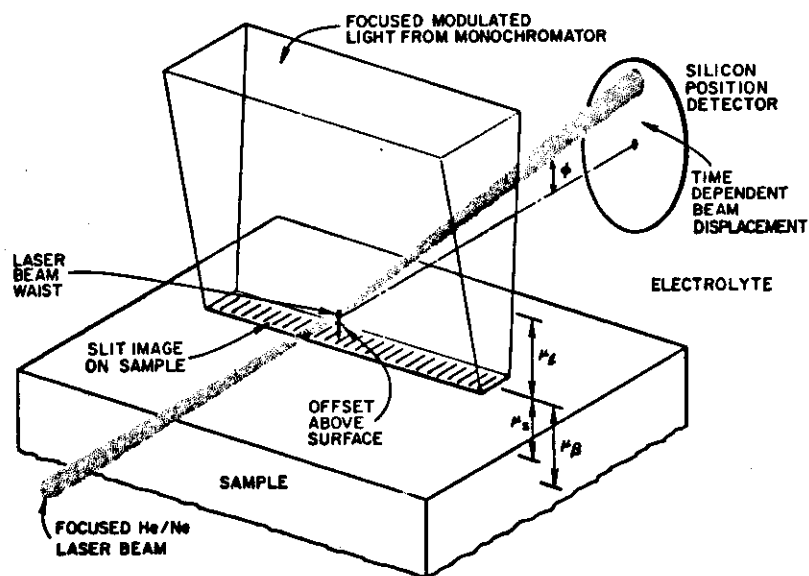
A Mirage Effect Detector may be used with either a Dispersive or Interferometric Spectrometer. Over the Visible Spectral Range the Transducer Fluid may be Water, Carbon Tetrachloride, Methanol or a Gas such as Nitrogen or Air. In the Infrared Spectral Region a Gas will provide the widest Absorption Free Range. Dry Nitrogen is a Good Choice. For Limited Ranges Liquids can be found that have Transmission Windows.

The Optical Configuration Employed for a Mirage Effect Detector is Illustrated below.



The Sample must be Positioned so that the Beam Waist of the Probe Laser Passes within about a Thermal Diffusion Length Above the Surface for air at 100 Hz. $\mu_f = 2.5 \times 10^{-2} \text{ cm} = 250 \text{ } \mu\text{m}$ for Water at 100 Hz. $\mu_f = 2.1 \times 10^{-3} \text{ cm} = 21 \text{ } \mu\text{m}$.

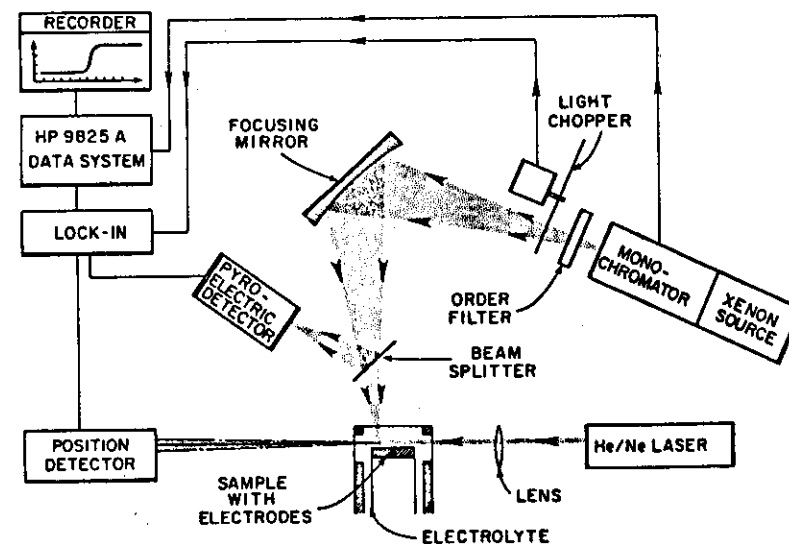
The Beam Waist Diameter for a 1 mm Beam Diameter from the Laser is about $40\text{ }\mu\text{m}$. The Beam samples a Large Fraction of μ_s for most Systems. The Sample Should have Translation and Rotation Capabilities with this Degree of Precision of Motion.



The Silicon Position Detector should also be Adjustable so that the Beam can be Centered on the Detector once it is Correctly Positioned with Respect to the Sample Surface.

Both the Pointing Stability of the Laser and Beam Deflection due to Air Currents are Important Sources of Noise.

Table Vibrations Causing Relative Motion between the Laser and the Position Detector must also be Avoided. Optical Breadboard Tables are Good in this Respect and a Configuration Similar to that for the Gas-Microphone Cell may be used for Spectroscopy.



This Configuration can also be used to study Concentration Gradient Effects. For Photocorrosion Studies a Steady State Illumination is used to Promote the Reaction and to Ensure Overlap between the Spectroscopic Probe Light and the Photo-Corroded Region the Same Light Source and Monochromator are used.

PHOTOACOUSTIC MEASUREMENT ON BIOLOGICAL SYSTEMS

- 1) Photoacoustic Spectroscopy in the Visible and Infrared Spectral Regions.
- 2) Depth Profile Data
- 3) Photosynthesis -- Photoacoustic Spectroscopy in the Presence of a Photochemical Reaction.

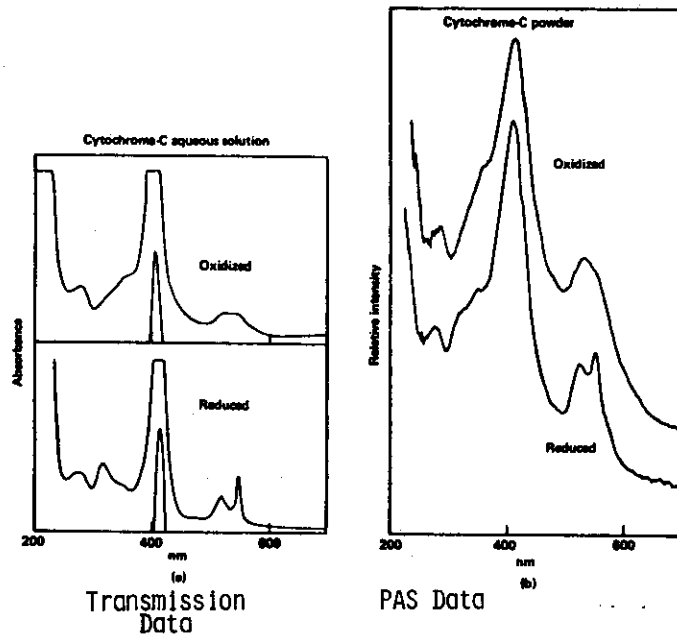
BIOSPECTROSCOPY

- Photoacoustic Spectroscopy has an Advantage of Not Requiring Sample Preparation and being able to Provide Spectral Data on Light Scattering and Optically Thick Samples.
- Quantitative Measurements are Difficult Unless the Sample is Thermally and Optically Homogeneous.
- In the Infrared Spectral Region Gas Phase Impurities (CO_2 and H_2O) provide Strong Signals and may Mask the Response from a Condensed Phase Solid Sample.
- With Special Cell Design in situ Measurements are Possible. As for all PAS Measurements the Signal to Noise Ratio is the Major Problem for in situ Data.

HEMOPROTEINS

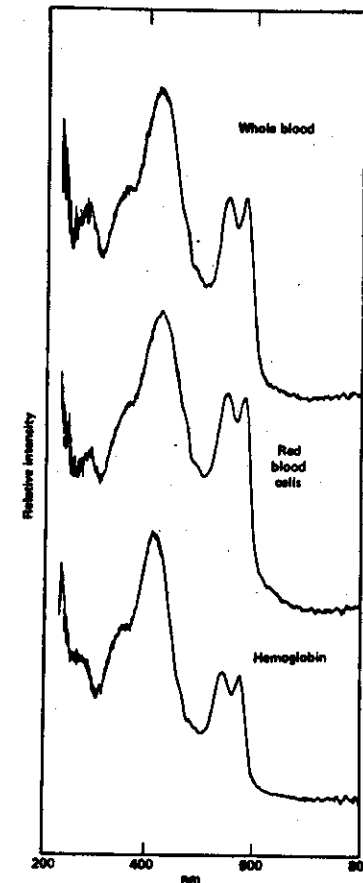
A. Rosencwaig, Science 181 (1973) 657.

Demonstration of the Similarity of Spectra Obtained by PAS and Transmission Methods. PAS Spectra of Cytochrome-C obtained on a Powder Sample in Both its Oxidized and Reduced State. This is Compared to the Transmission Spectrum Obtained from the Material in Aqueous Solution.



Visible Spectral Range. Powdered PAS Sample will give a Stronger Signal than the Same Material in Solution due to the Pressure Term. Light Scattering will Influence the Energy Deposition Profile. Peak Locations are Correct. Peak Height Ratios may be Different.

Oxyhemoglobin also Studied in the Visible Spectral Range in Several Physical Forms. Spectra Exhibit the Same Features in Each Case. Choice of the Form of the Sample can Therefore be Based on the Desired Experiment. Light Scattering is the Main Barrier to Conventional Transmission Spectroscopy.



G. Alter, J. Biological Chem. 258 (1983) 14960: 14966.

- Use of Visible PAS Spectra to Look at Conformation Changes due to Various Adducts and Dehydration. Comparison Between Computed and Measured PAS Spectra.
- Samples: Oxyhemoglobin, Aquomethemoglobin, Cyanide, Azide and Fluoride Methemoglobin in Crystalline, Lyophilized or Solution State. Horse, Bovine or Human Source.
- Spectral Range: 200 nm \rightarrow 700 nm using a Commercial Photoacoustic Spectrometer.

Spectra of $\text{Hb}^{\text{III}}\text{CN}$ and $\text{Hb}^{\text{III}}\text{N}_3$ are Insensitive to the State of the Material. The CN and N_3 Adducts are Strongly Bound and the Spectral Features are Insensitive to Perturbations of the Globin Structure. Computed and Observed Spectra are in Good Agreement.

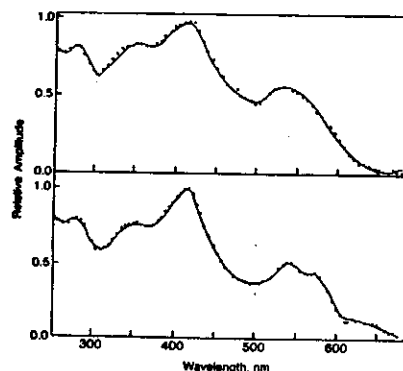


FIG. 2. Predicted (—) and observed (.....) PA spectra of lyophilized $\text{Hb}^{\text{III}}\text{CN}$ (top) and ammonium sulfate-precipitated $\text{Hb}^{\text{III}}\text{N}_3$ (bottom). Preparations were made and spectra predicted as described in the text.

Spectra of $\text{Hb}^{\text{III}}\text{F}$ and $\text{Hb}^{\text{III}}\text{H}_2\text{O}$ show strong Differences Between the Solution Spectra (which yield the predicted PAS Spectra) and the Actual PAS Spectra observed for Lyophilized and Precipitated Samples.

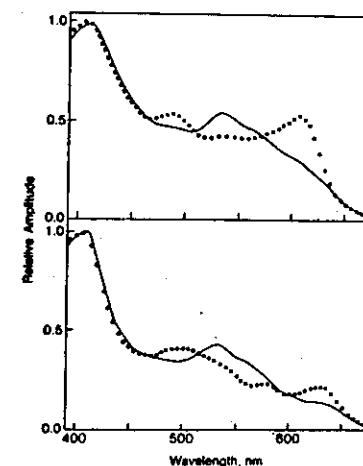


FIG. 4. Predicted (.....) and observed (—) PA spectra of lyophilized $\text{Hb}^{\text{III}}\text{F}$ (top) and ammonium sulfate-precipitated $\text{Hb}^{\text{III}}\text{H}_2\text{O}$ (bottom). Preparations were made, and predicted spectra were calculated as described in the text.

Spectral Shifts Suggest that Imidazol Methemoglobin Contributes to the Solid State Samples Spectra.

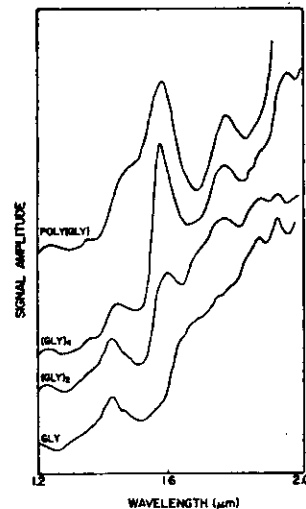
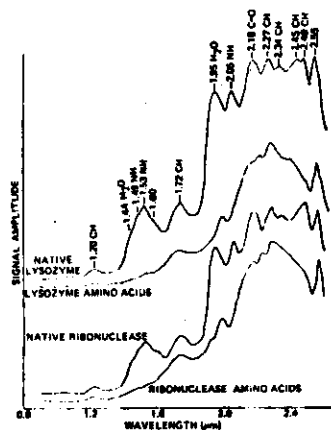
The Processes Causing the Spectral Changes tend to Dehydrate the Protein.

- Direct Removal of H_2O during Lyophilization.
 - Ammonium Sulphate Precipitation Competing with the Protein for Water of Hydration during the Precipitation Reaction.
- Both Mechanisms Perturb the Heme Pocket so that the Distal Histidine can associate with the Heme Ion.

A.J. Sadler et al., Analytical Biochemistry **138** (1984) 44.

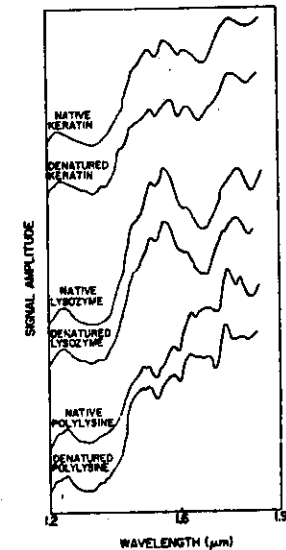
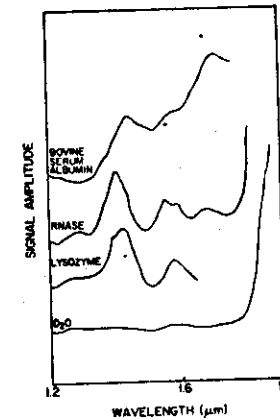
- Use of Near IR PAS to Study Proteins.
- Spectral Range 260 nm \rightarrow 2800 nm.
- Powdered Samples and D₂O Solution Spectra.
- Commercial PAS Spectrometer, EDT OAS-400. Samples Normally Fill the Complete Sample Cup which Request 5 to 50 mg of Protein.
- Lock in Amplifier Detector for PAS Signal.
- Normalization Using a Pyroelectric Detector.
- Modulation Frequency Range 20 \rightarrow 160 Hz.

Spectral Assignments Made for Egg White Lysozyme and Bovine Ribonuclease. Comparison made with Amino Acid Mixtures of Similar Global Composition.



Solid Glycine In Various Polymeric States also Examined.

Solution PAS Spectra were made in D₂O to avoid strong water absorption in this spectral region. Concentrations of About 100 mg/ml are required. Peaks in the Spectra are Tentatively Identified.



Some Samples were Denatured by Dissolving in H₂O, heating to 90°C for 30 min and Lyophilized. Powders so produced were compared to Native Material. Parallel Circular Dichroism Measurements suggest some Renaturation by the drying process. Spectral Locations are Reproducible. Quantitative Data are hard to obtain. Method Good for Protein on Opaque Substrate. Makes Optical Probe in this Spectral Region Relatively Easy.

Fourier Transform Photoacoustic Spectroscopy has been Used to Extend Data on Systems of this type out to Circa 400 cm^{-1} .

Rockley et al., Science 210 (1980) 918, Demonstrated that Spectra could be obtained with Dry Samples of Various Biological Materials Including Bovine Hemin, Hemoglobin and Horseradish Peroxidase.

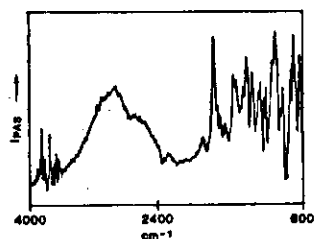


Fig. 2. Spectrum of a 14-mg sample of bovine hemin (grade 1 purity, Sigma Chemical Co.); 800 scans, resolution 8 cm^{-1} .

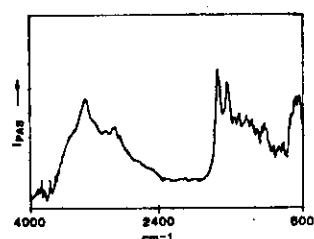


Fig. 3. Spectrum of a 1-mg sample of hemoglobin from beef blood (Sigma Chemical Co.); 800 scans, resolution 8 cm^{-1} .

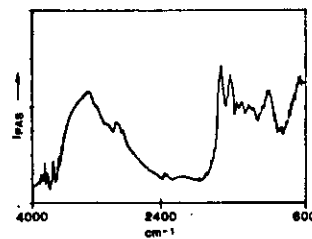


Fig. 4. Spectrum of a 0.5-mg sample of horseradish peroxidase (type VI, Sigma Chemical Co.); 200 scans, resolution 8 cm^{-1} .

These Spectra were taken with a Digilab FTS 20 Spectrometer, 1 cm^3 Cell Volume and a General Radio 1962 Electret Microphone.

Signal Averaging is Achieved by Adding Together Several Interferograms before Fourier Transforming to obtain the Spectrum. This provides a \sqrt{N} noise Reduction.

The Mirror Velocity on the FT20 is High (0.16 cm/sec) and so the Modulation Frequencies are High.

PAS Signal $\propto (\text{Frequency})^{-n}$

V. Renugopalakrishnan and R.S. Bhatnagar

J. Am. Chem. Soc. 106 (1984) 2217, have used FTIR-PAS to Look at the Spectroscopy of Poly(γ -Benzylglutamate). Peak Positions of the Amide Bands are taken to Indicate an α -Helical Conformation for this Material.

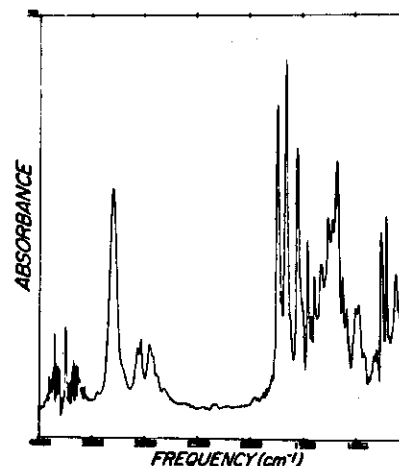


Figure 1. Fourier transform infrared photoacoustic spectrum of poly(γ -benzyl glutamate) per se, M_n 28,000 and degree of polymerization of 130, at room temperature. The spectrum shown represents 512 scans; 0.25 mg of the sample was used to obtain the spectrum.

These Spectra were also taken with a Digilab Spectrometer. Band Positions Agree well with those Obtained from Transmission Data. Gas Phase H_2O is Present in the Cell. This can be Removed by Purging or with a Zeolite Getter in the Sample Cell.

Table 1. Frequency^a of Major Bands of Poly(γ -benzyl glutamate)

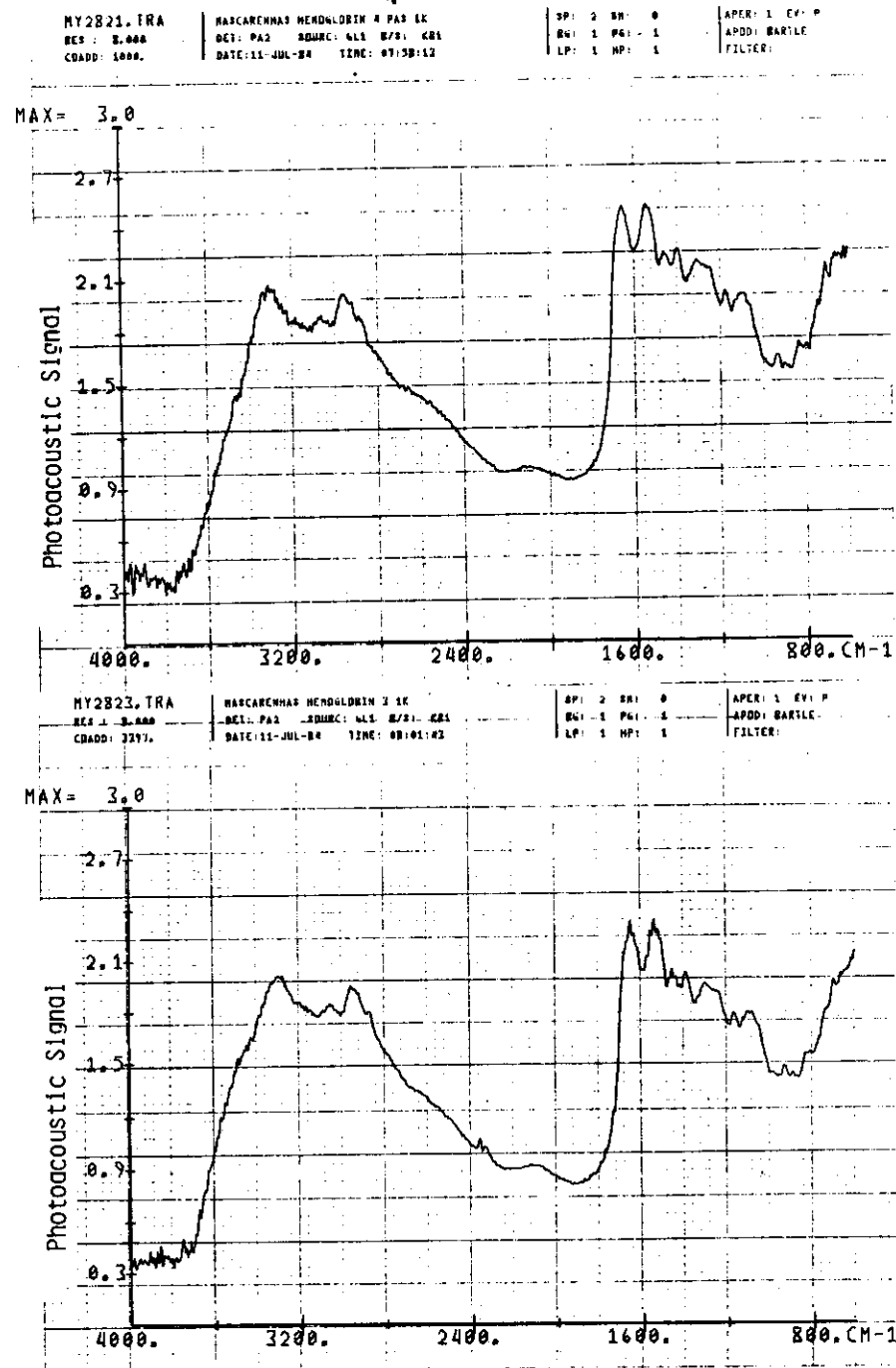
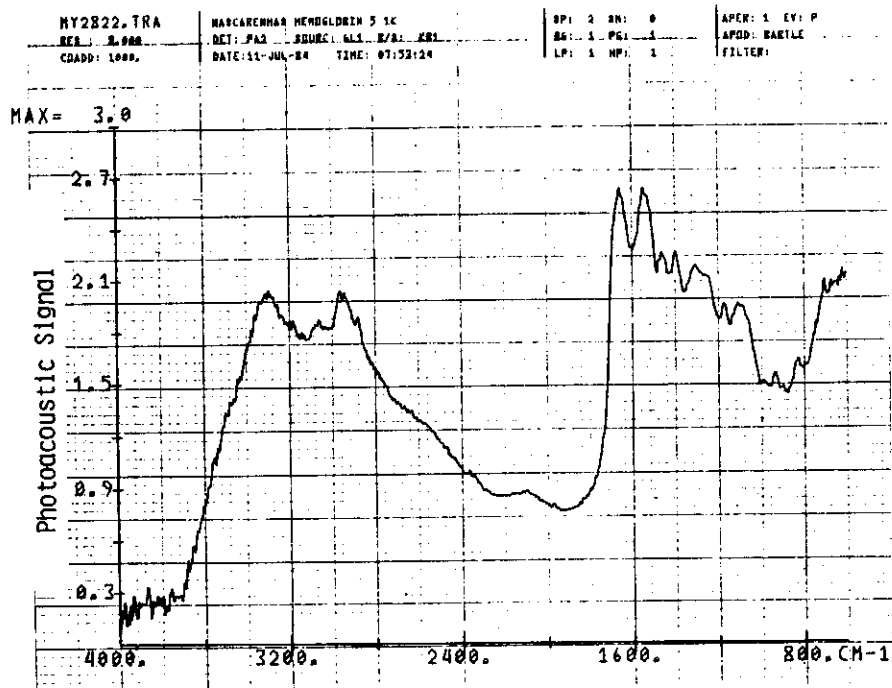
FT-IR PAS	E _i species mode ^b				assignment
	FT-IR poly(γ - benzyl glutamate) in KBr pellet	mean value from previous IR studies	calcd		
3300	3295				amide A
1737	1736				ester carbonyl
					stretch
1656	1650	1654	1657		amide I
1549	1548	1548	1544		amide II
1267	1256				amide III

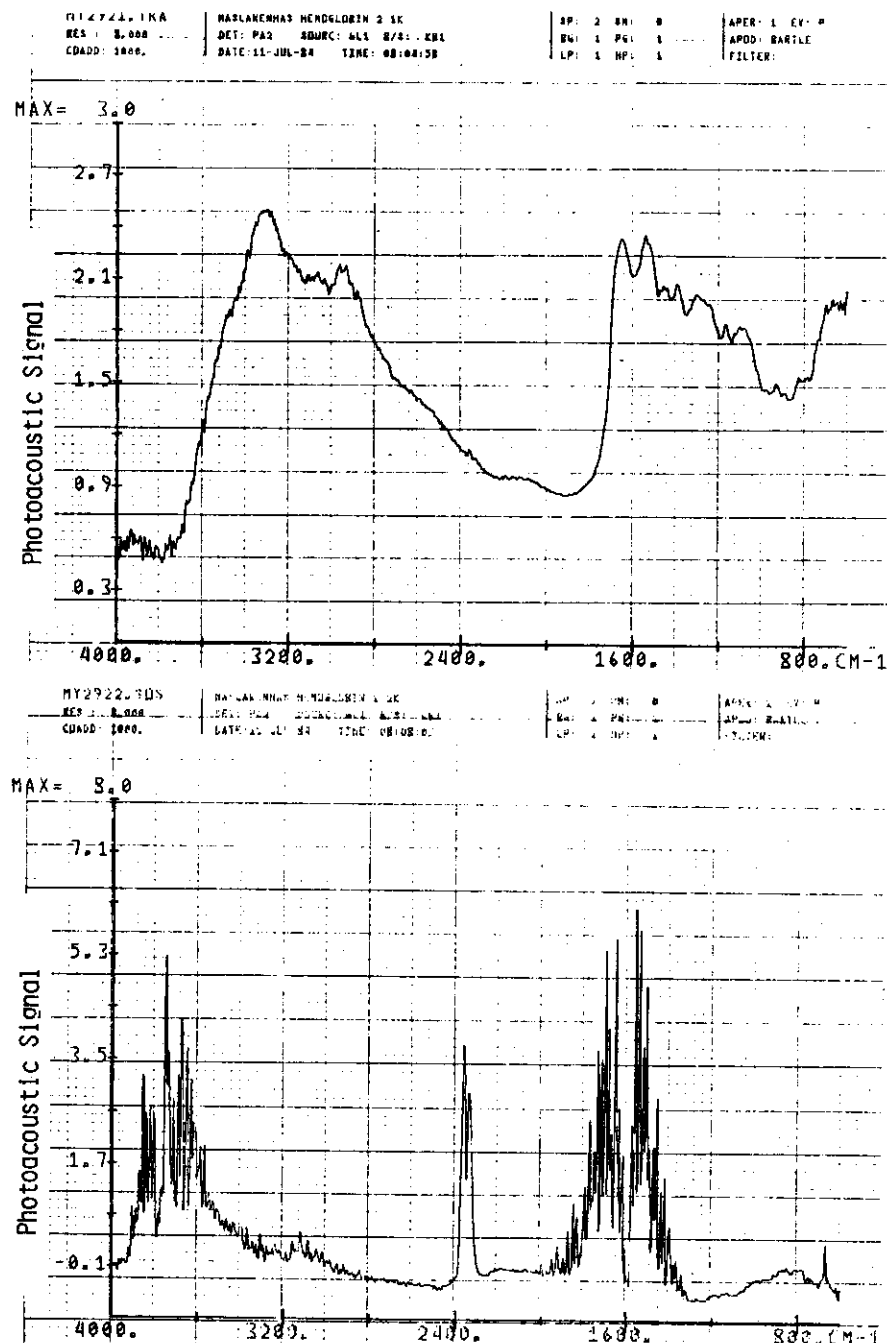
^a In cm^{-1} . ^b Nevskaya and Chirgadze.⁹

Mascarenhas and Royce have Obtained FTIR-PAS Spectra of Hemoglobin at Various Stages of Hydration. These were taken with the Bomem Spectrometer and Photoacoustic Cell Previously Described. Samples were in the Form of a Lyophilised Powder.

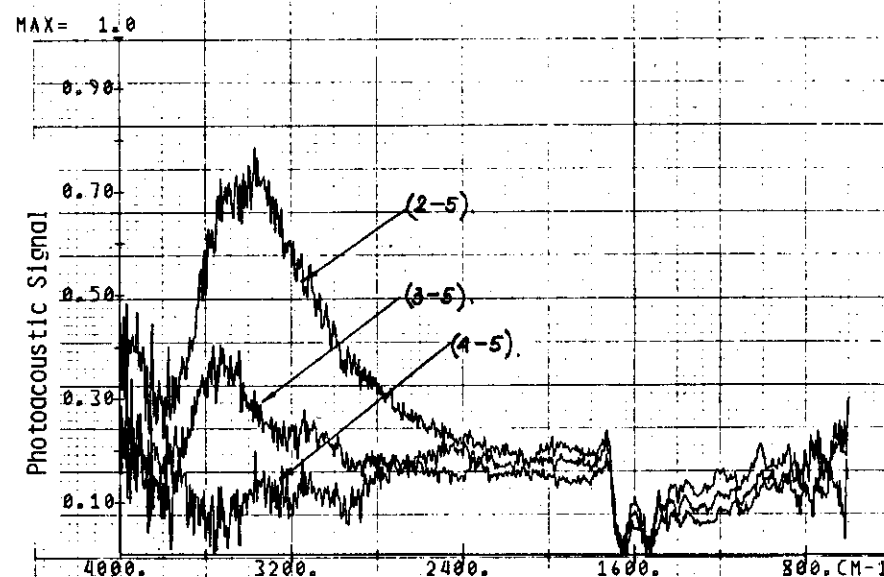
Sample Number	mg H ₂ O/mg Hb
1	0.78
2	0.23
3	0.11
4	0.08
5	0.02

Mirror Velocity = 0.02 cm sec. Dry N₂ Transducer Gas Signal Normalized with a Graphite Spectrum.



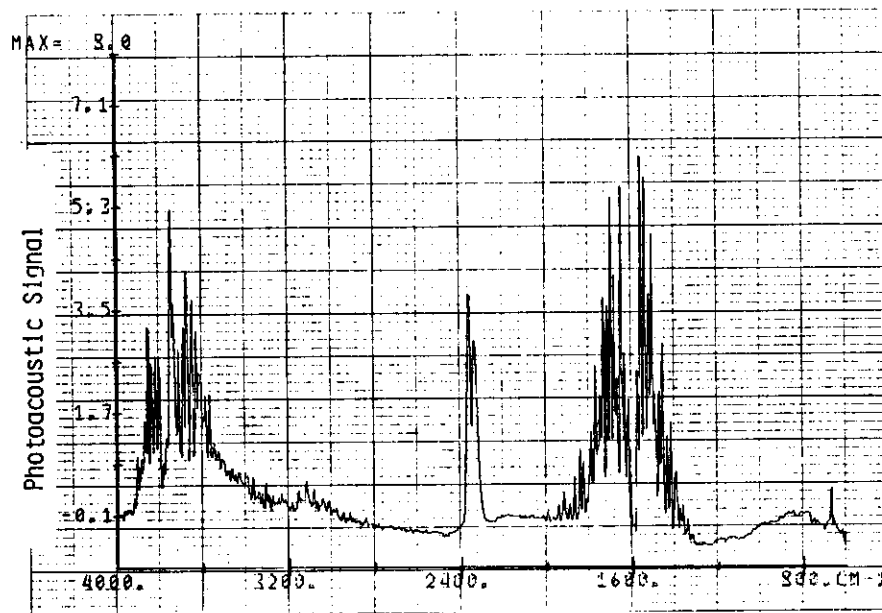


These Spectra may be Subtracted from each other to Display the Spectral Changes produced by the Increased Water Content. For the Diagram Below the Spectrum of Sample 5 with 0.02 mg H_2O /mg Hb is Subtracted from the Spectra for the other Samples.



The Data is Normalized so that the Spectra have the same Value at 1653 cm^{-1} . The peaks between 1650 cm^{-1} and 800 cm^{-1} are seen not to be Strongly Dependent on the H_2O content. The General Feature between 3600 cm^{-1} and 2400 cm^{-1} is Strongly Dependent on the H_2O Content.

The Difference Spectrum Shown Below Results from the Subtraction of the Sample 5 Spectrum from that of Sample 1. This shows a Major Problem with this Spectral Region and PAS Detection Gas Phase Contributions from H_2O and CO_2 are Clearly Shown and due to their Favored Energy Conversion Path tend to Mask the Solid Phase Signal.



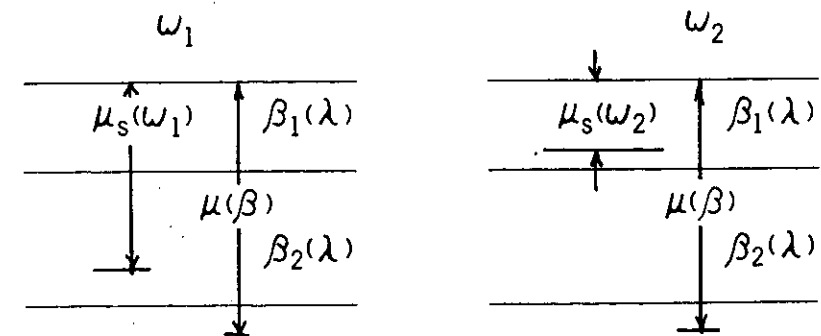
DEPTH PROFILE METHODS

The Photoacoustic Response of a System Contains an Optical Term $\beta(\lambda)$ and a Thermal Term $\mu_s(\omega)$. For an Optically Thick, Thermally Thick Sample the Signal Amplitude Scales as the Product of these Quantities for a Homogeneous Material.

Since $\mu_s(\omega)$ can be Reduced by Increasing ω :

$$\mu_s = \sqrt{\frac{2K}{\omega \rho c}}$$

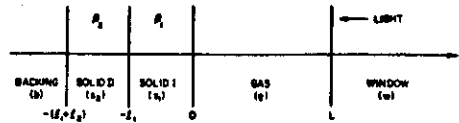
Measurements at Different Modulation Frequencies Provide Information about the Spatial Distribution of $\beta(\lambda)$.



For a Simple Layered Structure a Spectral Scan at ω_1 will give PAS Data about β_1 and β_2 . A Scan at ω_2 will only give data about β_1 .

The AC Heat Wave from Various Distances within the Sample is Attenuated Exponentially with the Characteristic Length being the Thermal Diffusion Length. A Signal from a Depth x is therefore reduced in Amplitude by $\exp(-x/\mu)$. In Addition this Contribution to the Total Signal Experiences a Phase Lag $\psi(x) = x/\mu$.

A General Expression for the PAS Amplitude in a Two Layer System as Shown Below was Developed by Mandellis et al.



Geometry for a double-layer PAS system.

The Signal has the Form:

$$\langle p(t, \omega) \rangle = Q_d \exp \left[i(\omega_0 t - \frac{\pi}{4}) \right]$$

For the Case of a Transparent Overlayer, i.e. $\beta_1 = 0$ the Complex Amplitude of the Signal is Given by:

$$Q_d = \left(\frac{p_0 I_0}{2\sqrt{2a_s T_0 L}} \right) \left(\frac{\eta_2 \beta_2}{k_2 (\beta_2^2 - \sigma_2^2)} \right) \left(\frac{1}{\exp(\sigma_1 l_1) + \exp(-\sigma_1 l_1)} \right) \times \left(\frac{(r_2 - 1)(b_2 + 1) \exp(\sigma_2 l_2) - (r_2 + 1)(b_2 - 1) \exp(-\sigma_2 l_2) + 2(b_2 - r_2) \exp(-\beta_2 l_2)}{(b_2 + 1) \exp(\sigma_2 l_2) + (b_2 - 1) \exp(-\sigma_2 l_2)} \right)$$

As the thickness of the Layer 1 increases l_1 increases and $\exp(\sigma_1 l_1)$ increases taking Q_d to zero. This also occurs for a Constant Overlayer Thickness as σ_1 increases due to an Increase in the Modulation Frequency.

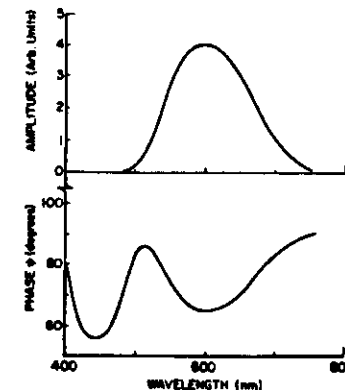
The Phase of the Signal for the Transparent Overlayer Situation is given by:

$$\psi = \tan^{-1}(-\omega_0 \tau_{\beta 2}) + \left(\frac{\omega_0}{2a_1} \right)^{1/2} l_1 - \tan^{-1} \left(\frac{-1}{1 - (2\omega_0 \tau_{\beta 2})^{1/2}} \right)$$

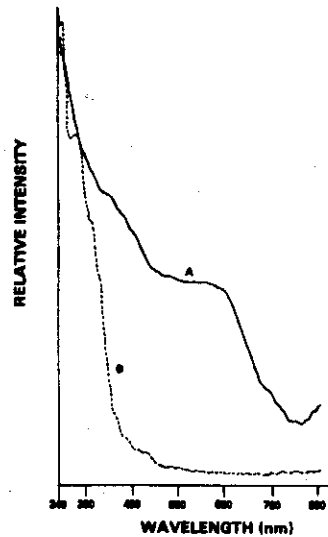
As the Absorption of the Second Layer Increases Phase Delays due to the Spatial Distribution of Energy in this Layer go to Zero. For this Case $\omega_0 \tau_{\beta 2} \gg 0$ and:

$$\psi = \frac{\pi}{4} + \left(\frac{\omega_0}{2a_1} \right)^{1/2} l_1$$

This was the Situation Considered by Adams and Kirkbright. When Both Layers have Optical Absorption Coefficients the full Equation for Q_d must be used. Results of Amplitude and Phase Computations for $\beta_1(500 \text{ nm}) = 50 \text{ cm}^{-1}$, $\beta_2(600 \text{ nm}) = 500 \text{ cm}^{-1}$ are shown below.

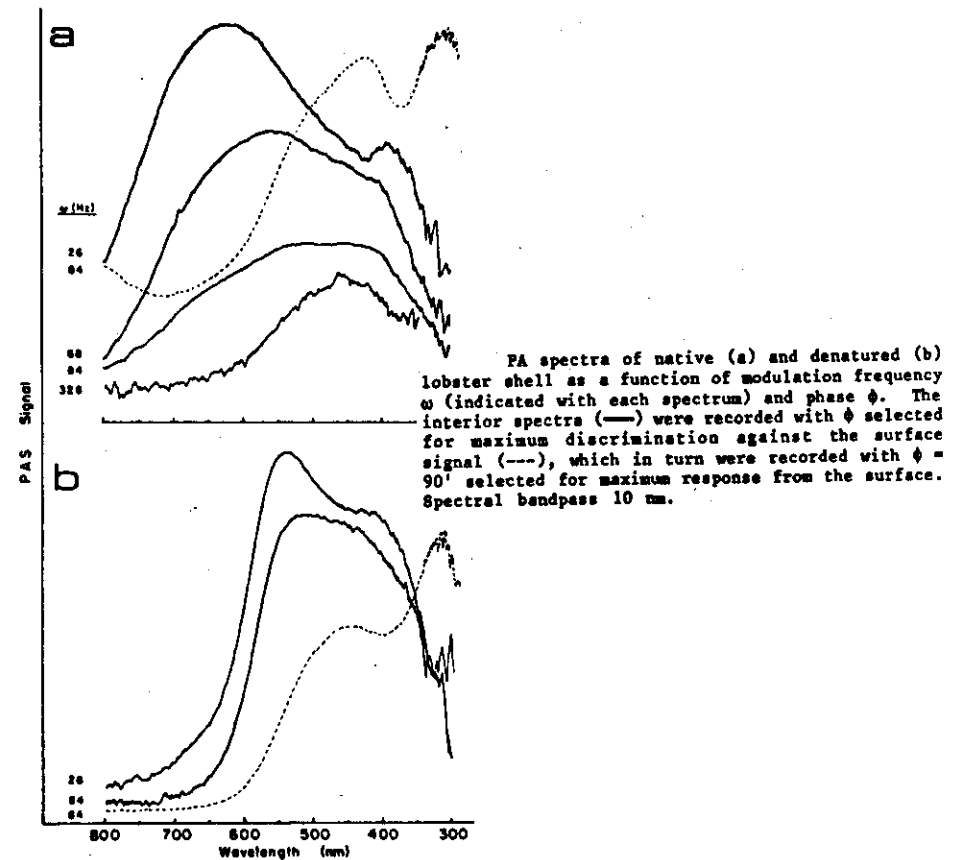


Rosencwaig used Spectra taken at two different Modulation Frequencies to look at the Layered Optical Structure of an Apple Peel. The High Frequency Spectrum (B) gives only the Optical Properties of the Surface Waxy Layer that has a UV Absorption. The Low Frequency Data (A) Contains Optical contributions from this layer and also Carotenoids and Chlorophyll Material at Greater Depths.



The Exponential Weighting of Signal Contribution with Depth of the Source must be taken into account in Deconvoluting Data of this Type.

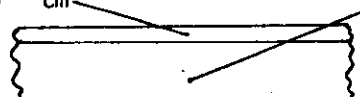
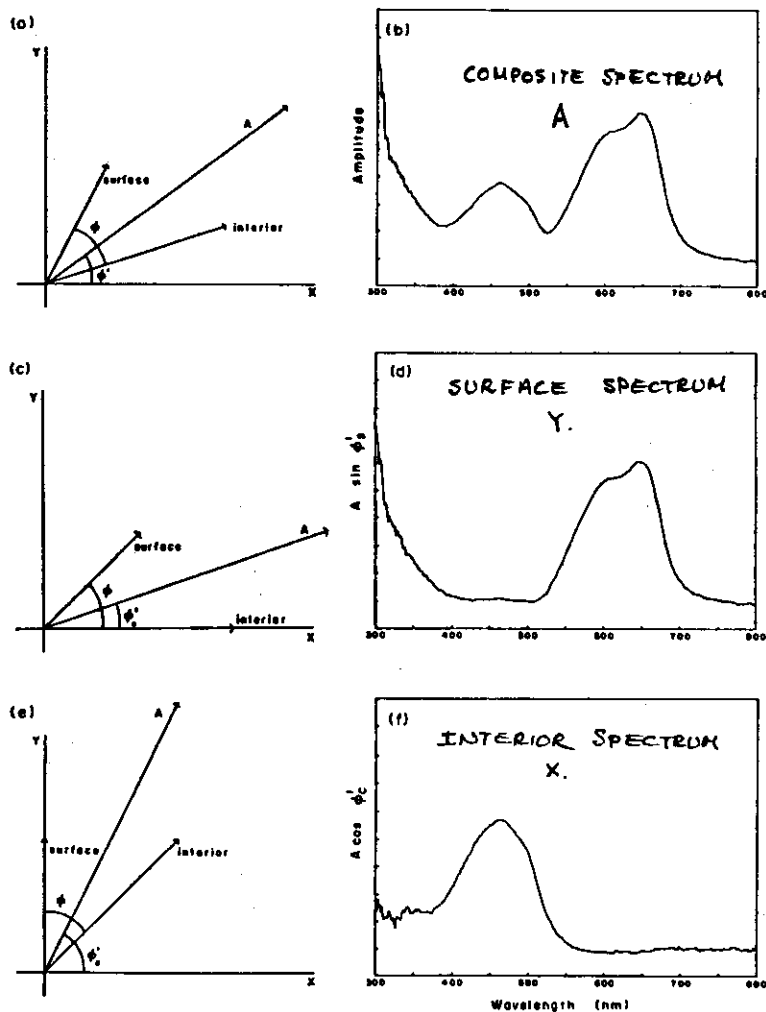
T.A. Moore (Nature 279 (1979) 265) has used a Combination of Modulation Frequency and Phase Control to Improve the Contrast in Spectral Data from Different Depths in a Layered Structure. The Diagram Below Indicates the Effect of the Phase Control on the Spectrum. Great Care must be taken in the Interpretation of Data of this Type. Absorption of Overlayers must be taken into account and a Good Knowledge of the Structure and Thermal Properties of the Sample is Required.



E. P. O'Hare et al. (Photochemistry and Photobiology 36 (1983) 709) constructed a two layer system to test the vector concept of interior and surface signals.

Surface Layer 1×10^{-3} cm
Methylene Blue

Interior Layer 6×10^{-2} cm
 β -Carotene

This type of Model and Method were then applied to studies of the Lichen *Acarospora schleicheri*.

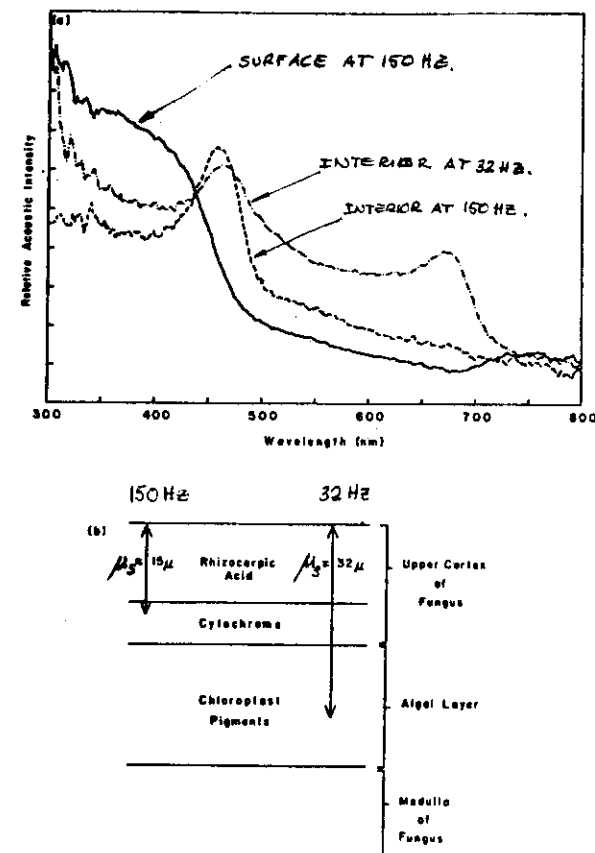


Figure 2. Pigment depth profile and schematic diagram of the lichen *A. schleicheri*. (a) Pigment depth profile of the lichen (—) is associated with a spectral component of Rhizocarpic acid ($A \sin \phi_s$ photoacoustic component at 150 Hz). (---) is associated with the bulk cytochrome absorption ($A \cos \phi_c$ photoacoustic component at 150 Hz). (---) is the absorption of the chloroplast of the algae ($A \cos \phi_c$ photoacoustic component at 32 Hz). (b) schematic cross-sectional view of the lichen.

REACTIVE SYSTEMS

A Photoacoustic Cell Provides an Environment in which Chemical or Photochemical Reactions can take place and be Monitored Spectroscopically. The Transducer Gas of the Cell can be one of the Reactions and DC as well as Periodically Modulated Radiation may be Employed.

Velux and Bae (J. Op. Soc. Am. 70 (1980) 560) have used PAS to Study Gas Exchange with Macroporous Hemoglobin Particles and to Compare this with Solution Data. Visible Spectral Region covered with a Two Beam Spectrometer using a PAS Cell containing Carbon Black to Monitor the Incident Intensity. An Identical Cell contained the Sample. The Gas in the Sample Compartment was of Controlled Humidity but was Static during the PAS Measurements. Comparison Made to Transmission Spectroscopic Data in Dilute Aqueous Solution.

Solution and PAS Data are shown below. In the Spectral Region covered the Oxygenated Hb shows Similar Spectral Features in the Transmission and PAS Data.

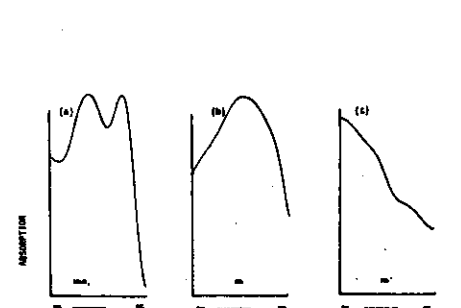


FIG. 2. Conventional absorption spectra from pure hemoglobin in diluted aqueous solution: (a) after rapid oxygenation by oxygen bubbling (oxyhemoglobin HbO_2); (b) in the presence of excess sodium dithionite 0.05-M (deoxyhemoglobin Hb); and, (c) after treatment with 0.05-M potassium ferricyanide (methemoglobin Hb^+ , $\text{Fe}^{++} \rightarrow \text{Fe}^{+++}$), obtained with a Beckman DK 2A spectrophotometer.

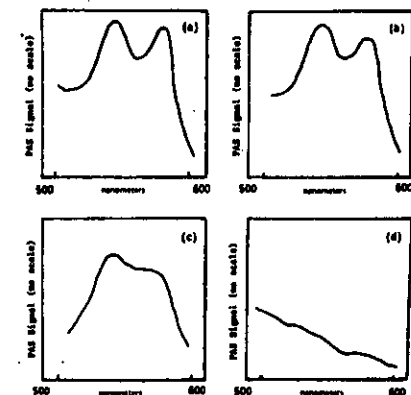


FIG. 3. Photoacoustic spectra from macroporous hemoglobin particles: (a) as prepared; (b) after 3 h under pure N_2 (atmospheric pressure); (c) treated in 0.05-M sodium dithionite; and (d) treated in 0.05-M potassium ferricyanide.

Deoxygenation of the Particulate Hemoglobin (3b) was not possible with a N_2 Flow through the Cell. Solution Phase Deoxyhemoglobin (2b) was Produced by Reaction with Sodium Dithionite but Similar Reaction with the Particulate Material (3c) did not Completely remove the 575 nm Band of the Oxyhemoglobin.

Similar Conversions were obtained in Solution and Solid Phase by Treatment with Potassium Ferricyanide.

D. Balasubramanian (Bioscience Reports 3 (1983) 981) has Studied the Effects of 200 → 300 nm Radiation on the Photolysis of TPP (Thiaminepyrophosphate). As a result of in situ Exposure in the PAS Cell the Sample develops an Absorption Band at 355 nm. The Sample examined was in the Solid State.

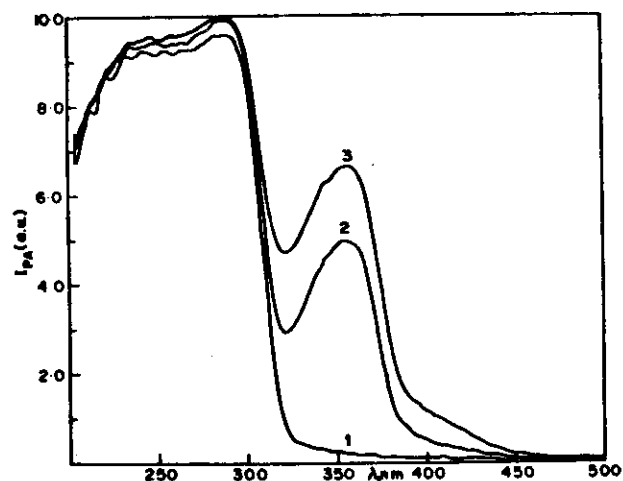
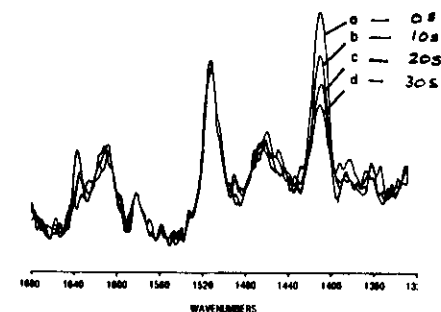


Fig. 2. PA spectra of thiamine pyrophosphate in the solid state. Modulation frequency 40 Hz, spectral band width ± 3 nm, temperature ambient, and spectral scanning speed 200 nm/min in the direction 500 nm downwards.
Curve 1, fresh sample with no prior u.v. irradiation; 2, after an exposure for 30 s in the 300-200-nm range in situ from the lamp source of the spectrometer during the first scan; 3, after the additional 30-s exposure in the 300-200-nm range during the second scan.

Similar Measurements were made on Samples in Solution and no Photochemical Reaction was Observed.

When Photochemical Processes are being followed it is Important to be sure that changes in the Thermal Properties of the Sample do not occur since the Photoacoustic Signal Depends on $\beta\mu_s$.

When Photopolymerization is taking place Changes in Thermal Conductivity and Heat Capacity per unit volume may take place and it is desirable to use an Internal Standard for Normalizing the PAS Signal. Such a Standard is associated with a Chromophore that is known to remain unchanged by the Photochemical Process.



Royce, Teng and Ors (Proc. IEEE 1981) used this Method in the Photopolymerization of Acrylate Polymers. The Bisphenol A Peak at 1509 cm^{-1} is used as a Reference. Photopolymerization Causes the $\text{C} = \text{C}$ peak at 1407 cm^{-1} to Decrease. Oxygen Inhibition of this Process was also Followed.

PHOTOSYNTHETIC REACTIONS WITH GAS EVOLUTION

- Processes in which the pressure in the Photoacoustic Cell can be Changed Periodically other than by Heat Addition will Contribute to the Measured Signal;
- In Photosynthesis Gas Evolution occurs when the sample is illuminated by Light in the Visible Spectral Region. A Steady Light will give rise to a Steady Evolution rate. This will increase the Pressure in the Cell but will not Contribute to the periodic PAS Signal directly.
- Periodic Illumination with a Photosynthetically Active Wavelength may give rise to a Periodic Gas Evolution which will contribute to the Measured Signal.
- Absorbed Energy may be stored as Chemical Products which will not contribute to the PAS Signal.
- Both the Photosynthetic Gas Evolution process and the Heat Conduction Process involved in the PAS Signal are characterized by some Relaxation Time. These will, in general, not be the same and so the Two Signal Contributions will have a Different Phase with Respect to the Modulated Illumination of the Sample.

Poulet, Cohen and Malkin (Biochimica and Biophysica Acta 724 (1983) 433) have considered the effect of Oxygen Evolution during a PAS Reaction. Measurements are made at Different Modulation Frequencies and in the presence of DC Illumination which can Saturate the AC Photosynthetic Process.

The Total Signal in the Absence of DC Light results from non-radiative (Thermal) Processes and Gas Evolution. In the presence of a DC Light the periodic gas evolution is reduced to zero and only the thermal term contributes to the PAS Signal.

The Vector Diagram below is used to separate these two components of the Signal.

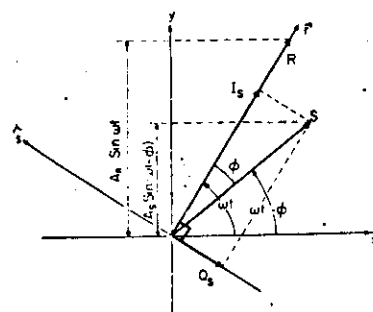


Fig. 1. A vectorial representation of sinusoidal signals. The (rotating) reference vector R produces a projection on the (fixed) y -axis equal to $A_R \sin \omega t$ while the (rotating) signal vector S produces a projection equal to $A_S \cos \phi \sin \omega t - A_S \sin \phi \cos \omega t$. The constant coefficients of this expression are, respectively, the projections of S on the (rotating) axes r and s (in-phase and quadrature).

$$I = I_{th}(1 - L) + I_{ox}$$

$$Q = Q_{th}(1 - L) + Q_{ox}$$

L = Photochemical Loss

th = thermal term

ox = oxygen evolution term

In the presence of the Saturating DC Light the Oxygen Evolution term is removed together with the Photochemical Loss.

$$I^* = I_{th} \quad Q^* = Q_{th}$$

Vector Subtraction of the Signal with and without the DC Light Gives:

$$-\Delta I \equiv (I - I^*) = I_{ox} - LI_{th} = I_{ox} - LI^*$$

$$-\Delta Q \equiv (Q - Q^*) = Q_{ox} - LQ_{th} = Q_{ox} - LQ^*$$

At High Modulation Frequencies the Oxygen Evolution Contribution is Found to be Negligible so that:

$$\Delta I(\omega \rightarrow \infty) = LI_{th} = LI^*(\omega \rightarrow \infty)$$

$$\Delta Q(\omega \rightarrow \infty) = LQ_{th} = LQ^*(\omega \rightarrow \infty)$$

Assuming L to be frequency independent enables it to be evaluated from these equations and this value used for ΔI ; ΔQ , so that

$$I_{ox} = I - (1 - L)I^*$$

$$Q_{ox} = Q - (1 - L)Q^*$$

The Oxygen Evolution Vector Contribution is then:

$$A_{ox} = \sqrt{I_{ox}^2 - Q_{ox}^2} \quad ; \quad \phi_{ox} = \tan^{-1}(-Q_{ox}/I_{ox})$$

Similarly the thermal contribution is

$$A_{th} = \sqrt{I_{th}^2 + Q_{th}^2} \quad ; \quad \phi_{th} = \tan^{-1}(-Q_{th}/I_{th})$$

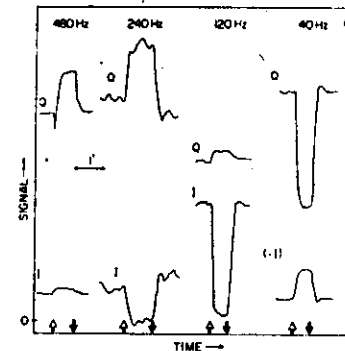
The Diagrams below show the effect of Frequency and DC Light on the Measured PAS Signal obtained with Tobacco Leaf.

I = In Phase Signal

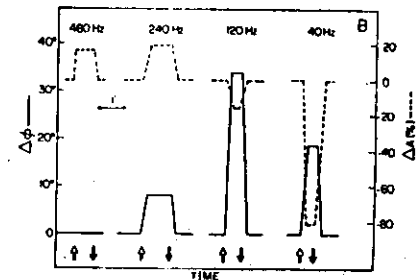
Q = Quadrature Signal

⬆ = Background DC Light On

⬇ = Background DC Light Off



COMPUTED VALUES ON THE BASIS OF THE ABOVE MODEL



The Signals Amplitude and Phase take some time to reach their "Steady State" values after these changes in condition.

There is no Change in Phase Angle with the DC Light when only the Thermal Term is present (480 Hz). At Lower Frequencies a Phase Change occurs. At 120 Hz the Amplitude Change is small but the Phase Change is Large.

The Oxygen and Thermal Contributions as well as the Photochemical Loss were Calculated from the Data and are shown in the Table below.

Signal components are expressed in arbitrary but consistent units (mV), as measured at the input of the lock-in amplifier (after preamplification). Phase angles are expressed in degrees. r, raw data; c, calculated.

		Frequency (Hz)	
		480	60
I	(r)	0.95	22
Q		6.70	96
A _i	(c)	6.77	98.5
φ		82	77
I* = I _{th}	(r)	1.10	-10
Q* = Q _{th}		8.10	60
A* = A _{th}	(c)	8.17	61
φ* = φ _{th}		82	99.5
L	(c)	0.17	0.17 ^b
I _{ox}	(c)	0*	30
Q _{ox}		0*	46
A _{ox}	(c)	0	55
φ _{ox}		0	57
A _{ox} /A _{th}	(c)	0	0.90
Δφ = φ _{ox} - φ _{th}		-	-42.5

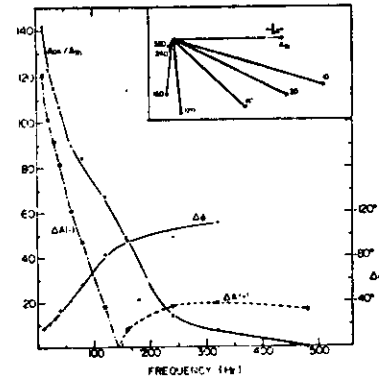
* Assumed.

^b Assumed to be equal to the L value at 480 Hz.

As $\omega \rightarrow \infty$ (A_{ox}/A_{th}) $\rightarrow 0$ and $\Delta\phi = (\phi_{ox} - \phi_{th})$ increases as shown in the Figure above.

At Low Frequencies Thermal and Gas Signal are Approximately in Phase. DC Light removes Gas Signal and therefore decreases the Total Response.

At Higher Frequencies the Thermal and Gas Signals have Opposite Phase and Partly Cancel. DC Light removes the Gas Signal and the PAS Amplitude increases.



Both the Periodic Thermal Diffusion and Oxygen Diffusion exhibit Exponential Damping of the Amplitude of the Periodic Term. For the Oxygen Diffusion Term this is of the Form

$$A_{ox} \propto \exp\left[-\sqrt{\frac{\omega}{2D_{ox}}} \cdot x\right]$$

As the Modulation Frequency of the Radiation increases the Amplitude Damping of the Oxygen Diffusion Term at a given location increases. Its contribution to the PAS Signal will therefore decrease.

At High Modulation Frequencies changes due to the DC Light can Therefore be Attributed to L \rightarrow the Photochemical Loss Term.

The Oxygen Evolution Term also exhibits a Frequency Dependence through the Kinetic Processes involved in its Generation for each Step Describable by First Order Kinetics and having a Rate Constant k_1 . This Attenuation Factor is of the form:

$$\left[\frac{k_1}{\sqrt{k_1^2 + \omega^2}} \right] \rightarrow 1 \quad \omega \ll k_1$$

$$\rightarrow (k_1/\omega) \quad \omega \gg k_1$$

The Thermal Contribution to the Signal shows a similar frequency dependence with the Thermal Diffusion Coefficient replacing the Matter Diffusion Coefficient

$$A_{th} \propto \exp\left[-\sqrt{\frac{\omega}{2D_{th}}} \cdot x\right]$$

$$\frac{A_{ox}}{A_{th}} = \exp\left[-\sqrt{\pi f} (D_{ox}^{-1/2} - D_{th}^{-1/2})x\right] \prod_1 \left[\frac{k_1}{\sqrt{k_1^2 + 4\pi^2 f^2}} \right]$$

when $f \ll k$ the second term goes to unity and a plot of $\ln(A_{ox}/A_{th})$ vs. \sqrt{f} should be linear. D_{th} is usually $\sim 100 \times D_{ox}$ so that the slope of this plot is approximately $(D_{ox})^{-1/2} \cdot \sqrt{\pi} \cdot L$.

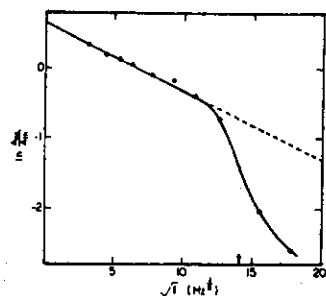


Fig. 4. A plot of $\ln A_{ox}/A_{th}$ vs. the square root of the frequency (cf. Eqn. 7). The arrow on the abscissa indicates the point where the second attenuation (due to electron-transport reactions) is half maximum (from the same data as those shown in Fig. 3).

For tobacco leaf:

$$D_{ox} \approx 3.7 \times 10^{-6} \text{ cm}^2 \text{ sec}^{-1}$$

For H_2O :

$$D_{ox} = 2.1 \times 10^{-5} \text{ cm}^2 \text{ sec}^{-1}$$

Above 150 Hz

$$\prod_1 \left[\frac{k_1}{\sqrt{k_1^2 + 4\pi^2 f^2}} \right]$$

becomes important

In Situ Measurements with a Differential Photoacoustic Cell.

In Situ Measurements are often complicated by Noise from the Signal Source. Poulet and Chambron (Journal de Physique 44 (1983) C6-413), have used a Differential Photoacoustic Cell to Minimize Noise. A Light Pipe is used to provide the Modulated Radiation to the Measuring Cell.

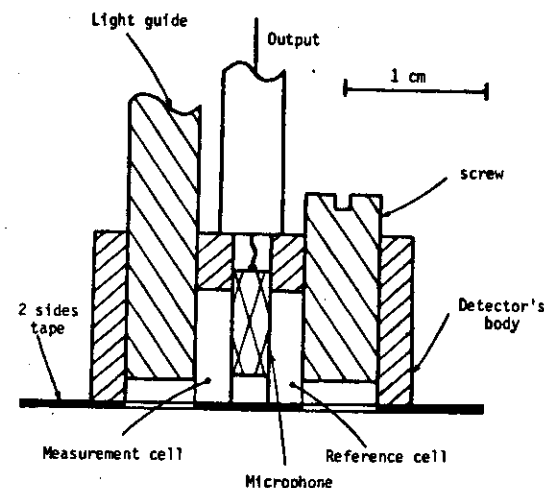


FIGURE 1 - Diagram of the differential photoacoustic detector for in situ spectroscopy.

REFERENCES

A. BOOKS AND REVIEWS ON PHOTOACOUSTIC SPECTROSCOPY

1. "Photoacoustic Spectroscopy and Detection," Yoh-Hau Pao, Editor, Academic Press (1977).
2. "Photoacoustics: Principles and Applications," H. Coufal, Editor, Vieweg Verlag (1981).
3. "Photoacoustics and Photoacoustic Spectroscopy," A. Rosencwaig, John Wiley and Sons (1980).
4. "Fourier Transform Infrared Spectroscopy," J. Ferraro and L. Basile, Editors, Academic Press (1982).
5. "Photoacoustics: Spectroscopy and other Applications," A.C. Tam. Review Article in the book "Ultrasensitive Spectroscopic Techniques," D. Kliger, Editor, Academic Press (1982).
6. "Photoacoustic Spectroscopy of Solids and Surfaces," P. Ganguly and C.N.R. Rao, Proc. Indian Acad. Sciences (Chem. Sci.) 90 (1981) 153.
7. "Optical Spectroscopy using an Open Photoacoustic Cell," P.O.F. Helander, Linköping Studies in Science and Technology. Dissertation #90, Linköping, Sweden (1983).
8. "Applications of Photoacoustic Spectroscopy," J.B. Kinney and R.H. Staley, Annual Reviews of Materials Science 12 (1982) 295.

B. SELECTED PAPERS ON THE THEORY OF THE PHOTOACOUSTIC PROCESS

1. "Theory of the Photoacoustic Effect with Solids," A. Rosencwaig and A. Gersho, J. Appl. Phys. 47 (1976) 64.
2. "Generalized Theory of the Photoacoustic Effect," F.A. McDonald and G.C. Wetzel, J. Appl. Phys. 49 (1978) 2313.
3. "Phase Measurements in the Frequency Domain PAS of Solids," A. Mandelis, Y.C. Teng and B.S.H. Royce, J. Appl. Phys. 50 (1979) 7136.
4. "Photothermal Spectroscopy in Scattering Media," Z.A. Yasa, W.B. Jackson and N.M. Amer, Applied Optics 21 (1982) 21.
5. "Absolute Optical Absorption Coefficient Measurements using PAS Amplitude and Phase Information," Y.C. Teng and B.S.H. Royce, J. Op. Soc. Am. 70 (1980) 557.
6. "Quantitative FTIR-PAS of Condensed Phases," Y.C. Teng and B.S.H. Royce, Applied Optics 21 (1982) 77.

7. "Photothermal Spectroscopy using Optical Beam Probing: Mirage Effect," J.C. Murphy and L.C. Aamodt, J. Appl. Phys. 51 (1980) 4580.
8. "Photothermal Deflection Spectroscopy and Detection," W.B. Jackson, N.M. Amer, A.C. Boccara and D. Fournier, Applied Optics 20 (1981) 1333.
9. "Absolute Optical Absorption Coefficient Measurements Using Transverse Photothermal Deflection Spectroscopy," A. Mandelis, J. App. Phys. 54 (1983) 3404.
10. "High Luminosity Visible and Near IR Fourier Transform Photoacoustic Spectrometer," D. Debarre, A.C. Boccara and D. Fournier, Applied Optics 20 (1981) 4281.
11. "Fourier Transform Photoacoustic Spectroscopy," M.M. Farrow, R.K. Burnham, E.M. Eyring, Appl. Phys. Lett. 33 (1978) 735 and Anal. Chem. 52 (1980) 253.
12. "Fourier Transform Photoacoustic Spectrometer," L.L. Lloyd, S.M. Riseman, R.K. Burnham and E.M. Eyring, Rev. Sci. Inst. 51 (1980) 1488.
13. "Phase Modulation in FIR Interferometers, I. Mathematical Formulation," J. Chamberlain, InfraRed Physics 11 (1971) 25.

C. GAS-MICROPHONE PHOTOACOUSTIC CELL DESIGNS

1. A. Rosencwaig; Rev. Sci. Inst. 48 (1977) 1133.
2. E.M. Monahan and A.W. Nolle; J. Appl. Phys. 48 (1977) 3519.
3. S.O. Kanstad and P.E. Nordal; Opt. Comm. 26 (1978) 367.
4. A.C. Tam and Y.H. Wong; Appl. Phys. Lett. 36 (1980) 471.
5. D. Cahen; Rev. Sci. Inst. 52 (1982) 1306.

D. PAPERS ON BIOLOGICAL SYSTEMS AND PAS

1. "Photoacoustic Spectroscopy and Related Techniques Applied to Biological Materials," T.A. Moore; Photochem. and Photobiol. Rev. 7 (1983) 187-221.
2. "Photoacoustic Spectroscopy and its use in Biology," D. Balasubramanian; Bioscience Reports 3 (1983) 981-995.
3. A. Rosencwaig, Science 181 (1973) 657.
4. G. M. Alter, J. Biological Chem. 258 (1983) 14960 and 14966.
5. R. Haire and B. Hedlund, Biochemistry 22 (1983) 327.

6. A. J. Sedler, J.G. Horsch, E.Q. Lawson, D. Harmatz, D.T. Brandan and C.R. Middaugh, *Analytical Biochemistry* **138** (1984) 44.
7. A.M. Vejux and P. Bae, *J. Op. Soc. Am.* **70** (1980) 560.
8. M.G. Rockley, D.M. Davis and H.H. Richardson, *Science* **210** (1980) 918.
9. V. Renngopalakrishnan and R.S. Bhatnagar, *J. Am. Chem. Soc.* **106** (1984) 2217.
10. S.L. Castleden, G.F. Kirkbright, and K.R. Menon, *Analyst* **105** (1980) 1076.
11. M.L. Mackenthun, R.D. Tom, T.A. Moore, *Nature* **278** (1979) 861 and *Nature* **279** (1979) 265.
12. M.J. Adams and G.F. Kirkbright, *Analyst* **102** (1977) 678.
13. A. Mandelis, Y.C. Teng and B.S.H. Royce, *J. App. Phys.* **50** (1979) 7138.
14. B.S.H. Royce, Y.C. Teng and J.A. Ors, *IEEE Ultrasonics Symposium* (1981) 784.
15. S. Malkin and D. Cahen, *Photochemistry and Photobiology* **29** (1979) 803.
16. P. Poulet, D. Cahen and S. Malkin, *Biochimica et Biophysica Acta* **724** (1983) 433.
17. R. Carpentier, B. Lare, R.M. Leblanc, *Arch. Biochem. Biophys.* **228** (1984) 534.
18. E.P. O'Hara, R.D. Tom and T.A. Moore, *Photochem. Photobiol.* **38** (1983) 709.
19. S. Malkin, N. Lasser-Ross, G. Bults, and D. Cahen, *Photosynthesis. Proc. 5th Int. Congress* **3** (1980) 1031.
20. R. Carpentier, B. LaRue and R.M. Leblanc, *Journal de Physique* **44** (1983) C6-335.
21. K. Veeranjanyulu and V.S.R. Das, *Journal de Physique* **44** (1983) C6-337.
22. P. Poulet and J. Chambron, *Journal de Physique* **44** (1983) C6-413.

Theory of the photoacoustic effect with solids

Allan Rosencwaig and Allen Gersho

Bell Laboratories, Murray Hill, New Jersey 07974
(Received 24 July 1975)

When chopped light impinges on a solid in an enclosed cell, an acoustic signal is produced within the cell. This effect is the basis of a new spectroscopic technique for the study of solid and semisolid matter. A quantitative derivation is presented for the acoustic signal in a photoacoustic cell in terms of the optical, thermal, and geometric parameters of the system. The theory predicts the dependence of the signal on the absorption coefficient of the solid, thereby giving a theoretical foundation for the technique of photoacoustic spectroscopy. In particular, the theory accounts for the experimental observation that with this technique optical absorption spectra can be obtained for materials that are optically opaque.

PACS numbers: 78.20.H, 43.35., 07.45.

I. INTRODUCTION

In 1880, Alexander Graham Bell¹ discovered that when a periodically interrupted beam of sunlight shines on a solid in an enclosed cell, an audible sound could be heard by means of a hearing tube attached to the cell. Motivated by Bell's discovery, Tyndall² and Röntgen³ found that an acoustic signal can also be produced when a gas in an enclosed cell is illuminated with chopped light. Bell⁴ subsequently experimented with a variety of solids, liquids, and gases and his work generated a brief flurry of interest. The photoacoustic effect was evidently regarded as a curiosity of no practical value and was soon forgotten. Fifty years later the photoacoustic or photoacoustic effect with gases was reexamined. It has since become a well-established technique for gas analysis and is well understood. Photons absorbed by the gas are converted into kinetic energy of the gas molecules, thereby giving rise to pressure fluctuations within the cell. The photoacoustic effect with solids, however, was apparently ignored for 90 years and a satisfactory theoretical explanation of the effect with solids was never published.

Recently, interest in the photoacoustic effect with solids has been revived with the development of a very useful technique for spectroscopic investigation of solid and semisolid materials.⁵⁻⁹ The name change from optoacoustic to photoacoustic has been instituted to reduce confusion with the acousto-optic effect in which a laser beam is deflected by acoustic waves in a crystal.

In photoacoustic spectroscopy of solids, or PAS, the sample to be studied is placed inside a closed cell containing a gas, such as air, and a sensitive microphone. The sample is then illuminated with chopped monochromatic light. The analog signal from the microphone is applied to a tuned amplifier whose output is recorded as a function of the wavelength of the incident light. In this way photoacoustic spectra are obtained and these spectra have been found to correspond, qualitatively at least, to the optical absorption spectra of the solids.

One of the principal advantages of photoacoustic spectroscopy is that it enables one to obtain spectra similar to optical absorption spectra on any type of solid or semisolid material, whether it be crystalline, powder, amorphous, smear, gel, etc. This capability is based on the fact that only the absorbed light is converted to sound. Scattered light, which presents such a

serious problem when dealing with many solid materials by conventional spectroscopic techniques, presents no difficulties in photoacoustic spectroscopy. Furthermore, it has been found experimentally that good optical absorption data can be obtained, with the photoacoustic technique, on materials that are completely opaque to transmitted light.¹ Photoacoustic spectroscopy has already found some important applications in research and analysis of inorganic, organic, and biological solids and semisolids.⁶⁻⁹ It furthermore has very strong potential as a spectroscopic technique not only in the study of bulk optical properties, but also in surface studies and deexcitation studies.¹ With the rapid growth of interest in PAS, a quantitative understanding of the production of the acoustic signal is of utmost importance. In this paper we lay the groundwork for this analysis. In addition we have, for the first time, been able to account for the capability of the photoacoustic technique to derive optical absorption spectra from systems that are completely opaque to transmitted light.

Bell⁴ attributed the photoacoustic effect observed with spongy solids such as carbon black to a cyclic driving off of pulses of air from, and readorption onto, the pores of the solid in response to the cyclical heating and cooling of the solid by the chopped light. He also supported the theory of Rayleigh¹⁰ who concluded that the effect is also probably due to a mechanical motion of the solid. However, Preece¹¹ inferred from his experiments that the solid does not undergo any substantial mechanical motion, and suggested that the effect was due to an expansion and contraction of the air in the cell. Mercadier¹² who also experimented with the effect concluded that the sound is due to "vibratory movement determined by the alternate heating and cooling produced by the intermittent radiations, principally in the gaseous layer adhering to the solid surface hit by these radiations."

We have found, from experiments in which we first thoroughly evacuated the photoacoustic cell and then refilled it with nonadsorbing noble gases and from experiments with two-dimensional solids and other materials with weak surface adsorption properties, that absorbed gases do not play a significant role in the production of the acoustic signal. Furthermore, it can be readily shown that thermal expansion and contraction of the solid, and any thermally induced mechanical vibration of the solid are generally too small in magnitude to account for the observed acoustic signal. From

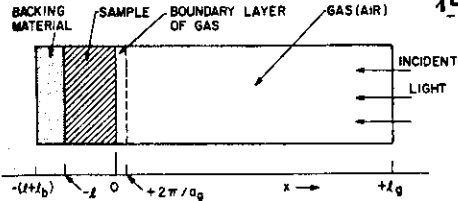


FIG. 1. Cross-sectional view of a simple cylindrical photoacoustic cell, showing the positions of the solid sample, backing material, and gas column.

both experimental and theoretical considerations we feel that the primary source of the acoustic signal in the photoacoustic cell arises from the periodic heat flow from the solid to the surrounding gas as the solid is cyclically heated by the chopped light.¹³ Only a relatively thin layer of air (~0.2 cm for a chopping rate of 100 Hz) adjacent to the surface of the solid responds thermally to the periodic heat flow from the solid to the surrounding air. This boundary layer of air can then be regarded as a vibratory piston, creating the acoustic signal detected in the cell. Since the magnitude of the periodic pressure fluctuations in the cell is proportional to the amount of heat emanating from the solid absorber, there is a close correspondence between the strength of the acoustic signal and the amount of light absorbed by the solid.

II. HEAT-FLOW EQUATIONS

Any light absorbed by the solid is converted, in part or in whole, into heat by nonradiative deexcitation processes within the solid. We formulate a one-dimensional model of the heat flow in the cell resulting from the absorbed light energy. Consider a simple cylindrical cell as shown in Fig. 1. The cell has a diameter D and length L . We assume that the length L is small compared to the wavelength of the acoustic signal and the microphone (not shown) will detect the average pressure produced in the cell. The sample is considered to be in the form of a disk having diameter D and thickness l . The sample is mounted so that its front surface is exposed to the gas (air) within the cell and its back surface is against a poor thermal conductor of thickness l_b . The length l_g of the gas column in the cell is then given by $l_g = L - l - l_b$. We further assume that the gas and backing materials are not light absorbing.

We define the following parameters: k_i , the thermal conductivity of material i (cal/cm sec °C); ρ_i , the density of material i (g/cm³); C_i , the specific heat of material i (cal/g °C); $\alpha_i = k_i/\rho_i C_i$, the thermal diffusivity of material i (cm²/sec); $a_i = (\omega/2\alpha_i)^{1/2}$, the thermal diffusion coefficient of material i (cm⁻¹); $\mu_i = 1/a_i$, the thermal diffusion length of material i (cm). i can take the subscripts s , g , and b for the solid, gas, and backing material, respectively, and ω denotes the chopping frequency of the incident light beam in radians per second.

We assume a sinusoidally chopped monochromatic light source with wavelength λ incident on the solid with intensity

$$I = \frac{1}{2} I_0 (1 + \cos \omega t),$$

where I_0 is the incident monochromatic light flux (W/cm²). Let β denote the optical absorption coefficient of the solid sample (in cm⁻¹) for the wavelength λ . The heat density produced at any point x due to light absorbed at this point in the solid is then given by

$$\frac{1}{2} \beta I_0 \exp(\beta x) (1 + \cos \omega t),$$

where x takes on negative values since the solid extends from $x = 0$ to $x = -l$ with the light incident at $x = 0$. Note also from Fig. 1 that the air column extends from $x = 0$ to $x = l_g$ and the backing from $x = -l$ to $x = -(l + l_b)$.

The thermal diffusion equation in the solid taking into account the distributed heat source can be written

$$\frac{\partial^2 \phi}{\partial x^2} = \frac{1}{\alpha_s} \frac{\partial \phi}{\partial t} - A \exp(\beta x) [1 + \exp(j\omega t)],$$

for $-l \leq x \leq 0$, (1)

with

$$A = \beta I_0 \eta / 2k_s,$$

where ϕ is the temperature and η is the efficiency at which the absorbed light at wavelength λ is converted to heat by the nonradiative deexcitation processes. In this paper we shall assume $\eta = 1$, a reasonable assumption for most solids at room temperature. For the backing and the gas,¹⁴ the heat diffusion equations are given by

$$\frac{\partial^2 \phi}{\partial x^2} = \frac{1}{\alpha_g} \frac{\partial \phi}{\partial t}, \quad -l - l_b \leq x \leq -l \quad (2)$$

$$\frac{\partial^2 \phi}{\partial x^2} = \frac{1}{\alpha_g} \frac{\partial \phi}{\partial t}, \quad 0 \leq x \leq l_g, \quad (3)$$

The real part of the complex-valued solution $\phi(x, t)$ of Eqs. (1)–(3) is the solution of physical interest and represents the temperature in the cell relative to ambient temperature as a function of position and time. Thus the actual temperature field in the cell is given by

$$T(x, t) = \text{Re}[\phi(x, t)] + \Phi,$$

where Re denotes the "real part of" and Φ is the ambient (room) temperature.

To completely specify the solution of Eqs. (1)–(3), the appropriate boundary conditions are obtained from the requirement of temperature and heat-flux continuity at the boundaries $x = 0$ and $x = -l$, and from the constraint that the temperature at the cell walls $x = +l_g$ and $x = -l - l_b$ is at ambient. The latter constraint is a reasonable assumption for metallic cell walls but in any case it does not affect the ultimate solution for the acoustic pressure.

Finally, we note that we have assumed the dimensions of the cell are small enough to ignore convective heat flow in the gas at steady-state conditions.

III. TEMPERATURE DISTRIBUTION IN THE CELL

The general solution for $\phi(x, t)$ in the cell neglecting transients can be written

$$\begin{aligned} \phi(x, t) &= (1/l_b)(x + l + l_b)W_0 + W \exp[\sigma_s(x + l) + j\omega t], & \phi_s(0, t) &= \phi_s(0, t), & (8a) \\ & & -l - l_b \leq x \leq -l & & \phi_b(-l, t) &= \phi_s(-l, t), & (8b) \\ &= e_1 + e_2 x + d \exp(\beta x) + [U \exp(\sigma_s x) + V \exp(-\sigma_s x) & k_s \frac{\partial \phi_s}{\partial x}(0, t) &= k_g \frac{\partial \phi_g}{\partial x}(0, t), & (8c) \\ &\quad - E \exp(\beta x)] \exp(j\omega t), & -l \leq x \leq 0 & & \text{and} & & \\ &= (1 - x/l_g)\theta_0 + \theta \exp(-\sigma_g x + j\omega t), & 0 \leq x \leq l_g, & & k_b \frac{\partial \phi_b}{\partial x}(-l, t) &= k_g \frac{\partial \phi_g}{\partial x}(-l, t), & (8d) \end{aligned}$$

where W , U , V , E , and θ are complex-valued constants, e_1 , e_2 , d , W_0 , and θ_0 are real-valued constants, and $\sigma_i = (1 + j)a_i$ with $a_i = (\omega/2\alpha_i)^{1/2}$. In particular it should be noted that θ and W represent the complex amplitudes of the periodic temperatures at the sample-gas boundary ($x = 0$) and the sample-backing boundary ($x = -l$), respectively. The dc solution in the backing and gas already make use of the assumption that the temperature (relative to ambient) is zero at the ends of the cell. The quantities W_0 and θ_0 denote the dc component of the temperature (relative to ambient) at the sample surfaces $x = -l$ and $x = 0$, respectively. The quantities E and d , determined by the forcing function in Eq. (1), are given by

$$d = -\frac{A}{\beta^2}, \quad (5a)$$

and

$$E = \frac{A}{(\beta^2 - \sigma_s^2)} = \frac{\beta I_0}{2k_s(\beta^2 - \sigma_s^2)}. \quad (5b)$$

In the general solution, Eq. (4), we have omitted the growing exponential component of the solutions to the gas and backing material, because for all frequencies ω of interest the thermal diffusion length is small compared to the length of the material in both the gas and the backing. That is, $\mu_s \ll l_b$ and $\mu_g \ll l_g$ ($\mu_g \sim 0.02$ cm for air when $\omega = 630$ rad/sec), and hence the sinusoidal components of these solutions are sufficiently damped so that they are effectively zero at the cell walls. Therefore, the growing exponential components of the solutions would have coefficients that are essentially zero in order to satisfy the temperature constraint at the cell walls.

The temperature and flux continuity conditions at the sample surfaces are explicitly given by

$$\theta = \frac{\beta I_0}{2k_s(\beta^2 - \sigma_s^2)} \left(\frac{(r-1)(b+1) \exp(\sigma_s l) - (r+1)(b-1) \exp(-\sigma_s l) + 2(b-r) \exp(-\beta l)}{(g+1)(b+1) \exp(\sigma_g l) - (g-1)(b-1) \exp(-\sigma_g l)} \right), \quad (9)$$

where

$$b = \frac{k_g \mu_g}{k_s a_s}, \quad (10)$$

$$g = \frac{k_g \mu_g}{k_g \mu_g}, \quad (11)$$

$$r = (1 - j) \frac{\beta}{2a_s}, \quad (12)$$

and as stated earlier $\sigma_s = (1 + j)a_s$. Thus, Eq. (9) can be evaluated for specific parameter values yielding a complex number whose real and imaginary parts θ_1 and θ_2 , respectively, determine the in-phase and quadrature components of the periodic temperature variation at the

where the subscripts s , b , and g identify the solution to Eq. (4) for the temperature in the solid, backing, and gas, respectively. These constraints apply separately to the dc component and the sinusoidal component of the solution. From Eqs. (8), we obtain for the dc components of the solution

$$\theta_0 = e_1 + d, \quad (7a)$$

$$W_0 = e_1 - e_2 l + d \exp(-\beta l), \quad (7b)$$

$$-(k_s/l_b)\theta_0 = k_s e_2 + k_s \beta d, \quad (7c)$$

$$(k_g/l_g)W = k_g e_2 + k_g \beta d \exp(-\beta l). \quad (7d)$$

Equations (7) determine the coefficients e_1 , e_2 , W_0 , and θ_0 for the time-independent (dc) component of the solution. Applying Eqs. (8) to the sinusoidal component of the solution yields

$$\theta = U + V - E, \quad (8a)$$

$$W = U \exp(-\sigma_s l) + V \exp(\sigma_s l) - E \exp(-\beta l), \quad (8b)$$

$$-k_s \sigma_s \theta = k_s \sigma_s U - k_s \sigma_s V - k_s \beta E, \quad (8c)$$

and

$$\begin{aligned} k_g \sigma_g W &= U \exp(-\sigma_g l) - k_g \sigma_g V \exp(\sigma_g l) \\ &\quad - k_g \beta E \exp(-\beta l). \end{aligned} \quad (8d)$$

These equations together with the expression for E in Eq. (5b) determine the coefficients U , V , W , and θ . Hence the solutions to Eqs. (7) and (8) allow us to evaluate the temperature distribution, Eq. (4), in the cell in terms of the optical, thermal, and geometric parameters of the system. The explicit solution for θ , the complex amplitude of the periodic temperature at the solid-gas boundary ($x = 0$), is given by

surface $x = 0$ of the sample. Specifically, the actual temperature at $x = 0$ is given by

$$T(0, t) = \Phi + \theta_0 + \theta_1 \cos \omega t - \theta_2 \sin \omega t,$$

where Φ is the ambient temperature at the cell walls and θ_0 is the increase in temperature due to the steady-state component of the absorbed heat.

IV. PRODUCTION OF THE ACOUSTIC SIGNAL

As stated in Sec. I, it is our contention that the main source of the acoustic signal arises from the periodic heat flow from the solid to the surrounding gas. The

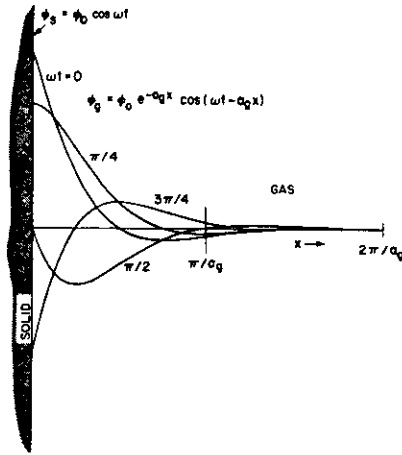


FIG. 2. Spatial distribution of the time-dependent temperature within the gas layer adjacent to the solid surface.

periodic diffusion process produces a periodic temperature variation in the gas as given by the sinusoidal (ac) component of the solution, Eq. (4),

$$\phi_{ac}(x, t) = \theta \exp(-\sigma_g x + j\omega t). \quad (13)$$

Taking the real part of Eq. (13), we see that the actual physical temperature variation in the gas is

$$T_{ac}(x, t) = \exp(-a_g x) [\theta_1 \cos(\omega t - a_g x) - \theta_2 \sin(\omega t - a_g x)], \quad (14)$$

where θ_1 and θ_2 are the real and imaginary parts of θ , as given by Eq. (9). As can be seen in Fig. 2, the time-dependent component of the temperature in the gas attenuates rapidly to zero with increasing distance from the surface of the solid. At a distance of only $2\pi/a_g = 2\pi\mu_g$, where μ_g is the thermal diffusion length, the periodic temperature variation in the gas is effectively fully damped out. Thus we can define a boundary layer, as shown in Fig. 1, whose thickness is $2\pi\mu_g$ (≈ 0.1 cm at $\omega/2\pi = 100$ Hz), and maintain to a good approximation that only this thickness of gas is capable of responding thermally to the periodic temperature at the surface of the sample.

The spatially averaged temperature of the gas within this boundary layer as a function of time can be determined by evaluating

$$\bar{\phi}(t) = (1/2\pi\mu_g) \int_0^{2\pi\mu_g} \phi_{ac}(x, t) dx.$$

From Eq. (13) this gives

$$\bar{\phi}(t) \approx (1/2\sqrt{2}\pi)\theta \exp[j(\omega t - \frac{1}{2}\pi)], \quad (15)$$

$$Q = \frac{\beta l \gamma P_0}{2\sqrt{2} k_s \mu_s T_0 (\beta^2 - \sigma_s^2)} \left(\frac{(\gamma-1)(b+1) \exp(\sigma_s l) - (\gamma+1)(b-1) \exp(-\sigma_s l) + 2(b-\gamma) \exp(-\beta l)}{(g+1)(b+1) \exp(\sigma_s l) - (g-1)(b-1) \exp(-\sigma_s l)} \right), \quad (21)$$

where $b = k_s \mu_s / k_g \mu_g$, $g = k_s \mu_s / k_g \mu_g$, $\tau = (1-j)\beta/2a_s$, and $\sigma_s = (1+j)a_s$, as previously defined. At ordinary tem-

using the approximation $\exp(-2\pi) \ll 1$.

Because of the periodic heating of the boundary layer, this layer of gas expands and contracts periodically and thus can be thought of as acting as an acoustic piston on the rest of the gas column, producing an acoustic pressure signal that travels through the entire gas column. A similar argument has been used successfully to account for the acoustic signal produced when a conductor in the form of a thin flat sheet is periodically heated by an ac electrical current.¹⁵

The displacement of this gas piston due to the periodic heating can be simply estimated by using the ideal gas law,

$$\delta x(t) = 2\pi\mu_g \frac{\bar{\phi}(t)}{T_0} = \frac{\theta\mu_g}{\sqrt{2}T_0} \exp[j(\omega t - \frac{1}{2}\pi)], \quad (16)$$

where we have set the average dc temperature of this gas boundary layer equal to the dc temperature at the solid surface, $T_0 = \Phi + \theta_0$. Equation (16) is a reasonable approximation to the actual displacement of the layer since $2\pi\mu_g$ is only ~ 0.1 cm for $\omega/2\pi = 100$ Hz and even smaller for higher frequencies.

If we assume that the rest of the gas responds to the action of this piston adiabatically, then the acoustic pressure in the cell due to the displacement of this gas piston is derived from the adiabatic gas law

$$PV^\gamma = \text{const},$$

where P is the pressure, V the gas volume in the cell, and γ the ratio of the specific heats. Thus the incremental pressure is

$$\delta P(t) = \frac{\gamma P_0}{V_0} \delta V = \frac{\gamma P_0}{V_0} \delta x(t),$$

where P_0 and V_0 are the ambient pressure and volume, respectively and δV is the incremental volume. Then from Eq. (16)

$$\delta P(t) = Q \exp[j(\omega t - \frac{1}{2}\pi)], \quad (17)$$

where

$$Q = \frac{\gamma P_0 \theta}{\sqrt{2} l \mu_s T_0}. \quad (18)$$

Thus the actual physical pressure variation, $\Delta P(t)$, is given by the real part of $\delta P(t)$ as

$$\Delta P(t) = Q_1 \cos(\omega t - \frac{1}{2}\pi) - Q_2 \sin(\omega t - \frac{1}{2}\pi), \quad (19)$$

or

$$\Delta P(t) = q \cos(\omega t - \psi - \frac{1}{2}\pi), \quad (20)$$

where Q_1 and Q_2 are the real and imaginary parts of Q and q and ψ are the magnitude and phase of Q , i.e.,

$$Q = Q_1 + jQ_2 = q \exp(-i\psi).$$

Thus Q specifies the complex envelope of the sinusoidal pressure variation. Combining Eqs. (9) and (18) we get the explicit formula

peratures $T_0 \approx \Phi$ so that the dc components of the temperature distribution need not be evaluated. Thus Eq.

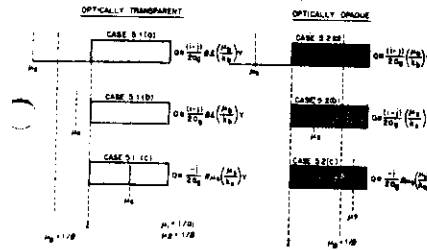


FIG. 3. Schematic representation of special cases discussed in the text.

(21) may be evaluated for the magnitude and phase of the acoustic pressure wave produced in the cell by the photoacoustic effect.

V. SPECIAL CASES

The full expression for $\delta P(t)$ is somewhat difficult to interpret because of the complicated expression for Q as given by Eq. (21). However, physical insight may be gained by examining special cases where the expression for Q becomes relatively simple. We group these cases according to the optical opaqueness of the solids as determined by the relation of the optical absorption length,

$$\mu_s = 1/\beta$$

to the thickness l of the solid. For each category of optical opaqueness, we then consider three cases according to the relative magnitude of the thermal diffusion length μ_s , as compared to the physical length l and the optical absorption length l . For all of the cases evaluated below, we make use of the reasonable assumption that $g < b$ and that $b \sim 1$, i.e., that $k_s \mu_s < k_g \mu_g$ and $k_s \mu_s \sim k_g \mu_g$.

The six cases are illustrated in Fig. 3. It is convenient to define

$$Y = \frac{\gamma P_0 l_0}{2\sqrt{2} l \mu_s T_0}, \quad (22)$$

which always appears in the expression for Q as a constant factor.

A. Case 5.1: Optically transparent solids ($\mu_s > l$)

In these cases, the light is absorbed throughout the length of the sample.

1. Case 5.1 (a): Thermally thin solids ($\mu_s \gg l$; $\mu_g > \mu_s$)

Here we set $\exp(-\beta l) \approx 1 - \beta l$, $\exp(\pm \sigma_s l) \approx 1$, and $|\tau| > 1$ in Eq. (21). We then obtain

$$Q = \frac{lY}{2a_s k_s \mu_s} (\beta - 2a_s b - j\beta) \approx \frac{(1-j)\beta l}{2a_s} \frac{\mu_g}{k_s} Y. \quad (23)$$

The acoustic signal is thus proportional to βl and, since a_s is proportional to $1/\omega$, the acoustic signal has a ω^{-1} dependence. For this thermally thin case of $\mu_s \gg l$, the thermal properties of the backing material come into play in the expression for Q .

2. Case 5.1 (b): Thermally thin solids ($\mu_s > l$; $\mu_s < \mu_g$)

Here we set $\exp(-\beta l) \approx 1 - \beta l$, $\exp(\pm \sigma_s l) \approx (1 \pm \sigma_s l)$, and $|\tau| < 1$ in Eq. (21). We then obtain

$$Q = \frac{\beta l Y}{4k_s \mu_s a_s b} [(\beta^2 + 2a_s^2) + j(\beta^2 - 2a_s^2)] \approx \frac{(1-j)\beta l}{2a_s} \left(\frac{\mu_g}{k_s} \right) Y. \quad (24)$$

The acoustic signal is again proportional to βl , varies as ω^{-1} , and depends on the thermal properties of the backing material. Equation (24) is identical to Eq. (23).

3. Case 5.1 (c): Thermally thick solids ($\mu_s < l$; $\mu_s \ll \mu_g$)

In Eq. (21) we set $\exp(-\beta l) \approx 1 - \beta l$, $\exp(\pm \sigma_s l) \approx 0$, and $|\tau| < 1$. The acoustic signal then becomes

$$Q = -j \frac{\beta \mu_s}{2a_s} \left(\frac{\mu_g}{k_s} \right) Y. \quad (25)$$

Here the signal is now proportional to $\beta \mu_s$, rather than βl . That is, only the light absorbed within the first thermal diffusion length μ_s contributes to the signal, in spite of the fact that light is being absorbed throughout the length l of the solid. Also, since $\mu_s < l$, the thermal properties of the backing material present in Eq. (24) are replaced by those of the solid. The frequency dependence of Q in Eq. (25) varies as $\omega^{-3/2}$.

B. Case 5.2: Optically opaque solids ($\mu_s \ll l$)

In these cases, most of the light is being absorbed within a distance small compared to l .

1. Case 5.2 (a): Thermally thin solids ($\mu_s \gg l$; $\mu_s \gg \mu_g$)

In Eq. (21) we set $\exp(-\beta l) \approx 0$, $\exp(\pm \sigma_s l) \approx 1$, and $|\tau| \gg 1$. We then obtain

$$Q \approx \frac{(1-j)}{2a_s} \left(\frac{\mu_g}{k_s} \right) Y \quad (26)$$

In this case, we have photoacoustic "opaqueness" as well as optical opaqueness, in the sense that our acoustic signal is independent of β . This would be the case of a very black absorber such as carbon black. The signal is quite strong, [it is $1/\beta l$ times as strong as that in case 5.1(a)], and depends on the thermal properties of the backing material, and varies as ω^{-1} .

2. Case 5.2 (b): Thermally thick solids ($\mu_s < l$; $\mu_s > \mu_g$)

In Eq. (21) we set $\exp(-\beta l) \approx 0$, $\exp(\pm \sigma_s l) \approx 0$, and $|\tau| > 1$. We obtain

$$Q \approx \frac{Y}{2a_s k_s \mu_s} (\beta - 2a_s b - j\beta) \approx \frac{(1-j)}{2a_s} \left(\frac{\mu_g}{k_s} \right) Y. \quad (27)$$

Equation (27) is analogous to Eq. (26), but the thermal parameters of the backing are now replaced by those of the solid. Again the acoustic signal is independent of β and varies as ω^{-1} .

3. Case 5.2 (c): Thermally thick solids ($\mu_s \ll l$; $\mu_s < \mu_g$)

We set $\exp(-\beta l) \approx 0$, $\exp(\pm \sigma_s l) \approx 0$, and $|\tau| < 1$ in Eq. (21). We obtain

$$Q = \frac{-j\beta Y}{4a_s \mu_s k_s} (2a_s - \beta + j\beta) = \frac{-j\beta \mu_s}{2a_s} \left(\frac{\mu_g}{k_s} \right) Y. \quad (28)$$

This is a very interesting and important case. Optically we are dealing with a very opaque solid ($\beta l \gg 1$). However, as long as $\beta \mu_s < 1$, i.e., $\mu_s < \mu_g$, this solid is not photoacoustically opaque, since, as in case 5.1(c), only the light absorbed within the first thermal diffusion length, μ_s , will contribute to the acoustic signal. Thus even though this solid is optically opaque, the photoacoustic signal will be proportional to $\beta \mu_s$. As in case 5.1(c), the signal is also dependent in the thermal properties of the solid and varies as $\omega^{-3/2}$.

VI. CONCLUSIONS

A theoretical analysis of the photoacoustic effect with solids has been performed. In this analysis we have assumed that the primary source of the acoustic signal arises from the periodic heat flow from the solid to the surrounding gas. This periodic heat flow causes an oscillatory motion of a narrow layer of gas at the solid-gas boundary, and it is this motion of the gas layer that produces the acoustic signal detected in the photoacoustic cell. We have derived the exact solutions for the acoustic pressure produced in the cell due to the process and have evaluated explicit formulas for certain cases of physical significance.¹⁶ The formulas developed for the special cases have been found to give numerical results for magnitude and phase of the acoustic signal that are in good agreement with the experimental data. This agreement supports our explanation for the mechanism underlying the photoacoustic effect with solids. A full comparison of theory and experiment will be published in a later paper.

Our formulas show that the photoacoustic signal is ultimately governed by the magnitude of the thermal diffusion length of the solid. Thus even when a solid is optically opaque, it is not necessarily opaque photoacoustically and, in fact, as long as $\beta \mu_s < 1$, the photoacoustic signal will be proportional to β , even though

the optical thickness βl of the sample may be much greater than unity. Since the thermal diffusion length μ_s can be changed by changing the chopping frequency ω , it is therefore possible, with the photoacoustic technique, to obtain optical absorption spectra on any, but the most highly opaque, solids. This capability of the PAS technique together with its insensitivity to scattered light makes its use as a spectroscopic tool for the investigation of solid and semisolid materials highly attractive. In particular, these features give the photoacoustic technique a unique potential for noninvasive *in vivo* studies of human tissues, a potential which may have important implications in biological and medical research and in medical diagnostics.

¹A. G. Bell, Am. J. Sci. 20, 305 (1880).

²J. Tyndall, Proc. R. Soc. London 31, 307 (1881).

³W. C. Röntgen, Philos. Mag. 11, 308 (1881).

⁴A. G. Bell, Philos. Mag. 11, 510 (1881).

⁵T. H. Maugh II, Science 188, 38 (1975).

⁶A. Rosencwaig, Opt. Commun. 7, 305 (1973).

⁷A. Rosencwaig, Science 181, 657 (1973).

⁸A. Rosencwaig and S. S. Hall, Anal. Chem. 47, 548 (1975).

⁹A. Rosencwaig, Phys. Today 28(No. 9), 23 (1975); Anal. Chem. 47, 592A (1975).

¹⁰Lord Rayleigh, Nature 23, 274 (1881).

¹¹W. H. Preece, Proc. R. Soc. London 31, 506 (1881).

¹²M. E. Mercadier, C.R. Acad. Sci. (Paris) 92, 409 (1881).

¹³A recent treatment of the photoacoustic effect with solid by Parker [Appl. Opt. 12, 2974 (1973)] also assumes that the signal is produced by heat conduction from solid sample to surrounding gas. His treatment, however, assumes an anomalously high absorption coefficient for a thin surface layer of the solid.

¹⁴A more exact treatment for the gas can be derived using equations of fluid dynamics. However, the approximate treatment given here gives results consistent with the more exact method, and has the advantage of presenting a simpler physical description of the process.

¹⁵H. D. Arnold and I. B. Crandall, Phys. Rev. 10, 22 (1917).

¹⁶It should be noted that we have not considered here the effects of reflection losses at the surface.

Generalized theory of the photoacoustic effect

F. Alan McDonald and Grover C. Wetsel, Jr.

Department of Physics, Southern Methodist University, Dallas, Texas 75275
(Received 22 July 1977; accepted for publication 14 November 1977)

The theory of the photoacoustic effect is extended to include the contribution of mechanical vibration of the sample. Coupled equations for thermal and acoustic waves are solved in both sample and gas. It is shown that the pressure signal in the gas may be significantly affected by acoustic coupling in the sample, and experimental confirmation of this extended theory is given. The results of the fully coupled treatment are shown to be accurately reproduced by an extension of the Rosencwaig piston model: the pistonlike motion of the gas boundary layer adjoining the sample is superimposed on the mechanical vibration of the sample surface to give a composite piston displacement which then produces the pressure signal in the gas. The composite-piston model provides relatively simple algebraic results applicable to many cases of physical interest.

PACS numbers: 43.35.Sx, 78.20.Hp, 07.65.-b, 82.80.Di

I. INTRODUCTION

The photoacoustic effect was discovered by Alexander Graham Bell,¹ who found that an acoustic signal was produced when a sample in an enclosed cell was illuminated with light having a periodically varying intensity (i.e., "chopped" light). This effect provides a means for the study of optical absorption in the sample, such studies being called photoacoustic spectroscopy (PAS). Photoacoustic spectroscopy has been used in studies of gases² and, more recently, solid³⁻⁵ and liquid⁴⁻⁶ samples as well. Theoretical models for the effect in solids have been developed by Parker,⁷ and by Rosencwaig and Gersho⁸ (RG), with further development by the present authors⁹ and by Aamodt, Murphy, and Parker¹⁰ (AMP). These models have been found to give reasonably good agreement with experimental results (for both solid and liquid samples), and, thus, the basic mechanisms responsible for the photoacoustic effect seem to be well understood.

The main goal of theoretical models of the photoacoustic effect is to allow interpretation of the PAS signal in terms of optical absorption in the sample. In the work of RG and AMP, the effect of physical and thermal properties of the system on the PAS signal has been delineated in order to show the relation of PAS spectra to normal absorption spectra. The present authors have shown¹¹ that absolute absorption coefficients (as distinct from relative spectra) may be determined at any optical wavelength by measuring the PAS signal as a function of chopping frequency. In that work, the theoretical model for solids was assumed to be valid for liquids as well. Adams and Kirkbright¹² have used the phase of the PAS signal to determine thermal properties of transparent materials. All of these applications require a proper theoretical basis to interpret the experimental data.

The acoustic signal in a typical PAS cell (see Fig. 1) has been understood as due to the periodic heating of the enclosed gas as a result of absorption of chopped light by the sample. Thermal diffusion from the sample causes a temperature variation in a thin layer of the gas at the gas-sample boundary. The resulting pistonlike behavior of this layer was used by RG⁸ to calculate the pressure variation in the gas. The present authors and AMP¹⁰ have used a more complete hydrodynamic treatment of the gas in order to consider cell lengths for

which the piston argument is inadequate. Bennett and Forman¹³ have used a similar treatment to study weak absorption in glasses used as cell windows (i.e., the window is also the sample). In all previous work, the effect of mechanical vibration of the sample has not been included in calculation of the PAS signal.

In the present work, we allow for acoustic waves in the (solid or liquid) sample as well as the gas by solving coupled equations for pressure and temperature in both media. We show that the PAS signal may be appreciably affected within the frequency range usually used for spectroscopic studies. The results of the full coupled treatment are shown to be equivalent to an amplification of the piston model in which the thermal piston vibration and the mechanical vibration of the sample surface are superimposed. This latter view enables us to specify the conditions under which sample motion will be important in a form easily accessible to the potential PAS experimentalist. The modification necessary for resonant or near-resonant cells is also presented. In the course of our discussion, we present some graphical representations of the theoretical results as aids to experimental considerations.

II. THEORY

A. Outline of theory

We consider a one-dimensional treatment of the acoustic and thermal processes in the PAS cell of Fig. 1, assuming that absorption of the modulated light beam gives an (essentially) instantaneous source of thermal energy. This requires use of coupled equations for acoustic-wave motion and thermal diffusion in sample and gas, with proper account of boundary conditions;

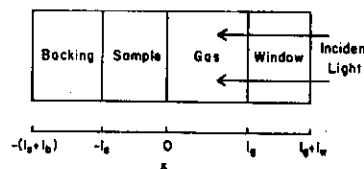


FIG. 1. Schematic diagram of typical photoacoustic cell, showing coordinates used in text.

only thermal diffusion is considered in the window and backing, but the numerical solutions obtained could easily be modified to include mechanical vibration here as well.

The coupled linear equations for the time-dependent pressure and temperature in a fluid are written (ignoring viscosity)¹⁴

$$\nabla^2 p - \frac{\rho_0}{B} \frac{\partial^2 p}{\partial t^2} = -\rho_0 \beta_T \frac{\partial^2 T}{\partial t^2}, \quad (1)$$

$$\kappa \nabla^2 T - \frac{\kappa}{\alpha} \frac{\partial T}{\partial t} + S = -T_0 \beta_T \frac{\partial p}{\partial t}, \quad (2)$$

where ρ_0 and T_0 are ambient density and temperature, respectively, B is the isothermal bulk modulus, β_T is the (volume) coefficient of thermal expansion, κ is the thermal conductivity, α is the thermal diffusivity ($= \kappa/\rho_0 C_p$, with C_p the heat capacity at constant pressure), and S (present in the sample only) represents the thermal-energy source due to optical absorption. If the intensity of incident light is I_0 (assumed uniform), and the optical-absorption coefficient is β , then the heat density at any point in the sample (where x is negative) is

$$H(x, t) = \beta I_0 \exp(\beta x) \left(\frac{1}{2} + \frac{1}{2} \cos \omega t \right),$$

where it is assumed for simplicity that all absorbed light is converted to thermal energy and that the light is sinusoidally chopped. If p and T have time dependence $\exp(j\omega t)$ (with the real parts of the solutions representing the physical variables, as usual), then Eqs. (1) and (2) become

$$\frac{\partial^2 p}{\partial x^2} - \frac{\rho_0 \omega^2}{B} p = \rho_0 \beta_T \omega^2 T, \quad (3)$$

$$\frac{\partial^2 T}{\partial x^2} - j \frac{\omega}{\alpha} T + A \exp(\beta x) \exp(j\omega t) = -j \frac{T_0 \beta_T \omega}{\kappa} p, \quad (4)$$

where $A = \beta I_0 / 2\kappa$. It has been shown¹⁵ that plane-wave solutions of the appropriate coupled equations (for temperature and displacement) in isotropic solids have the same form as plane-wave solutions of Eqs. (3) and (4), so that our basic approach applies to both liquid and isotropic solid samples.

Solutions to Eqs. (3) and (4) for the sample have the form (suppressing the time dependence)

$$p = P_A \exp(jkx) + P'_A \exp(\beta x), \quad (5)$$

$$T = T_A \exp(jkx) + T'_A \exp(\beta x); \quad (6)$$

substitution of these forms into Eqs. (3) and (4) leads to four equations for the amplitude factors:

$$(-k^2 + \rho_0 \omega^2/B) P_A - \rho_0 \beta_T \omega^2 T_A = 0, \quad (7)$$

$$(-k^2 - j\omega/\alpha) T_A + (j\omega T_0 \beta_T / \kappa) P_A = 0;$$

$$(\beta^2 + \rho_0 \omega^2/B) P'_A - \rho_0 \beta_T \omega^2 T'_A = 0,$$

$$(\beta^2 - j\omega/\alpha) T'_A + (j\omega T_0 \beta_T / \kappa) P'_A = -A. \quad (8)$$

Equations (7) combine to give a quadratic equation in k^2 , with solutions

$$k^2 = -\frac{1}{2} (j\omega/\alpha - \rho_0 \omega^2/B) \pm \left\{ \frac{1}{4} (j\omega/\alpha - \rho_0 \omega^2/B)^2 - j\omega^3 \rho_0 [T_0 \beta_T / \kappa - (B\alpha)^{-1}] \right\}^{1/2}. \quad (9)$$

Study of typical values of the constants shows that one solution is essentially that for an uncoupled acoustic wave in the sample,

$$k_a^2 \equiv k_s^2 = \rho_0 \omega^2/B, \quad (10)$$

while the other is essentially that for the thermal "wave",

$$-k_t^2 \equiv \sigma_s^2 = j\omega/\alpha. \quad (11)$$

(This thermal wave is rapidly attenuated.) At typical PAS frequencies (10–1000 Hz), the corrections to these approximate expressions are negligible. The amplitude ratio (P_A/T_A) has a distinct value for each solution, k_a^2 for the acoustic mode ($k^2 = k_s^2$),

$$d_{aa} = (P_A/T_A)_a = \kappa/(\alpha \beta_T T_0), \quad (12)$$

and for the thermal mode ($k^2 = -\sigma_s^2$),

$$d_{tt} = (P_A/T_A)_t = -j\rho_0 \beta_T \alpha \omega. \quad (13)$$

Finally Eqs. (8) have solutions

$$T'_A = -A/(\beta^2 - \sigma_s^2), \quad (14)$$

$$P'_A = d_{tt} T'_A, \quad (15)$$

where

$$d_{tt} = \rho_0 \beta_T \omega^2 (\beta^2 + \rho_0 \omega^2/B)^{-1}. \quad (16)$$

The harmonic solution in the sample is, thus,

$$T_s = A_s \exp(-jk_s x) + B_s \exp(jk_s x) + C_s \exp(-\sigma_s x) + D_s \exp(\sigma_s x) + T'_A \exp(\beta x), \quad (17)$$

$$p_s = d_{aa} [A_s \exp(-jk_s x) + B_s \exp(jk_s x)] + d_{tt} [C_s \exp(-\sigma_s x) + D_s \exp(\sigma_s x)] + d_{tt} T'_A \exp(\beta x). \quad (18)$$

Solutions to Eqs. (3) and (4) for the gas (omitting the source term S) are obtained in the same way. However, the gas is assumed to obey the ideal gas law, so that $B = P_0$ (the ambient pressure), and $\beta_T = (T_0)^{-1}$. Then the two solutions for k^2 are, for the acoustic mode,

$$k_g^2 \approx \omega^2 \rho_g / (\gamma P_0) \quad (19)$$

(γ is the ratio of specific heats C_p/C_v) and, for the thermal mode,

$$\sigma_g^2 = j\omega/\alpha_g, \quad (20)$$

where subscripts on ρ and α emphasize that these are gas density and thermal diffusivity, respectively. The pressure-temperature ratios are

$$d_{ag} = \kappa_g/\alpha_g, \quad (21)$$

$$d_{tg} = -j\omega \alpha_g \rho_g / T_0. \quad (22)$$

The solution in the gas is, then,

$$T_g = A_g \exp(-jk_g x) + B_g \exp(jk_g x) + C_g \exp(-\sigma_g x) + D_g \exp(\sigma_g x), \quad (23)$$

$$p_g = d_{ag} [A_g \exp(-jk_g x) + B_g \exp(jk_g x)] + d_{tg} [C_g \exp(-\sigma_g x) + D_g \exp(\sigma_g x)]. \quad (24)$$

The temperature distributions in window and backing are easily seen to have the form

$$T = C \exp(-\alpha x) + D \exp(\alpha x), \quad (25)$$

with α or b subscripts on T, C, D , and D .

The 12 coefficients (A_s, B_s, \dots) in Eqs. (17), (18), and (23)–(25) are determined by imposing eight boundary conditions on the continuity of temperature and heat flux,

$$T_w = 0 \quad \text{at } x = l_w + l_g, \quad (26)$$

$$T_w = T_g \quad \text{at } x = l_g, \quad (27)$$

$$\kappa_w \frac{\partial T_w}{\partial x} = \kappa_g \frac{\partial T_g}{\partial x} \quad \text{at } x = l_g, \quad (28)$$

$$T_g = T_s \quad \text{at } x = 0, \quad (29)$$

$$\kappa_g \frac{\partial T_g}{\partial x} = \kappa_s \frac{\partial T_s}{\partial x} \quad \text{at } x = 0, \quad (30)$$

$$T_s = T_b \quad \text{at } x = -l_s, \quad (31)$$

$$\kappa_s \frac{\partial T_s}{\partial x} = \kappa_b \frac{\partial T_b}{\partial x} \quad \text{at } x = -l_s, \quad (32)$$

$$T_b = 0 \quad \text{at } x = -l_s - l_b, \quad (33)$$

three boundary conditions on velocity (with $v = (j/\omega \rho_0) \times (dp/dx)$),

$$v_g = 0 \quad \text{at } x = l_g, \quad (34)$$

$$v_g = v_s \quad \text{at } x = 0, \quad (35)$$

$$v_s = 0 \quad \text{at } x = -l_s, \quad (36)$$

and the continuity of pressure

$$p_g = p_s \quad \text{at } x = 0. \quad (37)$$

Equations (26) and (33) allow immediate elimination of two coefficients (e.g., D_w and C_b), leaving a set of ten inhomogeneous linear equations for the remaining coefficients; the last terms in Eqs. (17) and (18) give the inhomogeneous elements of this set of equations. These equations may be solved algebraically, but the resulting expressions are very involved and, thus, not very instructive. Numerical solution by matrix techniques is almost as fast as numerical evaluation of the algebraic expressions for the coefficients. (Approximate algebraic expressions are given in Sec. IV.)

The spatial dependence of the solutions suggests the introduction of several length parameters which will be useful in the subsequent discussion. The thermal diffusion length μ_t is the distance over which a thermal wave is damped by e^{-1} ; if $\alpha_t = \text{Re}(\sigma_t)$, then $\mu_t = \alpha_t^{-1} = (2\alpha_t/\omega)^{1/2}$, where t indicates gas, sample, etc. The optical-absorption length is the distance over which the light intensity is reduced by e^{-1} : $\mu_s = \beta^{-1}$.

B. Comparison with previous work

Before turning to the results of these calculations in Sec. III, it seems appropriate to indicate how our present approach differs from previous work. Thermal-

diffusion equations only were solved by RG, so no acoustic mode was coupled in. They also assumed that the gas and backing are "thermally thick" (i.e., $\mu_g \ll l_g$, etc.) so that some terms in τ are negligible; this is achieved in our equations by setting C_w, D_w, D_g , and C_s zero, as well as setting all A_i and B_i zero. Then one has four coefficients left which satisfy the four boundary conditions of Eqs. (29)–(32). The result for C_g establishes the amplitude of temperature variation in the boundary layer of gas near $x = 0$, which is converted to an amplitude of vibration for a thermal "piston" which, in turn, gives the pressure variation in the cell (see Appendix B). The RG piston model assumes uniform pressure throughout the gas, so one might expect correct results when $l_g \ll \lambda_g$, where λ_g is the acoustic wavelength in the gas for the chosen chopping frequency.

Interest in the chopping-frequency dependence of the PAS signal led the present authors to reconsider the approximate treatment of the gas and to use a coupled-equation treatment of the gas pressure and temperature.⁹ That work (which we will refer to as MW1) assumed no acoustic mode in the sample ($A_s = B_s = 0$), assumed that $v_s = 0$ at $x = 0$ [cf. Eq. (35)], and did not use Eqs. (36) and (37); the algebraic result is given in Appendix A. The results essentially confirmed those of RG under their stated assumptions, but allowed one to consider the case of "thermally thin" gas ($l_g \ll \mu_g$) which will occur as either $\omega \rightarrow 0$ or $l_g \rightarrow 0$. The possibility of acoustic resonances in the cell is also included in this treatment.

Recent work of AMP emphasized the dependence of the PAS signal on the gas length. Their approach differs from MW1 only in that they assume the window and backing to be thermally thick, which is equivalent to setting D_w and C_b zero and omitting Eqs. (26) and (33). For normal PAS frequencies, this is quite adequate, but it does not allow the limit $\omega \rightarrow 0$. The algebraic expression of MW1 is compared with the result of AMP in Appendix A.

Finally, we note a similarity between the basic mechanisms involved in the photoacoustic effect and those involved in some recent work on thermoacoustics,¹⁶ wherein thermal expansion caused by the absorption of modulated laser light gives rise to an acoustic wave in the absorbing medium. The essential differences, in principle, are that the PAS signal is detected in the gas, not in the absorbing sample, and that the signal has been considered as caused by heat flow from the sample, not by thermal expansion of the sample. Clearly, the work reported here, showing an appreciable effect due to acoustic waves in the sample, makes the similarity between photoacoustic effect and thermoacoustic effect more apparent. Nevertheless, the emphasis in PAS is on the study of sample absorption, not on the generation of acoustic waves.

C. Theoretical results

The results of the full coupled-equations treatment outlined in the previous Sec. IIB (labeled MW2) are shown in Fig. 2, along with those of RG, for a dye solution in water. This type of sample has been used previously because one can readily vary the absorption co-

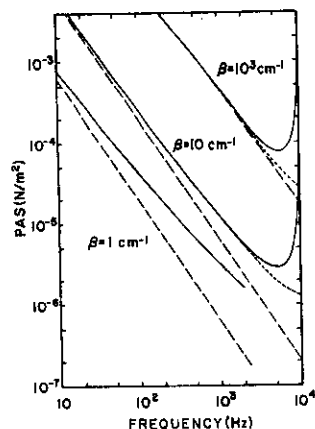


FIG. 2. Theoretical values of photoacoustic signal (PAS) for three values of absorption coefficient β . Solid curves show values from the present work (MW2) with $x = l_s$, short-dashed (---) curves with $x = 0.5 l_s$, illustrating the effect of resonance on the signal near 10 kHz. Long-dashed (---) curves show values from the theory of Rosenzweig and Gersho (RG). Material parameters are given in Table I: for water, $\beta_T = 2.1 \times 10^{-4}/^\circ\text{C}$, $B = 2 \times 10^9 \text{ N/m}^2$. Cell parameters are $l_s = 0.48 \text{ cm}$, $l_r = 1.74 \text{ cm}$, $l_w = l_b = 0.2 \text{ cm}$.

efficient in order to compare theoretical calculations with experimental data. (The material properties used in these calculations are listed in Table I.) As the absorption coefficient is reduced, the effect of acoustic coupling in the sample becomes appreciable, the relative effect increasing with chopping frequency. At $f = 100 \text{ Hz}$, the acoustic coupling effect gives $\sim 20\%$ of the signal for $\beta = 10 \text{ cm}^{-1}$ and $\sim 50\%$ of the signal for $\beta = 1 \text{ cm}^{-1}$. At $f = 1000 \text{ Hz}$, the effect is $\sim 80\%$ of the signal for $\beta = 1 \text{ cm}^{-1}$. The frequency range shown extends to the first resonance frequency for the gas length used in order to show how this resonance affects the PAS signal (acoustic resonance might also occur in this sample, but at $f \approx 7 \times 10^4 \text{ Hz}$). In this frequency range, RG and MW1 differ significantly only where resonance effects are important.

The low-frequency behavior of the calculated results is shown in Fig. 3. Although these frequencies are not expected to be used in PAS, the behavior in this range helps to elucidate the mechanisms responsible for the

TABLE I. Material properties used in theoretical calculations of photoacoustic signal.

Material	$\alpha \text{ (m}^2/\text{s)}$	$\kappa \text{ (W/m}^2\text{K)}$	$\rho \text{ (kg/m}^3)$
Air	2.15×10^{-5}	0.0258	1.2
Water	1.48×10^{-7}	0.61	1000.
Brass	2.9×10^{-5}	96.3	
Plexiglas	1.13×10^{-7}	0.16	
Glass	5.1×10^{-7}	0.88	

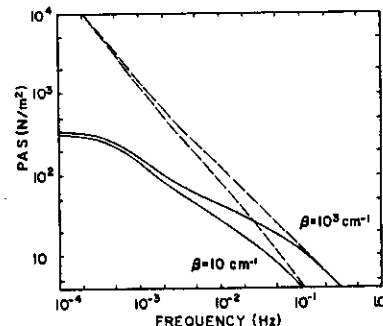


FIG. 3. Theoretical values of photoacoustic signal (PAS) at low chopping frequency. Notation is that of Fig. 2.

varying-frequency dependence of the signal. It was pointed out by RG that the signal decreases as ω^{-1} when the sample thermal-diffusion length μ_s is much greater than the optical-absorption length μ_a , but as $\omega^{-3/2}$ when $\mu_s \ll \mu_a$ (see Appendix B). The transition occurs near 400 Hz for $\beta = 1000 \text{ cm}^{-1}$ in the dye-water sample, but for $\beta = 10 \text{ cm}^{-1}$, the transition occurs near 0.04 Hz. The other significant transitions occur when the gas, sample, backing, or window become thermally thin (viz., $l_g < \mu_g$, etc.). For the sample-cell parameters used here, these transitions occur in the range 0.01–0.2 Hz (e.g., $\mu_g \approx l_g$ at $\sim 0.02 \text{ Hz}$). Below this region, the signal “rolls over” (with decreasing ω) and approaches a finite limit depending on cell and thermal parameters; this limit is clearly related to the time-independent solution for the temperature due to an unmodulated light beam. The correct limit is obtained from MW1

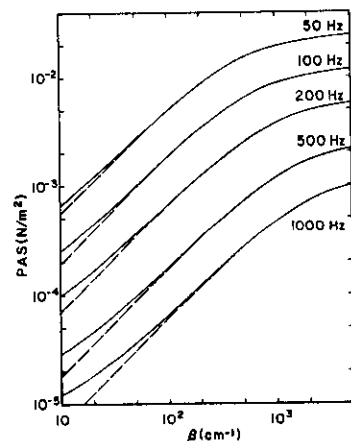


FIG. 4. Dependence of photoacoustic signal on absorption coefficient β for opaque samples. Notation is that of Fig. 2.

F.A. McDonald and G.C. Wetsel, Jr.

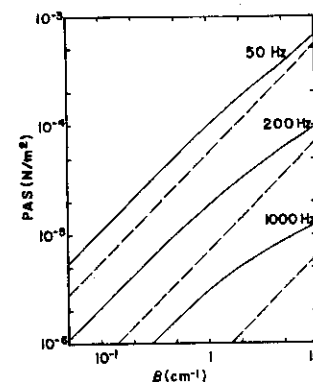


FIG. 5. Dependence of photoacoustic signal on absorption coefficient β for transparent samples. Notation is that of Fig. 2.

and MW2, provided one is careful with the considerable algebraic cancellation which occurs in taking the limit. The difference in MW1 and MW2 is negligible at these low frequencies.

The dependence of the PAS signal on absorption coefficient β is illustrated for opaque samples in Fig. 4. In order to interpret a PAS spectrum as equivalent to a normal absorption spectrum, one wishes the PAS signal to be proportional to β . For the water-dye sample used here, the effect of acoustic coupling in the sample becomes appreciable as β decreases, such that the signal does not decrease linearly with decreasing β . In the intermediate region between low β and signal saturation at high β , the signal is still essentially linear in β . The choice of chopping frequency allows some flexibility in achieving linearity for a given sample.

The dependence of PAS signal on β , for transparent samples, is illustrated in Fig. 5. If $\beta_s \ll 1$, the effect of acoustic coupling is proportional to β_s (see Sec. IV). Thus, the net signal is also linear in β , but at a significantly higher level than is predicted without acoustic coupling. When viewed together, Figs. 4 and 5 suggest that the PAS signal is roughly linear over a broad range of β values up to the point of signal saturation ($\beta_s > 1$) with some distortion when $\beta_s \sim 1$.

III. EXPERIMENTAL RESULTS

In order to evaluate the theoretical model of Sec. II, the photoacoustic signal was measured as a function of chopping frequency for samples having widely disparate values of optical-absorption coefficient. Two concentrations of a common pH indicator, phenol red sodium salt dissolved in distilled water, were used as samples. Light of 488-nm wavelength and about 70-mW power from an argon-ion laser was chopped by a Princeton Applied Research Corp. Model 192 variable-speed chopper and directed through a fused-silica window into an O-ring-sealed sample cell. A General Radio Model

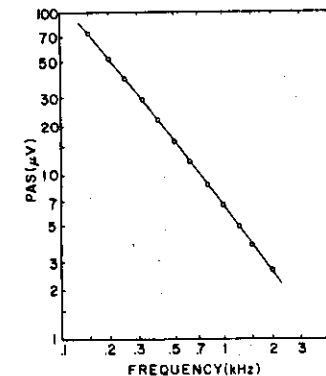


FIG. 6. Experimentally determined photoacoustic signal for phenol red sodium salt in distilled water, 25 g/l. The solid curve represents the best fit to the data using the full theoretical treatment given in the text: $\beta = 1.1 \times 10^3 \text{ cm}^{-1}$, $I_0 = 380 \text{ W/m}^2$.

1962 Electret-Condenser microphone with Model 1972-9600 preamplifier was used to detect the photoacoustic signal which was then processed by a Princeton Applied Research Corp. Model 186A Lock-In amplifier or by a Princeton Applied Research Corp. Model 5204 Lock-In Analyzer. The data-taking procedure, described previously,¹¹ allowed correction for coherent noise. The sample-cell parameters were as follows: $l_s = 0.63 \text{ cm}$, $l_r = 1.7 \text{ cm}$, $l_b = 0.32 \text{ cm}$, and $l_w = 0.32 \text{ cm}$.

The experimental points for two concentrations, 25 g/l and 0.25 g/l, are shown in Figs. 6 and 7, respectively, along with theoretical curves. The values of β indicated in Figs. 6 and 7 were determined by compari-

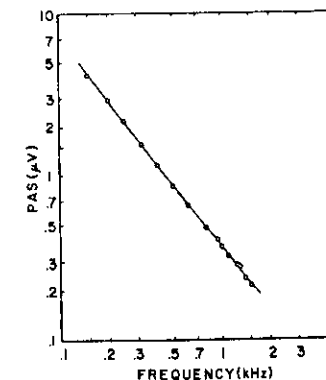


FIG. 7. Experimentally determined photoacoustic signal for phenol red sodium salt in distilled water, 0.25 g/l. The solid curve represents the best fit to the data using the full theoretical treatment given in the text: $\beta = 9.6 \text{ cm}^{-1}$, $I_0 = 870 \text{ W/m}^2$.

F.A. McDonald and G.C. Wetsel, Jr.

son of data with theory using a computer-search procedure which minimizes the rms percentage deviation of the theoretical from the experimental value by allowing both β and l_0 to vary.¹¹ The relative frequency dependence of the data essentially determines the value of β , with l_0 simply a normalizing factor. The agreement of theory (MW2) with data is apparent for both values of β . For the higher value of β , the theoretical curves of RG and MW2 are only slightly different over the frequency range of the data, as shown in Fig. 2. For the lower value of β , however, there is a marked difference in frequency dependence between RG and MW2 due to the effect of acoustic coupling. In fact, if one assumes that acoustic coupling is negligible in the case of the lower-concentration sample and attempts to force a fit of the RG theory to the data of Fig. 7 using the procedure described above, one obtains a value of β about two orders of magnitude too high ($\sim 1200 \text{ cm}^{-1}$)

The values of β determined by the above fitting procedure may be checked independently by extrapolating from values measured with a spectrophotometer at substantially lower concentrations. Assuming a power-law relation between absorption coefficient and concentration, a straight-line extrapolation (on a log-log plot) gives 1100 ± 100 and $10.5 \pm 0.4 \text{ cm}^{-1}$ for the higher and lower concentrations, respectively. The two β values for the higher concentration agree quite well, while those for the lower concentration differ by about 10%. If the two data points at 1250 and 1300 Hz are excluded from the photoacoustic data in Fig. 7, a value of $\beta = 10.1 \text{ cm}^{-1}$ is obtained for the lower concentration. Thus, the theory gives β values which are in very good agreement with the spectrophotometric determination, allowing for some experimental uncertainty.

These experimental results, when interpreted using the theoretical model of the Sec. II, demonstrate that the photoacoustic signal can be significantly affected by coupling of thermal and acoustic waves in the sample.

IV. THE COMPOSITE-PISTON MODEL

A. Outline of the model

The solution of the full set of coupled equations [Eqs. (17), (18), and (23)–(25) with boundary conditions given in Eqs. (26)–(37)] has been shown to be a valid representation of the PAS signal. The complexity of those equations may tend to obscure the basic mechanisms involved, however, and so we present in this section a simplified approach which, in fact, reproduces the results of the full calculation (within $\sim 2\%$) over the normal PAS frequency range (10–1000 Hz).

The essential features of this simplified model are first briefly described. Absorption of chopped light causes periodic heating in the sample which produces pressure variations propagating in both directions (i.e., acoustic waves). The superposition of these waves at the sample surface gives rise to a surface motion which then serves as a boundary condition for the acoustic wave in the gas. Periodic heat flow to the gas simultaneously causes expansion and contraction within a thin boundary layer next to the sample which RG have characterized as a vibrating piston. If this thermal piston

is superimposed on the mechanical surface motion, the resulting "composite piston" produces the signal detected in the gas.

Implementation of this simplified approach rests on two facts: the temperature distribution in the system is hardly affected by the term coupling it to the pressure [right-hand side of Eq. (2) or (4)]; the surface motion of the sample is virtually independent of the periodic pressure variation in the gas. One may then obtain the final signal by the following sequential calculations: (1) Determine the temperature distribution in the system, ignoring the acoustic mode [set A_s, B_s, A_g , and B_g zero and use Eqs. (26)–(33)]. (2) Obtain the thermal-piston displacement as prescribed by RG. The displacement δx_s is equal to the boundary-layer thickness ($2\pi\mu_g$) times the ratio of spatially averaged temperature to ambient temperature in the gas layer (also see Appendix B). (3) Determine the surface displacement of the sample by solving Eq. (3) in the sample, with the temperature distribution from step (1) as a source term. The form of the pressure p_s is that of Eq. (18), but A_s and B_s are now determined by the boundary conditions that $p_s = 0$ at $x = 0$ and $v_s = 0$ at $x = -l_s$. Then the mechanical piston (i.e., sample surface) displacement is

$$\delta x_m = -\frac{i}{\omega} v_s(x=0) = (\omega^2 p_s)^{-1} \left(\frac{\partial p_s}{\partial x} \right)_0 \quad (38)$$

If the sample is thermally thick ($\mu_s \ll l_s$) and acoustically thin ($k l_s \ll 1$), the expression for δx_m becomes particularly simple:

$$\delta x_m(t) \approx \frac{1}{2} (-j\beta l_s / \omega \rho_s C_{ps}) [1 - \exp(-\beta l_s)] \exp(j\omega t). \quad (39)$$

One can see that the effect is proportional to the optical energy absorbed in the sample [viz., $\frac{1}{2} l_s [1 - \exp(-\beta l_s)]$] and inversely proportional to ω . This contrasts to δx_s , which is proportional to the energy absorbed only in the thermal diffusion length μ_s and inversely proportional to $\omega^{1/2}$ (for thermally thick samples). If the sample is transparent, $[1 - \exp(-\beta l_s)] \rightarrow \beta l_s$, so δx_m is proportional to βl_s . [Alternatively, one may solve Eqs. (3) and (4) for a point oscillating source term at arbitrary position in the sample, subject to the same boundary conditions on p_s and v_s . The thermal-mode terms are rapidly attenuated, leaving only acoustic-mode terms at the boundaries. The result for the sample-surface velocity amplitude is simply¹² $v_s(x=0) = (\beta_T / \rho_s C_{ps}) A_s$, where A_s is the point-source amplitude, provided (as above) $\mu_s \ll l_s$, $k l_s \gg 1$. Equation (30) follows immediately by integrating over the source distribution.] (4) Add the thermal and mechanical piston displacements, taking account of phase as well as amplitude. The net displacement causes a gas-pressure variation consistent with the adiabatic gas law, viz.,

$$p_g = (\gamma P_0 / V_0) \delta V = (\gamma P_0 / l_s) \delta x(t). \quad (40)$$

This result might be characterized as multiplying the expression for p_g in Appendix A by the factor $[1 + (\delta x_m / \delta x_s)]$.

We may now assess the need to include acoustic coupling in the sample by comparing the two components. Using the limit for β_s given in Eq. (A9) for thermally thick samples, the complex signal amplitude becomes

$$p_g = \frac{j \gamma P_0}{\omega l_s} \frac{l_0}{2 \rho_s C_{ps}} \left(\frac{\beta}{\sigma_s T_0 (\gamma + 1) (\gamma + 1)} + \beta_T [1 - \exp(-\beta l_s)] \right), \quad (41)$$

where the second term in the large parentheses is the contribution of acoustic coupling. Inserting the thermal parameters of air, and $T_0 = 297^\circ \text{K}$, we find

$$\delta x_m / \delta x_s \approx 17 \times 10^4 \exp(j\pi/2) f^{1/2} \beta_T (\gamma + 1) (\gamma + 1) \times [1 - \exp(-\beta l_s)] \beta^{-1}. \quad (42)$$

For the water-dye sample at 200 Hz, $\beta = 10 \text{ cm}^{-1}$ ($\beta_s \approx 5$), the ratio is $0.48 \exp(j\pi/2)$, so

$$|1 + (\delta x_m / \delta x_s)| \approx 1.4.$$

For a transparent sample ($\beta_s \ll 1$), the ratio is essentially independent of β but is proportional to l_s , giving $\beta_s = 0.476 \text{ cm}$ a ratio of $2.3 \exp(j\pi/2)$, so

$$|1 + (\delta x_m / \delta x_s)| \approx 3.0.$$

These numbers are seen to correspond to those obtained by comparing curves for MW2 and RG in Figs. 4 and 5.

The expressions in Eqs. (41) and (42) enable one to make some general comments. Acoustic coupling does not alter the linear relation between the PAS signal and β when $\beta l_s \ll 1$. As β increases, this effect reaches a limit for a given ω when $\mu_s = l_s$, while the thermal-piston term continues to increase linearly with β until $\mu_s \approx \mu_g$. The relative effect of acoustic coupling increases as $f^{1/2}$, provided $\mu_g > \mu_s$. All of these characteristics are evident in Figs. 2, 4, and 5.

The essential feature causing the acoustic coupling to become important is the limitation inherent in thermal diffusion: only light energy absorbed within a thermal-diffusion length (approximately) of the sample surface can contribute to the periodic heat flux at the surface. The surface vibration is, in contrast, proportional to the total energy absorbed in the sample. The latter may exceed the former if $l_s > \mu_s$, with $\mu_g > \mu_s$.

As the chopping frequency increases, the pressure amplitude becomes dependent on position, since the acoustic wavelength is no longer much larger than the gas length l_g . If one assumes the piston displacement δx at $x = 0$, as well as $v_s = 0$ at $x = -l_s$, the pressure amplitude is easily determined: it is simply p_g of Eq. (41) times the factor

$$R(x) = k l_g \cos(k l_g - k x) / \sin(k l_g). \quad (43)$$

For $f < 1000 \text{ Hz}$ and $l_g = 1.74 \text{ cm}$, $R(x) \approx 1$, but for $f > 1000 \text{ Hz}$, the spatial dependence affects the PAS signal, depending on microphone placement. Use of this factor enables one to extend the frequency range over which the composite-piston model is valid.

The complete composite-piston model (CPM), including the factor of Eq. (43), gives results which are indistinguishable from the curves of MW2 in Figs. 2, 4,

and 5 over the entire range of f and β shown, including the resonance region near $f = 10 \text{ kHz}$. This model then provides a convenient representation of the full one-dimensional theory for use in planning experiments and interpreting data.

B. Acoustic coupling in solids

The composite-piston model is applicable to isotropic solid samples, provided the same boundary conditions are assumed (see discussion in the next paragraph). The key parameter is the coefficient of thermal expansion β_T . Since this coefficient is smaller for typical solids than for water, the contribution of acoustic coupling to the PAS signal will be correspondingly less important for solid samples. Nevertheless, the acoustic term may have to be included in interpreting experimental data accurately.¹³ The CPM provides a convenient basis for determining the relative magnitudes of acoustic and thermal contributions, as well as their dependence on absorption coefficient, chopping frequency, and thermal parameters.

The "rigid-wall" boundary condition at the sample-backing interface is clearly an approximation, one which might appear to be less appropriate for solid samples than for liquids. To justify this approximation, we have considered the effect of replacing Eq. (36) by an impedance relation, $v_s = p_s / Z_s$ at $x = l_s$, where Z_s is the impedance of the backing. The backing impedance should have terms related to the backing mass and stiffness, with the stiffness dominant at low frequencies. Estimates of the stiffness effect for brass backing give an impedance Z_s which is quite large, such that negligible differences occur in the calculated results. In addition, we find that the frequency dependence is significantly affected if the impedance is assumed small, such that the agreement between measurements and calculations would be much poorer. For these reasons, we have some confidence in the application of this model to solid samples. There may occur situations with other backing materials or other experimental arrangements where this point must be reconsidered.

C. Effect of sample thickness

The dependence of the PAS signal on sample thickness may be important in interpreting PAS spectra or even in designing an experimental setup. We give a brief discussion of this dependence as indicated by our theoretical results.

In transparent thermally thick samples, the composite-piston model shows that the PAS signal will be enhanced by increasing the sample thickness l_s , provided β_s is still small. Figure 8 illustrates the dependence on l_s for several absorption coefficients ($f = 100 \text{ Hz}$). As β becomes small, the effect of acoustic coupling can be much larger than the thermal effect. This might be useful in improving the signal-to-noise ratio in some cases (while still maintaining approximate linearity in β). It is also clear that comparison spectra must be taken with samples of the same thickness, to avoid ambiguities in interpretation.

The dependence of PAS signal on l_s for nonthermally thick samples is illustrated in Fig. 9. The effect of

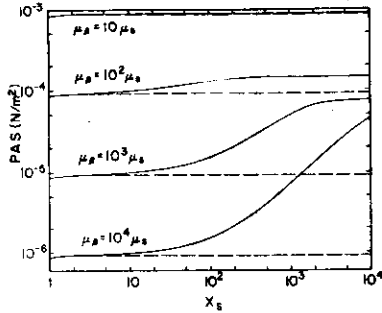


FIG. 8. Dependence of photoacoustic signal on sample thickness for thermally thick samples ($f=100$ Hz). X_e is the ratio of sample thickness to thermal-diffusion length. Notation is that of Fig. 2.

acoustic coupling is negligible, with that due to the thermal wave predominating. When $l_s < \mu_s$, the thermal wave is not strongly damped before reaching the gas-sample interface, so the signal can be affected by the total energy absorbed in the sample. If $\beta_s \ll 1$, this absorbed energy is proportional to β_s , but as β or l_s is increased, the absorbed energy approaches the incident energy and the signal saturates. As l_s is increased such that $l_s > \mu_s$, the thermal waves originating at depths given by $|x| > \mu_s$ are damped before reaching the surface and do not contribute to the signal; hence, the signal is independent of l_s (for given β).

The effect of the backing material can also be seen in Fig. 9. For thermally thin samples, the thermal wave reflected at $x = -l_s$ also contributes to the signal. A Plexiglas backing gives a reflected wave in phase with the original,¹⁷ increasing the signal when $l_s \ll \mu_s$. As $l_s \sim \mu_s$, the reflected wave is damped out so that the signal is reduced, as evidenced in the top two curves of Fig. 9. In the lower curves for Plexiglas ($\mu_s > \mu_p$), the direct signal is still increasing as $l_s \sim \mu_p$, more than compensating for the loss of the reflected wave. A brass backing gives a reflected thermal wave with a 180° phase change, canceling the direct wave to a great degree. The signal is thus greatly reduced with a thermally thin sample and brass backing, compared to the same sample with a Plexiglas backing. However, as $l_s \sim \mu_s$, the reflected wave becomes unimportant, and so the signal is independent of the backing material. Note that it is the difference in thermal parameters of the backing which leads to the variation shown in Fig. 9; the acoustic term in the PAS signal is negligible for thermally thin samples.

V. CONCLUSIONS

It has been shown that mechanical motion of liquid and solid samples can significantly affect the photoacoustic signal and can be the dominant effect for some liquid samples. A composite-piston model has been shown to be valid for thermally thick samples which should include most common samples unless in thin-

film form, and this model [particularly Eq. (41)] then provides the basis for interpretation of most PAS data. The simple form of the model may easily be modified for resonant cells. The dependence of the PAS signal on the absorption coefficient is approximately linear over a wide range, with some distortion in the transition region where $\beta_s \approx 1$, so that PAS spectra can be interpreted as would other absorption spectra. For thermally thin samples, PAS spectra should not be appreciably affected by acoustic coupling, and the simple piston model of RG will suffice. If the gas is thermally thin, the expression of MW1 or AMP must be used to describe the signal.

A more complete understanding of the photoacoustic effect will also be useful in other applications than spectroscopy. The aforementioned possibility of determining absolute absorption coefficients¹¹ requires detailed knowledge of the chopping-frequency dependence of the PAS signal. The phase shift caused by the acoustic term may be important in applications¹² depending on the relative phase of signal and reference. The range of possible uses clearly extends to many areas of science, engineering, and medicine.

ACKNOWLEDGMENT

We gratefully acknowledge the kindness of Phil Elrod of Princeton Applied Research Corp. who provided temporary use of lock-in amplifiers.

APPENDIX A

The approximate treatment of acoustic signal generation given by Rosencwaig and Gersho⁸ (RG) must be modified if the gas is thermally thin (i.e., $l_s \ll \mu_p$) or if the gas length is an appreciable fraction of the acoustic wavelength in the gas. The necessary modification has been made by the present authors⁹ and by Aamodt, Murphy, and Parker¹⁰ (AMP). We give the result here in our notation for reference; in the text of the article, it is referred to as MW1.

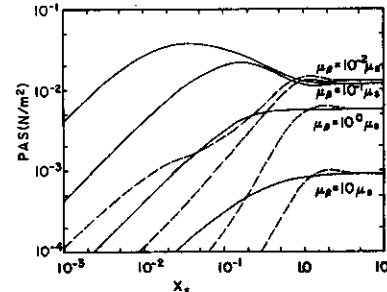


FIG. 9. Dependence of photoacoustic signal on sample thickness for thermally thin samples ($f=100$ Hz). X_e is the ratio of sample thickness to thermal-diffusion length. In this figure, the solid curves show values for Plexiglas backing, dashed curves for brass backing. Cell parameters are those of Fig. 2.

This treatment assumes no acoustic wave in the sample. Equations (17) and (23)–(25) give the form of the solution ($A_s = B_s = 0$) with boundary conditions of Eqs. (26)–(34), plus $v_s = 0$ at $x = 0$. To evaluate the pressure at any point in the gas, one needs the four coefficients A_s , B_s , C_s , and D_s ; the latter three may each be written in terms of A_s , so we first state A_s . This coefficient has the form

$$A_s = N/D, \quad (A1)$$

To display the form of N and D , we define (as in RG)

$$r = \beta/\sigma_s, \quad g = \kappa_p \sigma_p / \kappa_s \sigma_s, \quad b = \kappa_p \sigma_p / \kappa_s \sigma_s.$$

Then

$$N = [A/(\beta^2 - \sigma_s^2)] [rR_{ab} - 1 + S(1 + R_{ab}) \exp(-\sigma_p l_s - \beta_s)], \quad (A2)$$

$$D = F_2 + gR_{ab}F_3, \quad (A3)$$

where

$$\begin{aligned} R_{ab} &= [1 - R_s \exp(-2\sigma_p l_s)] / [1 + R_s \exp(-2\sigma_p l_s)], \\ R_s &= (b - T_s) / (b + T_s), \\ S &= (b - rT_s) / (b + T_s), \\ T_s &= \tanh(\sigma_p l_s). \end{aligned} \quad (A4)$$

The factors F_2 and F_3 require the following definitions:

$$\begin{aligned} G &= jk_p d_{ss} / (\sigma_p d_{sp}), \quad G^* = G \pm 1, \\ W &= G(1 - d_{sp}/d_{ss}) (\kappa_p \sigma_p / \kappa_s \sigma_s), \\ T_w &= \tanh(\sigma_w l_w), \\ E_s &= \exp(-jk_p l_s), \quad E_p = \exp(-\sigma_p l_s), \\ F_1 &= -2GE_s E_p + (G^* + W) + (G^* - W)E_p^2. \end{aligned} \quad (A5)$$

Then

$$\begin{aligned} F_2 &= [-8GE_s E_p + G^*(G^* + W)E_p^2 + G^*(G^* - W)E_p^2 \\ &\quad - G^*(G^* + W) - G^*(G^* - W)E_p^2 E_p^2] (F_1)^{-1}, \\ F_3 &= G(1 - d_{sp}/d_{ss}) [(G^* + W)E_p^2 - (G^* - W)E_p^2 \\ &\quad - (G^* + W) + (G^* - W)E_p^2 E_p^2] (F_1)^{-1}. \end{aligned} \quad (A6)$$

Finally,

$$\begin{aligned} B_s &= A_s [-2GE_s E_p + (G^* + W)E_p^2 + (G^* - W)E_p^2 E_p^2] (F_1)^{-1}, \\ C_s &= A_s [-2GE_s E_p + G(G^* + W)E_p^2 - G(G^* + W)] (F_1)^{-1}, \end{aligned} \quad (A7)$$

$$D_s = A_s [-2GE_s E_p - G(G^* - W)E_p^2 E_p^2 + G(G^* - W)E_p^2] (F_1)^{-1}.$$

If the pressure is evaluated at $x = l_s$, then

$$p_s = d_{ss}(A_s E_s + B_s E_s^{-1}) + d_{sp}(C_s E_s + D_s E_s^{-1}); \quad (A8)$$

this is essentially the result given by AMP, provided the window and backing are thermally thick ($T_w = 1$, $T_b = 1$ in Eqs. (A4) and (A5)). One must multiply their result by $-1/2$ to get the same expression as Eq. (A8); the negative sign is apparently due to a sign error in their source term; the factor of $1/2$ occurs because their I_0 is our $1/2 I_0$ (our I_0 is the overall beam intensity, but their I_0 is the intensity of the harmonic term only).

The expression given by RG is obtained from Eq. (A8) if one assumes the window, backing, and gas are

thermally thick and that the gas length is small compared to the acoustic wavelength. Then, if one further assumes the sample to be thermally thick, the limit of p_s is

$$p_s = (-jI_0 P_0 / 2\sigma_p l_s T_0) (\beta / \omega \rho_s C_p) (g + 1)^{-1} (r + 1)^{-1}. \quad (A9)$$

This expression is used in the text in constructing the composite-piston model.

APPENDIX B

We present a slight variant of the thermal-piston argument of RG,⁸ primarily as a basis for discussing the frequency dependence of the piston "displacement" δx_i .

The periodic heat flux from sample to gas causes a periodic temperature variation in the gas near $x = 0$, having the form $\tau_s = C_s \exp(-\sigma_p x)$. [This is the dominant term in Eq. (23) for usual PAS conditions.] Each infinitesimal layer of the gas in this region undergoes fractional (essentially isobaric) expansion/contraction proportional to the ratio of periodic temperature to ambient temperature T_0 . The net displacement of this boundary region is the sum of these infinitesimal displacements:

$$\delta x_i = \int_0^L (\tau_s / T_0) dx. \quad (B1)$$

This expression includes the effect of phase differences in the infinitesimal displacements. The upper limit need only be chosen such that $\exp(-\sigma_p L) \approx 0$ (RG chose $L = 2\pi\mu_p$).

The above expression allows the frequency dependence of δx_i to be understood as follows. Assume, first, that the optical energy is absorbed within a distance less than the thermal diffusion length ($\mu_s \ll \mu_p$), such that all the absorbed energy contributes to the heat flux at the boundary. The flux then has an amplitude which is independent of frequency. Since the heat flux is equal to $\kappa_p (-d\tau_s/dx)_0 = \kappa_p \sigma_p C_s$, we infer that C_s is inversely proportional to σ_p and, thus, proportional to $\omega^{-1/2}$ [cf. Eq. (20)]. The exponential dependence of τ_s shows that the region over which the integrand [of Eq. (B1)] is appreciable shrinks as σ_p increases, such that an additional factor of $\omega^{-1/2}$ occurs in δx_i . For these conditions, δx_i is thus inversely proportional to ω .

The thermal-diffusion length of the sample decreases as $\omega^{-1/2}$, such that at higher frequencies $\mu_s < \mu_p$. When this occurs, only the energy absorbed within a distance proportional to μ_s contributes to the heat flux at the boundary, and the flux amplitude is no longer constant but proportional to $\omega^{-1/2}$. When this factor is combined with that already discussed, δx_i is seen to be proportional to $\omega^{-3/2}$. The transition in ω dependence obviously occurs near the point at which $\mu_s = \mu_p$.

The piston argument clearly becomes inadequate if the gas is thermally thin ($\mu_p < \mu_s$). The temperature variation extends over the entire gas, and one cannot then define a region to be considered as the "piston". If the heat flux from the sample is independent of frequency, then so is the temperature amplitude [both C_s and D_s of Eq. (23) must now be included]. The pressure amplitude is essentially that due to uniform heating of the gas, and it is likewise independent of frequency. The

curves for MW2 in Fig. 3 show the pressure amplitude becoming independent of frequency as $\omega \rightarrow 0$.

Note added in proof. Subsequent work has shown that the mechanical displacement given in Eq. (39) must be modified for solid samples by a factor (of order 1) which depends on the elastic constants of the solid.

¹A. G. Bell, *Am. J. Sci.* **20**, 305 (1980).

²D. W. Hill and T. Powell, *Non-Dispersive Infrared Gas Analysis in Science Medicine, and Industry* (Plenum, New York, 1968).

³A. Rosencwaig, *Opt. Commun.* **7**, 305 (1973); *Anal. Chem.* **47**, 592A (1975); A. Rosencwaig and S. S. Hall, *Anal. Chem.* **47**, 648 (1975).

⁴G. C. Wetsel, Jr. and F. A. McDonald, *J. Acoust. Soc. Am.* **60**, S. 3 (1976).

⁵G. C. Wetsel, Jr. and F. A. McDonald, *Bull. Am. Phys. Soc.* **22**, 295 (1977).

⁶J. F. McClelland and R. N. Knisley, *Appl. Opt.* **15**, 2658 (1976).

⁷J. G. Parker, *Appl. Opt.* **12**, 2974 (1973).

⁸A. Rosencwaig and A. Gersho, *J. Appl. Phys.* **47**, 64 (1976).

⁹F. A. McDonald and G. C. Wetsel, Jr., *J. Acoust. Soc. Am.* **60**, S52 (1976).

¹⁰L. C. Aamodt, J. C. Murphy, and J. G. Parker, *J. Appl. Phys.* **48**, 927 (1977).

¹¹G. C. Wetsel, Jr. and F. A. McDonald, *Appl. Phys. Lett.* **30**, 252 (1977).

¹²M. J. Adams and G. F. Kirkbright, *Spectrosc. Lett.* **9**, 255 (1976).

¹³H. S. Bennett and R. A. Forman, *J. Appl. Phys.* **48**, 1432 (1977) and references therein.

¹⁴P. M. Morse and K. U. Ingard, *Theoretical Acoustics* (McGraw-Hill, New York, 1968).

¹⁵R. N. Thurston, *Physical Acoustics Part A* (Academic, New York, 1964), Vol. 1.

¹⁶For example, T. G. Muir, C. R. Culbertson, and J. R. Clyne, *J. Acoust. Soc. Am.* **59**, 735 (1976) and references therein.

¹⁷F. A. McDonald (unpublished).

¹⁸G. C. Wetsel and F. A. McDonald, 1977 *Ultrasonics Symposium Proceedings* (IEEE, New York, 1977), p. 347.

Phase measurements in the frequency domain photoacoustic spectroscopy of solids

A. Mandelis, Y. C. Teng, and B. S. H. Royce

Materials Laboratory, Princeton University, Princeton, New Jersey 08544

(Received 5 March 1979; accepted for publication 6 June 1979)

Photoacoustic spectroscopy provides information about both the amplitude and phase of the response of a system to an optical excitation process. This paper presents a theoretical model of photoacoustic processes in the frequency domain which includes the relaxation time of the radiationless deexcitations and a two-layer absorbing system. Emphasis is placed on the effect of these conditions on the phase of the photoacoustic signal and the utility of this measurement in evaluating material parameters. Circumstances under which the phase may be used to measure the optical absorption coefficient of the solid and the nonradiative relaxation times are defined. The value of the phase measurement in the study of surface films is discussed.

PACS numbers: 78.20. — e, 78.65. — s, 42.80. — f, 07.65. — b

1. INTRODUCTION

Photoacoustic spectroscopy (PAS) provides information about both the amplitude and phase of the response of a photoacoustic system to an optical excitation process. The phase data contains contributions from a number of sources associated with the sample under study, the geometry of the photoacoustic cell, the response of the detecting system, etc. In an actual photoacoustic measurement many of the non-sample related parameters may be maintained constant and the phase data may therefore be used to provide information about the optical and thermal properties of the solid under study as well as the relaxation times associated with the non-radiative deexcitation processes that give rise to the PAS signal.

Measurements of the photoacoustic phase have been used with gaseous samples to obtain information about relaxation rates and photochemical processes. These measurements have been discussed in a recent review by Robin.¹ For the case of solids various contributions to the phase of the PAS signal have been considered by several authors.

In their one-dimensional theory of the photoacoustic response of solid samples, Rosencwaig and Gersho² discussed the effect of the optical absorption coefficient of the solid on the phase for the limiting cases of optically transparent and optically opaque specimens in which the nonradiative deexcitation processes occurred instantaneously. In a subsequent paper Rosencwaig³ took the generalized expression for the photoacoustic signal from this initial paper and used it to obtain computer-generated curves for both the amplitude and the phase of the photoacoustic response as a function of the modulation frequency and the sample dimensions. The dependence of these signals upon the thermal properties of the sample support was also considered.

Aamodt *et al.*⁴ developed a more exact one-dimensional model for the PAS response of a solid specimen which differs from the model of Rosencwaig and Gersho by using a thermal transport equation for the gas developed by Parker⁵ which includes the finite velocity of sound. In this paper the effects of the dimensions of the photoacoustic cell on the phase of the signal are considered and it is shown that the

phase is insensitive to cell length once the length of the gas in the cell is large compared to the corresponding thermal diffusion length at the chopping frequency of the radiation. Similarly the effect of the thermal properties of the sample backing on the phase was found to be unimportant in that range of chopping frequencies for which the thermal diffusion length in the solid was short compared to its thickness.

PAS phase has been discussed in a series of papers by Kirkbright and his co-workers.^{6,7} These authors considered instantaneous nonradiative deexcitation processes and were largely concerned with the phase shifts in a multilayered sample which result from the thermal transit time through a transparent overlayer deposited on an absorbing substrate.

The use of PAS phase to measure the lifetime associated with the nonradiative deexcitation paths has been employed by Merkle and Powell.^{8,9} These authors took the relationship between the nonradiative lifetime and the phase shift employed for a gaseous sample by Harshbarger and Robin¹⁰ and used it to interpret radiationless relaxation rates of Eu^{2+} ions in a KCl matrix. A large relative phase shift was observed between the PAS signals resulting from excitation in the f_2 and e_2 bands of the Eu^{2+} ion and was attributed to a long-lived excited state of the $4f^7$ configuration. Peterson and Powell¹¹ have employed the same analytical approach to compare the nonradiative decay modes for Cr^{3+} ions in Al_2O_3 , MgO , SrTiO_3 , and BaTiO_3 lattices.

Recently, Roark *et al.*¹² presented data on the absorption coefficient dependence of the photoacoustic phase. They suggested that measurement of the phase angle provides a means of computing the absolute optical absorption coefficient of a sample and indicated that the phase angle continues to be dependent upon the absorptivity of the sample after the PAS amplitude has saturated so that phase measurements provide a method of extending absorption coefficient determinations to higher values.

This paper is concerned with the extension of the Rosencwaig photoacoustic model to include the relaxation time of the radiationless deexcitation processes and two-layer absorbers supported on a nonabsorbing backing material. The emphasis is on the effects of these quantities on the phase of



FIG. 1. Geometry of a single-layer PAS system.

the photoacoustic response and the utility of this measurement in obtaining material parameters. It is shown that the phase of the photoacoustic signal can be used to measure the optical absorption coefficient of a solid but that this measurement exhibits the same saturation behavior at high absorption coefficients as does the PAS amplitude. The phase may also be used to measure the relaxation time of the nonradiative deexcitation processes responsible for the PAS signal; however, the relaxation time is only proportional to the tangent of the phase angle in certain limiting cases. For a multilayer absorber the phase measurement provides useful information about both a transparent overlayer on an absorbing substrate and a two-layer system with widely differing optical absorption coefficients.

II. MODEL

A. Single-layer sample with a finite nonradiative relaxation rate

An idealized configuration of a photoacoustic system is shown in Fig. 1. The solid sample, of thickness l , contains a two-level optical absorption band which has an excited-state lifetime τ and a wavelength-dependent optical absorption coefficient β . The sample is supported by a transparent backing material of large thickness and is in thermal contact with a transparent gas. Heat transfer between the solid and the gas results in pressure fluctuations which constitute the PAS signal. The cell is closed by a nonabsorbing thick window. By choosing both the transparent cell window and sample backing to be infinitely thick the growing exponential solutions for the thermal transport equations in these components can be eliminated by application of the boundary conditions. This geometry is essentially the same as that used by other authors²⁻⁴ but the system differs in that a finite relaxation time is associated with the nonradiative decay processes.

The light incident upon the solid is assumed to be modulated sinusoidally so that the irradiance at a distance x from the front surface is given by

$$I(x,t) = \frac{1}{2} [J_0 \beta \exp(-\beta|x|)] (1 + \cos \omega_0 t) \\ = A(x) \operatorname{Re} [1 + \exp(i\omega_0 t)],$$

where ω_0 is the modulation frequency. Absorption of this radiation by the electronic state gives rise to a time-dependent energy associated with the excited level and given by

$$\frac{dE(x,t)}{dt} = I(x,t) - \frac{E(x,t)}{\tau}$$

Solving this equation for $E(x,t)$ gives

$$E(x,t) = A(x) \tau \operatorname{Re} \left[S(t) - \left(1 + \frac{1}{(1 + i\omega_0 \tau)} \right) \right. \\ \left. \times \exp\left(-\frac{t}{\tau}\right) + \left(\frac{\exp(i\omega_0 t)}{1 + i\omega_0 \tau} \right) \right].$$

The first two terms are associated with the transient resulting from turning on the radiation at $t = 0$. Only the steady-state component of this solution is of interest for this paper so that

$$E(x,t) = A(x) \tau \operatorname{Re} \left(\frac{\exp(i\omega_0 t)}{1 + i\omega_0 \tau} \right).$$

The nonradiative decay of the excited-state population to the ground state provides a spatial- and time-dependent heat source in the solid

$$\dot{H}(x,t) = \frac{\eta}{\tau} E(x,t) \\ = \frac{\eta I_0 \beta \exp(-\beta|x|)}{2} \operatorname{Re} \left(\frac{\exp(i\omega_0 t)}{1 + i\omega_0 \tau} \right), \quad (1)$$

where η is the efficiency of the nonradiative processes. It is this alternating steady-state heat source that is responsible for the periodic temperature fluctuation of the sample. Thermal conduction processes then transfer energy to the sample backing and to the gas in the cell. In the approximation employed by Rosencwaig and Gersho² the appropriate thermal diffusion equations have the form

$$\frac{\partial^2}{\partial x^2} T_s(x,t) - \frac{1}{\alpha_s} \frac{\partial}{\partial t} T_s(x,t) = -\frac{\dot{H}(x,t)}{k_s} \quad (2)$$

for the solid in which the absorption of the incident radiation occurs, and

$$\frac{\partial^2}{\partial x^2} T_i(x,t) - \frac{1}{\alpha_i} \frac{\partial}{\partial t} T_i(x,t) = 0 \quad (3)$$

for the transparent window ($i = w, x > L$), gas ($i = g, 0 < x < L$), and backing ($i = b, x < -l$) regions of the cell. The quantities $\alpha_i = (k_i/\rho_i c_i)$ are the thermal diffusivities of various regions of the cell where ρ_i and c_i are the material densities and specific heats, respectively, and k_i is the corresponding thermal conductivity. These four coupled equations may be solved using Fourier transform techniques subject to the boundary conditions of temperature and heat flux continuity at each material interface so that

$$T_i(\text{boundary}, t) = T_j(\text{boundary}, t) \quad (4)$$

and

$$k_i \frac{\partial}{\partial x} T_i(\text{boundary}, t) = k_j \frac{\partial}{\partial x} T_j(\text{boundary}, t). \quad (5)$$

The resulting expression for the Fourier transform of the temperature distribution in the gas has the form

$$\hat{T}_g(x, \omega) = \left(\frac{\beta I_0 \eta}{2k_g(\beta^2 - \sigma_g^2)} \right) \operatorname{Re} \left[\left(\frac{\delta(\omega - \omega_0)}{1 + i\omega_0 \tau} \right) \right. \\ \times \left(\frac{(r-1)(b+1) \exp(\sigma_s l) - (r+1)(b-1) \exp(-\sigma_s l) + 2(b-r) \exp(-\beta l)}{(g+1)(b+1) \exp(\sigma_s l) - (g-1)(b-1) \exp(-\sigma_s l)} \right) \\ \left. \times \sum_{n=0}^{\infty} ((1+D) \exp[-\sigma_g(2nL+x)] - (1-D) \exp[-\sigma_g(2(n+1)L-x)]) \right], \quad (6)$$

where

$$r = (1-i) \left(\frac{\beta}{2\alpha_s} \right), \quad b = \left(\frac{a_s k_s}{a_i k_i} \right), \quad g = \left(\frac{a_s k_s}{a_w k_w} \right), \quad D = \left(\frac{a_s k_s}{a_w k_w} \right), \quad \sigma_j = (1+i)\alpha_j, \quad \text{and} \quad a_j = \left(\frac{\omega}{2\alpha_j} \right)^{1/2}, \quad j = s, b, g, w.$$

The above relationship can be transformed from the frequency to the time domain and the presence of the multiplicative term $\delta(\omega - \omega_0)$ results in the frequency dependence implicit in the terms containing σ_j , contributing only at $\omega = \omega_0$. The temperature distribution in the gas is then given by

$$T_g(x,t) = \left(\frac{\beta I_0 \eta}{2k_g} \right) \operatorname{Re} \left[\left(\frac{1}{(\beta^2 - \sigma_g^2)} \right) \left(\frac{(r-1)(b+1) \exp(\sigma_s l) - (r+1)(b-1) \exp(-\sigma_s l) + 2(b-r) \exp(-\beta l)}{(g+1)(b+1) \exp(\sigma_s l) - (g-1)(b-1) \exp(-\sigma_s l)} \right) \right. \\ \left. \times \left[\left(\frac{1}{1 + i\omega_0 \tau} \right) \sum_{n=0}^{\infty} ((1+D) \exp[-\sigma_g(2nL+x)] - (1-D) \exp[-\sigma_g(2(n+1)L-x)]) \right] \exp(i\omega_0 t) \right]. \quad (7)$$

This periodic and spatially dependent temperature distribution generates a periodic but spatially uniform pressure in the gas given by

$$\langle p_g(t; \omega_0) \rangle = \frac{p_0}{T_0 L} \int_0^L T_g(x,t; \omega_0) dx, \quad (8)$$

where p_0 and T_0 are the initial pressure and temperature of the gas in the cell.

The PAS signal then has the form

$$\langle p_g(t; \omega_0) \rangle = \left(\frac{p_0 I_0 \eta \beta}{2k_g T_0 L} \right) \operatorname{Re} \left[\left(\frac{\exp[i(\omega_0 t - \frac{1}{2}\pi)]}{\sqrt{2\alpha_s(1 + i\omega_0 \tau)(\beta^2 - \sigma_g^2)}} \right) \right. \\ \left. \times \left(\frac{(r-1)(b+1) \exp(\sigma_s l) - (r+1)(b-1) \exp(-\sigma_s l) + 2(b-r) \exp(-\beta l)}{(b+1) \exp(\sigma_s l) + (b-1) \exp(-\sigma_s l)} \right) \right] \quad (9)$$

since $\sigma_g^{-1} = [1/(2\alpha_s)]^{1/2} \exp(-\frac{1}{2}i\pi)$ and where it has been assumed that $D < 1$, $g < 1$, and that $\alpha_s L > 1$ so that only the $n = 0$ term in the summation needs to be retained. Equation (9) is a generalization of Eq. (17) in Ref. 2 to include the effects of a noninstantaneous deexcitation process.

In order to separate the amplitude and the phase of the photoacoustic signal it is convenient to follow Rosencwaig and Gersho and define

$$\langle p_g(t; \omega_0) \rangle \equiv \operatorname{Re} \{ Q \exp[i(\omega_0 t - \frac{1}{2}\pi)] \} \equiv \operatorname{Re} \{ q \exp[i(\omega_0 t - \frac{1}{2}\pi - \psi)] \}$$

such that $Q = Q_1 + iQ_2 = q \exp(-i\psi)$.

The amplitude of the measured photoacoustic signal

$$|\langle p_g(t; \omega_0) \rangle| = |Q| = q = (Q_1^2 + Q_2^2)^{1/2}$$

and the phase lag of the signal with respect to the light source modulation

$$\Phi = (\frac{1}{2}\pi + \psi) \quad \text{with} \quad \psi = \tan^{-1} [-(Q_2/Q_1)].$$

These quantities may be most conveniently evaluated by writing the components of Q in the polar notation for complex quantities so that

$$\beta^2 - \sigma_g^2 = Z_1 = |Z_1| \exp(i\phi_1) = \beta^2 [1 + (\omega_0 \tau)^2]^{1/2} \exp(i\phi_1), \\ 1 + i\omega_0 \tau = Z_2 = |Z_2| \exp(i\phi_2) = [1 + (\omega_0 \tau)^2]^{1/2} \exp(i\phi_2), \\ r-1 = Z_3 = |Z_3| \exp(i\phi_3) = [(\omega_0 \tau)^{-1} + 1 - (2/\omega_0 \tau)^{1/2}]^{1/2} \exp(i\phi_3), \\ r+1 = Z_4 = |Z_4| \exp(i\phi_4) = [(\omega_0 \tau)^{-1} + 1 + (2/\omega_0 \tau)^{1/2}]^{1/2} \exp(i\phi_4), \\ b-r = Z_5 = |Z_5| \exp(i\phi_5) = [(\omega_0 \tau)^{-1} + b^2 - b(2/\omega_0 \tau)^{1/2}]^{1/2} \exp(i\phi_5), \\ \text{and} \\ (b+1) \exp(\sigma_s l) + (b-1) \exp(-\sigma_s l) = Z_6 = |Z_6| \exp(i\phi_6) = [(b+1)^2 \exp(2\alpha_s l) + (b-1)^2 \exp(-2\alpha_s l) \\ + 2(b^2 - 1) \cos(2\alpha_s l)]^{1/2} \exp(i\phi_6), \quad (10)$$

where $\tau \equiv 1/\beta^2 \alpha_s$ is a characteristic relaxation time for the system corresponding to the thermal transit time from a depth μ_B ($\equiv 1/\beta$) within the solid.

Using these definitions the real and imaginary parts of Q can be evaluated and have the form

$$\begin{aligned} Q_1 = \operatorname{Re} Q &= K [(b+1)|Z_1| \exp(a_1 l) \cos(\phi_1 + \phi_2 + \phi_6 - \phi_3 - a_1 l) - (b-1)|Z_4| \exp(-a_1 l) \\ &\quad \times \cos(\phi_1 + \phi_2 + \phi_6 - \phi_4 + a_1 l) + 2|Z_5| \exp(-\beta l) \cos(\phi_1 + \phi_2 + \phi_6 - \phi_5)], \\ Q_2 = \operatorname{Im} Q &= -K [(b+1)|Z_1| \exp(a_1 l) \sin(\phi_1 + \phi_2 + \phi_6 - \phi_3 - a_1 l) - (b-1)|Z_4| \exp(-a_1 l) \\ &\quad \times \sin(\phi_1 + \phi_2 + \phi_6 - \phi_4 + a_1 l) + 2|Z_5| \exp(-\beta l) \sin(\phi_1 + \phi_2 + \phi_6 - \phi_5)], \end{aligned} \quad (11)$$

where

$$K = \frac{p_0 I_0 \eta \beta}{2\sqrt{2k_s T_0 L_a |Z_1| |Z_2| |Z_4|}}$$

The amplitude of the photoacoustic signal is seen to be directly proportional to K and the relaxation time, τ , associated with the nonradiative decay process is contained in the term $|Z_1|$ in the denominator. For a modulation frequency $\omega_0 < 1/\tau$ the PAS amplitude becomes independent of τ , as expected, and the expression for the pressure is identical to that obtained by Rosenzweig and Gersho.² When $\omega_0 \tau$ cannot be neglected compared to unity, the PAS signal decreases as the relaxation time τ increases.

The variable contribution to the phase, $\phi = \tan^{-1}(-Q_2/Q_1)$, is seen to depend upon the optical absorption coefficient of the solid and its physical dimensions, the ratio of the thermal properties of the solid and the backing material, the relaxation time of the nonradiative deexcitation processes, the modulation frequency of the light, and the thermal properties of the solid and the gas in the cell. For certain limiting cases the expression for the phase can take on a particularly simple form.

For an optically opaque and thermally thick sample both the optical absorption depth, μ_B , and the thermal diffusion length, μ_s , are much less than the sample thickness. Under these conditions $\exp(-\beta l) \approx 0$ and $\exp(-a_1 l) \approx 0$ so that the variable component of the PAS phase is given by

$$\phi(\beta, \tau, \omega_0) = \tan^{-1}(-\omega_0 \tau \beta) + \tan^{-1}(\omega_0 \tau) - \tan^{-1}\left(\frac{-1}{1 - (2\omega_0 \tau \beta)^{1/2}}\right), \quad (12)$$

At chopping frequencies for which $\mu_s > \mu_B$ and $\omega_0 \tau \beta \approx 0$

$$\phi(\tau, \omega_0) = \frac{1}{2}\pi + \tan^{-1}(\omega_0 \tau) \quad (13)$$

and the phase information provides a direct measure of the relaxation time, τ , of the nonradiative processes.

A similar expression is obtainable for an optically transparent thermally thick solid for which $\exp(-\beta l) \approx (1 - \beta l)$ and $\mu_s < l$. In this case

$$\phi(\tau, \omega_0) = \frac{1}{2}\pi + \tan^{-1}(\omega_0 \tau). \quad (14)$$

Expressions (13) and (14) indicate that the PAS phase only provides a direct measurement of the relaxation time of the nonradiative processes in certain limiting cases. From an experimental viewpoint the preferred configuration would probably be that of Eq. (13) since the signal amplitude would be largest for this case.

The full expression for the phase may be evaluated numerically and Fig. 2 shows the dependence of the phase upon the modulation frequency of the light for a system in which the nonradiative relaxations are instantaneous. Fig. 2 is

equivalent to Fig. 2 in Ref. 3, however, an error of sign occurs in the expression for Q given in that paper and is responsible for the indicated nonsystematic dependence of the phase upon the properties of the backing material. If the data displayed in Fig. 2 of the present paper is plotted in terms of the parameter $l/\mu_s \propto \omega_0^{1/2}$ it reduces to the form shown in Fig. 3 of Ref. 4. For this optically transparent sample the phase of the photoacoustic signal already displays a strong dependence upon the thermal properties of the backing at a modulation frequency for which $\omega_0 \tau = 1$. τ may be considered to be a modified thermal diffusion time across the solid of thickness l and is defined by $\tau \equiv (k_s \rho_s c_s / k_b \rho_b c_b) \times (l^2/a_s) = (l/b)^2(1/a_s)$. The quantity l/b may be treated as an effective thickness of the sample which increases for a given sample as the thermal conductivity of the support material becomes smaller. When $\omega_0 \tau \gg 25$ the phase of the PAS signal is independent of the properties of the backing material. This is equivalent to a value of $l/\mu_s \approx 5$. For very large values of b , e.g., in the case of a solid in contact with a good thermal conductor, the phase changes by more than 45° at experimentally realistic values of the chopping frequency, but tends asymptotically to the 45° value at very low frequencies ($\sim 10^{-3}$ Hz). However, in this limit, the signal is small and phase shifts may not be easy to measure accurately. For very small values of b , such as expected if the solid under study is a self-supporting film with a gas backing, the phase changes by less than 45° at intermediate values of the modulation frequency since the condition $\mu_s \sim l/b$ which determines the phase change is met at lower frequencies. In this case also the phase tends asymptotically to the 45° value at very low frequencies. In the limit of $b = 0$, there is no observable phase shift between the backing-independent frequency range and this intermediate region.

The amplitude of the PAS signal is also dependent upon the ratio of μ_s to this effective thickness and, as expected for

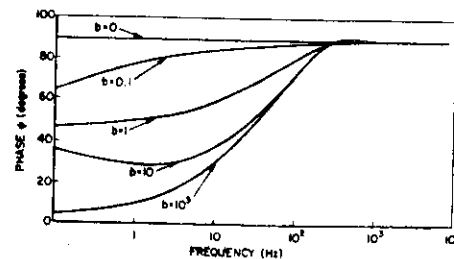


FIG. 2. Dependence of the PAS phase upon modulation frequency for various values of b , for an optically transparent solid ($\beta = 20 \text{ cm}^{-1}$, $l = 50 \text{ } \mu\text{m}$).

Mandelis, Teng, and Royce

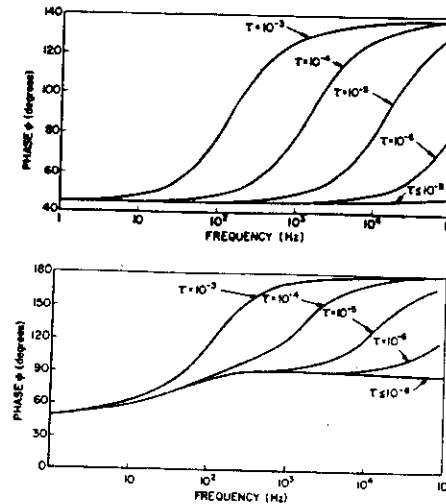


FIG. 3. (a) Frequency dependence of the PAS phase for various nonradiative lifetimes and an optically opaque thermally thick sample ($\mu_B < \mu_s$, $\mu_B < l$). (b) Corresponding data for an optically transparent sample ($\mu_B > l$, $l = 50 \text{ } \mu\text{m}$, $b = 1$).

a transparent solid, when μ_s is greater than the effective thickness for materials for which $b > 1$ the signal magnitude is reduced due to the large heat flux to the backing material.

Figure 3 shows the dependence of the phase upon the modulation frequency for solids in which the relaxation time of the nonradiative deexcitations is taken into account. In Fig. 3 it has been assumed that $b = 1$. As seen in Fig. 3a which applies to a material of high optical absorption coefficient ($\beta = 2 \times 10^5 \text{ cm}^{-1}$), no contribution to the phase shift arises from the optical absorption depth since over the full range of modulation frequencies $\mu_s > \mu_B$. The complete phase shift displayed in this part of the diagram results from effects due to the nonradiative lifetime and, as expected, such processes become important for frequencies greater than that for which $\omega_0 \tau \approx 1.0$. The phase shift produced by any given relaxation time is seen to saturate as the frequency increases. Figure 3b shows the response expected for a material of lower β (20 cm^{-1}). Two contributions to the phase are now seen to be involved. The phase shift of approximately 45° associated with the instantaneous relaxation time curve results from a reversal of the relative magnitudes of μ_s and l as μ_s decreases with increasing ω . Superimposed on this contribution is that due to the relaxation time phenomena. As was shown in Eq. (14), in the limit of high frequencies for which μ_s is always less than l and the sample is therefore thermally thick, the additional increment of phase is directly related to the relaxation time.

In Figs. 2 and 3 the PAS signal is associated with a particular value of the absorption coefficient. In most actual PAS situations the wavelength of the exciting light is changed through a region associated with an absorption

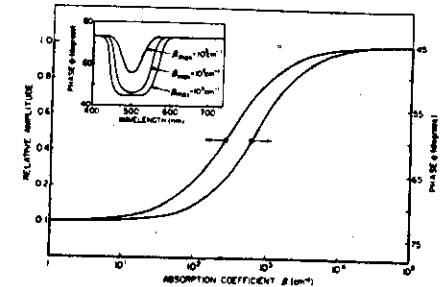


FIG. 4. Comparison between PAS amplitude and phase as a function of the absorption coefficient of the solid. ($f = 50 \text{ Hz}$, $l = 50 \text{ } \mu\text{m}$, $b = 1$). Inset: Phase Response in passing through a Gaussian absorption band having different values of β_{max} .

band. The phase of the PAS signal will then depend upon $\beta(\lambda)$. This dependence is illustrated in Fig. 4, the phase lag and the relative amplitude of the signal being displayed as a function of $\log \beta$. The inset in Fig. 4 shows the effect of this β dependence of the phase upon the system response to a Gaussian-shaped absorption band centered at 500 nm and with a full width at half-maximum of 0.1 eV . Both diagrams indicate that saturation occurs in the phase response at large values of β and the corresponding amplitude curve indicates that both phase and amplitude saturate at essentially the same value of β . As shown in the inset, for low values of β_{max} in an absorption band the phase response follows the form of the wavelength-dependent optical absorption coefficient and may therefore be used to measure this quantity. As $\beta(\lambda)$ increases, the phase angle decreases from an upper limit determined by the chopping frequency and by the coefficient b towards the 45° angle expected for a sample for which the optical absorption depth is less than the μ_s . "Phase saturation" therefore occurs for samples having high optical absorption coefficients.

The dependence of the thermal diffusion length, μ_s , upon the modulation frequency of the light means that for a sample with instantaneous nonradiative deexcitation processes the amplitude of the PAS signal has an ω^{-1} dependence at low modulation frequencies and an $\omega^{-3/2}$ dependence at high frequencies. For a sample in which the nonradiative processes have a finite relaxation time, the high-frequency slope is changed as is shown in Fig. 5. The

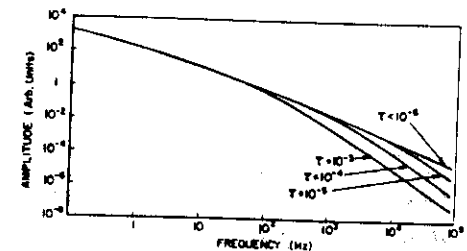


FIG. 5. Dependence of PAS amplitude on modulation frequency for different nonradiative lifetimes ($\beta = 20 \text{ cm}^{-1}$, $b = 1$, $l = 50 \text{ } \mu\text{m}$).

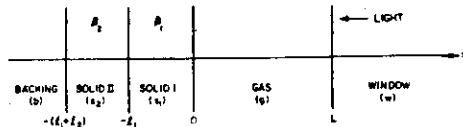


FIG. 6. Geometry for a double-layer PAS system.

curves for the finite relaxation times break away from the instantaneous curve at a point for which $\omega_0 \tau \approx 1.0$ and for all values of τ approach a limiting logarithmic slope higher by one than that of the instantaneous curve. For a material for which the instantaneous slope would be -1 that with relaxation is -2 ; for the case shown in Fig. 5 where the instantaneous slope is $-\frac{1}{2}$ that with relaxations is $-\frac{3}{2}$.

B. Two-layer sample with instantaneous nonradiative relaxations

Many systems of physical interest may be approximated by a two-layer model of a solid with each layer having independent optical absorption properties. Examples might be absorbing coatings on optical components, molecular films on an absorbing catalytic support, or biological systems such as the skin or a plant leaf. Such a system may be represented in the same approximation employed in Sec. II A as shown in Fig. 6. As before, the modulated light enters

the photoacoustic cell through a thick window at $x = L$. The surface of the first solid is at $x = 0$ and this material, with an absorption coefficient β_1 , extends to $x = -l_1$. The second solid of thickness l_2 and optical absorption coefficient β_2 is supported on a transparent backing material that extends to $x = -\infty$. The finite thickness of the second solid makes the solutions for the two absorbing regions symmetric and avoids the problem of the second layer being optically opaque for all nonzero values of β_2 .

Since only instantaneous nonradiative processes are being considered the distributed time-dependent heat source term associated with light absorption in the two solids has the form

$$\frac{\dot{H}(x,t)}{k_i} = \left(\frac{\beta_i I_0}{2k_i} \right) \exp(-\beta_i y) \text{Re}[1 + \exp(i\omega_0 t)], \quad (15)$$

where for solid 1, $i = 1$, $I = I_0$, the irradiance of the incident radiation, and $y = -x$. For solid 2, $i = 2$, $I = I_0 \exp(-\beta_1 l_1)$, and $y = -(x + l_1)$. There are now five coupled thermal diffusion equations for the system, two having the form of Eq. (2) but with Eq. (15) being substituted for $\dot{H}(x,t)/k_i$, and three having the same form as Eq. (3). As before these equations can be solved using Fourier transform techniques and invoking temperature and heat flux continuity at the boundaries between the various elements in the cell. It is only the ac component of the temperature in the gas that is of interest since this is responsible for the pressure fluctuations in the gas that are the PAS signal. In the general case this temperature is

$$T_g(x,t) = \left[\left(\frac{\eta_2 \beta_2 I_0 b_1 \exp(-\beta_1 l_1)}{k_2 (\beta_2^2 - \sigma_2^2)} \right) \{ (r_2 - 1)(b_2 + 1) \exp(\sigma_2 l_2) - (r_2 + 1)(b_2 - 1) \exp(-\sigma_2 l_2) + 2(b_2 - r_2) \times \exp(-\beta_2 l_2) \} + \left(\frac{\eta_1 \beta_1 I_0}{2k_1 (\beta_1^2 - \sigma_1^2)} \right) \{ (r_1 - 1)(b_1 + 1)(b_2 + 1) \exp(\sigma_1 l_1 + \sigma_2 l_2) - (r_1 + 1)(b_1 - 1)(b_2 + 1) \times \exp[-(\sigma_1 l_1 - \sigma_2 l_2)] + (b_1 - 1)(b_2 - 1) \exp(\sigma_1 l_1 - \sigma_2 l_2) - (r_1 + 1)(b_1 + 1)(b_2 - 1) \times \exp(\sigma_1 l_1 + \sigma_2 l_2) + 2[(b_1 - r_1)(b_2 + 1) \exp(\sigma_2 l_2) + (b_1 + r_1)(b_2 - 1) \exp(-\sigma_2 l_2)] \exp(-\beta_1 l_1) \} \times \{ (b_1 + 1)(b_2 + 1) \exp(\sigma_1 l_1 + \sigma_2 l_2) + (b_1 - 1)(b_2 + 1) \exp[-(\sigma_1 l_1 - \sigma_2 l_2)] + (b_1 + 1)(b_2 - 1) \exp[-(\sigma_1 l_1 + \sigma_2 l_2)] + (b_1 - 1)(b_2 - 1) \exp(\sigma_1 l_1 - \sigma_2 l_2) \}^{-1} \right] \times \sum_{n=0}^{\infty} \{ (1 + D) \exp[-\sigma_n (2nL + x)] - (1 - D) \exp[-\sigma_n (2(n+1)L - x)] \} \exp(i\omega_0 t) \quad (16)$$

or

$$T_g(x,t) = [N][M]^{-1} \sum_{n=0}^{\infty} [R(n)] \quad (16)$$

with $b_i \equiv k_2 a_2 / k_1 a_1$ and $b_i \equiv k_b a_b / k_2 a_2$ and the other symbols having their previous meanings with the subscripts referring to solids 1 or 2. With either l_1 or l_2 zero this expression reduces to that for a single-layer system given in Eq. (13) of Ref. 2.

The modulated pressure in the gas is obtained by substituting Eq. (16) into Eq. (8). If L is large compared to the thermal diffusion length in the gas, only the $n = 0$ term in the summation $\sum_{n=0}^{\infty} [R(n)]$ is retained and the expression for the pressure is

$$p(t; \omega_0) = \left(\frac{p_0 I_0 \exp[i(\omega_0 t - \frac{1}{2}\pi)]}{\sqrt{2a_g T_0 L}} \right) \frac{[N]}{[M]} \equiv Q_d \exp[i(\omega_0 t - \frac{1}{2}\pi)]. \quad (17)$$

By writing $[N]$ and $[M]$ in complex polar notation, as was done previously, this expression may be evaluated to obtain the amplitude and the phase of the photoacoustic response for the two-layer system.

For the case of a transparent overlayer on an absorbing substrate, as considered by Adams and Kirkbright,⁷ $\beta_1 = 0$ and $b_1 = 1$, then Q_d can be written as

$$Q_d = \left(\frac{p_0 I_0}{2\sqrt{2a_g T_0 L}} \right) \left(\frac{\eta_2 \beta_2}{k_2 (\beta_2^2 - \sigma_2^2)} \right) \left(\frac{1}{\exp(\sigma_1 l_1) + \exp(-\sigma_1 l_1)} \right) \times \left(\frac{(r_2 - 1)(b_2 + 1) \exp(\sigma_2 l_2) - (r_2 + 1)(b_2 - 1) \exp(-\sigma_2 l_2) + 2(b_2 - r_2) \exp(-\beta_2 l_2)}{(b_2 + 1) \exp(\sigma_2 l_2) + (b_2 - 1) \exp(-\sigma_2 l_2)} \right) \quad (18)$$

It is seen from the third term in Eq. (18) that Q_d , and hence the amplitude of the PAS signal, goes to zero as l_1 increases or as σ_1 increases due to an increased modulation frequency. Physically this is due to the thickness of the transparent overlayer on the absorbing substrate becoming considerably greater than the thermal diffusion length in that overlayer so that no ac component of the temperature fluctuation due to the absorbing substrate reaches the surface of the transparent overlayer. This modulated thermal signal from the absorbing underlayer decays to zero in the transparent overlayer in a distance of approximately $2\pi\mu$, from the intralayer boundary, just as occurs at the boundary between a single solid and the gas in a photoacoustic cell.

The phase of the PAS signal in the presence of a transparent overlayer can be written as

$$\psi = \tan^{-1}(-\omega_0 \tau_{\beta 2}) + \left(\frac{\omega_0}{2\alpha_1} \right)^{1/2} l_1 - \tan^{-1} \left(\frac{-1}{1 - (2\omega_0 \tau_{\beta 2})^{1/2}} \right) \quad (19)$$

When the absorption coefficient of the second layer is high and at normal modulation frequencies $(\omega_0 \tau_{\beta 2}) \rightarrow 0$, the phase becomes

$$\psi = \frac{\pi}{4} + \left(\frac{\omega_0}{2\alpha_1} \right)^{1/2} l_1. \quad (20)$$

This is the same expression given by Adams and Kirkbright.⁷ When the second solid has a lower optical absorption coefficient, an additional contribution will be made to the phase by the thermal diffusion times in that material.

Another case of interest is that of an absorbing thin film

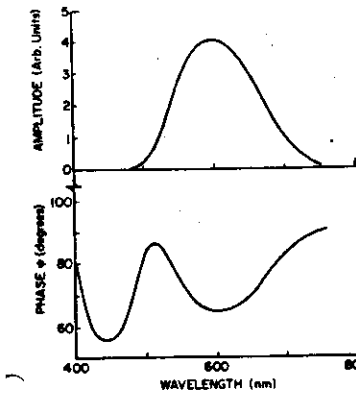


FIG. 7. A comparison between the amplitude and the phase response of a double-layer PAS system [$\beta_1(\text{max}) = 50 \text{ cm}^{-1}$, $\beta_2(\text{max}) = 500 \text{ cm}^{-1}$, $l_1 = 10^{-4} \text{ cm}$, $l_2 = 0.1 \text{ cm}$, $b_1 = b_2 = 1$].

with its absorption band overlapping the tail of the substrate absorption band. This case can be treated numerically using the full expressions for the PAS amplitude and phase derivable from Eq. (17). The results of such a calculation are shown in Fig. 7 for which it has been assumed that both the substrate and the film have Gaussian absorption bands situated at 600 and 500 nm respectively, with maximum absorption coefficients of 0.15 and 0.10 eV, respectively. As shown in Fig. 7 the presence of the surface film gives rise to a very small shoulder on the tail of the bulk PAS amplitude response. Provided the amplitude of the signal is large enough for the phase of the signal to be accurately measured this channel provides a clearer indication of the presence of the film. The wavelength dependence of the phase is, however, complex and depends upon both the amplitude and phase of the contributions from the two layers. As the wavelength of the light is scanned from short wavelengths the variable contribution to the phase of the signal changes from the 90° characteristic of a transparent material toward the value of 45° characteristic of an optically opaque material. Initially this signal is controlled in both amplitude and phase by the absorbing front solid. As the absorption coefficient of the back solid starts to become important, a contribution to the PAS signal is made by this second layer. The phase of this additional response is modified by the thermal transit time through the front film as well as by the changing absorption depth in the back solid. The amplitude of this signal also depends upon the absorption coefficients of both layers. Since for the case illustrated the second film has a much higher absorption coefficient than the surface film, the amplitude of the signal from this layer is much larger than that from the front solid and the phase of the response of the composite is finally dominated by the signal from the second layer. As the wavelength of the light is increased, the absorption coefficient of the front solid goes to zero and the phase of the signal depends only on the second solid and the thermal transit time characteristic of the first solid and is described by Eq. (19). Although this phase behavior does not provide a ready measure of the absorption coefficient of the front solid it does indicate the presence of such a solid and enables the correct interpretation to be made of the shoulder present in the amplitude signal. As has been pointed out by Rosencwaig and Gersho,² provided the PAS amplitude is high enough, the absorption behavior of the front solid can also be separated from that of an absorbing underlayer by making measurements at chopping frequencies for which $\mu_s \lesssim l_1$.

III. DISCUSSION

As indicated by the models outlined above, the phase data that is available in addition to amplitude information in frequency domain photoacoustic spectroscopy provides ad-

ditional insight into the properties of the system under study. The phase information, however, contains contributions from many sources and only in special limits of sample optical and thermal properties can the phase be unambiguously associated with one particular mechanism. In addition to phase contributions from the sample, the photoacoustic cell, the position of the sample within the cell, the preamplifier for the microphone, and the microphone itself will also produce phase shifts that will, in general, be dependent upon the modulation frequency of the radiation. It is therefore experimentally difficult to make accurate absolute phase measurements, however relative phase can be measured with considerable precision provided the signal-to-noise ratio of the P/S system is high enough and that calibration curves are available for those sources other than the sample.

For a sample in which the nonradiative relaxation processes are instantaneous the phase data can provide an alternate measure of the optical absorption coefficient of the solid. As this optical absorption coefficient increases, the phase lag of the PAS signal with respect to the modulated light source is reduced. As shown in the inset in Fig. 4 the phase data can replicate the shape of an optical absorption band, however phase saturation occurs at high optical absorption coefficients. It was suggested by Roark *et al.*¹¹ that the phase of the PAS signal enabled measurements to be extended to higher optical absorption coefficients than were measurable using the PAS amplitude. Both the theory presented above and measurements made in this laboratory suggest that this is not the case. Figure 4 also shows a comparison between the relative amplitude of the photoacoustic signal as a function of the absorption coefficient and the corresponding phase of the signal for a thermally thick sample. It is seen that the two measurements essentially coincide and the parallelism between the amplitude and phase response increases at higher chopping frequencies and sample thicknesses. At the low β limit both the phase and the amplitude depend linearly upon β . As β increases the curves pass through a region for which the amplitude and the phase have an approximately logarithmic dependence upon β after which saturation occurs. One advantage of the phase measurement however, is that it is insensitive to light intensity fluctuations whereas the amplitude will follow these fluctuations.

For optically thin samples the angular range of the phase measurement is dependent upon the relative values of the effective sample thickness and the thermal diffusion length in the solid. This behavior is indicated in Fig. 2 and shows that for modulation frequencies for which $\omega_0 \tau_s \ll 1$ the angular range of the phase response decreases as b decreases. The dependence of the phase change on sample thickness at a given modulation frequency is exactly analogous to the corresponding dependence of PAS phase on the length of the gas in the cell compared to the thermal diffusion length in the gas as discussed by Aamodt *et al.*⁴ Once the sample thickness is greater than about five times the thermal diffusion length in the sample the photoacoustic phase is sample thickness independent (the thermally thick limit).

The measurement of the nonradiative lifetime can be made without contributions to the phase arising from the optical absorption coefficient of the solid only in the optical-

ly thick or the optically thin limit. At intermediate values of the optical absorption coefficient the phase will contain a contribution due to the optical absorption depth in the solid and this contribution must be subtracted from the total phase to obtain the correct value of the nonradiative lifetime. The optically thick limit for which $\mu_\beta < \mu_s$ seems to be the most satisfactory choice for experimental measurement since the amplitude of the PAS signal has saturated together with any phase contribution from the optical absorption coefficient. Only changes in the nonradiative lifetime will contribute to the sample related phase shift under these conditions.

In their measurements of radiationless relaxation processes in various solid systems Powell and co-workers^{9,10,12} have used the gas phase relationship developed by Harshbarger and Robin¹¹ to obtain a measure of this lifetime. Although this expression is similar to that which applies for the case of an optically thick solid with $\mu_\beta < \mu_s$, Eq. (13), it is not clear from the data presented in their papers that this was the experimental situation. The photoacoustic amplitude data does not seem to show saturation, as would be expected in this limit, and consequently the optical absorption depth will be making a contribution to the measured relative phase angle. Only if this contribution was the same in the e_g and t_{2g} bands of the Eu^{2+} ions would the measured phase angle be directly related to the lifetime. Similar comments apply to the measurement of the relative lifetime for nonradiative processes of a given ion type in several host lattices. Only if all of the systems are studied in the optically thick region or if the absolute absorption coefficient of the host lattice plus the solute ion are the same in each case will it be possible to avoid contributions due to the absorption depth of the radiation. It would also seem to be fortuitous that the maximum response of the PAS signal occurred at 0° with the lock in amplifier since a $\frac{1}{2}\pi$ phase shift is to be expected due to the heat transfer process between the solid and the gas in the cell¹ and another $\frac{1}{2}\pi$ due to the fact that the heat flow leads the temperature wave by 45°. These contributions are in addition to any phase shifts due to the optical absorption processes in the solid or contributions from the cell, sample position, and microphone. Such a zero phase shift cannot be correctly interpreted as an instantaneous relaxation process without detailed knowledge of these other contributions.

The phase calculations for the multilayer solid suggest that use of this information together with the PAS amplitude is a good method for detecting surface films. This was also suggested by Bennett and Forman.¹³ Conversion of the phase data into a value of the optical absorption coefficient is complicated for this configuration since signals from an absorbing substrate will have both a phase shift due to the thermal transport time through the surface film and a phase shift due to the wavelength-dependent optical absorption coefficient of the substrate. In the limit of a transparent overlayer on a substrate of high optical absorption coefficient for which the β -dependent phase shift is saturated, the present calculations are in agreement with those of Adams and Kirkbright.⁴ For a substrate of lower optical absorption coefficient a phase shift arising from the thermal transport time in the substrate will be added to the constant phase shift due to

transport through the transparent overlayer.

In conclusion, the phase of a photoacoustic signal from a solid sample can provide valuable information concerning its structure, thermal properties, optical absorption characteristics, and the lifetimes of the nonradiative transitions responsible for the photoacoustic signal. In the general case contributions to the measured phase will arise from all of these sources; however, for various limiting cases discussed above individual contributions may be isolated. The theory developed in this paper is applicable to samples having a planar form and in good thermal contact with their supporting substrate and consequently is applicable to liquid as well as solid specimens. Experimental measurements indicate that powdered specimens exhibit phase behavior, however, for certain conditions of powder size and optical absorption coefficient phase reversals can occur. This data will be discussed in a later paper.

ACKNOWLEDGMENTS

One of us (BSHR) would like to thank H.S. Reichard for starting his interest in photoacoustic phase measure-

ments. This work was supported in part by ARO contract No. DAAG29-76-C-0054.

- ¹M.B. Robin, *Photoacoustic Spectroscopy and Detection*, edited by Yoh-Han Pao (Academic, New York, 1977), p. 167 *et seq*.
- ²A. Rosencwaig and A. Gersho, *J. Appl. Phys.* **47**, 64 (1976).
- ³A. Rosencwaig, *J. Appl. Phys.* **49**, 2905 (1978).
- ⁴L.C. Aamodt, J.C. Murphy, and J.G. Parker, *J. Appl. Phys.* **48**, 927 (1977).
- ⁵J.G. Parker, *Appl. Opt.* **12**, 2974 (1973).
- ⁶M.J. Adams and G.F. Kirkbright, *Spectrosc. Lett.* **9**, 255 (1976).
- ⁷M.J. Adams, B.C. Beadle, A.A. King, and G.F. Kirkbright, *Analyst* **101**, 353 (1976).
- ⁸M.J. Adams and G.F. Kirkbright, *Analyst* **102**, 281 (1977).
- ⁹L.D. Merkle and R.C. Powell, *Chem. Phys. Lett.* **46**, 303 (1977).
- ¹⁰L.D. Merkle and R.C. Powell, *J. Phys. C* **11**, 3103 (1978).
- ¹¹W.R. Harshbarger and M.B. Robin, *Acco. Chem. Res.* **6**, 329 (1973).
- ¹²R.G. Peterson and R.C. Powell, *Chem. Phys. Lett.* **53**, 366 (1978).
- ¹³J.C. Roark, R.A. Palmer, and J.S. Hutchison, *Chem. Phys. Lett.* **60**, 112 (1978).
- ¹⁴H.S. Carslaw and J.C. Jaeger, *Conduction of Heat in Solids*, 2nd ed. (Oxford U. P., London, 1952) Chap. 2, Sec. 6.
- ¹⁵H.S. Bennett and R.A. Forman, *J. Appl. Phys.* **48**, 1432 (1977).

Photothermal spectroscopy of scattering media

Zafer A. Yasa, Warren B. Jackson, and Nabil M. Amer

We present a general unified theoretical analysis of the role of scattering in photothermal spectroscopy, e.g., photoacoustic and photothermal deflection. We show that while the photothermal signal is significantly affected in the case of highly scattering media, it is independent of scattering for optically thin samples. Numerical estimates of the scattering contribution and comparison with experimental results are given. We also elucidate the relationship between photothermal and diffuse reflectance spectroscopies.

1. Introduction

Insensitivity to scattering has generally been assumed to be an inherent characteristic of photoacoustic spectroscopy,¹ since the photoacoustic signal is proportional to the fraction of absorbed energy which is converted to heat. Consequently, even for a highly scattering medium, the photoacoustic signal is presumed to be a direct measure of its absorption cross section. However, it is well known that the reflectance of such a medium, which is conventionally studied by diffuse reflectance spectroscopy, is a complicated function of its scattering properties^{2,3} as well as its absorption. The total absorbed energy, while proportional to the absorption cross section α_a , is also a function of the intensity distribution in the sample, which can deviate significantly from Beer's law when multiple scattering is important. Therefore, in principle, the thermal signal generated is affected by scattering. This was first discussed by Helander and Lundstrom,⁴ who considered the special case of a semi-infinite (optically and thermally thick) and isotropically scattering sample.

In this paper, we present a general unified analysis of the effects of light scattering in most common photothermal (photoacoustic and photothermal deflection⁵) spectroscopies (PTS) for arbitrary sample thicknesses and scattering characteristics. By simultaneously analyzing the heat diffusion equation and the radiative

transport equation, we determine the photothermal signal S in terms of the optical and thermoelastic constants of the sample. We thereby rigorously establish the relationship between (1) photothermal spectroscopies and (2) optical transmission and reflectance spectroscopies. We show that, in general, PTS is significantly affected by strong scattering.

For low modulation frequencies such that $l_{th} \gg l$ or $l_{th} \gg l_{op}$, where l , l_{th} , and l_{op} are the sample, thermal, and optical lengths, respectively (i.e., when energy is deposited in a distance much shorter than the thermal length), we determine exactly that $S \propto [1 - (R + T)]$, where $R(T)$ is the diffuse and specular reflectance (transmittance) of the sample. For an optically thick sample ($T = 0$), this expression implies that $S \propto (1 - R)$ and, therefore, that the photothermal spectrum of a sample is in principle equivalent to its diffuse reflectance spectrum in this limit. As the modulation frequency is increased, we show that S varies from $S \propto [1 - (R + T)]$ to $S \propto \alpha_a [1 + 2R(1 + r_0)/(1 - r_0)]$ (where r_0 is the sample surface reflectance for internally incident diffuse light), depending on the optical properties (scattering, absorption) and the thermal diffusivity of the sample. This variation of S occurs because of the dependence of the heat flow on modulation frequency. Hence we stress that PTS can yield important information unavailable by optical methods, which, combined with optical measurements, can be very useful for the determination of the optical constants of highly scattering media.

Using the above results, we also show that, for optically thin media, S is independent of scattering when $\alpha_s l \leq 0.1$ (α_s = scattering coefficient). This independence is in significant contrast to an optical measurement which would be dominated by scattering if $\alpha_s l \geq \alpha_a l$.

In Sec. II, we derive the general expression for S for the most commonly encountered cw PTS experimental configurations. In general, the PTS signal is given by

Table I. Definition of Parameters for Various PTS Methods

Method	$T_r(\omega)$ (transducer sensitivity)	$T_t(\omega)$	$G(x, \rho, \phi)$	Description of parameters (f : fluid; s : sample)
Sample-fluid -transducer (SFT)	V/dyn/cm ²	$\frac{\beta_f}{V_s K_{Tf}}$	$\frac{\delta(x)}{k_f} + \frac{\beta_s}{\beta_f}$	K_T = isothermal compressibility β = coefficient of thermal expansion $k = (1 + i)(\omega \rho C_p / 2\kappa)^{1/2}$ ω = modulation frequency ρC_p = heat capacity/unit volume at constant pressure V_s = effective cell volume = $V_f + V_s K_{Ts}/K_{Tf}$ ρ = density κ = thermal conductivity
Fluid- transducer (FT)	V/dyn/cm ²	$\frac{\beta}{K_T V}$	1	α = cell radius
(a) nonresonant (b) resonant		$\frac{i2\beta}{Q_s \pi V K_{Tf} J_0(\pi \alpha_f)}$	$J_0\left(\frac{\pi}{\alpha} \alpha_f \rho\right) - 1$	$\frac{d}{d} J_0(\pi \alpha) _{\alpha=\alpha_f} = 0$ $\frac{d}{d} Q_s$ = cavity Q (nth mode)
Solid- transducer (ST)	V/unit strain	$\beta(1 + \nu)$	$1 \pm 3\left(1 - \frac{2x}{l}\right)$	l = sample length ν = Poisson's ratio
Transverse photothermal deflection (PDS)	V/rad	$\frac{1}{n_0} \frac{dn}{dT} \sqrt{\frac{2}{\pi}}$ $\times k_f^2 \frac{\exp(k_f/2\alpha)}{\alpha_0}$	$\frac{\delta(x)}{k_f}$	α_0 = pump beam radius $\frac{1}{n_0} \frac{dn}{dT}$ = relative change of refractive index with temperature

Table II. Effective Parameters for Porous Media⁷

Parameter	Effective parameter	Remarks
K_T	$K_s \Omega$	Ω = volume fraction of fluid (porosity) Accounts for thermal and mechanical properties of the fluid-sample system
β	$\beta_s \Omega$	
κ	κ_s	
ρC_p	$(\rho C_p)_s$	

a weighted average of the sample temperature distribution, which we determine in terms of an arbitrary intensity distribution in Sec. II.A. In Sec. II.B, utilizing the equation of radiative transfer for diffuse photons, we solve for the integrals of the sample intensity distribution which appear in the temperature solutions. In Sec. II.C, we determine the low frequency, high frequency, and semi-infinite sample limits. The results in Sec. II.A-II.C involve the measurable (external) optical properties of samples R and T . These can be determined in terms of the intrinsic optical parameters (e.g., α_a , α_s) from the equation of radiative transfer by approximate analytical methods or numerically. The approximate expressions for R and T using three-flux calculation are given in Sec. II.D, and S is evaluated in the limits of Sec. II.C.

In Sec. III, we evaluate our theoretical results for some special cases and compare our theoretical findings with the experimental measurements of Helander and Lundstrom.⁴ We discuss the implications of our results for the photothermal spectroscopy of highly scattering media.

II. Theory

A. General Solution for the Photothermal Signal in Terms of the Photon Distribution in the Sample

We consider media with isotropic and homogeneous thermoelastic and optical properties but which may be porous (Table I). Porous media are taken into account by effective values of these properties,^{6,7} which may also be complex and frequency dependent (Table II). We neglect fluorescence, thermal radiation, energy migration, etc.

The signal S , generated in the most common cw photothermal experiments, can be written^{5,8-10}

$$S(\omega) = T_r(\omega) \int_V \int G(r) \tau(r) d^3r,$$

where $T_r(\omega) = T_r(\omega) T_t(\omega)$, $T_t(\omega)$ is a thermoelastic transduction factor, $T_r(\omega)$ is the transducer response (including a possible Helmholtz resonance response), $\tau(r)$ is the temperature distribution in the sample, V is the sample volume, and ω is the frequency. $G(r)$ is a geometrical weighting factor describing the relative contributions of the sample temperature distribution in the thermoacoustic conversion. In Table I, the expressions for $T_r(\omega)$ and $G(r)$ are given for the four major groups of cw PTS configurations (Fig. 1), and the various material parameters are defined.

In the case of resonant fluid-transducer (FT) detection, we consider cylindrically symmetric, zero-order longitudinal, and low-order radial modes, for which the

When this work was done all authors were with University of California, Lawrence Berkeley Laboratory, Applied Physics & Laser Spectroscopy Group, Berkeley, California 94720; W. B. Jackson is now with Xerox Research Center, Palo Alto, California 94304.

Received 22 June 1981.

0003-6935/82/010021-11\$01.00/0.

© 1982 Optical Society of America.

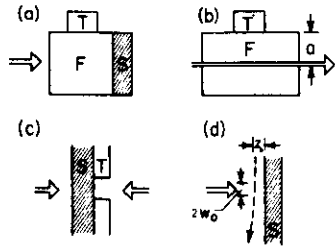


Fig. 1. Continuous-wave photothermal techniques considered in this paper: (a) SFT technique (nonresonant). If the fluid is a gas, this describes the sample-gas-microphone (SGM) technique. If the fluid is a liquid, the transducer (hydrophone) is usually a PZT. (b) FT technique (resonant or nonresonant). For a gas, it describes the gas-microphone spectrophone. For a liquid, the transducer is generally a PZT. (c) ST technique (nonresonant). The sample is epoxied to a flat PZT transducer which has a hole at the center to minimize the scattered light directly hitting the transducer. The beam can be incident from either side.¹⁰ (d) Transverse PDS technique. Pump beam of radius w_0 is normally incident on the sample. A probe beam of much smaller radius propagates parallel to the sample a distance z_0 away from the surface and through the center of the pump beam. The deflection of the probe beam is given by the average temperature gradient along its propagation path.⁵

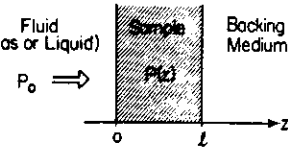


Fig. 2. Typical sample geometry: l is the length of the sample. The fluid and backing regions are assumed to be thermally thick.

laterally diffused beam diameter is much smaller than the mode diameter. Hence $G(r) \rightarrow 1$. (This assumption may not be valid for high-order modes excited by large diameter beams in highly scattering fluids.) Thus FT detection (resonant and nonresonant) is a special case of sample-fluid-transducer (SFT) detection with a fluid sample completely filling the cell.

Photothermal deflection spectroscopy (PDS) is also a special case of SFT detection. The equation in Table I for PDS has a somewhat restricted validity. When the scattering length is much less than the beam diameter, this equation is exact. Using the photon diffusion equation or intuitive arguments, we find that, when the scattering length is much larger than the beam diameter, the scattering contribution to the PDS signal is reduced by the scattering length divided by the beam diameter when compared with the scattering contribution to SFT.

$$\bar{T}(z) = \frac{\alpha_0}{2\pi k} \left[C_0 \{ (1+g) \exp(kz) + (1-g) \exp(-kz) \} + \exp(-kz) \int_0^l P(\xi) \exp(k\xi) d\xi - \exp(kz) \int_0^l P(\xi) \exp(-k\xi) d\xi \right] \quad (3)$$

where

Continuous wave solid-transducer (ST) detection is not widely applicable to highly scattering media due to scattered light incident directly on the transducer. However, for completeness, we derive the fundamental equations pertaining to this technique in the Appendix.

Since the SFT case is general, we write

$$S(\omega) = T_s(\omega) \left[\frac{1}{k_f} \bar{T}(0) + \frac{\beta_s}{\beta_f} \int_0^l \bar{T}(z) dz \right] \quad (1)$$

where

$$\bar{T}(z) = \iint_S \bar{T}(r) d^2\rho$$

is the average sample temperature in the transverse plane at z . The first term in the brackets in Eq. (1) gives the signal contribution due to the heat diffusion from the sample into the fluid. Form $\bar{T}(0)$ implies that only the energy deposited near (within a thermal length) the surface contributes to the signal. However, the contribution of the second term, which is due to the thermal expansion of the sample, depends on all the energy deposited in the sample. We assume that the contribution due to the buckling of a solid sample is negligible. For FT detection, only the second term contributes, and for PDS only the first term contributes.

In Fig. 2, the sample geometry is sketched. We have assumed that the incident beam size \ll transverse sample dimensions, and that the media on either side of the sample are thermally thick. We have also assumed that the cell boundaries are perfectly rigid and that the pressure within the sample equalizes with the pressure in the fluid. For porous media this condition may be violated since the sample may be larger than the pressure diffusion length.⁶ This results in a modification of the second term in the expression for V_s (Table I). However, if the sample volume V_s is much less than the volume of the fluid V_f , $V_s \approx V_f$, and this effect is then negligible.

Integrating the heat equation over the transverse plane in the sample and using the condition that the flux reaches the sample sides, the average temperature at plane z in the sample (oscillating at frequency ω) satisfies

$$\left(\frac{d^2}{dz^2} - k^2 \right) \bar{T}(z) = -\frac{\alpha_0}{k} P(z) \quad (2)$$

with the boundary conditions

$$\kappa \frac{d\bar{T}}{dz} \Big|_{z=0} = \kappa_f k_f \bar{T}(0), \quad \kappa \frac{d\bar{T}}{dz} \Big|_{z=l} = -\kappa_b k_b \bar{T}(l) \quad (2a)$$

$P(z) = \iint_S I(r) d^2\rho$ is the power distribution in the sample (oscillating at frequency ω), $k^2 = i\omega\rho C_p/k$, $k_f^2 = i\omega\rho_f C_{pf}/k_f$, $k_b^2 = i\omega\rho_b C_{pb}/k_b$, and $\kappa, \kappa_f, \kappa_b$ = thermal conductivity, and $\rho C_p, \rho_f C_{pf}, \rho_b C_{pb}$ = heat capacity/unit volume at constant pressure of the sample, fluid, and backing, respectively.

The general solution of Eq. (2) subject to Eq. (2a) is

$$C_0 = \frac{[(1-b) \exp(-kl) \int_0^l P(z) \exp(kz) dz + (1+b) \exp(kl) \int_0^l P(z) \exp(-kz) dz]}{[k(1+b)(1+g) \exp(kl) - (1-b)(1-g) \exp(-kl)]} \quad (3a)$$

$$g = \frac{\kappa_f k_f}{\kappa k}, \quad b = \frac{\kappa_b k_b}{\kappa k}$$

Integrating Eq. (2) over $0 \leq z \leq l$ and using Eq. (2a), we find

$$\int_0^l \bar{T}(z) dz = \frac{1}{\kappa k^2} \left[\alpha_0 \int_0^l P(z) dz - \kappa_b k_b \bar{T}(l) - \kappa_f k_f \bar{T}(0) \right] \quad (4)$$

in which, from Eqs. (3) and (3a),

$$\bar{T}(0) = \frac{\alpha_0 \left[(1-b) \exp(-kl) \int_0^l P(z) \exp(kz) dz + (1+b) \exp(kl) \int_0^l P(z) \exp(-kz) dz \right]}{\kappa k [(1+b)(1+g) \exp(kl) - (1-b)(1-g) \exp(-kl)]} \quad (5)$$

$$\bar{T}(l) = \frac{\alpha_0 \left[(1+g) \int_0^l P(z) \exp(kz) dz + (1-g) \int_0^l P(z) \exp(-kz) dz \right]}{\kappa k [(1+b)(1+g) \exp(kl) - (1-b)(1-g) \exp(-kl)]} \quad (6)$$

The terms in Eq. (4) have a simple physical interpretation. The first term is the total energy/sec deposited in the sample. The second and third terms are the heat flux/sec out of the back and front surfaces of the sample, respectively. Hence the terms within the brackets give the net energy increase/sec of the sample. The multiplication factor converts the energy increase/sec into a temperature rise/cycle.

Equations (4), (5), and (6) substituted into Eq. (1) yield the photothermal signal in terms of weighted averages of the optical power distribution in the sample, of the form $\int_0^l P(z) \exp(\pm kz) dz$. In the next section, these integrals are determined for a sample which has both absorption and scattering.

B. Solution for $\int_0^l P(z) \exp(kz) dz$

Assuming that a collimated beam of power P_0 is incident on the sample at $z=0$, the optical power distribution in the sample $P(z)$, is the sum of diffuse and collimated components:

$$P(z) = \int_{-1}^1 P_d(z, \mu) d\mu + P_0 \exp(-\alpha z) \quad (7)$$

where $P_d(z, \mu)$ is the diffuse power (diffuse intensity distribution integrated over the transverse plane) at z , propagating at an angle θ ($\mu = \cos\theta$) relative to the z direction (Fig. 3). The collimated beam decays by the total attenuation coefficient $\alpha = \alpha_0 + \alpha_s$.

Assuming macroscopically homogeneous and isotropic media, assuming incoherent and elastic scattering, and neglecting depolarization effects, the diffuse power distribution satisfies¹¹⁻¹³

$$\mu \frac{d}{dz} P_d(z, \mu) = -\alpha P_d(z, \mu) + \alpha \int_{-1}^1 s(\mu, \mu') P_d(z, \mu') d\mu' + \alpha_0 P_0 \exp(-\alpha z) s(\mu, 1) \quad (8)$$

where $s(\mu, \mu') \equiv s(\theta - \theta')$ is the indicatrix of anisotropic scattering describing the angular distribution of scattered photons (relative amount scattered from the cone θ to θ'). $s(\mu, \mu')$ is symmetric [$s(\mu, \mu') = s(\mu', \mu)$] and

normalized [$\int_{-1}^1 s(\mu, \mu') d\mu = \int_{-1}^1 s(\mu, \mu') d\mu' = 1$]. It is a function of the diameter d relative to wavelength λ and of the shape of the refractive-index inhomogeneities; it is specified as a mean over a distribution of sizes and shapes. For isotropic scattering $s(\mu, \mu') = 1/2$. For $\lambda/d \leq 1$ (Mie scattering), $s(\mu, \mu')$ is elongated in the forward direction ($\mu = \mu'$). For $\lambda/d \gg 1$ (Rayleigh scattering) $s(\mu, \mu') = [\cos^2(\theta - \theta') + 1]/3$.

Equation (8) is the radiative transfer equation describing the energy balance for the net change of $P_d(z, \mu)$ per unit length in the propagation direction. It states that the diffuse light $P_d(z, \mu)$ at z , propagating in the μ direction, is decreased by absorption and scattering (first term), increased by the diffuse light scattered in the μ direction from the diffuse photons propagating in all other directions (second term), and increased by photons scattered diffusely into the μ direction from the collimated beam propagating in the $\mu = 1$ direction (third term). For simplicity, we have neglected the specular reflections of the collimated beam at the boundaries. These reflections, which are generally small, can be taken into account by a simple modification of the last term in Eq. (8). The boundary conditions for diffuse light are to be taken into account by defining the relevant reflection coefficients at the boundaries.

It is not possible to obtain exact analytical solutions of Eq. (8) for arbitrary $s(\mu, \mu')$ and sample length. A simplification follows, however, since only integrals of the form $\int_0^l P(z) \exp(\pm kz) dz$ are needed for the determination of S from Eqs. (1) and (4)-(6). We multiply Eq. (8) by $\exp(kz)$ and integrate over $0 \leq z \leq l$, obtaining

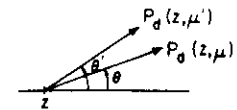


Fig. 3. Diffuse photons sec at position z , propagating in directions $\theta \cos \theta = \mu$ and $\theta' \cos \theta' = \mu'$ relative to the z axis.

$$\mu[P_d(l, \mu) \exp(kl) - P_d(0, \mu)] = (k\mu - \alpha)P_d(k, \mu) + \alpha \int_{-1}^1 P_d(k, \mu') s(\mu, \mu') d\mu' + \frac{\alpha_s}{(\alpha - k)} P_0 [1 - \exp(-\alpha + k)l] s(\mu, 1),$$

where

$$P_d(k, \mu) = \int_0^1 P_d(z, \mu) \exp(kz) dz$$

Defining

$$P_d^+ = \int_0^1 P_d(k, \mu) d\mu, \quad \Phi^+(x) = \int_0^1 P_d(x, \mu) \mu d\mu, \quad P_d^- = \int_{-1}^0 P_d(k, \mu) d\mu, \quad \Phi^-(x) = - \int_{-1}^0 P_d(x, \mu) \mu d\mu. \quad (9)$$

and adding and subtracting the integrals of the above equation over $0 \leq \mu \leq 1$ and $-1 \leq \mu \leq 0$, we obtain

$$\begin{aligned} [\Phi^+(l) \exp(kl) - \Phi^+(0)] - [\Phi^-(l) \exp(kl) - \Phi^-(0)] &= k \left[\int_0^1 \mu P_d(k, \mu) d\mu + \int_{-1}^0 \mu P_d(k, \mu) d\mu \right] - \alpha_s (P_d^+ + P_d^-) \\ &\quad + \frac{\alpha_s}{(\alpha - k)} P_0 [1 - \exp(-\alpha + k)l], \\ [\Phi^+(l) \exp(kl) - \Phi^+(0)] + [\Phi^-(l) \exp(kl) - \Phi^-(0)] &= k \left[\int_0^1 \mu P_d(k, \mu) d\mu - \int_{-1}^0 \mu P_d(k, \mu) d\mu \right] - \alpha (P_d^+ - P_d^-) \\ &\quad + \alpha_s \int_{-1}^1 P_d(k, \mu') \left[\int_0^1 s(\mu, \mu') d\mu - \int_{-1}^0 s(\mu, \mu') d\mu \right] d\mu' + \frac{\alpha_s}{(\alpha - k)} \eta P_0 [1 - \exp(-\alpha + k)l]. \quad (10) \end{aligned}$$

where $\eta = 1 - 2 \int_{-1}^0 s(\mu, 1) d\mu$.

Then we apply the Schuster-Schwarzschild (Kubelka-Munk) approximation commonly used in radiative transfer theory¹² by setting

$$\begin{aligned} \int_0^1 \mu P_d(k, \mu) d\mu &= \frac{1}{2} P_d^+, & \int_{-1}^0 \mu P_d(k, \mu) d\mu &= -\frac{1}{2} P_d^-, \\ \int_{-1}^0 \mu P_d(k, \mu) d\mu &= -\frac{1}{2} P_d^-, & \int_{-1}^0 \mu P_d(k, \mu) d\mu &= \frac{1}{2} P_d^-. \end{aligned} \quad (11)$$

Note that Λ and η are parameters that take into account the anisotropy of scattering. Λ describes the ratio of the backscattered to the forward-scattered diffuse photons, and η describes the difference between the relative number of photons diffusely scattered from the collimated beam into the forward and backward directions. In general, $0 \leq \eta \leq 1$, $0 \leq \Lambda \leq 1$, and $\Lambda = 1$, $\eta = 0$ for isotropic scattering. Equation (11) becomes exact if the diffuse light is uniformly distributed in each of the forward and backward hemispheres. Using Eq. (11), we obtain

$$\begin{aligned} [\Phi^+(l) \exp(kl) - \Phi^+(0)] - [\Phi^-(l) \exp(kl) - \Phi^-(0)] &= \frac{k}{2} (P_d^+ - P_d^-) - \alpha_s (P_d^+ + P_d^-) + \frac{\alpha_s}{(\alpha - k)} P_0 [1 - \exp(-\alpha + k)l], \\ [\Phi^+(l) \exp(kl) - \Phi^+(0)] + [\Phi^-(l) \exp(kl) - \Phi^-(0)] &= \frac{k}{2} (P_d^+ + P_d^-) - (\alpha_s + \alpha_s \Lambda) (P_d^+ - P_d^-) + \frac{\alpha_s}{(\alpha - k)} \eta P_0 [1 - \exp(-\alpha + k)l], \end{aligned}$$

which can be solved simultaneously for P_d^+ and P_d^- , giving the result

$$\begin{aligned} \int_0^1 P(z) \exp(kz) dz &= P_d^+ + P_d^- + \frac{P_0}{(\alpha - k)} [1 - \exp(-\alpha + k)l] \\ &= [k^2 - 4\alpha_s(\alpha_s + \alpha_s \Lambda)]^{-1} \\ &\quad \times \left\{ 2[k + 2(\alpha_s + \alpha_s \Lambda)] [\Phi^+(l) \exp(kl) - \Phi^+(0)] \right. \\ &\quad + 2[k - 2(\alpha_s + \alpha_s \Lambda)] [\Phi^-(l) \exp(kl) - \Phi^-(0)] \\ &\quad \left. + \frac{P_0}{(\alpha - k)} [k^2 - 4\alpha_s(\alpha_s + \alpha_s \Lambda) - 2\eta\alpha_s k] [1 - \exp(-\alpha + k)l] \right\}. \quad (12) \end{aligned}$$

In Eq. (12), the fluxes at the boundaries $\Phi^+(0)$ and $\Phi^-(l)$ can be written in terms of the total reflected and transmitted fluxes from the sample using the boundary conditions

$$\begin{aligned} \Phi^+(0) &= r_0 \Phi^-(0), \\ \Phi^-(l) &= r_l \Phi^+(l) + r_{cl} P_0 \exp(-\alpha l) \end{aligned} \quad (13)$$

and definitions

$$\begin{aligned} \Phi^+(l) - \Phi^-(l) &= \Phi^+(0) - \Phi^-(0) = RP_0, \\ \Phi^+(l) - \Phi^-(l) + P_0 \exp(-\alpha l) &= TP_0. \end{aligned} \quad (14)$$

In Eqs. (13) and (14), r_0 and r_l are the effective reflection coefficients for internally incident diffuse light at the sample boundaries, r_{cl} is the coefficient for diffuse reflection of the collimated flux at $z = l$, and R and T are the reflectance and transmittance of the sample, respectively. Due to total internal reflection for incidence angles greater than the critical angle, r_0 and r_l have values substantially higher than for normal incidence. (For isotropically diffuse light $r_{0,l} \approx 0.6$ for a refractive-index ratio of 1.5). In some experiments, the backing medium may be a high diffuse reflector¹⁴ for which r_l and r_{cl} assume values close to unity.

Substituting Eqs. (13) and (14) into Eq. (12), we obtain

$$\begin{aligned} \int_0^1 P(z) \exp(kz) dz &= \frac{P_0}{[k^2 - 4\alpha_s(\alpha_s + \alpha_s \Lambda)]} \left\{ 2R \left[2(\alpha_s + \alpha_s \Lambda) - k \left(\frac{1+r_0}{1-r_0} \right) \right] + 2T \exp(kl) [2(\alpha_s + \alpha_s \Lambda) + k \left(\frac{1+r_l}{1-r_l} \right)] \right. \\ &\quad \left. + \frac{[k^2 - 4\alpha_s(\alpha_s + \alpha_s \Lambda) - 2\eta\alpha_s k]}{(\alpha - k)} + \frac{k \exp(-\alpha + k)l}{(\alpha - k)} [k + 2\alpha_s + 2\alpha_s(2\Lambda + \eta - 1) + 4(\alpha - k) \frac{r_{cl}}{1-r_{cl}}] \right\}. \quad (15) \end{aligned}$$

For isotropic scattering ($\Lambda = 1$, $\eta = 0$) and $r_{cl} = 0$, Eq. (15) reduces to

$$\int_0^1 P(z) \exp(kz) dz = \frac{P_0}{(k^2 - 4\alpha_s \alpha)} \left\{ 2R \left[2\alpha - k \left(\frac{1+r_0}{1-r_0} \right) \right] + \left[2\alpha + k \left(\frac{1+r_l}{1-r_l} \right) \right] + 2T \exp(kl) - \frac{2\alpha + k}{(\alpha - k)} [2\alpha - k(1 + \exp(-\alpha + k)l)] \right\}. \quad (15a)$$

C. Special Cases

Equation (15) substituted into Eqs. (1) and (4)-(6) yields the photothermal signal in terms of the modulation frequency and the optical properties of the sample. Of particular interest are the limiting cases as $\omega \rightarrow 0$, $\omega \rightarrow \infty$, and $l \rightarrow \infty$, which are treated in this section.

1. $l_{th} \approx 1/|k| \gg l$ or $l_{th} \gg l_{op} \approx 1/\alpha$

This is the case when the energy is deposited in a region much shorter than the thermal length (see Fig. 4). We can set $\int_0^1 P(z) \exp(kz) dz \approx \int_0^1 P(z) dz$, which, by direct integration of Eq. (8) and using Eq. (4), is given by

$$\alpha_s \int_0^1 P(z) dz = [1 - (R + T)] P_0. \quad (16)$$

Using the above in Eqs. (1) and (4)-(6) implies that in this limit

$$S \rightarrow T_s(\omega) \frac{P_0}{\kappa k l} F(\omega) [1 - (R + T)], \quad (17)$$

where

$$F(\omega) = \frac{[(1-b) \exp(-kl) + (1+b) \exp(kl)] \left(1 + \frac{\beta_s k_l}{\beta_l k} \right) - \frac{2b\beta_s k_l}{\beta_l k}}{[(1+b)(1+g) \exp(kl) - (1-b)(1-g) \exp(kl)]}.$$

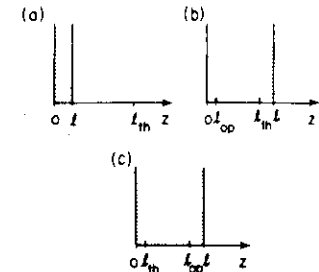


Fig. 4. Description of special cases (1) and (2). (a) and (b) describe the case in Sec. II.C.1; (c) is the case in Sec. II.C.2.

Note that in this limit, Eq. (17) is independent of the Schuster-Schwarzschild approximation [Eq. (11)] introduced for the general solution [Eq. (15)]. Equation (17) is always valid for FT detection [since thermal diffusion can be neglected and the signal is given in general by $\alpha_s \int_0^1 P(z) dz$]. Equation (17) formally proves the intuitive result that S is proportional to the absorbance of the sample. The expression $S \propto [1 - (R + T)]$ is also valid for pulsed FT detection¹⁵ of optically thin liquids in which the first peak of the transient PZT response yields the photoacoustic signal.

From Eq. (17) one can see by the following simple example that S is quite insensitive to scattering for optically thin media. For an isotropically scattering, optically thin medium ($\alpha l \ll 1$) (Fig. 5), $R \approx \alpha_s l (1 - r_0)/2$, and $T \approx 1 - \alpha l + \alpha_s l (1 + r_0)/2$ [see Eqs. (22a) and (22b)]. Hence, $S \propto [1 - (R + T)] \approx \alpha_s l$, whereas R and T measured alone are dominated by scattering.

On the other hand, for an optically thick medium for which $T = 0$, $S \propto (1 - R)$, and hence the photothermal signal is, in principle, equivalent to a reflectance measurement in this limit. This result is in good agreement with the experimental findings of Ref. 16. These conclusions will be further elucidated by the results of Sec. III.

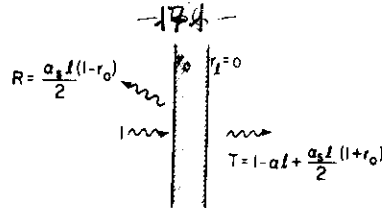


Fig. 5. Optically and thermally thin ($\alpha_s l \ll 1$) medium with the internal reflectances $r_0 \neq 0$, $r_1 = 0$, and isotropic scattering. The photothermal signal is given by $S \propto [1 - (R + T)] \propto \alpha_s l$.

2. $l_{th} \ll l_{op}, l$

From Eq. (15), it follows in this limit of very short thermal length that

$$S \rightarrow T_s(\omega) P_0 \left[\frac{\alpha_s}{k h_f (k h_f + k_s h_s)} \left(1 + \frac{2(1+r_0)}{(1-r_0)} R \right) + \frac{\beta_s}{\beta_f k h^2} [1 - (R + T)] \right] \quad (18)$$

The first term is the signal contribution from the heat diffused into the fluid (within a thermal length) at the sample-fluid boundary. The heat is proportional to α_s times the total power in that region which has increased by the factor $[1 + 2R(1+r_0)/(1-r_0)]$ due to scattering. This factor can be derived from a simple argument. The total power at the boundary is given by $P^-(0) + P^+(0) + P_0$, where $P^-(0)$ and $P^+(0)$ are the backward and forward propagating diffuse photons/sec, respectively. But $P^+(0) = r_0 P^-(0)$, and $P^-(0) = 2RP_0/(1-r_0)$. Hence $P^+(0) + P^-(0) + P_0 = [1 + 2(1+r_0)/(1-r_0)] P_0$. The second term in Eq. (18) (thermal expansion of the sample) can be significant at this high frequency limit⁸ or for porous media.

3. Semi-infinite Sample ($l \rightarrow \infty$)

In this limit, it is observed from Eqs. (5) and (6) that

$$\bar{T}(0) \rightarrow \frac{\alpha_s}{k h_f (1+g)} \int_0^\infty P(z) \exp(-kz) dz, \quad \bar{T}(l) \rightarrow 0.$$

Using the above and Eq. (16) in Eqs. (1) and (4), we derive

$$S(\omega) = T_s(\omega) P_0 \left(\frac{\alpha_s \left[2R \left[2(\alpha_s + \alpha_s \Lambda) + k \left(\frac{1+r_0}{1-r_0} \right) (\alpha + k) + k^2 - 4\alpha(\alpha_s + \alpha_s \Lambda) + 2\eta \alpha k \right] \right]}{k_f (k h_f + k_s h_s) [k^2 - 4\alpha(\alpha_s + \alpha_s \Lambda)] (\alpha + k)} + \frac{\beta_s}{\beta_f k h^2} (1 - R) \right). \quad (19)$$

Note that setting $k \gg 2\alpha$ in Eq. (19) leads to the limit in Sec. II.C.2 [Eq. (18) with $T = 0$], and $k \ll \alpha$ yields the limit in Sec. II.C.1 [Eq. (17) with $T = 0$].

D. Reflectance and Transmittance

The solution for the photothermal signal in terms of the measurable optical properties of the sample (R and T) can be employed in either of two ways: (1) photoacoustic measurements can be combined with optical measurements to provide information on sample properties, such as the internal reflectance r_0 , which is otherwise experimentally inaccessible; or (2) the radiative transfer equation [Eq. (8)] can be solved for R and

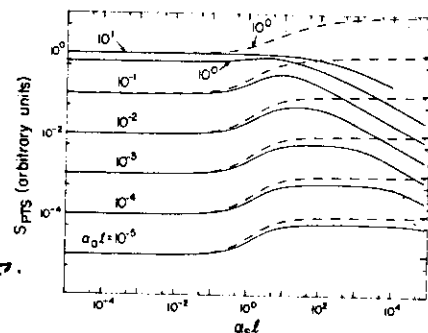


Fig. 6. Relative photothermal signal vs scattering, $\alpha_s l$ for various absorptions $\alpha_s l$. $r_0 = 0.6$, $r_1 = r_{cl} = 0$, and $\Lambda = 1$, $\eta = 0$ (isotropic scattering): —, theory (thermally thin); ---, theory (thermally thick). Note the independence of scattering $\alpha_s l \leq 0.2$.

T in terms of the intrinsic optical properties of the sample (α_s, α_s , scattering indicatrix and boundary reflectances). Substituting these expressions for R and T into the general solution for the photothermal signal, one obtains the dependence of the PTS on the scattering and absorption of the sample.

The well-developed numerical techniques of radiative transfer theory^{2,11,13} can be utilized for an accurate determination of R and T to be employed in Eqs. (15) and (17)–(19). However, the widely used three-flux (four-flux if the specular reflection at the $z = l$ boundary is non-negligible) calculations based on Eq. (11) have

been observed and accepted to be sufficiently accurate.¹⁷ Using this approach, we determine

$$R = \frac{(1-r_0)}{2D(\Gamma^2 - \alpha^2)} \left[\exp(-\Gamma l) \alpha_s (R_s - r_1) - R_s [(\alpha_s - \alpha_s)(1-\eta) + 2\alpha_s \Lambda] + (3\alpha_s + \alpha_s)(1+\eta) + 2\alpha_s \Lambda \right] + \exp(\Gamma l) \alpha_s (1-r_1 R_s) [(\alpha_s - \alpha_s)(1-\eta) + 2\alpha_s \Lambda - R_s [(3\alpha_s + \alpha_s)(1+\eta) + 2\alpha_s \Lambda]] + \exp(-\alpha l) (1-R_s^2) (2r_{cl}(\Gamma^2 - \alpha^2) - \alpha_s [(\alpha_s - \alpha_s)(1-\eta) + 2\alpha_s \Lambda - r_1 [(3\alpha_s + \alpha_s)(1+\eta) + 2\alpha_s \Lambda]]) \quad (20)$$

$$T = \frac{1}{2D(\Gamma^2 - \alpha^2)} \left[(1-r_1)(1-R_s^2) \alpha_s [r_0(\alpha_s - \alpha_s)(1-\eta) - 2\alpha_s \Lambda(1-r_0) - (3\alpha_s + \alpha_s)(1+\eta)] + \exp(-\alpha l) \alpha_s (1-r_1 R_s) [(\alpha_s - \alpha_s)(1-\eta) + 2\alpha_s \Lambda - R_s [(3\alpha_s + \alpha_s)(1+\eta) + 2\alpha_s \Lambda]] - (\alpha_s - \alpha_s)(1-\eta) + 2(\Gamma^2 - \alpha^2) [r_{cl} - r_1 + R_s(1-r_{cl})] + \exp(-\alpha l) \alpha_s (1-r_1 R_s) [(\alpha_s - \alpha_s)(1-\eta) + 2\alpha_s \Lambda - R_s [(3\alpha_s + \alpha_s)(1+\eta) + 2\alpha_s \Lambda]] - R_s [(\alpha_s - \alpha_s)(1-\eta) + 2(\Gamma^2 - \alpha^2) [1 - r_{cl} + R_s(r_{cl} - r_1)]] \quad (21)$$

where

$$\Gamma = 2\sqrt{\alpha_s(\alpha_s + \alpha_s \Lambda)}, \quad R_s = (2\alpha_s + \alpha_s \Lambda - \Gamma)/\alpha_s \Lambda,$$

$$D = (1-r_1 R_s)(1-r_0 R_s) \exp(\Gamma l) - (R_s - r_1)(R_s - r_0) \exp(-\Gamma l).$$

III. Results and Discussion

In Eqs. (15), (20), and (21), which determine the photothermal signal, there are five optical constants, $r_0, r_1, r_{cl}, \Lambda$, and η , in addition to the fundamental constants α_s and α_s . The values of these five constants can be judiciously chosen from theoretical considerations.¹⁷ The boundary reflectances r_0 and r_1 can be set equal to their theoretical values for perfectly diffuse light using the refractive index of the material.¹⁷ In general, $r_{cl} = 0$, but the diffuse reflectance characteristics of the backing medium must be taken into account. For example, if the backing medium is a highly diffuse reflector,¹⁴ $r_1 \approx r_{cl} \approx 1$ (also $T = 0$). The parameters Λ and η take into account the anisotropy of scattering and can be deduced from the scattering indicatrix. For a given λ/d , one can determine $s(\psi) = s(\theta - \theta')$ from Mie formulas¹⁸ (spherical particles) and evaluate its Legendre expansion coefficients $a_l = (2l+1) \int_{-1}^1 s(\psi) P_l(\cos \psi) d(\cos \psi)$. Then from Eqs. (10) and (11), one can set $\eta \approx (\alpha_s - \alpha_s/4 + \alpha_s/8)/2$ and $\Lambda \approx 1 - \alpha_s/4 - \alpha_s/64$ with good accuracy. Thus the only unknown parameters remaining are the important optical constants α_s and α_s .

In Fig. 6, the dependence of PTS on the optical thicknesses of the samples $\alpha_s l$ and $\alpha_s l$ is given for the low frequency and high frequency limits [Eqs. (17) and (18)]. Equation (20) and (21) are used with isotropic scattering ($\Lambda = 1, \eta = 0$). It is seen that the photothermal signal is not significantly affected for $\alpha_s l \ll 1$. In fact, it can be shown from Eqs. (20) and (21) that for $\alpha l \ll 1$

$$S \rightarrow 1 - (R + T) \approx \alpha_s l. \quad (22a)$$

$$S \rightarrow \alpha_s \left[1 + \frac{2(1+r_0)}{(1-r_0)} R \right] \approx \alpha_s [1 + (1+r_0)\Lambda \alpha_s l]. \quad (22b)$$

Therefore, Fig. 6 and Eqs. (22a) and (22b) demonstrate that, for the wide range of techniques considered, PTS is independent of scattering for $\alpha_s l \leq 0.1$. This result is not evident from the analysis of Helander and Lundstrom⁴ who only considered semi-infinite, and therefore optically thick, samples. They found that PTS was very sensitive to scattering when $\alpha_s \geq \alpha_s$. For larger $\alpha_s l$, it is seen from Fig. 6 that S is significantly

affected, initially increasing with $\alpha_s l$ and eventually decreasing for very large $\alpha_s l$.

Physically, for $\alpha_s l \ll 1$, the effective light path length within the sample is equal to its thickness, and the PTS is not affected. When $\alpha_s l \sim 1$ the mean path length of light increases and so does the absorption. At still higher scattering, the signal saturates as a function of $\alpha_s l$ since all the light is scattered without further increase in the effective path lengths. For very high scattering samples ($T \approx 0$), the reflectance becomes larger as $\alpha_s l$ is increased leading to a decrease in the light intensity within the sample. Hence the signal decreases.

For the thermally thick case, the signal rises as $\alpha_s l$ increases above 0.1 since scattering increases the flux at the surfaces (increases R). For $\alpha_s l \gg 1$, $R \approx 1$ (the surface flux can no longer increase), and the signal saturates at the level $\alpha_s l [1 + 2(1+r_0)/(1-r_0)]$.

Note that, in the region $\alpha_s l \sim 1$, S monotonically increases as a function of $\alpha_s l$ for a fixed $\alpha_s l$ (up to a factor of ~ 5 for $\alpha_s l < 0.1$). The scattering coefficient α_s is a decreasing function of λ/d for $\lambda/d > 1$. (The dependence of α_s on λ/d is given by the Rayleigh and Mie scattering formulas.¹⁸) Hence, for a fixed mean particle diameter and absorption coefficient, S may increase significantly as λ is decreased to approach $\lambda = d$, if $0.1 \leq \alpha_s l \leq 10$. For submicron particle sizes, this implies that there may be a monotonic increase in S as λ is decreased toward the UV if $\alpha_s l \sim 1$.

In Figs. 7 and 8, the ratio $R_0 = S(\alpha_s \neq 0)/S(\alpha_s = 0)$ is plotted as a function of $\alpha_s l$ for varying $\alpha_s l$, assuming isotropic scattering and neglecting the mechanical expansion, in the low and high frequency limits. The results of Fig. 7 can be explained as follows: (1) for low scattering ($\alpha_s l > 0.1$) and low absorption, the mean path through the sample is slightly increased, giving light a greater chance of being absorbed and resulting in $R_0 > 1$; (2) when the absorption increases sufficiently, the light is absorbed regardless of whether it scatters, so $R_0 \rightarrow 1$; (3) for very high scattering and low absorption, the light is more likely to be scattered out of the sample than to be absorbed, giving $R_0 < 1$; (4) as the absorption becomes larger than the scattering, the light absorption probability increases, giving $R_0 \rightarrow 1$. For Fig. 8, scattering increases the surface intensity up to a point, but for very high absorption the surface intensity decreases.

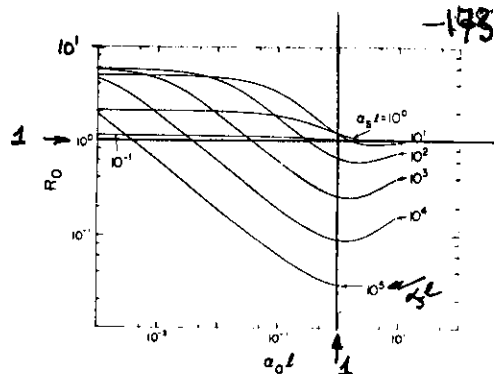


Fig. 7. R_0 (ratio of signal with scattering to signal without) vs absorption ($\alpha_a l$) for various values of $\alpha_s l$. The curves apply to the thermally thin limit [Eq. (17)], isotropic scattering ($\Lambda = 1, \eta = 0$), and $r_0 = 0.6, r_l = r_{cl} = 0$.

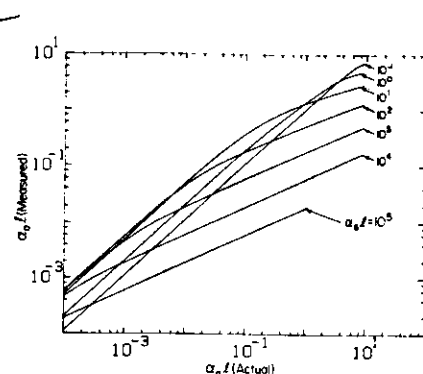


Fig. 9. $\alpha_a l$ (measured) (neglecting scattering) vs $\alpha_a l$ (actual) for various values of $\alpha_s l$ for the thermally thin limit [Eq. (17)]. Isotropic scattering ($\Lambda = 1, \eta = 0$) and $r_0 = 0.6, r_l = r_{cl} = 0$.

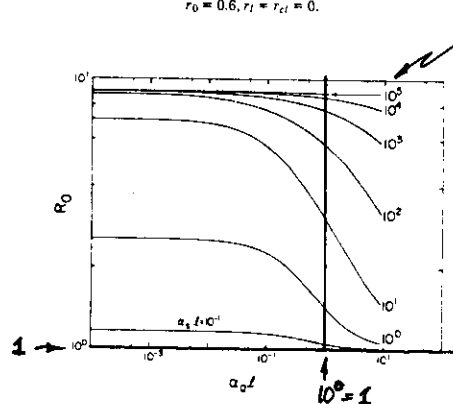


Fig. 8. R_0 vs absorption $\alpha_a l$ for various values of $\alpha_s l$. The thermally thick limit [Eq. (18)] with the mechanical expansion term neglected. Isotropic scattering ($\Lambda = 1, \eta = 0$) and $r_0 = 0.6, r_l = r_{cl} = 0$.

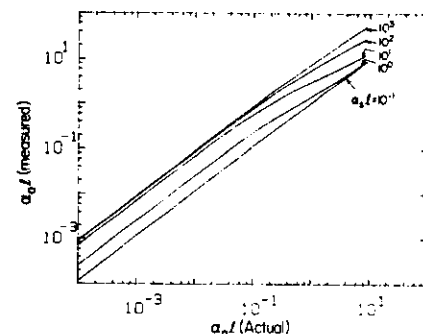


Fig. 10. $\alpha_a l$ (measured) (neglecting scattering) vs $\alpha_a l$ (actual) for various values of $\alpha_s l$ for the thermally thick limit [Eq. (18)] with $\chi = 0$. Isotropic scattering ($\Lambda = 1, \eta = 0$) and $r_0 = 0.6, r_l = r_{cl} = 0$.

Another important observation evident from Figs. 7 and 8 is that the general effect of scattering on a spectrum is to lower the peaks and raise the valleys.

In Figs. 9 and 10, curves of $\alpha_a l$ (measured) vs $\alpha_a l$ (actual) are given for the low frequency and high frequency limits (isotropic scattering). The physical interpretation is the same as in Figs. 7 and 8. These curves are useful for correcting spectra for the effects of scattering.

In Figs. 11-13, we compare our results with the experimental and theoretical results of Helander and Lundström.⁴ R_0 is computed using the thermal properties of water and air from Eqs. (19) and (20) ($t \rightarrow \infty, T = 0$). We use the theoretical value of $r_0 = 0.4$ (valid for uniformly diffused light incident on an interface

with index ratio of $n = 1.33$), which is more realistic¹⁵ than the smaller value ($r_0 = 0$) used in Ref. 4. Our curves for $r_0 = 0$ and isotropic scattering are very similar to those in Ref. 4 but are in better agreement with their data. Since the mean particle diameters used in Ref. 4 are comparable to the wavelength, the scattering indicatrix is likely to be peaked in the forward direction. Since we do not know the exact value of λ/d , we estimate $\Lambda = 0.5, \eta = 0.5$. Our results are in reasonably good agreement with their experimental measurements. In Fig. 13, the data may involve the changing of Λ and η as α_a is varied. This may explain the small discrepancy. A curve with $\Lambda = 0.2, \eta = 0.5$ agrees well with the data. In Figs. 11 and 12, the scattering properties are not being changed, and we obtain better agreement.

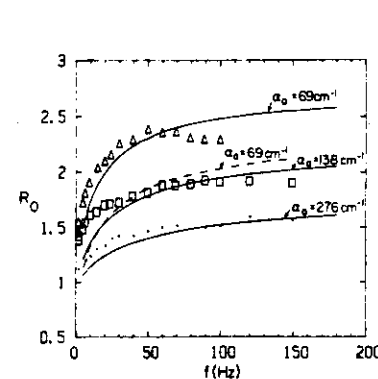


Fig. 11. R_0 vs chopping frequency for different absorption coefficients: —, present theory; ---, theory from Ref. 4; Δ , $\alpha_a = 69 \text{ cm}^{-1}$ data; \square , $\alpha_a = 138 \text{ cm}^{-1}$ data; \circ , $\alpha_a = 276 \text{ cm}^{-1}$ data. Data are from Ref. 4. $\alpha_s = 1145 \text{ cm}^{-1}, r_0 = 0.04, \Lambda = 0.5$, and the thermal properties of water were used in the calculations.

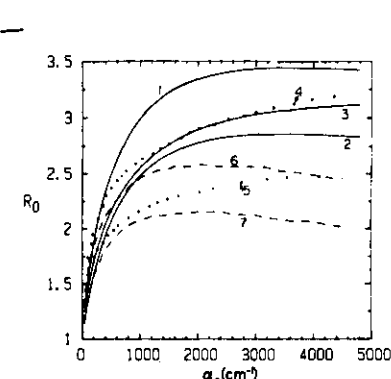


Fig. 13. R_0 vs scattering coefficient: 1, theory ($\alpha_a = 34.5 \text{ cm}^{-1}, \Lambda = \eta = 0.5$); 2, theory ($\alpha_a = 69 \text{ cm}^{-1}, \Lambda = \eta = 0.5$); 3, theory ($\alpha_a = 34.5 \text{ cm}^{-1}, \Lambda = 0.2, \eta = 0.5$); 4, data ($\alpha_a = 34.5 \text{ cm}^{-1}$); 5, data ($\alpha_a = 69 \text{ cm}^{-1}$); 6, theory ($\alpha_a = 34.5 \text{ cm}^{-1}$); 7, theory ($\alpha_a = 69 \text{ cm}^{-1}$). Other parameters are $f = 150 \text{ Hz}, r_0 = 0.4$, and thermal properties of water and air.

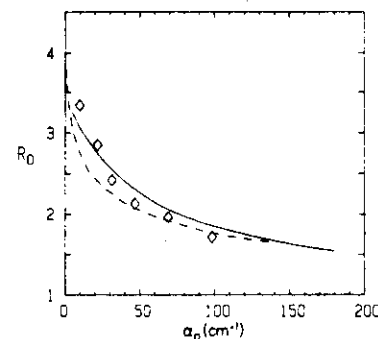


Fig. 12. R_0 vs absorption coefficient: —, present theory; ---, theory⁴. \diamond , data⁴ $\alpha_a = 500 \text{ cm}^{-1}, r_0 = 0.4, f = 150 \text{ Hz}, \Lambda = \eta = 0.5$. Thermal properties of water were used in the calculations.

Noting that the realistic value of $r_0 = 0.4$ is used, the agreement is remarkably good. One reason is that the mechanical expansion term is also included in our analysis and is not entirely negligible in their experiment.

In these computed curves, we made no attempt for a numerical fitting of parameters. Following the discussion at the beginning of this section, we chose reasonable values based on theoretical considerations. If more accurate values of the parameters were available, better agreement could be obtained.

The above theoretical results suggest the following ways to optimize PTS of scattering media. First, the scattering properties of the solid should be kept constant, and hence the particle size must not change

drastically from sample to sample. Second, because scattering flattens spectral features, it should be minimized by keeping the particle size small or by immersion in a liquid. Third, one can attempt to estimate the scattering length and use Figs. 9 and 10 to correct the signal. The curves may not be appropriate for every experimental configuration since they were generated neglecting the mechanical term and assuming isotropic scattering. Fourth, if $\alpha_a l > 0.01$ and the sample is optically thick, diffuse reflectance measurements give equivalent results and may be more convenient than PTS; for weakly absorbing samples, PTS gives better results.

In conclusion, we have shown that while photothermal spectroscopy is independent of scattering for optically thin media, it is significantly affected by scattering in general and is equivalent to diffuse reflectance spectroscopy in some limits. However, the general photothermal signal contains information which is not available by optical means and can be measured by variation of the chopping frequency. By parameter fitting our theoretical curves to the frequency dependent photothermal data, α_a and α_s can be numerically estimated. Optical measurements of R and T can be used to supplement this procedure. Utilized in this manner, photothermal spectroscopy can be an important tool for the determination of optical constants for highly scattering media.

We thank R. Gerlach for helpful discussions. This work was supported by the Office of Energy Research, Characterization and Measurement Division of the U.S. Department of Energy under contract W-7405-ENG-48.

This paper was presented (in part) at the Second Topical Meeting on photoacoustic spectroscopy, Berkeley, 22-25 June 1981.

Appendix: Solid-Transducer Detection

From the expression $G(r) = 1 \pm 3(1 - 2z/l)$ for the ST (PZT)¹⁰ scheme, it follows that

$$S_{PZT}(\omega) = T_r(\omega) \left[\int_0^l \tilde{r}(z) dz \pm 3 \int_0^l \left(1 - \frac{2z}{l} \right) \tilde{r}(z) dz \right]. \quad (A1)$$

The first term in brackets represents the thermal expansion of the sample and is given by Eq. (4) in the main text. To evaluate the second term, which represents the sample buckling due to the average temperature gradient along z , we multiply Eq. (2) by z and integrate, obtaining

$$k^2 \int_0^l z \tilde{r}(z) dz = \frac{\alpha_a}{\kappa} \int_0^l z P(z) dz - \left(1 + l \frac{\kappa_a k_0}{\kappa} \right) \tilde{r}(l) + \tilde{r}(0).$$

Using the above and Eq. (4) in Eq. (A1), we obtain

$$S_{PZT}(\omega) = \frac{T_r(\omega)}{\kappa k^2} \left\{ (1 \pm 3) \alpha_a \int_0^l P(z) dz \pm \frac{6}{l} \alpha_a \int_0^l z P(z) dz \right. \\ \left. \times (-1 \pm 3) \kappa_b k_0 \tilde{r}(l) - (1 \pm 3) \kappa_b k_0 \tilde{r}(0) \pm \frac{6}{l} \kappa_b [(\tilde{r}(0) - \tilde{r}(l))] \right\}. \quad (A2)$$

where

$$\int_0^l z P(z) dz = \int_{-1}^1 d\mu \int_0^l z P_d(z, \mu) dz \\ + \frac{1}{\alpha^2} P_0 [1 - (1 + \alpha l) \exp(-\alpha l)].$$

Multiplying Eq. (8) by z and integrating over $-1 \leq \mu \leq 1$ and $0 \leq z \leq l$ gives

$$l[\Phi^+(l) - \Phi^-(l)] - \int_{-1}^1 d\mu \int_0^l P_d(z, \mu) dz \\ = -\alpha_a \int_0^l z P(z) dz + \frac{1}{\alpha} P_0 [1 - (1 + \alpha l) \exp(-\alpha l)].$$

Applying the Schuster-Schwarzchild approximation [Eq. (11)] and using Eq. (14), the above equation can be written

$$\alpha_a \int_0^l z P(z) dz = \frac{1}{2} (P_0^+ - P_0^-) + \frac{P_0}{\alpha} [1 - \exp(-\alpha l)] - \alpha l T. \quad (A3)$$

where

$$P_0^+ = \int_0^1 d\mu \int_0^l dz P_d(z, \mu), \quad P_0^- = \int_{-1}^0 d\mu \int_0^l dz P_d(z, \mu).$$

From the equations following Eq. (11), we obtain

$$(\alpha_a + \alpha_s \Lambda) (P_0^+ - P_0^-) = \Phi^+(0) + \Phi^-(0) - [\Phi^+(l) \\ + \Phi^-(l)] + \eta \frac{\alpha_s}{\alpha} P_0 [1 - \exp(-\alpha l)].$$

Note added in proof: The recent paper by R. Tilgner [Appl. Opt. 20, 3780 (1981)] provides further experimental support for our theory.

which, using Eqs. (13) and (14), can be rewritten as ($r_{cl} = 0$)

$$(\alpha_a + \alpha_s \beta) (P_0^+ - P_0^-) = P_0 \left\{ \eta \frac{\alpha_s}{\alpha} [1 - \exp(-\alpha l)] \right. \\ \left. + \left(\frac{1 + r_0}{1 - r_0} \right) R - \left(\frac{1 + r_l}{1 - r_l} \right) [T - \exp(-\alpha l)] \right\}.$$

Substituting into Eq. (A3) gives

$$\alpha_a \int_0^l z P(z) dz = \frac{P_0}{\alpha} [1 - \exp(-\alpha l)] - \alpha l T \\ + \frac{P_0}{2(\alpha_a + \alpha_s \Lambda)} \left\{ \eta \frac{\alpha_s}{\alpha} [1 - \exp(-\alpha l)] \right. \\ \left. + \left(\frac{1 + r_0}{1 - r_0} \right) R - \left(\frac{1 + r_l}{1 - r_l} \right) [T - \exp(-\alpha l)] \right\}. \quad (A4)$$

Using Eqs. (A4), (5), (6), (15), and (16), Eq. (A2) yields the PZT signal in terms of the chopping frequency and the thermal and optical properties of the sample.

References

1. A. Rosencwaig, *Anal. Chem.* **47**, 592A (1975).
2. H. C. Van de Hulst, *Multiple Light Scattering*, Vol. 1 (Academic, New York, 1980).
3. G. Kortum, *Reflectance Spectroscopy* (Springer, Berlin, 1969).
4. P. Helander and I. Lundström, *J. Appl. Phys.* **51**, 3841 (1980).
5. W. B. Jackson, N. M. Amer, A. C. Boccara, and D. Fournier, *Appl. Opt.* **20**, 1333 (1981).
6. J. P. Monchalán, L. Bertrand, J. L. Parpal, and J. M. Gagne, in *Digest of Topical Meeting on Photoacoustic Spectroscopy* (Optical Society of America, Washington, D.C., 1981), paper MA-4.
7. P. Morse and K. Ingard, *Theoretical Acoustics* (McGraw-Hill, New York, 1968).
8. F. A. McDonald, *J. Opt. Soc. Am.* **70**, 555 (1980).
9. L. B. Kreuzer, *Photoacoustic Spectroscopy and Detection*, Y.-H. Pao, Ed. (Academic, New York, 1977).
10. W. B. Jackson and N. M. Amer, *J. Appl. Phys.* **51**, 3343 (1980).
11. S. Chandrasekhar, *Radiative Transfer* (Dover, New York, 1960).
12. F. Kottler, *Progress in Optics*, Vol. 3, E. Wolf, Ed. (Wiley, New York, 1964).
13. V. V. Sobolev, *Light Scattering in Planetary Atmospheres* (Pergamon, Oxford, 1975).
14. Z. A. Yasa, N. M. Amer, H. Rosen, A. D. A. Hansen, and T. Novakov, *Appl. Opt.* **18**, 2528 (1979).
15. A. C. Tam, C. K. N. Patel, and R. J. Kerl, *Opt. Lett.* **4**, 81 (1979).
16. J. J. Freeman, R. M. Friedman, and H. S. Reichard, *J. Phys. Chem.* **84**, 315 (1980).
17. P. S. Mudgett and L. W. Richards, *Appl. Opt.* **10**, 1485 (1971).
18. H. C. Van de Hulst, *Light Scattering by Small Particles* (Wiley, New York, 1957).

Reprinted from *Applied Optics*, Vol. 20, page 1333, April 15, 1981.
Copyright © 1981 by the Optical Society of America and reprinted by permission of the copyright owner.

Photothermal deflection spectroscopy and detection

W. B. Jackson, N. M. Amer, A. C. Boccara, and D. Fournier

The theory for a sensitive spectroscopy based on the photothermal deflection of a laser beam is developed. We consider cw and pulsed cases of both transverse and collinear photothermal deflection spectroscopy for solids, liquids, gases, and thin films. The predictions of the theory are experimentally verified, its implications for imaging and microscopy are given, and the sources of noise are analyzed. The sensitivity and versatility of photothermal deflection spectroscopy are compared with thermal lensing and photoacoustic spectroscopy.

1. Introduction

It is well known that upon the absorption of electromagnetic radiation by a given medium, a fraction of or all the excitation energy will be converted to thermal energy. In recent years, this de-excitation mechanism has provided the physical basis for a new class of sensitive photothermally based spectroscopies. Among the better known examples of these spectroscopies are interferometric techniques,¹ thermal lensing (TL),^{2,3} photoacoustic spectroscopy (PAS),⁴ and, most recently, photothermal deflection spectroscopy (PDS).⁵⁻¹⁰ While the theoretical foundation of interferometry,¹ TL,^{2,3} and PAS¹¹⁻¹⁶ are fairly well understood, this is not the case for PDS. Even though the concept of beam deflection by thermally induced changes in the index of refraction has been known for a long time,¹⁷ to the best of our knowledge, no one has published a complete systematic theoretical or experimental investigation of the applicability of this phenomenon to spectroscopy. In this paper, we develop and experimentally verify a general theoretical treatment of PDS.

Before proceeding with the theoretical treatment of PDS, a brief physical description of PDS is in order. The absorption of the optically exciting beam (pump beam) causes a corresponding change in the index of

refraction of the optically heated region. The absorption also causes an index-of-refraction gradient in a thin layer adjacent to the sample surface. By probing the gradient of the varying index of refraction with a second beam (probe beam), one can relate its deflection to the optical absorption of the sample. This is in contrast with probing thermally induced changes in optical path lengths, as in interferometric techniques or probing the curvature of the index of refraction as in TL. As can be seen from the above description, one has two choices in performing PDS: (1) collinear photothermal deflection^{6,7,10} where the gradient of the index of refraction is both created and probed within the sample (Fig. 1), or (2) transverse photothermal deflection^{8,9} where the probing of the gradient of the index of refraction is accomplished in the thin layer adjacent to the sample—an approach most suited for opaque samples and for materials of poor optical quality (Fig. 1). We have already demonstrated the high sensitivity of PDS for measuring *in situ* small absorptions in thin films, solids, liquids, and gases.⁵⁻⁸ Its potential for imaging and scanning microscopy has been demonstrated.¹⁸

In Sec. II, we present the theory of PDS for the cw collinear and transverse cases and the pulsed collinear case. In Sec. III we deal with experimental considerations. The experimental results are compared to theoretical predictions in Sec. IV. Noise and background analyses are described in Sec. V, and in Sec. VI, we discuss our findings and compare them with related techniques. Finally, the implications of our calculations for imaging and microscopy are presented in Sec. VII.

II. Theory

The calculation of the expected beam deflection for PDS can be divided into two parts. One first finds the temperature distribution in the sample and then solves for the optical beam propagation through an inhomogeneous medium. While temperature solutions have been reported in the literature,^{9,11-16} those reported are

W. Jackson and N. M. Amer are with University of California, Lawrence Berkeley Laboratory, Applied Physics & Laser Spectroscopy Group, Berkeley, California 94720; the other authors are with Ecole Supérieure de Physique et de Chimie Industrielles, Laboratoire d'Optique Physique—E.R.S. du CNRS, 10 rue Vauquelin, 75231 Paris, Cedex 05, France.

Received 16 October 1980.

0003-695/81/081333-12\$00.50/0.

© 1981 Optical Society of America.

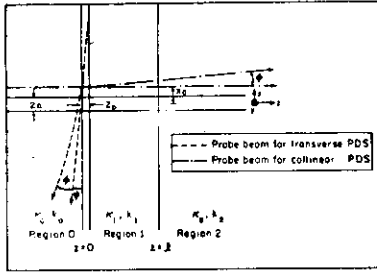


Fig. 1. Geometry for theory. Heat deposited diffuses into regions 0 and 2 as well as radially. For transverse PDS, the probe beam axis may be displaced along the y axis by a distance y_0 .

not applicable to our geometry and are not sufficiently general to provide a unified treatment for both collinear and transverse PDS of solids, thin films, gases, and liquids. We present a model which is sufficiently general to be applicable to most actual experimental cases.

A. Temperature Distribution

Consider the geometry shown in Fig. 1. Regions 0 and 2 are optically nonabsorbing media. Region 1 is the absorbing medium and can be either a thin film, gas, liquid, or solid. For simplicity, we assume that all three regions extend infinitely in the radial direction. This assumption does not significantly alter the applicability of the treatment, since focused laser beams are typically much smaller than the radial dimension of the sample, and the thermal diffusion length of most samples is less than typical sample dimensions for experimentally useful chopping frequencies.

In the three regions, the temperature rise T satisfies the equations

$$\nabla^2 T_0 - \frac{1}{k_0} \frac{\partial T_0}{\partial t} = 0 \quad \text{region 0,} \quad (1a)$$

$$\nabla^2 T_1 - \frac{1}{k_1} \frac{\partial T_1}{\partial t} = -\frac{Q(r,t)}{k_1} \quad \text{region 1,} \quad (1b)$$

$$\nabla^2 T_2 - \frac{1}{k_2} \frac{\partial T_2}{\partial t} = 0 \quad \text{region 2,} \quad (1c)$$

subject to the following boundary conditions:

$$T_{0|z=0} = T_{1|z=0}, \quad T_{1|z=l} = T_{2|z=l}, \quad (2a)$$

$$k_0 \frac{\partial T_0}{\partial z} \Big|_{z=0} = k_1 \frac{\partial T_1}{\partial z} \Big|_{z=0}, \quad k_1 \frac{\partial T_1}{\partial z} \Big|_{z=l} = k_2 \frac{\partial T_2}{\partial z} \Big|_{z=l}, \quad (2b)$$

where k_i is the conductivity, $k_i (k_i = \kappa_i / \rho_i C_i)$ is the diffusivity, T_i is the temperature rise of the i th medium above the ambient temperature, and l is the thickness of the absorbing medium. $Q(r,t)$ is the heat deposited per unit volume oscillating at the frequency ω in the absorbing medium and is given by

$$Q(r,t) = \frac{1}{2} \frac{4Pa}{\pi a^2} \exp(-\alpha z) \exp(-2r^2/a^2) \exp(i\omega t) + \text{c.c.} \quad (3)$$

for a square wave intensity modulated beam where P is the optically exciting beam (pump beam) power, α is the absorption coefficient, and a is the $1/e^2$ radius of the Gaussian beam. We have assumed above that over the interaction region between the pump and probe beams, the probe beam is focused to a smaller spot than that of the pump beam, and that the pump beam waist does not change over the confocal distance of the probe beam. In Eqs. (1a)–(1c) we have also neglected the effect of the acoustic wave which accompanies the temperature rise of the illuminated volume (see Appendix for details.)

Equation (1) is solved by making the following substitutions. For region 0, we have

$$T_0(r,t) = \frac{1}{2} \int_0^\infty \delta\delta J_0(\delta r) E(\delta) \exp(\beta_0 z) \exp(i\omega t) + \text{c.c.} \quad (4)$$

for region 2, we have

$$T_2(r,t) = \frac{1}{2} \int_0^\infty \delta\delta J_0(\delta r) D(\delta) \exp[-\beta_2(z-l)] \exp(i\omega t) + \text{c.c.} \quad (5)$$

and for region 1, we have

$$T_1(r,t) = \frac{1}{2} \int_0^\infty \delta\delta J_0(\delta r) [\Gamma(\delta) \exp(-\alpha z) + A(\delta) \exp(-\beta_1 z) + B(\delta) \exp(\beta_1 z)] \exp(i\omega t) + \text{c.c.}, \quad (6)$$

where $T_1(r,z)$ is the component of the temperature difference oscillating at frequency ω ,

$$\Gamma(\delta) = \frac{Pa \exp[-(\delta a)^2/8]}{\pi^2 k_1 \beta_1^2 - \alpha^2}, \quad (7)$$

$$\beta_i^2 = \delta^2 + i\omega/k_i. \quad (8)$$

Substituting into Eqs. (1) and satisfying the boundary conditions, we find that

$$A(\delta) = -[(1-g)(b-r) \exp(-\alpha l) + (g+r)(1+b) \times \exp(\beta_1 l)] \Gamma(\delta) / H(\delta),$$

$$B(\delta) = -[(1+g)(b-r) \exp(-\alpha l) + (g+r)(1-b) \times \exp(-\beta_1 l)] \Gamma(\delta) / H(\delta), \quad (9)$$

$$D(\delta) = \Gamma(\delta) \exp(-\alpha l) + A(\delta) \exp(-\beta_1 l) + B(\delta) \exp(\beta_1 l),$$

$$E(\delta) = \Gamma(\delta) + A(\delta) + B(\delta),$$

$$H(\delta) = [(1+g)(1+b) \exp(\beta_1 l) - (1-g)(1-b) \exp(-\beta_1 l)],$$

where

$$g = \kappa_0 \beta_0 / \kappa_1 \beta_1, \quad b = \kappa_2 \beta_2 / \kappa_1 \beta_1, \quad r = \alpha / \beta_1.$$

The final temperature distribution is obtained by combining Eqs. (4)–(9).

To gain insight into the physical picture described by the formulae and to relate our findings to previous work, we consider special cases.

To obtain the 1-D solution,¹⁵ we take $2\pi \int_0^\infty r dr$ of Eq. (6). Since $\int_0^\infty \delta\delta \int_0^\infty r dr J_0(\delta r) R(\delta) = R(0)$, one obtains

$$\bar{T}_1(z) = 2\pi [\Gamma(0) \exp(-\alpha z) + A(0) \exp(-K_1 z) + B(0) \exp(K_1 z)], \quad (10)$$

where

$$K_1^2 = i\omega/k_1 \quad \text{and} \quad T_1(z) = 2\pi \int_0^\infty r dr T_1(r,z)$$

Simplifying this expression, the result is

$$\begin{aligned} T_1(z) = & \frac{Pa}{H(0)\pi^2 k_1 (K_1^2 - \alpha^2)} [(1+g)(1+b) \exp(K_1 l - \alpha z) \\ & - (1-g)(1-b) \exp(K_1 l - \alpha z) - (1-g)(b-r) \\ & \times \exp(-\alpha l - K_1 z) - (g+r)(1+b) \exp(K_1 l - z)] \\ & - (1+g)(b-r) \exp(-\alpha l + K_1 z) - (g+r)(1-b) \\ & \times \exp(-K_1 l + K_1 z)]. \end{aligned} \quad (11)$$

Hence the physical interpretation of Eqs. (4)–(6) is that any temperature distribution can be decomposed into distributions of the form $J_0(\delta r) \exp(-\beta_1 z)$.

These distributions act independently of each other and have an effective thermal length given by $l_i = 1/\text{Re}(\beta_i) = [\text{Re}(K_i^2 + \delta^2)]^{1/2} - 1$. The case $\delta = 0$ gives a radially uniform temperature distribution, which, as expected, is similar to the 1-D case.

For region 1, $A(\delta)$ is the magnitude of the thermal wave diffusing in the positive z direction, $B(\delta)$ is the thermal wave diffusing in the negative z direction, and $\Gamma(\delta)$ is the temperature rise due to energy deposited at location (r,z) by the pump beam.

If heat diffusion into the bounding media is neglected and the temperature is integrated along the z direction, Eq. (6) reduces to

$$\begin{aligned} \int_0^l dz T_1(r,t) = & \frac{1}{2} \frac{P[1 - \exp(-\alpha l)]}{\pi^2 k_1} \\ & \times \int_0^\infty \frac{\delta J_0(\delta r) \exp[-(\delta a)^2/8]}{\delta^2 + K_1^2} d\delta \exp(i\omega t) + \text{c.c.} \end{aligned} \quad (12)$$

If the thermal length $(\text{Re}K_1)^{-1}$ is much smaller than the beam radius, the denominator in Eq. (12) becomes K_1^2 , and the integral can be performed. The result is⁶

$$\begin{aligned} \int_0^l dz T_1(r,t) = & \frac{1}{2} \frac{P[1 - \exp(-\alpha l)]}{\pi^2 k_1 r} \exp(-2r^2/a^2) \exp(i\omega t) + \text{c.c.} \end{aligned} \quad (13)$$

In the above case, the temperature distribution follows the beam profile because there is no diffusion of heat.

If the thermal length is much greater than the beam radius, K_1^2 can be neglected in the denominator of Eq. (12). The solution for the temperature gradient reduces to⁶

$$\begin{aligned} \int_0^l dz T_1(r,t) = & \frac{1}{2} \frac{P[1 - \exp(-\alpha l)]}{\pi^2 k_1 r} [1 - \exp(-2r^2/a^2)] \exp(i\omega t) \\ & + \text{c.c.} \end{aligned} \quad (14)$$

This result shows that the temperature distribution extends significantly beyond the beam profile for low chopping frequencies.

B. Optical Beam Propagation

We next calculate the effect of the temperature distribution on the probe beam. The index of refraction is, in general, a function of temperature and pressure. One can neglect the pressure contribution (Appendix). Hence

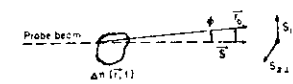


Fig. 2. Scattering geometry. Scattering region may focus the beam differently in the $S_{1\perp}$ and $S_{2\perp}$ directions (elliptical Gaussian beams).

$$n(r,t) = n_0 + \Delta n(r,t) = n_0 + \frac{\partial n}{\partial T} T(r,t), \quad (15)$$

where $(\partial n)/(\partial T)$ is typically 10^{-4}C^{-1} for liquids and 10^{-5}C^{-1} solids. The propagation of the Gaussian probe beam through the spatially varying index of refraction is given by¹⁹

$$\frac{d}{ds} \left(n_0 \frac{dr_0}{ds} \right) = \nabla_\perp n(r,t), \quad (16)$$

where r_0 is the perpendicular displacement of the beam from its original direction, n_0 is the uniform index of refraction, and $\nabla_\perp n(r,t)$ is the gradient of the index of refraction perpendicular to S (the ray path) (Fig. 2). The change in the complex beam parameter q is given by¹⁹

$$\frac{d}{ds} \left(\frac{1}{qs_{\perp}} \right) = - \left(\frac{1}{qs_{\perp}} \right)^2 - \frac{\partial^2 n}{n_0 \partial S_{\perp}^2}, \quad i = 1, 2, \quad (17)$$

where $1/qs_{\perp} = 1/Rs_{\perp} - i\lambda/(n_0 \pi w_0^2)$. Rs_{\perp} is the radius of curvature of the phase fronts, w_0 is the $1/e^2$ spot size, and λ is the vacuum wavelength of the probe beam. We also assume that the deflection is small compared with the temperature distribution. Since typical deflections are 10^{-5} rad over 1 cm, the total deviation is $0.1 \mu\text{m}$, which is much smaller than the typical $50\text{-}\mu\text{m}$ spot size of a focused laser. Integrating Eqs. (16) and (17) over the ray path S gives

$$\frac{dr_0}{ds} = \frac{1}{n_0} \int_{\text{path}} \nabla_\perp n(r,t) ds, \quad (18)$$

and

$$\begin{aligned} \frac{1}{qs_{\perp}} \Big|_{\text{end of interaction}} - \frac{1}{qs_{\perp}} \Big|_{\text{beginning of interaction}} = & \int_{\text{path}} ds \left(- \frac{1}{2} - \frac{\partial^2 n}{n_0 \partial S_{\perp}^2} \right) \quad i = 1, 2. \end{aligned} \quad (19)$$

Since the deviation is small,

$$\frac{dr_0}{ds} \approx \phi = \frac{1}{n_0} \frac{\partial n}{\partial T} \int_{\text{path}} \nabla_\perp T(r,t) ds, \quad (20)$$

where ϕ is the angular deviation from S , and Eq. (15) was used. Equation (20) is a 3-D generalization valid for Gaussian beams of the 1-D case reported in Ref. 8. From Eq. (19) we see that the effect of the curvature of the index of refraction is equivalent to an astigmatic lens of focal length F_i in the S_i direction where F_i is given by

$$\begin{aligned} 1/F_i = & - \frac{1}{n_0} \int_{\text{path}} \frac{\partial^2 n}{\partial S_{\perp}^2} ds \\ = & - \frac{1}{n_0} \frac{\partial n}{\partial T} \int_{\text{path}} \frac{\partial^2 T}{\partial S_{\perp}^2} ds \quad i = 1, 2. \end{aligned} \quad (21)$$

Equations (20) and (21) demonstrate one difference between PDS and TL. PDS probes the gradient of the temperature, while TL probes its curvature.

C. Solution for Beam Deflection

1. Collinear PDS

For collinear PDS, the beam is deflected by the temperature gradient in all three regions. For simplicity, we assume that the probe beam travels parallel to the pump beam axis and is deflected only in regions 1 and 2.²³ However, the interaction length is restricted to be consistent with an angle between the pump and probe beams (Fig. 3).

From Eqs. (5), (6), and (18), the deflection in this case is given by

$$\phi = \frac{-\exp(i\omega t)}{2n_0} \frac{\partial n}{\partial T} \left\{ \int_0^l dz \int_0^\infty \delta^2 d\delta J_1(\delta x_0) \right. \\ \times [\Gamma(\delta) \exp(-\alpha z) + A(\delta) \exp(-\beta_1 z) + B(\delta) \exp(\beta_2 z)] \\ + \int_0^{l_i} dz \int_0^\infty \delta^2 J_1(\delta x_0) \delta D(\delta) \exp[-\beta_2(z-l)] \} \\ + \text{c.c.} \quad l_i > l, \quad (22)$$

where $l_i = 2a/\sin\psi$ is the length of interaction of the two beams, x_0 is the displacement between the beams, and ψ is the angle of their intersection. If the beams overlap in region 1 only,

$$\phi = \frac{-1}{2n_0} \frac{\partial n}{\partial T} \exp(i\omega t) \int_0^l dz \int_0^\infty \delta^2 d\delta J_1(\delta x_0) [\Gamma(\delta) \exp(-\alpha z) \\ + A(\delta) \exp(-\beta_1 z) B(\delta) \exp(\beta_2 z)] + \text{c.c.} \quad l_i < l \quad (23)$$

Note that the assumption that the beams are parallel can be relaxed by integrating over an oblique path and evaluating the gradient in a perpendicular direction. This would add unnecessary complexity without introducing any significant effects.

2. Transverse PDS

For transverse PDS, the probe beam propagates completely within region 0. The probe beam path is (Fig. 1)

$$y = y_0 \quad z = (\tan\psi)x + z_0 \quad (24)$$

For small $\tan\psi$, $\nabla_1 T = (\partial T)/(\partial z)$. By substituting Eq. (4) into Eq. (20), the deflection is given by

$$\phi = \frac{1}{2} \frac{\exp(i\omega t)}{n_0} \frac{\partial n}{\partial T} \int_{-\infty}^{\infty} dx \int_0^\infty \delta \omega (\delta \sqrt{y_0^2 + x^2}) \beta_0 E(\delta) \exp(i \tan\psi x + z_0 \beta_0) \delta \delta + \text{c.c.} \quad (25)$$

3. Pulsed PDS

For pulsed PDS, the temperature solution as a function of time can be found by replacing $i\omega$ by p in Eqs. (22)–(25) and inverting the Laplace transform using the inversion formula

$$\phi(t) = \frac{1}{2\pi i} \int_{-i\infty}^{+i\infty} \phi(p) \exp(pt) dt. \quad (26)$$

Because of the integral form of the solution and the many poles of the integrand, this solution would be too

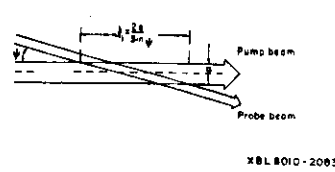


Fig. 3. Effective interaction length in collinear PDS. For simplicity, beams are assumed to be parallel but interact only over a distance l_i .

cumbersome to be of use. For an infinite weakly absorbing medium, the solution is much simpler and can be shown to be qualitatively similar to the more complicated solution. Hence we derive this solution for a square pulse.

In this case, the temperature is given by²¹

$$T(r, t) = \int_0^t dt' \int_0^\infty 2\pi r' dr' Q(r', t') G(r, r', t - t'). \quad (27)$$

where

$$Q(r', t') = \begin{cases} (2\alpha E_0 / \pi a^2 t_0) \exp(-2r'^2/a^2) & 0 \leq t' \leq t_0 \\ 0 & t' > t_0 \end{cases} \\ G(r, r', t - t') = \frac{1}{4\pi k_1(t - t')} \exp \left[\frac{-(r^2 + r'^2)}{4k_1(t - t')} \right] \\ \times I_0 \left[\frac{rr'}{2k_1(t - t')} \right];$$

E_0 is the pulse energy, t_0 is the pulse width, and $I_0(x)$ is a Bessel function.

Integrating and solving for $\partial T/\partial r$, we obtain

$$\frac{\partial T}{\partial r} = \frac{-\alpha E_0}{\pi k_1 t_0 2r} \left\{ \exp[-2r^2/(a^2 + 8k_1 t)] \right. \\ - \exp(-2r^2/a^2) \} \quad 0 \leq t \leq t_0, \quad (28) \\ \frac{\partial T}{\partial r} = \frac{-\alpha E_0}{\pi k_1 t_0 2r} \left\{ \exp[-2r^2/(a^2 + 8k_1 t)] \right. \\ - \exp[-2r^2/(a^2 + 8k_1(t - t_0))] \} \quad t > t_0.$$

This expression may be substituted into Eq. (20) (and letting $r = a/2$) to derive the expected signal vs time at the position of maximum deflection.

D. Numerical Evaluation

Equations (22) and (23) were evaluated using numerical quadrature routines. By varying the method of integration and the step size and by comparing the results with limiting cases and experiments, we verified that the routines were converging correctly. The equations were evaluated using appropriate material parameters, and the results of the calculations are shown in Figs. 6–13 and will be compared with the experimental results.

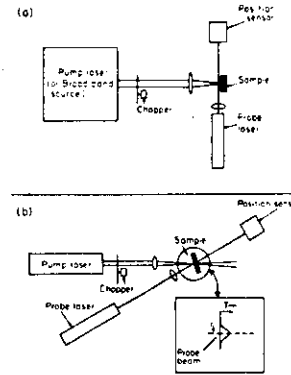


Fig. 4. Experimental apparatus: (a) transverse PDS; (b) collinear PDS.

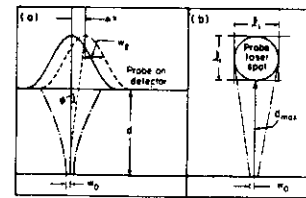


Fig. 5. (a) Probe spot on detector, (b) continuous detector. Maximum distance from probe focal spot to the detector is d_{\max} .

III. Experimental Considerations

A. Experimental Configurations

Experiments were performed to verify the theoretical results and to determine the ultimate sensitivity of PDS.⁵⁻⁸ The experimental configurations are given in Fig. 4. Figure 4(a) shows the experimental setup for transverse PDS. For exciting light sources (pump beams), we used either a cw dye laser, a pulsed dye laser, or a xenon arc lamp with a monochromator. When a cw dye laser or an arc lamp was used, a mechanical chopper modulated the output. The probe beam was a 0.5-mW He-Ne laser. Two types of position sensors²² were used to determine the amplitude and phase of the probe beam deflection: lateral and quadrant. The output of the sensor was fed into the (A-B) input of a lock-in amplifier.

In Fig. 4(b), the experimental arrangement for collinear PDS is presented. The pump beam must be a laser to permit tight focusing. To minimize the scattering of the pump beam on the position sensor, both

pump and probe beams were counterpropagating. Furthermore, a notch filter was placed between the sample and the detector to eliminate any remaining scattered light. To maximize the signal, the angle between the pump and probe beams can be minimized, although collinearity is rarely required. One further consideration is that the focal spot of the probe beam should be smaller than that of the pump beam.

In the case of pulsed PDS, the exciting light source was a Chromatix CMX-4 flashlamp-pumped dye laser. A quadrant position sensor detected the deflection of the He-Ne probe beam. The output of the sensor was fed into a differential preamplifier whose output was digitized by a Tektronix 7912AD digitizer. When necessary, this digitized waveform was averaged with a Tektronix 4052 computer. The laser power was monitored with a color corrected photodiode for the purpose of power normalization.

Sample materials included filtered spectroscopic grade benzene, a 0.5- μm thick film of indium and tin oxides deposited on a glass substrate, and a 600-nm glass edge filter.

B. Analysis of Detector Response

As indicated, the deflection of the beam due to the change in the index of refraction is detected by a position sensor which converts the deflection into an output voltage. The relationship between the deflection and the voltage depends on whether the position sensor is a quadrant or a lateral detector.

For a quadrant detector, the change of the signal ΔV above the dc level V is calculated using Fig. 5(a), assuming a Gaussian probe beam,

$$\frac{\Delta V}{V} = \frac{\Delta I}{I_0} = 4 \Delta x \int_0^\infty \frac{2}{\pi w_0^2} \exp(-2r^2/w_0^2) dr = (4/\sqrt{2\pi}) \frac{\Delta x}{w_2} \quad (29)$$

where $\Delta x = \phi d$, d is the distance from the focal spot to the detector, I_0 is the probe beam intensity, and w_2 is the spot radius on the detector. Since d is large,

$$w_2 \approx (\lambda d)/(\pi w_0 n_0), \quad (30)$$

where w_0 is the probe beam radius at the focal spot, and λ is the probe beam wavelength. Hence

$$\Delta V = \frac{4}{\sqrt{2\pi}} \frac{\phi \pi w_0 n_0}{\lambda} V, \quad (31)$$

and ϕ is given by Eq. (20).

We conclude that in the case of a quadrant position sensor, the signal is independent of the sample distance. For modulation frequencies of the order of a few hundred cycles per second, $\Delta V/V$ was found to be 10^{-6} . Thus we were able to measure a deflection of 1.5×10^{-9} rad/ $\sqrt{\text{Hz}}$ given typical laser parameters.

For a lateral detector, we use the sensitivity figure of 0.55P A/cm given by the manufacturer, where P is the probe beam power in watts. Then $\Delta V/V = 0.55 \Delta x = 0.55 \phi d$ (d is in centimeters). The signal depends on the distance from the focal spot to the detector. For a detector of size l_1 [Fig. 5(b)],

$$d_{\max} = (l_1 \pi w_0 n_0)/\lambda; \quad (32)$$

$$\frac{\Delta V}{V} = \frac{0.55a}{2} \frac{l_1 \pi \omega \eta_0}{\lambda} \quad (33)$$

Since $l_1 = 1$ cm, we see that both detectors are similar in sensitivity.

IV. Experimental Verification of the Theoretical Predictions

A. Continuous/Wave PDS

As noted above, PDS can be performed in two ways: collinear and transverse. Experiments were conducted to evaluate both approaches and to compare the results obtained with the theoretical predictions.

1. Collinear PDS

a. *Signal dependence on interbeam offset x_0 .* Figure 6(a) shows the dependence of the signal amplitude on the offset of the pump and probe beams for high and low modulation frequencies. Note that both theoretical curves are adjusted only by the identical amplitude factor, indicating that the correct relative magnitude and peak positions are predicted by the theory.

The discrepancy in the case of high modulation frequency and larger x_0 could be due to uncertainty in the precise thermal properties of the glass substrate. Similarly, the phase shown in Fig. 6(b) demonstrates good agreement between theory and experiment, except for large displacements.²⁰

For low frequencies, the thermal lengths in the sample and the substrate are much larger than the pump beam radius. Consequently, the temperature distribution extends significantly beyond the beam radius. Figure 6(b) shows that the phase changes continuously as the probe beam moves away from the pump beam. This is due to the propagation of the heat from the pump beam to the probe beam. For high frequencies, the thermal conduction becomes unimportant. Hence the curve describing the relationship between the amplitude and the offset of the pump and probe beams is the radial derivative of the beam profile. Using this fact, one can measure the radius of the Gaussian beam profile, if unknown, and check the focus of the pump beam. Far from the pump beam, the phase changes linearly with the distance x_0 , since it is due to the propagation delay of the heat wave traveling from the pump to the probe beam.

b. *Signal dependence on modulation frequency ω .* Figure 7(a) and (b) show the amplitude and phase vs the frequency for various offsets of the probe beam. The theoretical amplitude is adjusted by an amplitude factor, and the phase is adjusted with a constant offset. The theoretical and experimental curves show rapid change at the same frequency and approach the same limiting values at high frequencies. When the thermal length in the sample-substrate becomes smaller than the probe beam radius, the signal amplitude and the phase change rapidly. Thus by measuring the pump beam radius, using the technique outlined above, one can measure the thermal diffusivity of the sample. The

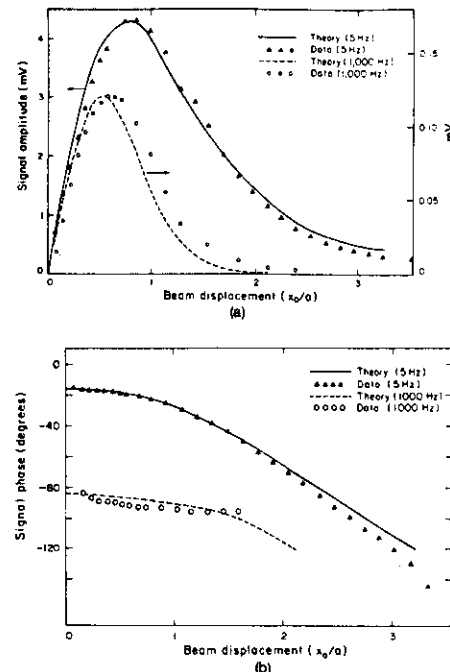


Fig. 6. Collinear PDS: (a) signal amplitude vs beam displacement x_0/a ; (b) signal phase vs beam displacement x_0/a .

high frequency limit of the signal amplitude has a $1/\omega$ dependence. When the probe beam is offset from the pump beam by more than one beam radius, the signal decreases faster than $1/\omega$. This occurs not only because the temperature of the central region decreases as $1/\omega$, but because the thermal length also decreases, preventing the heat from reaching the probe beam. If the two beams overlap significantly, there is no dependence on the thermal length. This causes the high frequency limit to follow $1/\omega$.

2. Transverse PDS

For the transverse PDS, several parameters were varied.

a. *Frequency dependence.* By examining Fig. 8 we see that the signal falls off very rapidly as a function of frequency. Because $T \propto \exp(-z_0/l_1)$, the signal falls off exponentially as the frequency increases. The important consequence of the above is that for high modulation frequencies, pulsed work, or solids immersed in liquids, the signal is bigger if the probe beam is carefully aligned close to the sample surface and hence should be focused. This condition shows that the signal is optimized for flat samples with small lateral dimensions.

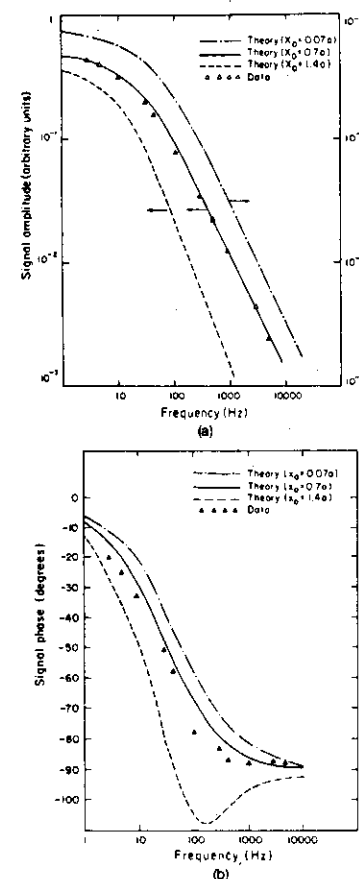


Fig. 7. Collinear PDS: (a) signal amplitude vs frequency; (b) signal phase vs frequency.

b. *Signal dependence on pump beam radius a .* Figure 9 shows the effect of varying the pump beam radius. The signal increases as $1/a$ as the pump beam is focused. The temperature rise has an a^2 dependence, while the interaction length goes as $1/a$. When the pump beam radius becomes as small as the lateral thermal length, no further increase in the signal is observed. For z_0 less than the thermal length in air l_a , the lateral thermal length is approximately the thermal length in the glass l_g ; for z_0 greater than l_a , the lateral thermal length is l_a .

c. *Signal dependence on probe and pump beam offset y_0 .* Figure 10 shows the effect of off-axis dis-

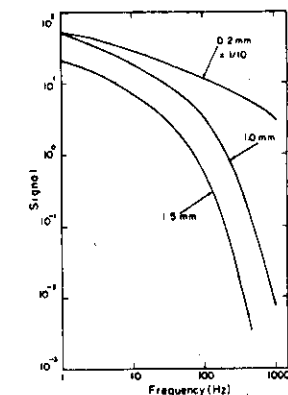


Fig. 8. Transverse PDS. Signal vs frequency for various offsets z_0 . Beam radius is 140 μ m.

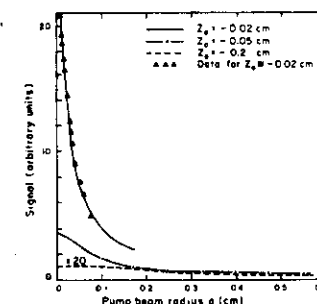


Fig. 9. Transverse PDS. Signal amplitude vs beam radius a for different beam offsets z_0 . Frequency is 48 Hz, and tilt angle is 0°.

placement y_0 of the probe beam relative to the pump beam (Fig. 1). By varying the offset y_0 of the beams, the profile of the temperature in region 0 is probed at the position z_0 of the probe beam. The main peak width is determined by the spot size of the pump beam and the sample thermal length. Because l_a is larger than l_g , the heat flows from the air back into the sample for y_0 greater than l_a (see inset in Fig. 10). This reversed heat flow causes the second, but weaker, maximum with its phase shifted 180° from that of the central peak. For z_0 greater than l_a , the heat flows away from the sample for all y_0 values, and the secondary peak will no longer be observed. Both the 180° phase shift and the disappearance of the secondary peak were verified experimentally.

d. *Signal dependence on the probe beam tilt angle ψ .* The effect of varying the tilt angle ψ of the probe

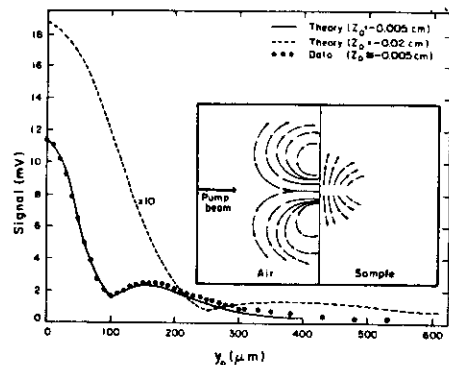


Fig. 10. Transverse PDS. Signal amplitude vs off-axis displacement y_0 for various z_0 offsets. Material is 600-nm edge filter glass, frequency is 48 Hz, tilt angle is 0° , and beam radius is 70 μm . Inset shows direction of heat flow and origin of the second maximum.

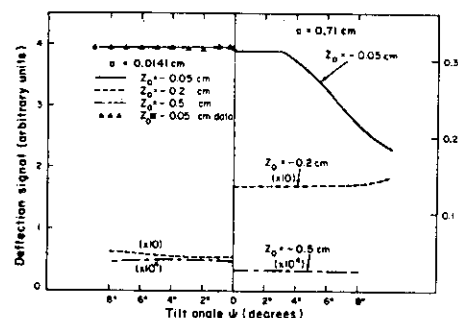


Fig. 11. Transverse PDS. Signal amplitude vs tilt angle ψ . Frequency is 48 Hz, and the sample is 600-nm edge filter glass.

beam relative to the sample surface is shown in Fig. 11. For a small pump radius (40 μm), the tilt angle is not important unless the sample actually intercepts the probe beam. In the case of a broadband pump beam (0.71 cm), the signal is more sensitive to the tilt angle because of the longer path grazing the sample. This often requires a longer focal length lens for the probe beam.

e. *Pump beam offset in the z_0 direction.* Figure 12 shows the effects of varying the beam offset z_0 from the sample. In general, the signal increases exponentially as the probe beam approaches the sample. As pointed out in Ref. 5, the exponential increase can be used to determine the diffusivity of the deflecting medium. For the more realistic case of a beam focused on a poor conducting substrate, the results are more complex.

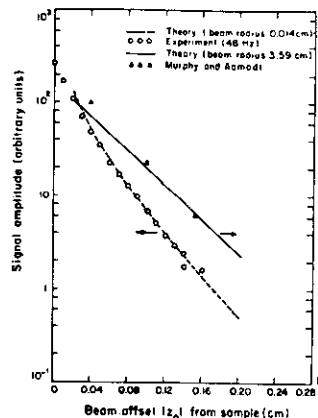


Fig. 12. Transverse PDS. Signal amplitude vs beam offset z_0 at 4 Hz. Tilt angle is 0° .

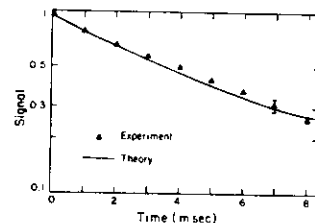


Fig. 13. Signal vs time for benzene at 607 nm. Collinear PDS with the probe beam at $x_0 = a/2$.

For z_0 increasing, the temperature distribution is determined by the thermal properties of the air (or an appropriate fluid) so the beam deflection falls off exponentially as z_0 . On the other hand, for z_0 decreasing, the temperature distribution gets smaller and more compressed (Fig. 10). Hence the signal rises faster than exponentially.

Spectra taken with cw PDS have been previously reported and will not be repeated here.⁶⁻⁸ For transverse PDS and for an interaction length of 1 cm, we were able to detect a temperature rise of 10^{-4}°C in air and 10^{-6}°C for CCl_4 . For collinear PDS, we have been able to measure an αl of 10^{-8} for liquids,⁶ 10^{-7} for solids,⁶ and 10^{-7} for gases.⁷

B. Pulsed Collinear PDS

We have investigated the case of collinear pulsed PDS. The signal as a function of time for pure benzene is shown in Fig. 13. The measured time constant ($1/\tau$)

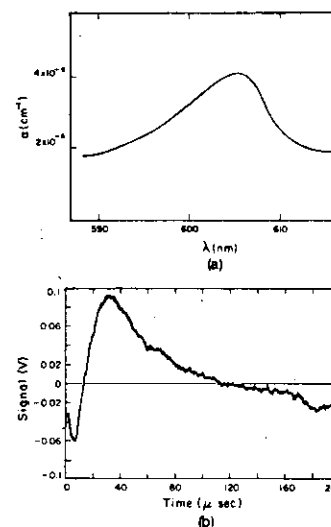


Fig. 14. (a) Absorption vs wavelength for 0.1% benzene in distilled CCl_4 . (b) Signal vs time. Horizontal scale is 1 msec/div, wavelength is 606 nm, and 1024 averages were taken.

is 6.2 msec. The magnitude of the expected signal was computed using Eq. (28) with $r = a/2 = 37 \mu\text{m}$. The pump radius a was found by measuring the distance the pump beam focusing lens moved between signal maxima. The agreement between theory and experiment is good, demonstrating that for thick uniform samples, the infinite sample approximation is appropriate.

To demonstrate the sensitivity of pulsed PDS, we have obtained the spectrum of the sixth harmonic of the C-H stretch of 0.1% of benzene in distilled CCl_4 [Fig. 14(a)]. The measured absorption coefficient is $2 \times 10^{-6} \text{ cm}^{-1}$. Since the interaction length was 0.1 cm or less, we measured an αl of 10^{-7} . We believe the background is due to impurities in the CCl_4 (since such a background was ten times larger before distillation of CCl_4), absorption in the CCl_4 itself, or is due to the signal caused by electrostriction.²⁴

Figure 14(b) shows the signal vs time for the peak absorption in 0.1% benzene. The rise time is determined by the shunt capacitance of the cables with a 50-k Ω load resistor. The fall time is determined by a 5000-Hz high pass filter in the preamplifier. The SNR for a single point can be conservatively estimated to be 10. (Actually, if one were to fit a curve through all points, the noise would be considerably less.) Assuming an SNR of 10, we find that we can measure an absorption coefficient of $2 \times 10^{-7} \text{ cm}^{-1}$ for a 1-mJ laser. Since the noise appears to be mostly shot noise, the He-Ne probe laser output could be increased by a factor of 20, giving an improvement of 4 in the SNR. If one fits a

curve through all points and takes more averages, the minimum measurable absorption coefficient can be lowered by a factor of 10-100. This assumes that problems with coherent electrical noise, electrostriction, and probe laser noise are insignificant.

V. Noise—Background Considerations

The background noise originates from the following sources: laser noise (pointing and intensity fluctuations); electronic noise; and sample and/or ambient environment noise (e.g., convection, turbulence, or mechanical vibration).

For cw PDS, the pointing noise of the probe laser predominates. The intensity fluctuations of the probe beam can be discriminated against by adjustment of the probe spot on the detector. Typically, the differential input can reject intensity fluctuations to 1 part in 1000. For a typical laser, the ratio of the intensity noise to the dc level was $5 \times 10^{-6}/\sqrt{\text{Hz}}$, while the observed noise ratio was $6 \times 10^{-7}/\sqrt{\text{Hz}}$. The expected contribution of laser intensity fluctuations is $5 \times 10^{-9}/\sqrt{\text{Hz}}$, which is much less than the observed noise. Also the observed noise cannot be attributed to room vibrations or air turbulence, since the noise decreased by a factor of 10 when we used a focused flashlight beam as the probe beam. We conclude that the noise must be due to pointing fluctuations. Testing a variety of He-Ne lasers, we found that they all exhibited a pointing noise of $\sim 5 \times 10^{-9} \text{ rad}/\sqrt{\text{Hz}}$ at low frequencies reaching shot noise at a few kilohertz. Spatially filtering or installation of an intracavity iris could improve this value.

The electronic noise is easily calculated and seldom limits the sensitivity. Following Van der Ziel's analysis,²⁵ the expected combined rms current noise contribution of the position sensor, the load resistor, and preamplifier is given by

$$i_{\text{rms}} = (4k_B T F_1)^{1/2} \left(\frac{1}{R_L} + \frac{e I_0}{2k_B T} + \frac{i_n^2}{4k_B T} + \frac{e_n^2}{4R_L^2 k_B T} + \frac{e_n^2 \omega^2 C'^2}{12k_B T} \right)^{1/2} \quad (34)$$

where k_B is Boltzmann's constant; T is the temperature; F_1 is the frequency bandpass of the detector and electronics; R_L is the load resistor; I_0 is the dc current; C' is the combined detector, cable, and preamplifier shunt capacitance; i_n is the preamplifier current noise; and e_n is the preamplifier voltage noise. Usually the third term in Eq. (34) can be neglected for a reasonably good amplifier by making the load resistor larger than 1 k Ω . Often the first and fourth terms can be neglected as well. This is feasible at low frequencies. Thus the most significant electronic noise term is the shot noise, the second term, which sets a detection limit of $3.4 \times 10^{-10} \text{ rad}/\sqrt{\text{Hz}}$ for a 1-mW probe laser.

For wideband or pulsed operation, the situation is more complicated. The high frequency cutoff F_1 is determined by $2\pi F_1 R_L C' = 1$. Consequently the load resistance cannot be made arbitrarily large. Furthermore, since the thermal signal fall time is very slow (Fig. 13), the high pass filter must be set at 25 Hz or less to avoid waveform distortion. Unfortunately a 25-Hz high pass filter allows significant low frequency noise and

Table I. Summary of Some Photothermally Based Spectroscopies

Technique	Samples Already Studied	Experimental Set Up	Sensitivity (αI) min. Pump Power (W) ^a	Probe Beam	Sensitivity to Scattered Light	Special Features
TL	Liquids	Difficult to align	10^{-7} - 10^{-8}	Sensitivity to pointing and intensity noise	No	No mechanical contact. Permits hostile environment and <i>in situ</i> measurements.
Microphone PAS	Solids (bulk, powders), liquids, & gases	Simple to align	$\sim 10^{-4}$ - 10^{-5} solids 10^{-7} gases		Yes	Sensitive to mechanical and acoustical noise.
PZT PAS	Solids (bulk) liquids	Simple to align	$\sim 10^{-3}$ (10^{-5} J pulsed)		Yes	Sample attachment difficult.
Collinear PDS	Optically clear transparent solids, liquids & gases	Difficult to align	$\sim 10^{-7}$ - 10^{-8} (10^{-10} J pulsed)	Sensitivity to pointing noise Sample transparent to probe	No	No mechanical contact. Permits hostile environment and <i>in situ</i> measurements.
Transverse PDS	Condensed phase samples	Simple to align	$\sim 10^{-5}$	Sensitivity to pointing noise	No	No mechanical contact. Permits hostile environment and <i>in situ</i> measurements.
Interferometry	Liquids & solids	Difficult to align	$\sim 10^{-7}$ - 10^{-8}	Sensitive to intensity noise Sample transparent to probe beam	No	No mechanical contact. Permits hostile environment and <i>in situ</i> measurements.

^aTypical ranges cited in the literature.

background into the detection electronics. We have found that a 3000-Hz high pass filter improves the SNR and eliminates the background significantly, even though it distorts the waveform and throws away part of the signal. The distorted waveform is shown in Fig. 14(b). With a high pass filter, the shot noise predominates over other noise sources.

Other factors which may contribute to the background noise are unwanted light scattered on the position sensor, spurious signals due to particulates, impurities in the sample, and window absorption. In the case of low modulation frequencies in liquids, turbulence may mask the true deflection of the probe beam. Obvious solutions to these problems include keeping thermal gradients small, filtering out particles, distilling the liquid, and insuring that the probe and pump beams do not overlap within the windows of the sample container.

VI. Discussion and Comparison with Related Spectroscopies

In this section we discuss the advantages and disadvantages of PDS and compare PDS with other photothermally based spectroscopies. A summary of our comparison is in Table I.

A. Comparison to Thermal Lensing

First we compare collinear PDS to TL given in Ref. 3. Using the recommendations found therein, we determine that for weak absorptions, the relative change

of intensity $\Delta I/I$ for TL is given by

$$(\Delta I/I)_{TL} = 0.8 \frac{u_0}{\alpha} \frac{\partial n}{\partial T} \frac{\lambda P_{TL}}{a^2 \kappa_1} \left(\frac{1}{1 + t_c/2l} \right), \quad (35)$$

where u_0 is the probe focal spot, α is the pump focal spot, t is the time after the pump is turned on, α is the absorption coefficient, P is the pump beam power, l_{TL} is the interaction length, κ_1 is the conductivity, λ is the vacuum wavelength of the probe beam, n_0 is the index of refraction of the media, and $t_c = a^2/4k$. Using Eq. (29) for the change of intensity $\Delta I/I$ for PDS and evaluating $\partial T/\partial r$ as in Ref. 3, we find that

$$(\Delta I/I)_{PDS} = \frac{4\alpha P}{\sqrt{2\pi}} \frac{u_0}{\lambda} \frac{\partial n}{\partial T} \frac{l_{PDS}}{a \kappa_1} \left[\exp[-1/2(1 + 2t/t_c)] - \exp(-1/2t) \right], \quad (36)$$

letting $t \rightarrow \infty$ and assuming that $n_0 = 1.5$,

$$\frac{(\Delta I/I)_{PDS}}{(\Delta I/I)_{TL}} = \frac{0.78 l_{PDS}}{l_{TL}}, \quad (37)$$

If the probe beam is aligned collinearly with the pump beam and if the pump is filtered out before reaching the position sensor, the following relation holds:

$$l_{PDS} = l_{TL} = 0.2\pi u_0^2 n_0 / \lambda. \quad (38)$$

Thus PDS and TL have almost the same sensitivity. Usually, however, for both collinear PDS and TL, the overlap of the beams within the notch filter can give rise to an appreciable background signal due to heating within the filter. To reduce the background, the pump

and probe beams should intersect at an angle. This reduces the interaction length and the signal by a factor of 1-2 orders of magnitude.

PDS has several distinct advantages over TL when one considers noise and background. The probe laser usually has relatively large intensity fluctuations. Such fluctuations give rise to significant noise in the case of TL but are reduced in PDS by a factor of 1000. The pointing noise of the probe laser, of course, affects both PDS and TL. When PDS and TL are used on semiconductors with a band gap near the probe wavelength, the probe beam intensity will be modulated by the shift of the band gap due to pump beam heating. This intensity modulation causes an additional signal which varies as the pump wavelength. The two contributions may be difficult to separate.

PDS also has versatility advantages over TL. Spectra of opaque samples or scattering samples can be measured using transverse PDS, 3-D depth profiling of absorption can be performed by moving the beam overlap region through the sample. Finally TL is more difficult to align. Hence PDS is as sensitive as TL and is more versatile and easy to use.

B. Comparison with Photoacoustic Spectroscopy

Because of the variety of detector-sample combinations of both PAS and PDS, we restrict our comparison to condensed matter samples.

Compared with microphone PAS, PDS has the following advantages: (1) it is more sensitive, particularly in the case of liquids; (2) it has the potential for remote sensing and *in situ* monitoring; (3) it works in hostile environments such as temperature extremes or caustic substances; (4) acoustic shielding requirements are less stringent; (5) there is no background due to window absorption; (6) the frequency response is greater; (7) spatial probing of absorption is possible; and (8) the complication of gas coupling physics is eliminated. Disadvantages of PDS are: (1) alignment is more difficult; (2) the sample surface cannot be exceedingly rough; and (3) the sample must be transparent to the probe beam for collinear PDS.

Compared with piezoelectric PAS, the advantages of PDS are: (1) it is at least as sensitive; (2) it can be employed in hostile environments; (3) there is no scattering background; (4) the attachment of the transducer to the sample is eliminated; (5) the mechanical properties and sample size are not limiting factors; (6) 3-D spatial profiling is possible; and (7) the relationships of the signal to the temperature rise and to the time dependence of the signal are far simpler. On the other hand, the disadvantages of PDS are: (1) in the case of collinear PDS it may be difficult to find a probe beam that is transmitted by some materials; (2) alignment is more difficult; and (3) the optical quality of the sample is more demanding for collinear PDS.

VII. Implications for Imaging and Microscopy

Recently, photoacoustic detection, which depends on both the optical and the thermal properties of a given material, has been put to use in performing scanned

imaging and microscopy of various materials.²⁶⁻²⁸ In this case, a new type of image is obtained which displays unique spatial and thermal information. Of particular interest is the ability of this imaging to detect subsurface structures or flaws which exist at depths exceeding the optical penetration of the probe light.

The discussion above suggests that photothermal deflection detection yields information similar to photoacoustic imaging. Photothermal deflection imaging has been reported elsewhere.¹⁸ In this section we discuss some of the implications of our theoretical treatment for imaging and microscopy.

A. Collinear Photothermal Deflection Microscopy and Imaging

This scheme is mainly suitable for optically thin samples and for weakly absorbing objects embedded in a transparent matrix. By scanning the interaction region of the focused pump and probe beams relative to the sample, a 3-D profile can be constructed. In this case, the optical resolution is determined by the size of the probe beam waist in the x and y directions and by the interaction length l ($= 2a/\sin\psi$) in the z direction. Consequently, the larger the intersection angle of the beams and the tighter the focal spot of the pump beam, the greater the optical resolution. On the other hand, we have shown that the thermal resolution is determined by the thermal length within the sample itself [see Eq. (12) and Fig. 6(a)]. Figure 6(a) shows that as the modulation frequency increases, the thermal resolution given by $(\text{Re}K_1)^{-1}$ also increases.

We have demonstrated⁶ that an αI of 10^{-7} can be measured with collinear PDS. Hence spatial profiling of weakly absorbing inhomogeneities can be probed with a resolution equal to the pump laser spot size. By changing the probe wavelength, one can get spectral information as well.

B. Transverse Photothermal Deflection Microscopy and Imaging

By performing transverse photothermal deflection microscopy, one probes the optical and thermal properties at and near the surface of the material of interest. The optical resolution will again be determined by the pump beam waist, while the thermal resolution for a focused pump beam will be the thermal wavelength in the material. For large pump beams or for large thermal sources, the thermal resolution is more complicated. In the case of small beam offsets ($|z_0|$), the thermal resolution is given by the thermal length in the sample. For large $|z_0|$, however, the thermal resolution is given by the thermal wavelength in deflecting media adjacent to the sample surface.

Transverse photothermal deflection microscopy also can yield information on the surface topography of a given material. Equation (25) and Fig. 12 show the strong dependence of the signal on the probe beam offset ($|z_0|$). If the material's surface varies in the z direction, both the phase and the amplitude of the photothermal deflection signal will reflect such a vari-

ation.¹⁸ In the case of a uniformly illuminated surface with a uniform absorption, surface roughness of the order of 0.1 μm can be resolved.

To account fully for the role of sample inhomogeneities and of geometrical boundaries and to determine the thermal resolution, one needs to generalize our theoretical treatment to include the spatial variation of the thermal properties of the sample. Such an extension will not be dealt with in this paper.

VIII. Summary

We have shown that photothermal deflection spectroscopy is a sensitive and versatile technique for measuring a wide range of absorption coefficients in solids, thin films, liquids, and gases. A model was presented which accurately predicts the experimental results. The model allows the experimenter to optimize the experimental setup and predict quantitatively the sensitivity and limitations of PDS. We also identified sources of noise, and ways to maximize the SNRs were discussed. Finally, we discussed the advantages and disadvantages of PDS and compared it with alternative spectroscopies. We believe that photothermal deflection spectroscopy will prove to be a unique and sensitive spectroscopic technique.

We express our sincere thanks to C. B. Moore, to members of his group, and to A. Kung for the generous use of a Chromatix CMX-4 laser. We also thank the other members of the Applied Physics and Laser Spectroscopy Group and M. Jackson for their helpful suggestions and comments. This work was supported by the U.S. Department of Energy.

Appendix

The acoustic wave deflects the probe beam in two ways. The acoustic wave propagates for the energy deposition region to the probe beam where it generates a temperature rise by adiabatic compression. The gradient of this temperature rise deflects the beam. The ratio of this term to the thermal deflection term is

$$(\text{acoustic/thermal}) = (h_0 B_T \omega T_0 / C_p) \exp(z_0/l_t), \quad (\text{A1})$$

where B_T is the volume expansion coefficient, $l_t = (2k_0/\omega)^{1/2}$, and z_0 is the distance between the heat deposition region and the probe beam. This ratio is the same as the ratio given in Ref. 9. For gases and liquids

$$\text{acoustic/thermal} \approx 10^{-11} \omega \exp(z_0/l_t), \quad (\text{A2})$$

which indicates that the acoustic term will be important only at very high frequencies and/or large probe displacements between the heat deposition region and the probe beam. When the acoustic and thermal contributions to the deflection are equal, the signal will be 10^{-10} times smaller than the thermal deflection signal for low frequencies and $z = 0$. Hence the acoustic terms add considerable complexity but are negligible in most practical experiments.

The acoustic wave also deflects the probe beam by the pressure generated at the sample surface. The pressure

wave propagates to the probe beam and deflects the probe beam through the pressure dependence of the index of refraction. The contribution of the pressure deflection term is of the same order of magnitude as the contribution in Eq. (A1) if a gas is the deflecting medium. For liquids, it is negligible. Reference 9 omits this term. Hence to be consistent one must solve the coupled pressure and temperature waves in the sample and deflecting medium and compute their combined effect on the index of refraction. The additional terms will be of nominal experimental importance only at high frequencies, large probe beam offsets, and/or high pump beam peak powers.

References

1. See, for example, J. Stone, *J. Opt. Soc. Am.* **62**, 327 (1972); *Appl. Opt.* **12**, 1828 (1973).
2. J. R. Whinnery, *Acc. Chem. Res.* **7**, 225 (1974) and references therein.
3. R. L. Swofford and J. A. Morrell, *J. Appl. Phys.* **49**, 3867 (1978) and references therein.
4. For an overview of photoacoustic spectroscopy, see Y.-H. Pao, Ed., *Optoacoustic Spectroscopy and Detection* (Academic, New York, 1977).
5. D. Fournier, A. C. Boccara, and J. Badoz, in *Digest of Topical Meeting on Photoacoustic Spectroscopy* (Optical Society of America, Washington, D.C., 1979), paper ThA1.
6. A. C. Boccara, D. Fournier, W. Jackson, and N. M. Amer, *Opt. Lett.* **5**, 377 (1980).
7. D. Fournier, A. C. Boccara, N. M. Amer, and R. Gerlach, *Appl. Phys. Lett.* **37**, 519 (1980).
8. A. C. Boccara, D. Fournier, and J. Badoz, *Appl. Phys. Lett.* **36**, 130 (1980).
9. J. C. Murphy and L. C. Aamodt, *J. Appl. Phys.* **51**, 4580 (1980).
10. M. Billardon and J. M. Ortega, E.S.P.C.I., private communication.
11. F. A. McDonald and G. C. Wetsel, Jr., *J. Appl. Phys.* **49**, 2313 (1978).
12. W. Jackson and N. M. Amer, *J. Appl. Phys.* **51**, 3343 (1980).
13. H. S. Bennett and R. A. Forman, *J. Appl. Phys.* **48**, 1432 (1977).
14. L. C. Aamodt and J. C. Murphy, *J. Appl. Phys.* **49**, 3036 (1978).
15. A. Rosencweig and A. Gershko, *J. Appl. Phys.* **47**, 64 (1976).
16. A. Mandelis and B. S. Royce, *J. Appl. Phys.* **50**, 4331 (1979).
17. D. C. Smith, *IEEE J. Quantum Electron.* **QE-5**, 600 (1969).
18. D. Fournier and A. C. Boccara, in *Scanned Image Microscopy*, E. A. Ash, Ed. (Academic, London, 1980).
19. L. W. Casperson, *Appl. Opt.* **12**, 2434 (1973).
20. For some high frequency modulation experiments with very tight focusing, we observed a small secondary maximum with a 180° phase shift. Because the pump and probe beams intersect at an angle and the probe beam deflects slightly in region 0, a mechanism similar to that discussed in Sec. IV.A.2.3, could be present.
21. H. S. Carslaw and J. C. Jaeger, *Conduction of Heat in Solids* (Oxford, Clarendon, 1959).
22. Silicon Detector Corp., Newbury Park, Calif.
23. In some cases, it is experimentally advantageous to use a liquid in region 0 to make use of the typically higher dn/dT for liquids. In this case, it is obvious that the role of regions 0 and 2 should be interchanged.
24. S. R. Brueck, H. Kildal, and L. J. Belanger, *Opt. Commun.* **34**, 199 (1980).
25. A. Van der Ziel, *Noise in Measurements* (Wiley, New York, 1976).
26. R. L. Thomas, J. J. Pouch, Y. H. Wong, L. D. Favro, P. K. Kuo, and A. Rosencweig, *J. Appl. Phys.* **51**, 1152 (1980) and references therein.
27. H. K. Wickramasinghe, R. C. Bray, V. Jipson, C. F. Quate, and J. R. Salcedo, *Appl. Phys. Lett.* **33**, 923 (1978).
28. G. Busse and A. Ograteck, *J. Appl. Phys.* **51**, 3576 (1980) and references therein.

Absolute optical absorption coefficient measurements using transverse photothermal deflection spectroscopy

Andreas Mandelis

Photoacoustics Laboratory, Department of Mechanical Engineering, University of Toronto, Toronto, Ontario, Canada M5S 1A4

(Received 4 November 1982; accepted for publication 8 March 1983)

Information about the optical absorption coefficient of solid materials in contact with a fluid phase can be obtained from photothermal deflection (PDS) measurements using both the signal amplitude and phase channels of the PDS response of a system to an optical excitation. This paper presents a theoretical model of photothermal processes in the transverse (TPDS) experimental configuration. The theory is used to determine the dependence of both signal channels on the optical absorption coefficient of the solid material and to define absorption coefficient ranges within which TPDS can be used as a spectroscopic technique. A method concerning the use of the combined amplitude and phase data for the absolute measurement of the absorption coefficient is presented for the experimentally important thermally thick limit.

PACS numbers: 78.20.Dj, 78.20.Nv, 84.60.Dn, 07.65. - b

INTRODUCTION

Photothermal deflection spectroscopy (PDS) has recently emerged as a sensitive method for the study of solid-fluid interfaces. Boccara *et al.*,¹ Murphy and Aamodt,² and Jackson *et al.*³ have applied this technique to studies of solid-gas interfaces. Royce *et al.*⁴ have used PDS to study *in situ* the optical properties of solid (electrode)-liquid (electrolyte) interfaces. In a PDS experiment the probe laser beam deflection is usually detected in the collinear or in the transverse modes in the frequency domain.⁵ However, the collinear configuration has the disadvantage that it requires samples which are transparent to the probe beam. For this reason the transverse mode (TPDS) has been favored by many workers.^{1,2,4}

Murphy and Aamodt² have studied the PDS response from a solid sample subject to a harmonic optical excitation. They derived expressions for the dependence of both signal amplitude and phase on the probe beam offset and verified their theory for sample surface temperatures ranging between 30.3 and 94 $^\circ\text{C}$. However, the usefulness of the PDS technique as a spectroscopic tool hinges on its success in providing a measurement of the absolute optical absorption coefficient of a material. Although Murphy and Aamodt's theory could in principle be used to provide expressions for the amplitude and phase dependence on the optical absorption coefficient, the derivation of such expressions is rather complicated, especially for certain limiting cases which are of interest to experimentalists. Complications in deriving explicit amplitude and phase expressions from the exact PDS theory presented by Murphy and Aamodt might arise because they considered acoustic transport phenomena similar to those which they reported in previous publications on the theory of photoacoustic spectroscopy (PAS).^{5,6} McDonald and Wetsel^{7,8} and Mandelis⁹ have shown that the acoustic transport phenomena in a PAS cell become unimportant for times greater than ca. 10^{-5} sec, or modulation frequencies below 10^4 Hz.

This paper is concerned with the development of one-dimensional theoretical model for the transverse PDS effect at a solid-fluid interface with emphasis on the relationship between signal amplitude/phase channels and the optical absorption coefficient of the solid sample under investigation. It is shown that under specific experimental conditions the combination of PDS amplitude and phase data can be used to determine the absolute value of the absorption coefficient.

THEORY

An idealized one-dimensional configuration is employed to determine the amplitude (TPDS) signal. The geometry of the system is shown in Fig. 1. A solid with optical

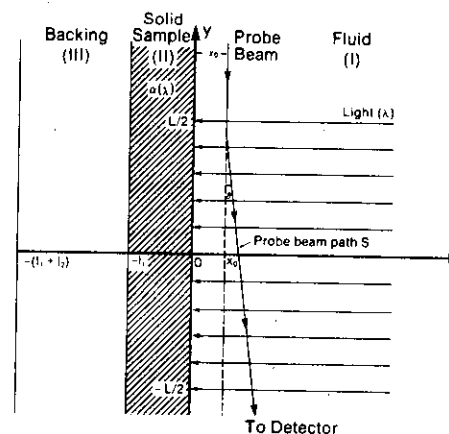


FIG. 1. Geometry of a one-dimensional TPDS system at a solid-fluid interface.

absorption coefficient $\alpha(\lambda)$ is illuminated uniformly with a light beam of wavelength λ , whose intensity is harmonically modulated in time at a frequency ω . The solid absorbs the incident radiation according to Beer's law and is in thermal contact with a transparent fluid (e.g., a liquid or a gas). The sample under investigation has thickness l_1 and is supported by a transparent backing material of thickness l_2 . It is further assumed that the extent of the solid surface along the y plane is large compared with the width L of the incident beam. Nonradiative deexcitations in the illuminated solid cause a harmonic modulation of the temperature at the sample surface and, through heat transfer, the temperature of the fluid layer adjacent to the surface. A laser probe beam passes through the fluid, parallel to the sample surface at a distance x_0 less than the thermal diffusion length in the fluid. It is deflected through an angle $\theta(\omega, \alpha)$ due to changes in the refractive index caused by the heat transfer from the absorbing solid.^{2,3}

In the three regions (I)–(III) shown in Fig. 1, the temperature rise satisfies the appropriate thermal diffusion equations:

$$\frac{\partial^2}{\partial x^2} T_i(x, t) = \frac{1}{\alpha_i} \frac{\partial}{\partial t} T_i(x, t) \quad (1)$$

$$= \begin{cases} \frac{H(x, t)}{k_i}, & \text{Region (II)} \\ 0, & \text{Regions (I), (III)} \end{cases}$$

$i = f$ (fluid), s (solid), b (backing).

In the solid (s) region for which $-l_1 < x < 0$, the sample heating rate \dot{H} (W cm^{-2}) is given by

$$\dot{H}(x, t) = \frac{1}{2} \eta I_0 \alpha \exp(-\alpha|x|) \text{Re}[1 + \exp(i\omega t)], \quad (2)$$

where η is the quantum efficiency of nonradiative processes. In this work it will be assumed that $\eta = 1$ (Ref. 10). I_0 is the irradiance of the incident light (W cm^{-2}); k_i is the thermal conductivity of material i [$\text{cal}(\text{cm sec}^\circ\text{K})^{-1}$]; $\alpha_i = k_i/\rho_i C_i$, the thermal diffusivity of material i ($\text{cm}^2 \text{sec}^{-1}$); ρ_i and C_i are the density (g cm^{-3}) and specific heat [$\text{cal}(\text{g}^\circ\text{K})^{-1}$] of material i .

The quantity of interest is $T_f(x, t)$ which describes the departure of the temperature from its ambient value T_A in the fluid region. Thus the actual temperature profile in the fluid is given by

$$T_f(x, t)_{\text{actual}} = \text{Re}[T_f(x, t)] + T_A. \quad (3)$$

The solution of the system of Eq. (1) can be separated into an ac and a dc (i.e., time-independent) component. The ac component of the solution in the fluid region is given by

$$T_f^{(ac)}(x, t) = \frac{A}{\alpha^2 - \sigma_f^2} \left\{ \frac{(r-1)(b+1)e^{\sigma_f x} - (r+1)(b-1)e^{-\sigma_f x} + 2(b-r)e^{-\alpha l_1}}{(f+1)(b+1)e^{\sigma_f l_1} - (f-1)(b-1)e^{-\sigma_f l_1}} \right\} \exp(-Gx), \quad (4)$$

where $A \equiv I_0 \alpha / 2k_s$, $\sigma_i \equiv (1 + i\alpha_i)$, $\alpha_i = (\omega/2\alpha_i)^{1/2} \equiv 1/\mu_i$, is the thermal diffusion coefficient of material i (cm^{-1}), and μ_i is the thermal diffusion length of material i ; $i = b, s, f$. The remaining parameters in Eq. (4) have been defined as

$$r \equiv (1 - i\alpha/2\alpha_s), \quad (5)$$

$$b \equiv (a_b k_b / a_s k_s), \quad (6)$$

$$f \equiv (a_f k_f / a_s k_s). \quad (7)$$

The dc component of the solution in the fluid region can be obtained by making the assumption that the loss of heat at any position above the illuminated area of the y plane to that surrounding fluid is proportional to the temperature at that position.² Then the time independent component of the fluid temperature can be written

$$T_f^{(dc)}(x) = -\frac{A}{\alpha^2} \left\{ \frac{(1 - e^{-\alpha l_1}(1 - F_{sb}\alpha l_2) - \alpha l_1)}{1 + F_{fs}G l_1 + F_{fs}G l_2} \right\} \exp(-Gx), \quad (8)$$

where G is the inverse of the distance above the sample surface at which the fluid temperature has decreased to the $1/e$ of its value at the solid-fluid interface.² The remaining parameters in Eq. (10) have been defined as

$$F_{ij} \equiv k_i/k_j, \quad i, j = b, s, \text{ or } f. \quad (9)$$

The refractive index $n(x, t)$ of the fluid region (I) varies spatially and temporally with the heating of the illuminated fluid column from $(+L/2)$ to $(-L/2)$, Fig. 1. The trajectory of the probe beam is given by the equation of ray propagation in an optically inhomogeneous medium¹¹

$$\frac{d}{ds} \left[n(r, t) \frac{dr}{ds} \right] = \nabla n(r, t), \quad (10)$$

where s is the distance along the ray measured from the entrance point, $y = L/2$, and r is the position vector of a point along s . For small changes of the refractive index from its ambient temperature value n_0 along the illuminated column and for small angles θ in the transverse geometry of Fig. 1, Eq. (10) can be simplified

$$n_0 \frac{\partial^2 x}{\partial y^2} = \frac{\partial}{\partial x} n(x, t). \quad (11)$$

Integrating Eq. (11) once over the deflected beam path s^{12} gives the following expression for the beam deflection θ to a good approximation on the order of $\cos \theta$:

$$\theta(x_0, t) = -\left(L/T_0 \right) \left[\frac{\partial}{\partial x} T_f(x, t) \right]_{x=x_0}, \quad (12)$$

where

$$T_f(x, t) = T_f^{(ac)}(x, t) + T_f^{(dc)}(x), \quad (13)$$

and we defined a material parameter T_0 as follows¹²

$$-\frac{1}{n_0} \frac{\partial n}{\partial T_f} \equiv \frac{1}{T_0}. \quad (14)$$

Equations (4), (8), and (12) indicate that the deflection θ

decreases exponentially with x_0 for both ac and dc components of the fluid temperature. θ tends to zero for beam offset values x_0 such that

$$x_0 \gg \min(G^{-1}, \mu_f).$$

T_0 is a slowly varying function of the wavelength of the exciting radiation. Ignoring the slow variation with wavelength, T_0 will be assumed constant for small fluid temperature departures from the ambient value.

The deflection angle θ consists of ac and dc components, which can be written explicitly using Eqs. (12), (4), and (8):

$$\theta^{(dc)}(x_0) = \left(\frac{LGI_0}{2T_0 k_s \alpha} \right) \left\{ \frac{\alpha l_1 - (1 - e^{-\alpha l_1})(1 - F_{sb}\alpha l_2)}{1 + F_{fs}G l_1 + F_{fs}G l_2} \right\} \times \exp(-Gx_0), \quad (15)$$

and, in the experimentally important thermally thick limit¹⁰

$$\theta^{(ac)}(x_0, t) = \left(\frac{LI_0 \alpha}{2T_0 k_s} \right) \times \text{Re} \left\{ \left[\frac{\sigma_f}{\alpha^2 - \sigma_f^2} \right] \left[\frac{(r-1)}{(f+1)} \right] \right\} \times \exp(-\sigma_f x_0 + i\omega t). \quad (16)$$

The dc contribution to the deflection angle θ which is described by Eq. (15) is a constant deviation of the probe beam path due to the steady-state thermal flux from the solid surface out into the fluid column adjacent to the solid. At offset distances from the solid-fluid interface such that $x_0 \gg G^{-1}$ thermal losses to the fluid column due to heat conduction from the solid will rapidly attenuate the dc component of the θ deflection. Experimentally only relative deflections of the probe beam can be measured accurately by means of position-sensitive diode detectors and lock-in amplifiers.² Therefore, it is the phase and amplitude of the ac component of the TPDS signal which can be measured and analyzed to give optical absorption data. For this reason the dc component of the signal will not be considered further in this work.

The ac contribution to the deflection angle θ can be used for the measurement of absolute optical absorption coefficients in the special case of a thermally thick solid. In this limit, the thickness l_1 of the solid must satisfy the condition¹⁰

$$l_1 \geq l_0 \equiv 2\pi\mu_s. \quad (17)$$

For a typical frequency of 100 Hz, $l_0 = 816.8 \mu\text{m}$ for KCl crystal¹³; 3.65 mm for crystalline Si (Ref. 14); and 167.6 μm for crystalline SiO_2 (Ref. 14). Therefore, condition (17) can be met easily in most experimental situations.

Using a polar coordinate method developed in Ref. 15, the phase of the ac thermally thick TPDS signal can be written as an explicit function of the product $(\alpha\mu_s)$:

$$\psi(x_0, \alpha\mu_s) \approx \alpha_f x_0 - \tan^{-1} [2/(\alpha\mu_s)^2] - \tan^{-1} \left(\frac{\alpha\mu_s}{2 - \alpha\mu_s} \right). \quad (18)$$

The TPDS deflection amplitude is also a function of

$(\alpha\mu_s)$:

$$|\theta^{(ac)}(x_0, \alpha\mu_s)| = \frac{LI_0 (\alpha_s)^{1/2}}{T_0 k_s (\alpha_f)} \times \left[\frac{1/2 (\alpha\mu_s)^2 - (\alpha\mu_s) + 1}{(\alpha\mu_s)^2 + 4/(\alpha\mu_s)^2} \right]^{1/2} \exp(-\alpha_f x_0). \quad (19)$$

Equations (18) and (19) give functional dependences of the phase and amplitude of the transverse PDS signal on the probe beam offset x_0 and on the material parameter product $(\alpha\mu_s)$ between $\alpha\mu_s \gg 1$ (optically opaque limit¹⁰) and $\alpha\mu_s \ll 1$ (optically transparent limit¹⁰). From an experimental viewpoint the ranges of $(\alpha\mu_s)$ values near the TPDS signal saturation ($\alpha\mu_s \gg 1$) and the low optical absorption coefficient region ($\alpha\mu_s \ll 1$) are of considerable spectroscopic interest.¹⁶ Near signal saturation Eqs. (18) and (19) reduce to the following expressions:

$$\psi(x_0, \alpha\mu_s \gg 1) \approx \alpha_f x_0 + \tan^{-1} \left(1 + \frac{2}{\alpha\mu_s} \right), \quad (20)$$

and

$$|\theta^{(ac)}(x_0, \alpha\mu_s \gg 1)| \approx \frac{LI_0 (\alpha_s)^{1/2}}{T_0 k_s (\alpha_f)} \left(\frac{1}{2} - \frac{1}{\alpha\mu_s} \right)^{1/2} \exp(-\alpha_f x_0), \quad (21)$$

where terms higher than $1/\alpha\mu_s$ were neglected. In the low absorption region, Eqs. (18) and (19) become

$$\psi(x_0, \alpha\mu_s \ll 1) \approx \alpha_f x_0 - \tan^{-1} [2/(\alpha\mu_s)^2], \quad (22)$$

and

$$|\theta^{(ac)}(x_0, \alpha\mu_s \ll 1)| \approx \frac{LI_0 (\alpha_s)^{1/2}}{2T_0 k_s (\alpha_f)} (\alpha\mu_s) \exp(-\alpha_f x_0). \quad (23)$$

In Eqs. (22) and (23) terms higher than $(\alpha\mu_s)$ were neglected.

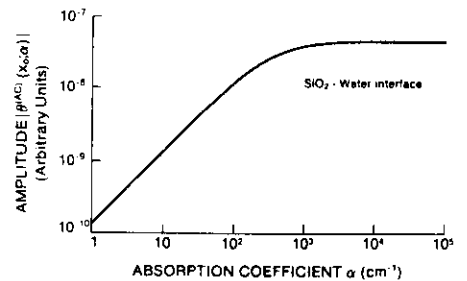


FIG. 2. Log-log plot of the transverse PDS amplitude as a function of the absorption coefficient of the solid. $\nu = 50 \text{ Hz}$, $l_1 = 30 \mu\text{m}$, $b = 1$, $f = 1.13$, $\alpha_s = 1.95 \times 10^{-3} \text{ cm}^2/\text{sec}$, $\sigma_f = 1.465 \times 10^{-3} \text{ cm}^2/\text{sec}$, $x_0 = 5 \times 10^{-2} \text{ cm}$.

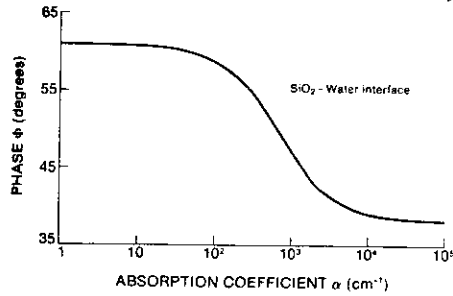


FIG. 3. Semi-log plot of the transverse PDS phase Φ as a function of absorption coefficient of the solid. $\nu = 50$ Hz, $l = 50$ μ m, $b = 1$, $f = 1.13$, $\alpha = 1.95 \times 10^{-3}$ cm²/sec, $\alpha_f = 1.465 \times 10^{-3}$ cm²/sec, $x_0 = 5 \times 10^{-2}$ cm.

DISCUSSION

A. General results of the theory

Full expressions for the TPDS deflection amplitude and phase were obtained from the polar coordinate model of Ref. 15 and evaluated numerically. Figure 2 shows the relative amplitude of the signal displayed as a function of $\ln(\alpha)$. In order to simulate PDS processes in an electrochemical environment, the system chosen was an SiO₂-water interface at a modulation frequency of 50 Hz. Figure 2 indicates that photothermal saturation occurs in the amplitude response at large values of α ($\approx 5 \times 10^3$ cm⁻¹). This range of amplitude saturation values of the absorption coefficient is similar to that for photoacoustic saturation.¹⁵ Figure 3 is a plot of the PDS phase Φ as a function of $\ln(\alpha)$, for the same set of param-

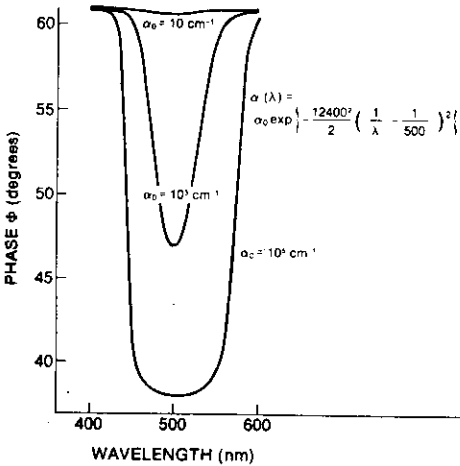


FIG. 4. Phase response in passing through a Gaussian absorption band having different values of α_m . ($\nu = 50$ Hz, $x_0 = 5 \times 10^{-2}$ cm.)

eters as that used in Fig. 2. Figure 3 shows that the phase anticorrelates with the PDS amplitude, in that it decreases with increasing α . Phase saturation occurs for both high and low values of α . The range of α values within which Φ exhibits sensitivity to changes in α lies approximately between 10 and 10^4 cm⁻¹. These features are similar to the behavior of the photoacoustic phase¹⁵ and indicate that Transverse PDS can be successfully used as a spectroscopic technique to measure absorption coefficients in the range $10 \leq \alpha \leq 10^4$ cm⁻¹. The effect of the phase dependence on the absorption coefficient of the solid is shown in Fig. 4, which exhibits the system response to a family of Gaussian lineshape absorption bands centered at 500 nm with linewidths of 0.1 eV. Saturation is seen to occur at large values of α , while Φ becomes essentially independent of the absorption coefficient for $\alpha < 10$ cm⁻¹.

Figure 5 is a plot of TPDS amplitude and phase in the thermally thick limit of Eqs. (18) and (19). $\theta^{(ac)}$ and Φ have been plotted versus the product $(\alpha\mu_s)$ for a chopping frequency of 50 Hz. Figure 5 shows that under thermally thick conditions PDS can be used as a spectroscopic technique for values of $(\alpha\mu_s)$ such that $0.05 \leq \alpha\mu_s \leq 100$. Both phase and amplitude saturate at large values of $(\alpha\mu_s)$ and exhibit similar degrees of sensitivity to changes in this product. Equation (18) shows that absolute phase is a linear function of the probe beam offset x_0 . This behavior has been previously described by Murphy and Aamodt² who also carried out an experimental verification using a 100-nm-thick platinum metal film as the absorbing sample in contact with air and sputtered on a glass substrate. Equations (18) and (19) give a precise definition of the undefined parameters K and θ_0 presented by Murphy and Aamodt in the form²

$$\ln(S_{opt}) = K - (\omega/2\alpha_f)^{1/2} x_0 \quad (24)$$

$$\theta_{opt} = \theta_0 - (\omega/2\alpha_f)^{1/2} x_0 \quad (25)$$

where $S_{opt} \equiv |\theta^{(ac)}|$ and $\theta_{opt} \equiv \psi$ of this work.

A comparison between Eqs. (24), (19), and (25), (18) identifies K and θ_0 as functions of $(\alpha\mu_s)$ in the thermally thick limit. It is, however, difficult to determine whether the experimental data presented in Ref. 2 in conjunction with Eqs. (24) and (25) satisfy the condition (17) because of the double layer structure of the sample-support system. If condition Eq. (17) is not satisfied, then general amplitude and

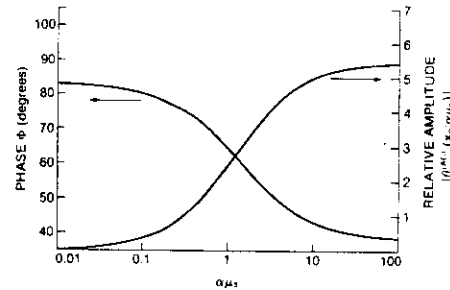


FIG. 5. Comparison between TPDS amplitude and phase as functions of the product $(\alpha\mu_s)$ in the thermally thick limit ($\nu = 50$ Hz, $x_0 = 5 \times 10^{-2}$ cm).

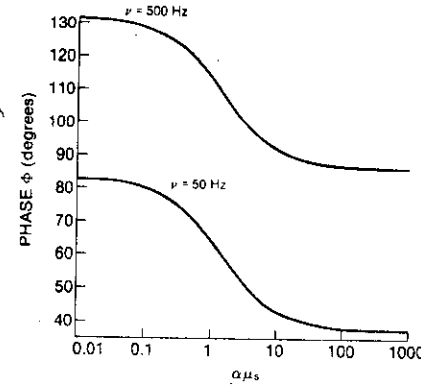


FIG. 6. TPDS deflection phase response as a function of chopping frequency in the thermally thick limit. $x_0 = 5 \times 10^{-2}$ cm, $\alpha_f = \alpha_{water} = 1.465 \times 10^{-3}$ cm²/sec.

phase equations must be used along the lines of those of Ref. 15, in which case the simple functional forms (24) and (25) are not strictly valid.

Figure 6 shows two TPDS phase plots as functions of $\ln(\alpha\mu_s)$ in the thermally thick limit for different chopping frequencies. The linear dependence of ψ on $\alpha_f = (\omega/2\alpha_f)^{1/2}$, Eq. (18), effects a phase shift of ca. 48° between the curves with $\nu = 50$ Hz and $\nu = 500$ Hz. It is clear from Fig. 6 that, unless the probe laser beam is very precisely positioned, it might be difficult to make absolute phase measurements, as Φ is very sensitive to beam position and chopping frequency changes.

B. The absolute absorption coefficient

From the point of view of absolute spectroscopic measurements, the transverse PDS amplitude and phase can be convoluted to yield absolute optical absorption coefficient values in the thermally thick range near signal saturation ($\alpha\mu_s \gg 1$) and for optically transparent materials ($\alpha\mu_s \ll 1$). In an experiment, an unknown instrumental contribution Φ'_0 will be added to the variable phase $\Phi(x_0; \alpha)$ in a manner similar to that described by Teng and Royce,¹⁷ and by Roark *et al.*¹⁸ in their discussion of the photoacoustic phase. Φ'_0 is independent of α , and the measured phase ψ_{exp} is the sum of two terms.

$$\psi_{exp} = \Phi(x_0; \alpha) + \Phi'_0; \quad \Phi_0 = \Phi'_0 + \pi/4, \quad (26)$$

where $\psi(x_0; \alpha)$ is the theoretically determined TPDS phase.

Similarly, the experimental TPDS amplitude $|\theta^{(ac)}|$ will include an instrumental contribution q'_0 , such as amplifier gain, semiconductor detector gain etc. Thus, the measured amplitude $|\theta^{(ac)}|_{exp} = q_{exp}$ will be the product of two terms

$$q_{exp} = q'_0 \cdot |\theta^{(ac)}(x_0; \alpha)|. \quad (27)$$

In the thermally thick limit near signal saturation Eqs. (26) and (27) can be combined with Eqs. (20) and (21) to give

$$\psi_{exp} \approx \Phi_0 + \alpha_f x_0 + \tan^{-1} \left(1 + \frac{2}{\alpha\mu_s} \right), \quad (28a)$$

and

$$q_{exp} \approx q'_0 \exp(-\alpha_f x_0) \sqrt{\frac{1}{2} - \frac{1}{\alpha\mu_s}}, \quad (28b)$$

where $q'_0 = q'_0(LI_0/T_0k_s)\sqrt{\alpha_f/\alpha}$ is also an unknown quantity. Upon inverting Eq. (28a), solving for $(\alpha\mu_s)$ and inserting the resulting expression in Eq. (28b), the following expression is obtained

$$q_{exp} = q'_0 \exp(-\alpha_f x_0) \left[1 - \frac{1}{2} \tan(\psi_{exp} - \Phi_0 - \alpha_f x_0) \right]^{1/2} \quad (29)$$

Equation (29) can be used with the Least-Squares Linear-Taylor Differential-Correction curve technique^{17,19} to determine the optimal values of q'_0 and Φ_0 from a set of experimental data point pairs $[(q_{exp})_i, (\psi_{exp})_i]$. Then the product $(\alpha\mu_s)$ may be calculated from either Eq. (28a) or (28b), once Φ_0 or q'_0 , respectively, are known, provided that μ_s is known.

In the low absorption coefficient region Eqs. (22) and (23) can be combined with Eqs. (26) and (27):

$$\psi_{exp} = \Phi_0 + \alpha_f x_0 - \tan^{-1} [2/(\alpha\mu_s)^{1/2}], \quad (30a)$$

and

$$q_{exp} = q'_0 \exp(-\alpha_f x_0) / (\alpha\mu_s). \quad (30b)$$

Equation (30) can be convoluted in a way similar to the convolution of Eq. (28). The result is

$$q_{exp} = q'_0 \exp(-\alpha_f x_0) \left[\frac{2}{\tan(\Phi_0 + \alpha_f x_0 - \psi_{exp})} \right]^{1/2}. \quad (31)$$

The numerical methods of Ref. 19 can be used with Eq. (31) to optimize the values of q'_0 and Φ_0 . The latter can then be inserted into Eq. (30) to yield absolute values of the product $(\alpha\mu_s)$, and hence of the absorption coefficient α .

CONCLUSIONS

A simplified one-dimensional theory of transverse mode photothermal deflection spectroscopy (TPDS) has been developed for a solid-fluid interface. Explicit expressions have been obtained for the ac and dc components of the signal, in terms of physical and geometrical parameters of the system. The amplitude and phase channels of the experimentally meaningful ac component were identified as carrying information about the optical absorption coefficient of the solid sample. Absorption coefficient ranges within which TPDS can be utilized as a sensitive spectroscopic tool have been defined, and expressions relating the experimental amplitude and phase have been obtained in the thermally thick limit in the regions of signal saturation and low absorption coefficient. These expressions can be used with optimizing fitting techniques to obtain absolute values of the absorption coefficient in the respective regions. Applications of the numerical methods will be discussed in a later publication.

ACKNOWLEDGMENTS

The author wishes to thank Professor B. S. H. Royce for many helpful suggestions and comments on the manuscript.

The kind assistance of S. Ho in the numerical calculations is acknowledged. The author gratefully acknowledges the financial support of the Natural Sciences and Engineering Research Council of Canada which made this publication possible.

- ¹A. C. Boccara, D. Fournier, and J. Badoz, *Appl. Phys. Lett.* **36**, 130 (1980).
- ²J. C. Murphy and L. C. Aamodt, *J. Appl. Phys.* **51**, 4580 (1980).
- ³W. D. Jackson, N. M. Aizer, A. C. Boccara, and D. Fournier, *Appl. Opt.* **20**, 1333 (1981).
- ⁴B. S. H. Royce, F. Sanchez-Sinencia, R. Goldstein, R. Muratore, R. Williams, and W. M. Yim, *Bull. Am. Phys. Soc.* **27**, 243 (1982).
- ⁵L. C. Aamodt and J. C. Murphy, *J. Appl. Phys.* **49**, 3036 (1978).
- ⁶L. C. Aamodt, J. C. Murphy, and J. G. Parker, *J. Appl. Phys.* **48**, 927 (1977).
- ⁷F. A. McDonald and G. C. Wetsel, *J. Appl. Phys.* **49**, 2313 (1978).

- ⁸F. A. McDonald, *Appl. Opt.* **18**, 1363 (1979).
- ⁹A. Mandelis, Ph.D. thesis, Princeton University, 1980.
- ¹⁰A. Rosencwaig and A. Gersho, *J. Appl. Phys.* **47**, 64 (1976).
- ¹¹M. Born and E. Wolf, in *Principles of Optics*, 3rd ed. (Pergamon, New York, 1965), Vol. 4, p. 1562.
- ¹²L. C. Aamodt and J. C. Murphy, *J. Appl. Phys.* **52**, 4903 (1981).
- ¹³A. Rosencwaig, in *Advances in Electronics and Electron Physics*, edited by L. Morton (Academic, New York, 1978), Vol. 46, pp. 207-311.
- ¹⁴Y. S. Touloukian, R. W. Powell, C. Y. Ho, and M. C. Nicolson, in *Thermal Diffusivity* (IFI/Plenum, New York 1973).
- ¹⁵A. Mandelis, Y. C. Teng, and B. S. H. Royce, *J. Appl. Phys.* **50**, 7138 (1979).
- ¹⁶B. S. H. Royce (private communication).
- ¹⁷Y. C. Teng and B. S. H. Royce, *J. Opt. Soc. Am.* **70**, 557 (1980).
- ¹⁸J. C. Roark, R. A. Palmer, and J. S. Hutchison, *Chem. Phys. Lett.* **60**, 112 (1978).
- ¹⁹T. R. McCalla, in *Introduction to Numerical Methods and FORTRAN Programming* (Wiley, New York, 1967), p. 255.

Photoacoustic Spectroscopy and Related Techniques Applied to Biological Materials

Thomas A. Moore

Department of Chemistry, Arizona State University, Tempe, Arizona 85287

1. Introduction	188
2. Description of the Photoacoustic Effect; Important Aspects for Biological Experiments	188
2.1. Photoacoustic Spectroscopy	188
2.2. Photoacoustically Detected Absorption Spectrum	190
2.3. Thermal Diffusion Length and Photoacoustic Saturation	191
2.4. Amplitude and Phase of the Photoacoustic Signal	192
2.4.1. Stratified Chromophores. Model Studies	193
2.4.2. Examples of Naturally Occurring Stratified Chromophores	197
2.5. Photoacoustically Detected Relaxation of Excited States; The Measurement of Photophysical Parameters	198
2.5.1. Quantum Yields, Energies, and Lifetimes of Metastable States	198
2.5.2. Fluorescence Quantum Yields	201
2.5.3. Photochemical Energy Conversion	201
2.5.4. Flash Calorimetry	202
2.6. Experimental Techniques Important in Photoacoustic Studies of Biological Systems	203
2.6.1. Two-Beam Experiments	203
2.6.2. Masking Unwanted Signals	203
2.6.3. Low Temperature Experiments	204
2.6.4. Photoacoustically Detected Circular and Linear Dichroism	204
2.6.5. Photothermal Radiometry (PTR)	205
2.6.6. Photothermal Deflection Techniques (Mirage Effect)	205
2.6.7. Transform Techniques in Photoacoustic Spectroscopy; Infrared Photoacoustic Spectroscopy	206
3. Photoacoustic Studies of Chlorophyll-Based Photosynthesis	207
3.1. Chloroplasts, Reaction Centers, and Leaves	207
3.2. Algae and Lichens	209
4. Photoacoustic Studies of <i>H. halobium</i> Photocycle	212
5. Photoacoustic Studies of Skin Tissue	213
6. Conclusion	214
7. Experimental Notes	215

7.1. Microphone	215
7.2. Light Scrambler	215
7.3. Bifurcated Light Guide	216
7.4. Stirred Arc	216
7.5. Photoacoustic Cell Signal	216
8. References	217

1. INTRODUCTION

The absorption of light by living organisms is important both as a probe of biochemical processes at the molecular level, and as the stimulus for myriad photobiological processes. Typically, light absorption may be characterized by measuring either the transmission or the reflectance spectrum; however, most biological systems *in situ* are not amenable to these measurements due to opacity, scattering, poorly defined or heterogeneous surface properties, etc. Thus, it is of interest to have a technique for measuring the absorption of light that is less constrained by the nature of the material under study. Photoacoustic spectroscopy (PAS) clearly meets this requirement while offering new information that arises uniquely from the combination of spectroscopic and calorimetric phenomena. In certain respects PAS is a qualitative spectroscopic technique, the spectra (except in special cases) are only similar to conventional absorption spectra; also for complex biological samples there is no general method of extracting extinction coefficients or concentrations from the observed signal. On the other hand, photophysical parameters such as quantum yields, lifetimes, and energies, characterizing the various excited states and relaxation pathways of photobiological systems *in situ*, can sometimes be measured by PAS. In considering PAS, it is perhaps useful to keep in mind that just as the fluorescence excitation spectrum is the action spectrum for fluorescence, the photoacoustic (PA) spectrum is the action spectrum for the production of heat.

Several general reviews have recently appeared (Rosencwaig, 1978; Cahen *et al.*, 1980; Somoano, 1978; Balasubramanian and Rao, 1981). The present review focuses on applications, examples, and techniques germane to biological systems.

2. DESCRIPTION OF THE PHOTOACOUSTIC EFFECT; IMPORTANT ASPECTS FOR BIOLOGICAL EXPERIMENTS

2.1. Photoacoustic Spectroscopy

A number of quantitative treatments of PAS have appeared, and an essential consensus has emerged regarding the origin of the phenomenon

(Rosencwaig and Gersho, 1976; Murphy and Aamodt, 1977; Aamodt *et al.*, 1977; Bennett and Forman, 1977; McDonald and Wetsel, 1978; McDonald, 1980). Consider Fig. 1 and assume a solid or liquid sample in an enclosed volume allowing a small air-space containing a coupling gas (air) above the sample. Light from a monochromator, which can be scanned, is chopped and is incident on the sample surface exposed to the air-space. A fraction of the light absorbed by a molecule at a point in the sample is converted to heat, which then diffuses, *via* thermal conduction, to the sample surface. At the surface, a thin boundary layer of gas is slightly heated, expands, and creates a pressure wave (sound wave) that fills the enclosed volume and is sensed by a transducer such as a microphone. This sequence of events, a thermal wave in the sample driving thermal expansion in the thin layer of gas that in turn drives a pressure wave in the cell chamber, accounts for the PA response in most cases.

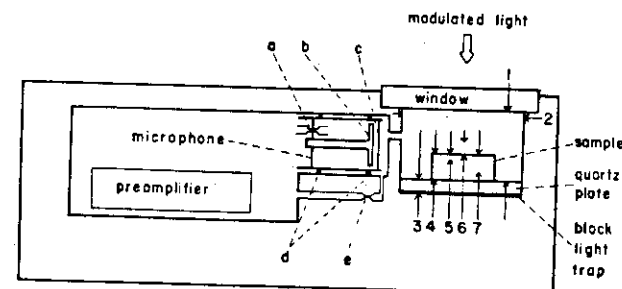


Fig. 1. Schematic diagram of a typical PAS cell including sample chamber, microphone, and preamplifier. The sample chamber is larger than scale. The numbers refer to the various lengths that determine the photoacoustic response of the sample and are defined as follows: (1), (2) sample chamber dimensions, (3) thickness of sample backing or transparent quartz plate covering a black light trap, (4) sample thickness, (5) one thermal diffusion length in the sample, μ_s , (6) one thermal diffusion length in the coupling gas, μ_g , (7) optical absorption length, $\beta_{\text{optical}}^{-1}$, where $\beta_{\text{optical}} = (2.303) (\text{optical density per cm})$. The letters refer to the principal parts of a condenser microphone installed in a PA cell: (a) controlled equalization vent for the microphone; this vent determines the low frequency limit of the microphone alone, (b) electrode or plate behind the diaphragm; the change in capacitance as the diaphragm is deflected between the diaphragm and this plate is the basis for signal generation by a microphone, (c) microphone diaphragm and this plate is the basis for signal generation around the microphone, (d) sealing rings preventing pressure leakage with the large chamber containing the microphone and preamplifier; this vent determines the low frequency limit of the PA cell. The cell must also have a means of changing the sample such as a removable window and electrical connectors for the signal and preamplifier power supply.

However, under certain conditions one may detect the much smaller acoustic wave produced in the sample along with the thermal disturbance upon relaxation of the excited state (McDonald and Wetsel, 1978). This acoustic wave propagates in the sample as sound (not according to thermal conduction), and is conveniently sensed by a piezo-electric detector attached to the sample itself. In the photoacoustic experiments discussed herein (involving solid or semisolid samples, a coupling gas, and microphone detection), this acoustic wave in the sample makes only a small contribution to the signal.

The periodic fluctuations in the coupling gas, driven at the chopping frequency of the incident light, produce a periodic alternating current (AC) signal at the microphone output, which is amplified and converted to a direct current (DC) signal by a lock-in amplifier. With microphone detection, the photoacoustic response is intrinsically AC; the microphone has an equalization vent across the diaphragm (Fig. 1a) that determines its limiting low frequency response. In other words, the microphone does not produce a signal at constant (DC) pressure. As can be seen from Fig. 1, the limiting low frequency response of the PA cell is determined by the equalization vent (e).

2.2. Photoacoustically Detected Absorption Spectrum

Provided PA saturation [in Fig. 1 the length (7) \gg (5), Section 2.3] is avoided, scanning the monochromator produces a spectrum with the signal (S) at each wavelength given by

$$S \propto \Phi_A \beta_{\text{optical}}(\lambda) P(\lambda) R(\omega) \quad (1)$$

where $R(\omega)$ describes the photoacoustic response of the sample and cell. $R(\omega)$ is a complex function of modulation frequency (ω) and, as indicated in Fig. 1, the sample thickness and thermal diffusion lengths in the sample and surrounding gas (Section 2.3). $P(\lambda)$ is the optical power as a function of wavelength of the incident, modulated light beam; $\beta_{\text{optical}}(\lambda)$ is 2.303 times the optical density per cm as a function of wavelength, and Φ_A is the fraction of the absorbed light converted to heat (Murphy and Aamodt, 1977; Rosencwaig and Gersho, 1976). The function $S[P(\lambda)]^{-1}$ is proportional to β_{optical} , and thus to the absorption spectrum. $P(\lambda)$ is obtained by measuring the spectrum of a black body absorber, usually soot or carbon powder. The general intent of detailed theories is the evaluation of R so that S can be quantitatively related to optical and calorimetric parameters of the sample. In certain cases, especially liquid samples,

Both bad in the IR
Use GRAPHITE POWDER
TO AVOID HYDROCARBON
FEATURES.

β_{optical} can be determined quantitatively (Poulet *et al.*, 1980; Malkin and Cahen, 1981). Work in this area is clearly important to future photobiological applications.

2.3. Thermal Diffusion Length and Photoacoustic Saturation

The modulation frequency of the incident light defines a key parameter, the thermal diffusion length (μ). μ is one of the lengths in R (Eq. 1) and is

$$\mu = \left(\frac{2\alpha}{\omega} \right)^{1/2} \quad (2)$$

where α is the thermal diffusivity ($\text{cm}^2 \text{s}^{-1}$), and ω ($\omega = 2\pi f$) is the modulation frequency. There is a thermal diffusion length in both the gas (μ_g) and in the sample (μ_s). μ_s defines the boundary layer of gas that is slightly heated upon diffusion of heat to the sample surface and for air has a value of 0.6 mm at a chopping frequency of 20 Hz. μ_s may be thought of as the distance that heat travels in the sample during the period of the modulation. Each successive cycle damps the fluctuation induced by its predecessor, thus limiting the depth from which a PA signal can be obtained. μ_s defines the optical path length in PAS experiments, and ranges from $\sim 4 \mu\text{m}$ (2 kHz modulation) to $\sim 170 \mu\text{m}$ (1 Hz modulation) for a thermal diffusivity of $0.001 \text{ cm}^2 \text{s}^{-1}$, a value characteristic of biological materials. Quantitatively, μ_s is the distance over which the thermal wave in the sample is damped to e^{-1} of its original magnitude.

Photoacoustic saturation (McClelland and Kniseley, 1976) occurs when $(\beta_{\text{optical}})^{-1} \leq \mu_s$, that is, a significant fraction of the incident light is absorbed within one μ_s . In this case, the signal amplitude no longer depends upon β_{optical} , and the spectrum becomes the power spectrum $P(\lambda)$ mentioned above. The onset of saturation is shown by peak flattening, since division by $P(\lambda)$ (a carbon soot sample is completely saturated at all wavelengths) yields a constant. It should be noted, however, that in certain cases spectra may be obtained from phase measurements even from very concentrated $[(\beta_{\text{optical}})^{-1} \leq \mu_s]$ samples (Poulet *et al.*, 1980). Also, several techniques have been presented for "diluting" concentrated (pure solid) samples so that saturation is avoided (Fuchsman and Silversmith, 1979; Lin and Dudek, 1979). In order to avoid complicated three dimensional effects (Quimby and Yen, 1979; McDonald, 1980, 1981) it is important that the edge of the sample not be illuminated, i.e., the exciting light should not be closer than several times μ_s to the edge of the sample.

BS

Saturation occurs
under very intense
conditions of light
also.

There should also be a space of several times μ_s between the illuminated portion of the sample and any cell wall or the cell window.

2.4. Amplitude and Phase of the Photoacoustic Signal

As mentioned above, the signal from the microphone is AC, and hence carries in addition to frequency two kinds of information, amplitude and phase (Mandelis *et al.*, 1979; Poulet *et al.*, 1980; Adams and Kirkbright, 1977). In general, PA spectra are plots of signal amplitude vs. wavelength. The amplitude of the PA signal is strongly dependent on a number of factors, including characteristics of the sample such as surface area, the presence and thickness of a waxy coat, and the reflectivity and opaqueness of the sample. Since PAS is a single beam technique, the major factors affecting signal amplitude are instrumental factors. Signal amplitude may be related to the concentration of the absorber by a calibration curve, provided sample preparation and instrumental factors are carefully controlled (Castleden *et al.*, 1979). Also, fluorescence quantum yields may be measured by a careful comparison of signal amplitudes between a nonfluorescent reference sample and the fluorescent unknown sample (Section 2.5.2). However, considerable information, especially in the case of *in situ* biological systems, is contained in the phase of the PA signal. Furthermore, except in the case of a two phase lock-in analyzer, one must, in fact, select a phase in order to record a spectrum.

The measured phase angle of the signal (θ_m) is defined with respect to the modulated incident light. Factors affecting θ_m include: (1) processes intrinsic to the PA phenomena such as thermal diffusion and the production of the pressure wave, and herein designated θ , (2) processes such as the relaxation of excited states with lifetimes of the order of the modulation period (ϕ), and (3) strictly experimental processes. Fortunately, it is often possible, in at least a semiquantitative way, to separate these contributions so that photobiologically significant information can be extracted from the phase of the signal.

Experimental contributions include such things as the phase shift due to the microphone, which is especially large and frequency dependent at low frequencies, and phase shifts in the signal processing electronics. It must be remembered that the major contribution to the absolute phase of the signal is the angular relationship (around the light chopping wheel) between the incident light beam and the electro-optic pick-up for the lock-in reference. Except in cells designed to operate at resonance, the dimensions of the enclosed volume [(1), (2) in Fig. 1] are usually much less than the wavelength of sound at usual frequencies so that acoustic resonance and concomitant phase shifts are not observed.

Don't need to be differential
PAS has been done:
Two samples in chamber.

Pressure pickup effect
are more important
as a rule.

As β changes
E must change if
 μ_s is constant.
Both amplitude and
phase change some small
with μ_s .
The standard is wavelength.

Better to change
(w) and so μ_s to
obtain a depth
profile.

For a homogeneous, thermally thick [in Fig. 1, (4) \gg (5)] sample the phase θ of the PA signal is given by (Poulet *et al.*, 1980).

$$\tan \theta = \beta_{\text{optical}} \mu_s + 1 \quad (3)$$

From this expression it is clear that for cases where $\beta_{\text{optical}} \mu_s \ll 1$ there is no appreciable phase shift as a function of β_{optical} , i.e., over the absorption band. In the case where $\beta_{\text{optical}} \mu_s \gg 0.1$, this equation may be used to determine β_{optical} , and thus the absorption spectrum quantitatively (Poulet *et al.*, 1980).

If one considers a biological sample in which different chromophores are present at different depths from the sample surface, the phase and modulation frequency dependence of the signal are quantitatively complicated (Fernelius, 1980). However, certain information about this chromophore distribution at depths ranging from $\sim 1 \mu\text{m}$ to $\sim 200 \mu\text{m}$ from the sample surface can be obtained from the frequency and phase of the PA signal. The phase of the signal is completely specified by the in-phase and 90° out-of-phase (quadrature) components. It is reasonable to think of one of these components as biased towards response from the upper half of μ_s , and the other component as biased towards response from the lower half of μ_s . Thus, the signal from the sample "interior" is phase shifted by the transit time for heat diffusing to the surface. In this way the overall depth of analysis is controlled by frequency (ω) through μ_s while the upper or lower parts of μ_s can be selected by the appropriate choice of phase. This approach is sometimes referred to as depth profiling, and has been described in detail by Adams and Kirkbright (1977).

2.4.1. Stratified Chromophores, Model Studies

An example of the use of phase information for a layered sample is presented in Fig. 2. A plastic film approximately $25 \mu\text{m}$ thick was marked on the upper surface with a blue dye and on the lower surface with a red dye. The lower surface was sealed with a light film of grease to the aluminum surface of the sample holder. The spectrum was scanned using a chopping frequency such that $\mu_s > 20 \mu\text{m}$. Referring to the inset, it can be seen that two pieces of information completely characterize the response of the sample to the modulated light: either the resultant $A(\lambda)$ and the angle $\theta_m(\lambda)$ or $A \cos \theta_m$ and $A \sin \theta_m$ may be recorded (the use of a two-phase lock-in analyzer and a two channel analog to digital converter allows simultaneous recording of both spectra during a single scan). Once these two spectra are obtained, there is no additional PA information available at the selected chopping frequency. From the phasor diagram it is clear, e.g., that measuring along the 0° axis will yield a signal that is

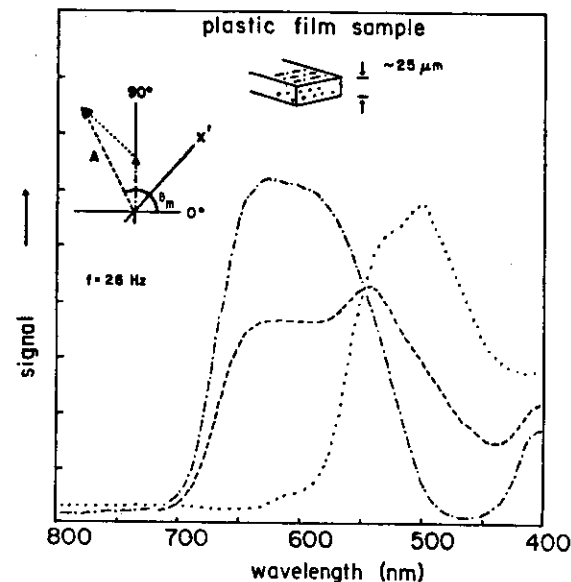


Fig. 2. Two-layer chromophore model. Plastic film, approximately 25 μm thick, with a blue dye (—) on the upper surface and a red dye (·····) on the lower surface, optical density at $\lambda_{\text{max}} \sim 0.5$ for each. The dyes did not diffuse significantly into the plastic, and the lower surface was sealed to the aluminum sample holder with a light film of silicon grease. The composite spectrum (-----) was recorded at a phase setting so that both dyes contributed to the signal. A mixed spectrum was also recorded with a two phase lock-in amplifier set in the phase independent, vector magnitude, or resultant mode. In the inset phasor diagram the phase of the signal from each dye is indicated by a vector of the appropriate symbol. θ_m is the measured phase angle and is with respect to the signal from the electro-optic pickup for the reference channel of the lock-in amplifier. Application of the phasor diagram is fully described in the text. The amplitudes of the spectra cannot be compared to each other.

the projection of the lower surface signal on the 0° axis, but contains no component from the upper surface. Likewise, measurement along the X' axis will be pure upper surface signal uncontaminated by signal from the lower surface. It is important to note that the 0° axis is not in general orthogonal to X' . It is very convenient to have a computer program rotate

the axis and calculate the two spectra at any desired phase setting (Bettleridge *et al.*, 1979). As can be seen from comparing Fig. 2 with Fig. 3, the spectra of each dye alone, an essentially uncontaminated spectrum of each dye can be extracted from the data (O'Hara *et al.*, 1981). Similar model studies have shown excellent agreement between the experimental phase shifts and those calculated from theory (Morita, 1981; Helander *et al.*, 1981).

This resolution of depth is unique to PAS; both transmission and reflectance techniques can only provide the sum of these absorbances.

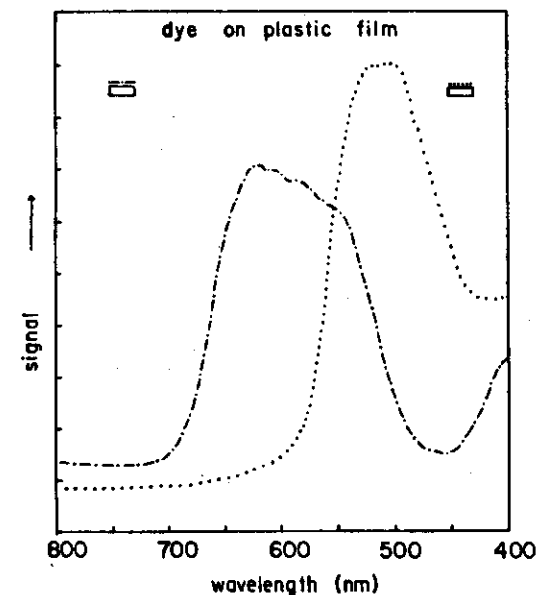


Fig. 3. PA spectra of red (·····) and blue (—) dyes on individual films recorded separately. Experimental conditions are similar to those in Fig. 2. The two phase lock-in amplifier was in the resultant mode. Notice that the spectrum of the blue dye (surface) in Fig. 2 matches exactly the spectrum shown here, whereas the spectrum of the red dye in Fig. 2 is slightly distorted by the filter effect (shading by absorption) of the long wavelength side of the blue dye.

One must, however, proceed with great caution when making measurements on unknowns. The key problem is to determine which phase angle yields the true spectrum. By examining a series of models similar to the one just described, and from a quantitative treatment of the phasor diagram, it is possible to develop certain guidelines for the investigation of unknowns.

(i) At high modulation frequency (1 kHz), and thus short μ_s , one can restrict the response to within a few μm of the surface. Then, at a phase setting shown from models to be surface sensitive at this frequency, one can be confident of recording a spectrum from approximately the first μm of sample. If the spectrum quadrature to the surface is the same as the surface spectrum, then it is likely that there is no layering of chromophores over this μ_s .

(ii) If, at lower modulation frequency and with the phase selected for interior sensitivity, spectra are recorded which differ from the spectra in (i), then it is likely that a different chromophore has been located. From the in-phase and quadrature spectra at this modulation frequency the spectra are calculated as a function of the rotation of the axis. An axis of rotation is searched for that nulls a known spectral band from the outermost chromophore. The spectrum at this rotation will be that of the interior relatively uncontaminated by the more surface chromophore.

(iii) Similarly, a rotation is searched for that nulls a specific band of the interior chromophore. The spectrum at this rotation will be relatively uncontaminated by the interior chromophore. This procedure is facile when one of the chromophores absorbs in a region where the other does not. The correct rotation yields a flat baseline in the spectral region where only the interior chromophore absorbs.

(iv) It is, in principle, possible to make use of specific stains to mark known regions of cells or organelles. For example, a cell wall stain could be used to mark the cell wall of an algae, thus allowing one to determine the correct phase for observing chromophores located in the cell wall.

It is important to realize that the spectral shapes of underlying chromophores may be distorted by the filter effect of the chromophores nearest the surface. In special cases it may be possible to correct for the filter effect by calculating the light attenuation from known absorption bands. Furthermore, referring to Eq. 3, in cases where $\beta_{\text{optical}} \mu_s \gg 0.1$ at the absorption maximum, then there will be a phase shift between the signal from the band maxima and the signal from other regions of the band or other bands of the same chromophore with lower β_{optical} . In these cases spurious spectra arise upon rotation of the axis. Our model studies have clearly shown that, subject to $\beta_{\text{optical}} \mu_s \leq 0.1$, rotation of the axis results

Overlapping bands
Do not chromophore
is measured

in uniform reduction of the spectrum to the baseline for samples having a nonlayered distribution of chromophores.

2.4.2. Examples of Naturally Occurring Stratified Chromophores

An early example of the resolution of a naturally occurring stratified system is the work by Adams *et al.* (1976), in which light absorption by the waxy cuticular layer of a green leaf was clearly resolved from the light absorbed by the chloroplasts. The chlorophyll-like spectrum was recorded at a phase setting optimizing the signal at 650 nm, and the spectrum rich in cuticular absorption recorded quadrature to this phase. Figure 4 presents the spectrum of an oat seedling taken in our spectrometer; spectra of a variety of leaf types have clearly reproduced the results of

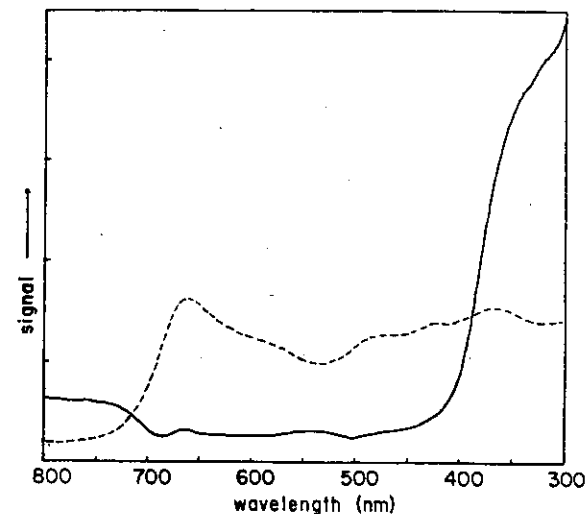


Fig. 4. PA spectrum of an oat seedling after axis rotation to null the 500–650 nm signal from the chloroplasts (—), and to null the cuticular signal in the near-UV region (---). The optical bandpass was 10 nm, the modulation frequency was 12 Hz, and the lock-in amplifier output bandwidth was 0.1 Hz.

Adams *et al.* (1976), and illustrate the use of (i)–(iii) above in selecting modulation frequencies and finding the best phase for a particular spectrum.

We have measured the PA spectrum of lobster shell at different modulation frequencies and phases, and have found an unexpected arrangement of protein–pigment complexes (carotenoproteins) in the pigmented layer of the shell (Mackenthun *et al.*, 1979). The carotenoproteins having the longest wavelength absorption maxima were found in the interior-most region of the pigmented layer. This anisotropic distribution of carotenoproteins as a function of depth is destroyed by denaturing the protein, clearly indicating that tertiary and quaternary structural features are involved in the pigment–protein interaction.

In Section 3.2, a study of pigment stratification in lichens is presented.

2.5. Photoacoustically Detected Relaxation of Excited States; The Measurement of Photophysical Parameters

2.5.1. Quantum Yields, Energies, and Lifetimes of Metastable States

A unique feature of the PA effect is that absolute values of photophysical parameters such as quantum yields, energies, and lifetimes of long-lived (from submillisecond to subsecond) metastable excited states can be determined from relative phase shift measurements (Moore, *et al.*, 1982). Consider the Jablonski diagram (Fig. 5) in which the metastable state in this case is the lowest excited triplet state. It can be seen that the relaxation rate from $T_1 \rightarrow S_0$ will be characteristic of the triplet lifetime, whereas the relaxation processes $S_1 \rightarrow S_0$ and $S_1 \rightarrow T_1$ will be much faster. Thus, at an appropriate modulation frequency the heat produced from $T_1 \rightarrow S_0$ relaxation ($h_{\text{slow}}(\omega)$) will be phase shifted from that produced by $S_1 \rightarrow S_0$ and $S_1 \rightarrow T_1$ processes (h_{fast}). Quantitatively, for sinusoidal modulation

$$h_{\text{slow}}(\omega) = \frac{k_{\text{isc}}}{k_s} \frac{\epsilon_T}{1 - i\omega\tau} \quad (4)$$

and

$$h_{\text{fast}} = \Delta\epsilon_1 + \frac{k_r}{k_s} \Delta\epsilon_0 + \frac{k_{nr}}{k_s} \epsilon_s + \frac{k_{\text{isc}}}{k_s} (\epsilon_s - \epsilon_T) \quad (5)$$

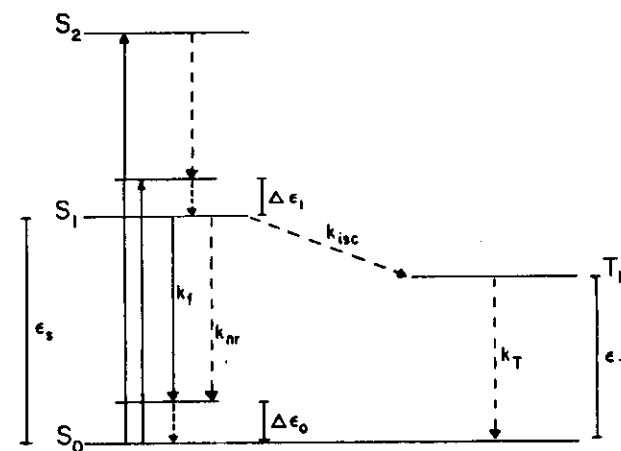


Fig. 5. Jablonski diagram. The vibrational levels in the ground (S_0) and first excited singlet (S_1) state are replaced with a single level corresponding in the case of absorption to the excitation wavelength, and in the case of emission to the fluorescence maximum, ϵ_s , $\Delta\epsilon_1$, $\Delta\epsilon_0$ and ϵ_T are the energy differences between the states indicated by vertical bars. Radiative (—) and non-radiative (---) processes are indicated, phosphorescence is ignored under the conditions of this experiment. k_r , k_{nr} , k_{isc} and k_T are the radiative, nonradiative, intersystem crossing and triplet decay rate constants, respectively.

where τ is the triplet lifetime and k_s is the total decay rate of S_1 . The complex amplitude $P(\omega)$ of the resulting PA signal has the form

$$P(\omega) = R(\omega)[h_{\text{fast}}(\omega) + h_{\text{slow}}(\omega)] \quad (6)$$

$$= P_{\text{fast}}(\omega) + P_{\text{slow}}(\omega)$$

where $R(\omega)$ is the response function describing the diffusion of heat in the sample and its coupling to the gas. Although $R(\omega)$ is not known explicitly, it is the same function for both fast and slow processes. This fact allows one to design experiments to measure the relative phase shift. The phase lag ϕ between the slow and fast components is determined by h_{slow} and h_{fast} , and is given by $\tan \phi = \omega\tau$, and the phase θ , between $P(\omega)$ and

P_{fast} is given by

$$\tan \theta_r = \frac{a\omega\tau}{a + b(1 + \omega^2\tau^2)} \quad (7)$$

where

$$a = \frac{k_{\text{isc}}}{k_s} \epsilon_T \quad (8)$$

and

$$b = \Delta\epsilon_1 + \frac{k_r}{k_s} \Delta\epsilon_0 + \frac{k_{nr}}{k_s} \epsilon_s + \frac{k_{\text{isc}}}{k_s} (\epsilon_s - \epsilon_T) \quad (9)$$

This function depends only on $\omega\tau$ and the parameters of the energy level scheme; from a plot of $\tan \theta_r$ vs ω values of a and b can be determined. From the value of the parameter a , one can determine either the energy of the metastable state or the quantum yield of its formation. In order to measure θ_r , it is necessary to prepare a reference sample in which there is no slow decay component. This can be accomplished by preparing a reference sample using an absorber such as β -carotene in which the triplet state is not populated, and therefore all relaxation is fast. It is extremely important that the optical, thermal, and geometric properties of the reference and sample be exactly matched in order that $R(\omega)$ is the same for each. Alternatively, the reference could be the sample in which the lifetime of the metastable state is markedly shortened by quenching processes. The necessity of a matched reference sample probably limits this method to solutions of biomolecules or subcellular preparations in either liquid solvents or plastics. It would be difficult to prepare the proper reference for chromophores *in situ* (however, see Section 2.5.3 for a reference system based on the PA signal in the presence of a strong continuous light).

Fortunately, it is possible to carry out this experiment in a way in which the sample itself acts as the reference. From the Jablonski diagram (Fig. 5) it can be seen that excitation to S_2 results in fast decay to S_1 followed by the photophysical processes, whereas excitation to S_1 results directly in these photophysical processes. In this way the fast relaxation from $S_2 \rightarrow S_1$ provides the reference fast heat. Quimby and Yen (1980) have used essentially this method to measure the quantum yield of fluorescence in ruby and report an accuracy of 0.90 ± 0.05 . It is expected that these experiments can be carried out *in situ* in some photobiological

systems, thus making possible the measurement of photophysical parameters of intact chromophore systems in their native environment.

2.5.2. Fluorescence Quantum Yields

By measuring the ratio of the signal amplitude of a fluorescent sample to that of a nonfluorescent reference material, the energy yield of radiationless relaxation γ can be determined. Φ_f is related to γ by

$$\Phi_f = \frac{\lambda_e}{\lambda_f} (1 - \gamma) \quad (10)$$

where λ_e is the excitation wavelength and λ_f is the mean fluorescence wavelength (Callis, 1976). These measurements rely on the fact that $R(\omega)$ is the same for sample and reference materials. This can be assured in solution studies since β_{optical} can be matched and the thermal, surface, and geometric properties are those of the solvent. Adams *et al.* (1977) have measured Φ_f for a series of dyes in solution by using the fully quenched dye as the reference.

Adams *et al.* (1980, 1981) have also devised a way to measure Φ_f of solid samples by using carbon soot as a reference, even though $R(\omega)$ is not the same for sample and reference. In this case Φ_f can be extracted from a plot of the ratio of the sample signal amplitude to the reference signal amplitude vs wavelength of exciting light over a range of wavelengths where the sample is photoacoustically saturated. This technique may well be the most accurate method for obtaining Φ_f of solids.

2.5.3. Photochemical Energy Conversion

Callis (1976) has pointed out that the heat produced (Q) in a photochemical process excited by N photons of energy E_{in} is

$$dQ = N(E_{\text{in}} - Q_p E_p) \quad (11)$$

where Q_p is the quantum yield of stable product with energy E_p above the ground state. Malkin and Cahen (1979) have developed a general theory for the photoacoustically detected enthalpy changes in a photoactive sample. The relative PA signal of a photoactive sample is given by

$$S(\omega, \lambda) = F_{B(\lambda)} G(\omega) \left[1 - \frac{\sum_i \Phi_p \Delta E_{p_{\text{rel}}, \omega}}{N h \nu} \right] \quad (12)$$

where $S(\omega, \lambda)$ is the PA signal compared to a photoacoustically saturated reference with no photochemical activity; $F_{BA}(\lambda)$ is the fraction of the incident radiation ($Nh\nu$) absorbed in the distance μ_z ; $G(\omega)$ is an instrumental factor and Φ_p and ΔE_p are the quantum yield and stored enthalpy of product p of photochemical reaction i . ΔE_p is a function of modulation frequency since in order to be observed, the product (in many cases intermediate) must have a lifetime of the order of ω^{-1} . By analyzing S as a function of ω , different intermediates are observed; the fastest ones at high frequency and the slowest ones at very low frequency. In favorable cases qualitative rate constants may be assigned. In addition to measuring energies of the intermediates above (or below) the reactant ground state this equation can be used to extract information about the wavelength dependency of photochemical processes. As described below (Section 4) the photocycle of *Halobacterium halobium* has been extensively studied using this approach.

2.5.4. Flash Calorimetry

Callis *et al.* (1972) have devised a strategy for directly determining the enthalpy changes of photophysical and photochemical processes by measuring the volume change of a solution with a capacitor microphone following flash excitation. This technique differs from the photoacoustic measurements discussed herein in two important ways. First, the measurement is in the time domain rather than the frequency domain, and second, the volume change of the liquid solution is measured by the deflection of the microphone diaphragm in contact with the solution (there is no air-space in the cell). An advantage of the time domain measurement for experiments on complicated photocyclic systems such as photosynthesis and *Halobacterium* photoconversion is that the system is allowed to return to a well-defined initial state between excitation flashes. Although volume changes for a given amount of heat production are much smaller in liquid than in gas, the time domain measurements are readily signal averaged and volume changes of $3 \times 10^{-10} \text{ cm}^3$ and enthalpy changes of 1 μcal in the interval of 100 μs to 1 s after the flash were reported.

Volume changes after the flash can arise from two sources (Arata and Parson, 1981, 1982). Expansion or contraction of the solution due to heating or cooling and, in the case of photochemical processes, a volume difference between reactants and products. The total volume change after the flash is given by

$$V = (nE_i - NE_p) \left(\frac{\zeta}{\rho C_p} \right) + N \Delta V, \quad (13)$$

where n is the number of systems excited by the flash; E_i is the average energy of the photons; N is the number of systems reaching product; E_p is the energy of the product relative to the ground state (defined as zero); ζ is the thermal expansion coefficient; ρ is the density; C_p is the heat capacity per g of solution, and ΔV is the difference in volume between reactants and products. By using the appropriate reference solutions and by making measurements at two temperatures, it is possible to separate the contributions to ΔV and to find the enthalpy changes of the photochemical process. Flash calorimetry has been used effectively in determining triplet state quantum yields in molecular systems (Callis, 1976), in studies of enthalpy changes and proton translocation in photosynthetic systems (Arata and Parson, 1981, 1982; Callis *et al.*, 1972), and in studies of the *H. halobium* photocycle (Ort and Parson, 1978, 1979a,b).

2.6. Experimental Techniques Important in Photoacoustic Studies of Biological Systems

2.6.1. Two-Beam Experiments

In spectroscopic studies of photobiological systems undergoing photocyclic or photochromic reactions, it is often desirable to apply two beams of light, one to hold the system in the desired state and one to use for interrogation. PAS is ideally suited for these kinds of measurements since only the modulated light beam will contribute to the signal. Furthermore, it is not possible to saturate the detector (microphone) with a very strong continuous beam even at the measuring wavelength, since DC levels are not detected.

Two beam experiments have been used in the study of the bacteriorhodopsin photocycle (Garty *et al.*, 1978; Cahen *et al.*, 1978a), in photosynthetic studies (Callis *et al.*, 1972; Lasser-Ross *et al.*, 1980; Bults *et al.*, 1981) and in our laboratory in the search for signals from phytochrome photoreceptors.

2.6.2. Masking Unwanted Signals

The nature of PAS offers a simple method for restricting the signal to desired regions of the sample. First, of course, the best signal-to-noise ratio will be obtained by tightly focusing the light on the portion of the sample of interest. In this connection, note that the window shown in Fig. 1 can be replaced by a lens. Further restriction of the photoacoustically active region of the sample is obtained by coating it with a film of transparent wax, plastic, or silicone grease. The coating should be several

it better be
transparent!

thermal diffusion lengths thick, and transparent to the wavelength range used in the experiment. Under these conditions the signal from the masked (coated) regions of the sample will be essentially completely attenuated (Fernelius, 1980; Helander *et al.*, 1981). In this way it is not necessary to dissect out for spectroscopic study a single region or organelle from an intact biological specimen. This procedure has been employed in our laboratory in the study of insect eye photopigments *in situ*, and to attenuate the signal from very near the cut edge of leaf samples.

2.6.3. Low Temperature Experiments

PAS experiments have been reported at temperatures as low as 5°K (Pichon, *et al.*, 1979; also Section 2.6.6). One technique is to cool the microphone with the sample, thus avoiding the large thermal gradient (noise) and volume necessary if the microphone is maintained at room temperature (Murphy and Aamodt, 1977). Inexpensive electret microphones such as the Radio Shack 33-1058 or Sony ECM 16 work well at low temperature after modification in which the original J-type FET impedance translator is replaced with a MOS-FET such as the RCA 3N 187. However, Bechthold *et al.* (1982) have developed a cell that can be used with a commercial PA spectrometer and is continuously variable from 90–320°K, and the microphone remains at room temperature. A similar variable temperature cell has been reported by Schneider *et al.* (1982). Boucher and LeBlanc (1981) have used low temperature to block the photobleaching sequence in cattle rhodopsin (rod outer segments), and have measured the spectrum of the photostationary mixture of rhodopsin, bathorhodopsin, and isorhodopsin. Although not yet reported, the use of two beams and low temperature should allow the observation of relatively pure rhodopsin and bathorhodopsin spectra in intact retina.

2.6.4. Photoacoustically Detected Circular and Linear Dichroism

There is an obvious interest in the study of conformationally sensitive chiroptical characteristics of biomolecules *in situ*. Generally, this is not possible using conventional transmission detected circular dichroism due to the opaque nature of biological material. Experiments on solid samples using PA detection of both linear and circular dichroism have been reported (Fournier *et al.*, 1978; Palmer *et al.*, 1979), and a theoretical analysis has been done defining conditions under which the PA amplitude and phase are directly related to $\Delta\epsilon$ (Saxe *et al.*, 1979). While this method may hold considerable promise, a potential problem is the loss of integrity of the circularly polarized light upon multiple reflections (scattering) prior to absorption (scattered light not absorbed within μ_a is of no concern).

In this connection, and subject to the above caveat, it should be feasible to measure photoacoustically the linear dichroism of chromophores *in situ*.

2.6.5. Photothermal Radiometry (PTR)

Nordal and Kanstad (1979) have shown that the periodic temperature fluctuation in the sample induced by the absorption of the modulated light may be detected directly as a change in the black body emission from the sample. From the Stefan-Boltzmann's Law

$$W = \epsilon \sigma T^4 \quad (14)$$

and

$$\delta W = 4 \epsilon \sigma T^3 \delta T \quad (15)$$

where W is the total radiant emittance, ϵ is the emissivity, σ is the Stefan-Boltzmann constant, and T is the temperature. It can be seen that modulation of T will modulate W . A detailed theoretical description of PTR has recently appeared in which the conditions under which the signal is linearly proportional to β_{optical} have been discovered (Tom *et al.*, 1982). Although δW may be considerably less than 10^{-7} W at the detector, the experiment is feasible since infrared detectors with noise-equivalent-powers of 10^{-12} W (Hz)^{1/2} are available.

This technique requires essentially no sample preparation and no sample cell or container. The emission from the sample is imaged onto the detector with appropriate lenses in much the same way fluorescence is gathered and focused onto a detector. The potential of this technique is illustrated by the spectrum of a green leaf with signal to noise ratio ≥ 50 obtained using an Xe arc lamp monochromator combination of modest output (≥ 1 mW) and an electrical time constant of 3 s (Nordal and Kanstad, 1981). It is also worth noting that infrared detectors with response times of 10^{-7} s are available, making it possible to monitor relatively fast kinetic processes *in vivo* by PTR.

2.6.6. Photothermal Deflection Techniques (Mirage Effect)

Recall from Section 2.1 that upon absorption of light by the sample a thin boundary layer of gas (μ_a) at the sample surface is heated. Boccara *et al.* (1980a,b) have shown that the resulting change in refractive index of the boundary layer of gas can be detected from the deflection of a laser beam passing through the gas boundary layer. For an opaque sample, the

$$\left(\frac{\delta W}{W}\right) = \left(\frac{4\delta T}{T}\right)$$

laser beam should be parallel to the sample surface and within one thermal diffusion length in the gas ($\mu_g \sim 0.4$ mm in air at 50 Hz modulation frequency) of the surface. A knife edge blocking half the beam diameter followed by a photodetector makes an excellent position sensitive detector. Boccara *et al.* (1980a) reported visible spectra at room temperature of both an inorganic powdered sample ($\text{Cs}_2\text{Cr}_2\text{Cl}_9$) and of a single crystal ($\text{Nd}_2(\text{MoO}_4)_3$) and, as an illustration of the versatility of this method of detection, they also measured absorption and magnetic circular dichroism of $\text{Nd}_3(\text{MoO}_4)_3$ at 2°K and 0.7°K, respectively. In the low temperature work the refractive index change in the superfluid helium was observed as a standing wave in the tail of the helium Dewar.

These authors reported sensitivity comparable to that of conventional microphone detection, and noted that there is essentially no sample preparation or sample cell (for room temperature work) needed for these experiments.

2.6.7. Transform Techniques in Photoacoustic Spectroscopy; Infrared Photoacoustic Spectroscopy

Due to the detector limited signal to noise ratio usually observed in PA experiments, transform techniques offer considerable time advantage. The need for this advantage was first felt in infrared PAS, where source intensity is especially weak. It is now relatively easy to convert a Fourier transform infrared (FTIR) spectrometer to PA detection (FTIR-PAS, Maugh, 1980) and, indeed, the major manufacturers of FTIR instruments offer PAS cells. Examples of FTIR instruments converted to PA detection include Digilab (Krishnan, 1981) and Nicolet (Chalmers *et al.*, 1981). This makes it possible to obtain infrared spectra of materials that do not transmit infrared light, e.g., most biological materials, without solubilization or other sample preparation techniques that destroy *in vivo* ultrastructures and interactions. Spectra of mg-amounts of protoporphyrin, bovine hemin, hemoglobin and horseradish peroxidase have been measured by Rockley *et al.* (1980). Although certain features in the spectral range where the protein absorbed strongly were unresolved, the structural information characteristically available from infrared spectroscopy is readily apparent.

Fourier transform techniques have been extended into the visible range, and a detailed comparison to the conventional technique presented (Lloyd *et al.*, 1980). In special cases the Fourier transform time advantage could be very useful, but it appears that applications in the visible range to biological systems will be limited by technological (interferometer alignment) and fundamental (it is difficult to extract phase and modulation

Not so in the
step and integrate method

frequency, i.e., depth, information) problems. Gray *et al.* (1977) have suggested the use of Hadamard transform techniques, perhaps a very good suggestion especially for improving the signal to noise ratio in the ultra-violet region where source intensity is weak.

3. PHOTOACOUSTIC STUDIES OF CHLOROPHYLL-BASED PHOTOSYNTHESIS

3.1. Chloroplasts, Reaction Centers, and Leaves

Callis *et al.* (1972), using the flash calorimeter, measured volume, and enthalpy changes upon flash excitation of *Chromatium* chromatophores in order to resolve into enthalpy and entropy components the free energy storage upon light-driven electron transfer from cytochrome C_{555} to a quinone acceptor (Q_B). Several novel experiments were pioneered with this work, and have been used in subsequent efforts. A photochemically saturating continuous light incident on the sample was used to provide a reference. This reference has exactly the thermal and optical characteristics of the sample; it differs only in that the flash does not elicit photochemical changes. Also, ionophores, uncouplers, and various buffers were used in order to perturb the chromatophores in a predictable way. These authors found that the increase in free energy upon flash excitation of these chromatophore preparations is almost totally in the form of a large negative entropy change.

Later work by Arata and Parson (1981, 1982) with light-driven electron transfer from P_{870} to quinone Q_A in reaction center preparations of *Rhodospseudomonas sphaeroides* indicates that in the state $P^+Q_A^-$ free energy is stored as negative entropy. However, in preparations containing both Q_A and Q_B , the formation of the state $P^+Q_AQ_B^-$ results in a substantial enthalpy increase and little change in entropy. These results and the contrast between the results from *Chromatium* chromatophores and *R. sphaeroides* reaction centers is fully discussed in the references above.

Cahen *et al.* (1978b) reported a study of photosynthesis in a chloroplast preparation using the more conventional coupling gas-microphone technique. They found that the PA spectrum very nearly matched the absorption spectrum obtained with an integrating sphere. In this preliminary report they also noted that treatment with 3-(3,4-dichlorophenyl)-1,1-dimethyl urea (DCMU) changed the ratio of blue to red region signal strength, and that the extent of this change depended on the chopping

frequency. In later work (Lasser-Ross, *et al.*, 1980) on this system, a strong continuous (DC) light was used to saturate the photochemical processes of photosynthesis and the expected increase in the PA signal was observed [e.g., less photochemical loss (Malkin and Cahen, 1979)]. Furthermore, measurements of this photochemical loss as a function of wavelength and electron acceptors such as methylviologen could be interpreted in terms of cyclic photodriven electron flow around Photosystem I. These authors made the observation that fluorescence and PA techniques seem to report on different aspects of the photosynthetic process.

When Bults *et al.* (1981) extended their work to include whole leaves, an important observation was made. At low modulation frequency the PA signal decreased upon application of a strong DC light. The authors interpreted this result in the following way. At low modulation frequency the PA signal consists in large part of modulated O_2 evolution. The strong DC light drives the O_2 evolution to saturation, and hence the modulated O_2 evolution and concomitant PA signal decreases. At high modulation frequency, above 200 Hz, the slower O_2 evolution process does not contribute to the PA signal and the expected increase in signal upon application of the DC light was observed. DCMU vacuum infiltrated into the leaf completely abolished the change in PA signal upon application of DC light at any modulation frequency. Further evidence was provided by the work of Bults *et al.* (1982) in which PTR was used in a similar experiment (see also Canaani *et al.*, 1982; Kanstad *et al.*, 1983). Since PTR is sensitive only to heat production, the evolution of O_2 will not contribute to the signal. Indeed, it was found that over the frequency range 15–120 Hz (poor signal to noise ratio prevented experiments at higher frequency) the application of a saturating DC light always resulted in an increase in the photothermal signal. This observation supports the interpretation that modulated O_2 evolution does contribute to the PA signal at low frequency. These results lay the groundwork for facile methods of measuring the action spectrum for the production of O_2 and the production of heat and should open up new avenues of research in photosynthetic energy conversion.

Inoue *et al.* (1979) reported the transient variation of the PA signal from intact leaf sections upon irradiation with modulated light. The transient signals are large, undergo light and dark adaptation reminiscent of the Kautsky effect, are inhibited by DCMU or heating, and are kinetically distinct from the transient fluorescence changes. In preliminary work in our laboratory we have observed large changes in the PA signal from oat seedlings over a period of minutes. These changes in signal amplitude depend on the light/dark history of the leaf and the wavelength and intensity of a continuous light. It seems clear that perturbations c

the photosynthetic process give rise to large changes in the PA signal. These signals contain information about the partitioning of excitation energy between the two pigment systems, the energies and kinetics of intermediate states, the extent of saturation of each photosystem, and the effects of drugs.

At this point we mention again (Section 2.4.2) the work by Adams *et al.* (1976) in which the spectrum of the waxy cuticula of a leaf was resolved from the spectrum of the interior chloroplasts. As Adams *et al.* (1976) suggested, it is clear from these results that the cuticular layer attenuates the near-UV light, and thus may play a role in protecting the photosynthetic membranes. However, it must also be pointed out that the intensities of the spectra in Fig. 4 are qualitative. One can say only that the absorption of near-UV radiation by the cuticular layer is similar in strength to the absorption of red light by the chloroplasts. We have found that, as expected, the very thick cuticular layer found on certain desert plants (*agave*) essentially masks the PA signal from the chloroplasts.

It is reasonable to expect that PA techniques will play a significant role in research on energy conversion in photosynthetic membranes. An understanding of the initial forms of free energy storage in the native system is not only of intrinsic value, but may also serve to guide efforts in biomimetic solar energy conversion schemes.

3.2. Algae and Lichens

The PA spectra of a series of freeze dried phytoplankton cultures has been reported by Ortner and Rosencwaig (1977). Excellent signal to noise ratios were obtained from as few as 200 cells mm^{-2} , and in several cases the spectra were better resolved than the corresponding absorption spectra. Recently Yoon *et al.* (1981) measured the PA spectra of several examples of *Porphyra* sp. in which the contributions of the light harvesting carotenoids, biliproteins and chlorophylls to the absorption over the entire visible range can clearly be distinguished. The various peaks correspond very well to those present in the absorption spectra; however, the relative intensities of the bands in the two types of spectra are markedly different. Probably the major factor affecting the relative band intensities in these systems is the disposition of excitation energy between Photosystem I and II. The spectra of these cells was found to be independent of modulation frequency indicating that there are no wavelength dependent photochemical rate processes in the ms to s range, and no layering of pigment systems along the direction normal to the cell surface (μm range).

The PA spectrum of a monolayer of living cells of *Porphyridium*

cruentum is shown in Fig. 6. Chromatic adaptation is easily shown by comparing the spectra of cells grown under different light conditions. The relative peak heights in these spectra depend strongly on the intensity and wavelength of a continuous light irradiating the cells. Furthermore, the amplitude of the signal from the accessory pigments phycocyanin, phycoerythrin, and carotene increases relative to the chlorophyll band at ~670 nm as the concentration of DCMU is increased from 1×10^{-8} M to 1×10^{-7} M (cells grown for several days in DCMU-treated agar). Even though a detailed analysis is not complete, it seems clear that these observations are related to energy distribution between the photosystems.

Figure 7 presents the spectrum at several modulation frequencies of a living sample (~4 mm²) of the lichen *Acarospora schleicheri* (O'Hara *et al.*, 1981). Note that at high frequency the response is limited to the fungal region of the lichen and yields the *in vivo* spectrum of the dominant

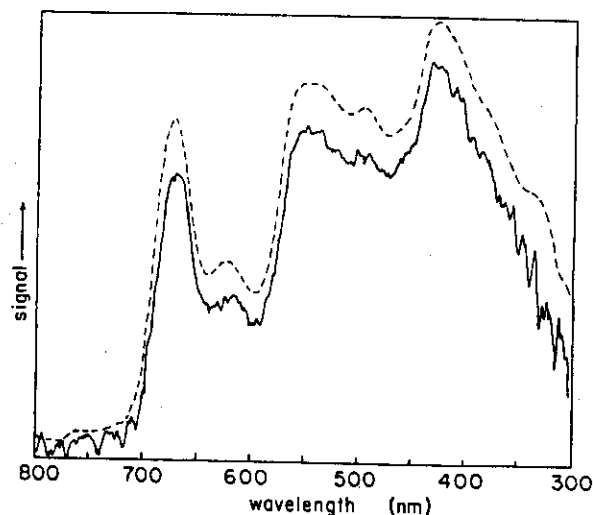


Fig. 6. PA spectra of a monolayer of living *Porphyridium cruentum* cells on agar. (---) Spectrum at 26 Hz modulation frequency and (—) spectrum taken at 1015 Hz. Note the change in signal to noise ratio as the modulation frequency is increased. The optical bandpass was 10 nm, and the lock-in amplifier output bandwidth was 0.1 Hz.

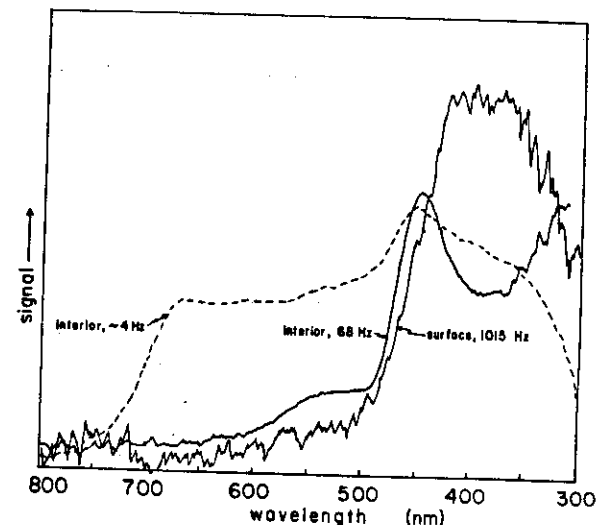


Fig. 7. PA spectra of the lichen *Acarospora schleicheri*. A small section ~4 mm² of lichen growing on a rock was placed in the sample chamber. The spectrum at 1015 Hz was taken with the phase optimized for surface response. The spectra of 68 Hz and 4 Hz were recorded with the phase optimized for response from the interior. The optical and electrical bandwidths were as in Fig. 6.

fungal pigment, rhizocarpic acid. It is worth noting that the spectrum of rhizocarpic acid in the native environment differs sharply from that in solution (peak 275 nm, shoulder 375 nm). At this frequency there was no evidence of absorption by the chloroplasts; in order to record a signal from the chloroplasts it was necessary to lower the frequency to 4 Hz (see Section 7.1 for information on microphones that operate at very low frequency). This spectrum clearly shows the chloroplast absorption, making it possible to monitor the algae photosynthesis *in vivo*. We have observed that simultaneous irradiation with a DC source decreases the PA signal, consistent with the results of Bults *et al.* (1981). This response only occurs with hydrated lichen samples. Dry samples, known to be dormant, do not respond to the application of a DC light.

4. PHOTOACOUSTIC STUDIES OF *H. halobium* PHOTOCYCLE

Ort and Parson (1978) reported studies of the purple membrane using the flash calorimeter to measure the solution volume change after flash excitation. A fast, buffer-dependent component of the volume increase following the flash was interpreted as electrostriction of the solvent due to proton release by the membrane. A slower, buffer-independent component of the volume increase could be due to proton translocation on the membrane. The kinetics of the volume change could not be correlated with the kinetics derived from the studies of the photocycle by optical spectroscopy. By making use of the large volume change occurring when protons enter the solution, it was possible to measure the quantum yield of proton release (Φ_{H^+}), an important parameter in the mechanism of the proton pump (Ort and Parson, 1979b). At low ionic strength a value of $\Phi_{H^+} = 0.25$ was found, in good agreement with the quantum yield for the formation of intermediate, *M*, and suggesting one proton per photocycle. However, at high ionic strength $\Phi_{H^+} = 0.43$ was found while the quantum yield for the formation of *M* was unchanged, implying that two protons are pumped per photocycle. Additionally, the work of Renard and Delmelle (1981) on the PAS of films of purple membranes demonstrates that the quantum yield of photocycle is independent of pH over the range 5–9. Taken with earlier work by these authors (Renard and Delmelle, 1980), the suggestion was made that $2H^+$ are pumped per photocycle at pH 5–7 and $1H^+$ is pumped per photocycle at alkaline pH. This conclusion is in contrast to the observation by Ort and Parson (1978) that Φ_{H^+} does not depend on pH over the range 6.0–8.75. However, a direct comparison is not possible since the work by Ort and Parson (1978) is on membrane fragments in solution while Renard and Delmelle (1981) used films of membrane on filter paper. It is also noted here that for solution samples the time domain liquid-coupled microphone technique used by Ort and Parson (1978) is perhaps better suited for measuring proton flux than the gas-coupled microphone in which the solution volume change makes only a very small contribution to the signal.

Enthalpy changes during the photocycle have also been reported by Ort and Parson (1979a). They find that fast relaxation, proton release and the slow component of expansion are exothermic, and that proton uptake to return to the original state is endothermic by approximately 35 kcal/mol. Since return to the starting state is spontaneous, entropy changes must be rather large, and thus play a significant role in the bioenergetics of the proton pump. It is noteworthy that Garty *et al.* (1980), using the gas-coupled microphone and modulation techniques (Section 2.5.3), reported a qualitatively similar picture of the enthalpy changes during the photo-

cycle and, using a continuous light in a two beam experiment, they have recorded a very nice spectrum of the intermediate *M*₄₁₂ in a film of purple membrane. Again, it appears that although some of the intermediate steps may correlate with those observed by optical techniques, there is no general agreement. However, complete agreement between photoacoustic and optical techniques is not expected since thermochemical changes do not necessarily result in observable optical changes, further illustrating the fact that these techniques are complementary. Garty *et al.* (1981) have discussed in detail the use of modulation techniques in *H. halobium* to extract enthalpy changes and the energy stored at each step of the photocycle.

Bechtold *et al.* (1982) have reported the spectrum of purple membranes in water and in a glycerol-water mixture at temperatures as low as 90°K. Marked spectral changes occur with irradiation time and as a function of temperature, but these results do not parallel those from transmission measurements.

In the case of visual rhodopsin, the only report of PAS is mentioned in Section 2.6.3.

5. PHOTOACOUSTIC STUDIES OF SKIN TISSUE

Rosenzweig and Pines (1977a,b) have reported a rather extensive study of newborn rat stratum corneum. Spectra with a good signal-to-noise ratio in the UV region (220–400 nm) were presented; the peak at 280 nm, due to the aromatic amino acids in the proteins, was clearly resolved. As the tissue matured from birth to age 60 h, a marked change in the 280 nm band was observed. The peak position shifted ~5 nm to the red, and the line width approximately doubled. After considering a variety of structural and chemical changes during keratinization, the authors tentatively suggested that the enzymatic modification of tyrosine, such as hydroxylation, could account for the observed changes. Also, since thermal properties of the tissue are affected by the extent of hydration, it was possible to correlate the signal amplitude with the tissue water content.

Campbell *et al.* (1977, 1979) have carried out extensive studies of the hydration profile or water concentration gradient of human skin. A multilayer theoretical model was developed for the dependence of signal on modulation frequency and thermal properties, and was used to interpret the experimental data. It was found that the transition from hydrated to dry tissue occurred approximately halfway through the stratum corneum, consistent with the view that the stratum corneum is the diffusional barrier

of the epidermis. Further illustrating the application of PAS to dermatological research, the authors reported the detection of tetracycline (down to ~0.01% solution topically applied), and its diffusion through both plantar and abdominal skin. The time constant for diffusion was found to be ~10 times greater in the case of abdominal skin.

Several other studies related to skin tissue have appeared. Sunscreen effectiveness is directly related to the attenuation of light as a function of penetration, wavelength, time, environment of the skin, etc. PA techniques can be used to measure *in situ* the absorption of light by the chemical sunscreen as a function of these parameters (Pines, 1978). Lermar *et al.* (1978) used PAS to measure the absorption of normal, aging, and cataractous human eye lenses. An analysis of skin lipids by infrared PAS at sensitivities of better than one μg can be accomplished simply by rubbing a cotton swab lightly against the skin and transferring a drying stain to a small aluminum plate (Kanstad *et al.*, 1981). Rather than a gas-microphone arrangement, these authors used a piezoelectric detector bonded directly to the aluminum plate.

These reports have clearly established the underpinning work for the use of PA techniques in studies of both photobiological and biochemical/biophysical properties and functions of skin tissue. It is expected that applications will expand in this area and include studies of photoproducts of skin sensitizing chemicals and their distribution in the epidermis, the diffusion of chemicals in tissue, and the disease conditions affecting surface and near surface tissue. In this connection, developments such as open-ended photoacoustic cells (Fishman and Bard, 1981) and radiometric detection (Section 2.4.5) could lead to true *in vivo* spectroscopy of a variety of living things.

6. CONCLUSION

Both qualitative and quantitative information can be extracted from measurements involving PA techniques. The observation from early experiments that it is in general extremely difficult to determine quantitatively β_{optical} , and hence the concentration of a chromophore, remains correct. On the other hand, calorimetric aspects of photoacoustics can be exploited to yield absolute values of energies or quantum yields of photoprocesses in an extremely wide range of samples including living things. Furthermore, with proper attention to experimental technique (saturation, phase, etc.) unambiguous absorption maxima can be measured and therefore the transition energy of chromophores *in vivo* determined.

Certainly the usefulness of PAS in certain types of strongly scattering materials is questionable (Tilgner, 1981). However, it is clear that the unique sensitivity of PA techniques to optical, thermal, and thermochemical properties of the sample will assure its place in studies of biochemical and especially energy-transducing photobiological systems. Capabilities are expanding rapidly, partly as a consequence of novel techniques such as PTR, mirage effect, and FTIR-PAS; it seems safe to continue the prediction (Smith, 1977) that PA techniques will find increasing use in the study of biological material.

7. EXPERIMENTAL NOTES

7.1. Microphone

We have found that the selection of a high quality microphone is rather important. This is especially true in the case of photobiological experiments, since achieving an acceptable signal to noise ratio by using a high light level may sometimes damage or alter the sample. In other words, choosing the most sensitive transducer will result in a given signal to noise ratio at a minimum light level. In order to derive maximum benefit from a sensitive microphone, it is necessary to have a cell with sufficient acoustic and seismic isolation so that the noise floor is electrical from the preamplifier stage. We have found that the Brüel and Kjaer model 4165 (condenser) or 4175 (electret) microphones to have the highest sensitivity and widest frequency response of any commercially available microphones; with special sealing kits these microphones have low frequency response to <0.1 Hz. Furthermore, they have quartz-coated diaphragms so that corrosive chemicals are less of a problem.

7.2. Light Scrambler

Since the PA spectrum results from the point by point division of the sample signal by the signal from a black body absorber, it is essential for the beam to have the same power spectrum when irradiating sample and reference. The power spectrum of a compact arc lamp (Xe) varies markedly over the distance between the electrodes, and if the source optics are of high quality, the image of the arc at the sample will not be homogeneous with respect to power spectrum. Since the sample is often not the same size or it is not in the same position in the cell as the black

body absorber, serious errors (up to 50%) can occur in the observed spectrum upon division. We partly solved this problem by installing a spherical mirror behind the arc lamp so that an inverted image of the arc falls on the arc, and completely solved the problem by having Maxlight (Phoenix, Arizona, USA) build a quartz light guide with the fibers randomized. The exit slit is imaged onto this light guide with an ellipsoidal mirror, and the light guide scrambles and transmits light to the cell.

Arc lamps with ellipsoid reflectors arranged such that the arc is coaxial with the ellipsoid axis may not suffer from this problem, since the heterogeneous power spectrum is along the optical axis, a direction not resolved when the image is formed on the sample.

7.3. Bifurcated Light Guide

An ideal way to carry out two beam experiments is a beam combiner in the form of a bifurcated light guide. Again, Maxlight custom builds these with randomized, quartz fibers.

7.4. Stirred Arc

A well-know technique for suppressing arc wander is to place a magnetic stirrer or solenoid near the lamp so that the arc is stirred or averaged over all available sites on the electrodes at relatively high frequency. In this way the random wander (noise), which can cause sudden intensity changes of as much as 50% every few minute (very low frequency noise), is translated up in frequency so that it is averaged by the time constants in the system.

7.5. Photoacoustic Cell Signal

Signals arising from absorption by the walls of the PA cell can distort the sample spectrum, and are especially troublesome in the case of phase measurements. We have experienced considerable difficulty with these spurious signals and have not completely solved the problem. The walls of the PA cell are illuminated by scattered light and sample fluorescence; it is difficult to remove these signals since the empty PA cell signal is not the correct blank for the PA cell contribution when the sample is present. A good strategy is to construct the PA cell from Plexiglass or aluminum with all interior surfaces polished. Additionally, a light trap, as shown in Fig. 1, may be used. The quartz cover plate must be carefully sealed at the edges with silicone grease. It is also important that the cell be designed

so that light does not fall on the microphone diaphragm. The design of PA cells is discussed in the general reviews cited earlier; good examples of useful reports of the sensitivities and signal to noise performance of cells are given by Cahen (1981), Ducharme *et al.* (1979) and Gray *et al.* (1977).

ACKNOWLEDGMENT

This work was supplied in part by NSF Grant CHE-8021718.

8. REFERENCES

- Aamodi, L. C., Murphy, J. C., and Parker, J. G., 1977, Size considerations in the design of cells for photoacoustic spectroscopy, *J. Appl. Phys.* 48:927-933.
- Adams, M. J., and Kirkbright, G. F., 1977, Analytical optoacoustic spectroscopy part III. The optoacoustic effect and thermal diffusivity, *Analyst* 102:281-292.
- Adams, M. J., Beadle, B. C., King, A. A., and Kirkbright, G. F., 1976, Analytical optoacoustic spectroscopy part II. Ultraviolet and visible optoacoustic spectra of some inorganic, biochemical and phytochemical samples, *Analyst* 101:553-561.
- Adams, M. J., Highfield, J. G., and Kirkbright, G. F., 1977, Determination of absolute fluorescence quantum efficiency of quinine bisulfate in aqueous medium by optoacoustic spectrometry, *Anal. Chem.* 49:1850-1852.
- Adams, M. J., Highfield, J. G., and Kirkbright, G. F., 1980, Determination of the absolute quantum efficiency of luminescence of solid materials employing photoacoustic spectroscopy, *Anal. Chem.* 52:1260-1264.
- Adams, M. J., Highfield, J. G., and Kirkbright, G. F., 1981, Determination of the absolute quantum efficiency of sodium salicylate using photoacoustic spectroscopy, *Analyst* 106:850-854.
- Arata, H., and Parson, W. W., 1981, Enthalpy and volume changes accompanying electron transfer from P_{680} to quinones in *Rhodospseudomonas sphaeroides* reaction centers, *Biochim. Biophys. Acta* 636:70-81.
- Arata, H., and Parson, W. W., 1982, Enthalpy and volume changes accompanying electron transfer from P_{680} to the primary and secondary quinones in photosynthetic reaction centers, in: *Function of Quinones in Energy Conserving Systems* (B. L. Trumpower, ed.), Academic Press, New York (in press).
- Balasubramanian, D., and Rao, CH. M., 1981, Yearly Review, Photoacoustic spectroscopy of biological systems, *Photochem. Photobiol.* 34:749-752.
- Bechthold, P. S., Kohl, K.-D., and Sperling, W., 1982, Low temperature photoacoustic spectroscopy of the purple membrane of *Halobacterium halobium*, *Appl. Opt.* 21:127-132.
- Bennett, H. S., and Forman, R. A., 1977, Frequency dependence of photoacoustic spectroscopy: Surface and bulk absorption coefficients, *J. Appl. Phys.* 48:1432-1436.
- Betteridge, D., Lilley, T., and Meyler, P. J., 1979, Computer generated optoacoustic spectra for a two-layer solid sample system, *Fresenius Z. Anal. Chem.* 296:28-31.
- Boccara, A. C., Fournier, D., and Badoz, J., 1980a, Thermo-optical spectroscopy: Detection by the "mirage effect," *Appl. Phys. Lett.* 36:130-132.
- Boccara, A. C., Fournier, D., Jackson, W., and Amer, N. M., 1980b, Sensitive photothermal deflection technique for measuring absorption in optically thin media, *Opt. Lett.* 5:377-379.

- Boucher, F., and LeBlanc, R. M., 1981, Photoacoustic spectroscopy of cattle visual pigment at low temperature, *Biochem. Biophys. Res. Commun.* 100:385-390.
- Bults, G., Horwitz, B. A., Malkin, S., and Cahen, D., 1981, Frequency-dependent photoacoustic signals from leaves and their relation to photosynthesis, *FEBS Lett.* 129:44-46.
- Bults, G., Nordal, P. E., and Kanstad, S. O., 1982, *In vivo* studies of photosynthesis in attached leaves by means of photothermal radiometry, *Biochim. Biophys. Acta* 682:234-237.
- Cahen, D., 1981, Photoacoustic cell for reflection and transition measurements, *Rev. Sci. Instrum.* 52:1306-1310.
- Cahen, D., Garty, H., and Caplan, S. R., 1978a, Spectroscopy and energetics of the purple membrane of *Halobacterium halobium*, *FEBS Lett.* 91:131-134.
- Cahen, D., Malkin, S., and Lerner, E. I., 1978b, Photoacoustic spectroscopy of chloroplast membranes; listening to photosynthesis, *FEBS Lett.* 91:339-342.
- Cahen, D., Bults, G., Garty, H., and Malkin, S., 1980, Photoacoustics in life sciences, *J. Biochem. Biophys. Methods* 3:293-310.
- Callis, J. B., 1976, The calorimetric detection of excited states, *J. Res. Nat. Bur. Stand.* 80A:413-419.
- Callis, J. B., Parson, W. W., and Gouterman, M., 1972, Fast changes of enthalpy and volume on flash excitation of *Chromatium chromatophores*, *Biochim. Biophys. Acta* 267:348-362.
- Campbell, S. D., Yee, S. S., and Aframowitz, M. A., 1977, Two applications of photoacoustic spectroscopy to measurements in dermatology, *J. Bioeng.* 1:185-188.
- Campbell, S. D., Yee, S. S., and Aframowitz, M. A., 1979, Application of photoacoustic spectroscopy to problems in dermatology research, *IEEE Trans. Biomed. Eng.* EME-26:220-227.
- Canaani, O., Cahen, D., and Malkin, S., 1982, Photosynthetic chromatic transitions and Emerson enhancement effects in intact leaves studied by photoacoustics, *FEBS Lett.* 150:142-146.
- Castleden, S. L., Elliott, C. M., Kirkbright, G. F., and Spillane, D. E. M., 1979, Quantitative examination of thin-layer chromatography plates by photoacoustic spectroscopy, *Anal. Chem.* 51:2152-2153.
- Chalmers, J. M., Stay, B. J., Kirkbright, G. F., Spillane, D. E., and Beadle, B. C., 1981, Some observations on the capabilities of photoacoustic Fourier transform infrared spectroscopy (PAFTIR), *Analyst* 106:1179-1186.
- Ducharme, D., Tessier, A., and LeBlanc, R. M., 1979, Design and characteristics of a cell for photoacoustic spectroscopy of condensed matter, *Rev. Sci. Instrum.* 50:1461-1462.
- Fernelius, N. C., 1980, Extension of the Rosencwaig-Gersho photoacoustic spectroscopy theory to include effects of a sample coating, *J. Appl. Phys.* 51:650-654.
- Fishman, V. A., and Bard, A. J., 1981, Open-ended photoacoustic spectroscopy cell for thin-layer chromatography and other applications, *Anal. Chem.* 53:102-105.
- Fournier, D., Boccara, A. C., and Badoz, J., 1978, Dichroism measurements in photoacoustic spectroscopy, *Appl. Phys. Lett.* 32:640-642.
- Fuchsman, W. H., and Silversmith, A. J., 1979, General method for overcoming photoacoustic saturation in highly colored organic and inorganic solids, *Anal. Chem.* 51:589-590.
- Garty, H., Cahen, D., and Caplan, S. R., 1978, Use of photoacoustic spectroscopy in the study of the bioenergetics of purple membranes, in: *Energetics and Structure of Halophilic Microorganisms*, (S. R. Caplan and M. Ginzburg, eds.), pp. 253-259, Elsevier/North-Holland Biomedical Press, Amsterdam.

Photoacoustic Spectroscopy

- Garty, H., Cahen, D., and Caplan, S. R., 1980, Photoacoustic calorimetry of *Halobacterium halobium* photocycle, *Biochem. Biophys. Res. Commun.* 97:200-206.
- Garty, H., Caplan, S. R., and Cahen, D., 1981, Photoacoustic photocalorimetry and spectroscopy of *Halobacterium halobium* purple membranes, *Biophys. J.* 37:405-415.
- Gray, R. C., Fishman, V. A., and Bard, A. J., 1977, Simple sample cell for examination of solids and liquids by photoacoustic spectroscopy, *Anal. Chem.* 49:697-700.
- Helander, P., Lundström, J., and McQueen, D., 1981, Photoacoustic study of layered samples, *J. Appl. Phys.* 52:1146-1151.
- Inoue, Y., Watanabe, A., and Shibata, K., 1979, Transient variation of photoacoustic signal from leaves accompanying photosynthesis, *FEBS Lett.* 101:321-323.
- Kanstad, S. O., Nordal, P. E., Helligren, L., and Vincent, J., 1981, Infrared photoacoustic spectroscopy of skin lipids, *Naturwissenschaften* 68:47-48.
- Kanstad, S. O., Cahen, D., and Malkin, S., 1983, Simultaneous detection of photosynthetic energy storage and oxygen evolution in leaves by photothermal radiometry and photoacoustics, *Biochim. Biophys. Acta* 722:182-189.
- Krishnan, K., 1981, Some applications of Fourier transform infrared photoacoustic spectroscopy, *Appl. Spectrosc.* 35:549-557.
- Lasser-Ross, N., Malkin, S., and Cahen, D., 1980, Photoacoustic detection of photosynthetic activities in isolated broken chloroplasts, *Biochim. Biophys. Acta* 593:330-341.
- Lerman, S., Yamanashi, B. S., Palmer, R. A., Roark, J. C., and Borkman, R., 1978, Photoacoustic fluorescence and light transmission spectra of normal, aging and cataractous lenses, *Ophthalmic Res.* 10:168-176.
- Lin, J. W.-p., and Dudek, L. P., 1979, Signal saturation effect and analytical techniques in photoacoustic spectroscopy of solids, *Anal. Chem.* 51:1627-1632.
- Lloyd, L. B., Burnham, R. K., Chandler, W. L., Eyring, E. M., and Farrow, M. M., 1980, Fourier transform photoacoustic visible spectroscopy of solids and liquids, *Anal. Chem.* 52:1595-1598.
- Mackenthun, M. L., Tom, R. D., and Moore, T. A., 1979, Lobster shell carotenoprotein organization *in situ* studied by photoacoustic spectroscopy, *Nature* 279:265-266.
- Malkin, S., and Cahen, D., 1979, Photoacoustic spectroscopy and radiant energy conversion: Theory of the effect with special emphasis on photosynthesis, *Photochem. Photobiol.* 29:803-813.
- Malkin, S., and Cahen, D., 1981, Dependence of photoacoustic signal on optical absorption coefficient in optically dense liquids, *Anal. Chem.* 53:1426-1432.
- Mandelis, A., Teng, Y. C., and Royce, B. S. H., 1979, Phase measurements in the frequency domain photoacoustic spectroscopy of solids, *J. Appl. Phys.* 50:7138-7146.
- Maugh, T. H. II, 1980, Fourier transform comes to photoacoustic spectroscopy, *Science* 208:167.
- McClelland, J. F., and Kniseley, R. N., 1976, Signal saturation effects in photoacoustic spectroscopy with applicability to solid and liquid samples, *Appl. Phys. Lett.* 28:467-469.
- McDonald, F. A., 1980, Three-dimensional heat flow in the photoacoustic effect, *Appl. Phys. Lett.* 36:123-125.
- McDonald, F. A., 1981, Three-dimensional heat flow in the photoacoustic effect-II: Cell-wall conduction, *J. Appl. Phys.* 52:381-385.
- McDonald, F. A., and Wetsel, G. C. Jr., 1978, Generalized theory of the photoacoustic effect, *J. Appl. Phys.* 49:2313-2322.
- Moore, T. A., Benin, D., and Tom, R., 1982, Photoacoustic measurement of photophysical properties. Lowest triplet state energy of a free base prophyrin, *J. Am. Chem. Soc.* 104:7356-7357.

- Morita, M., 1981, Theory and experiments on the photoacoustic effect in double-layer solids, *Jpn. J. Appl. Phys.* 20:835-842.
- Murphy, J. C., and Aamodt, L. C., 1977, Photoacoustic spectroscopy of luminescent solids: Ruby, *J. Appl. Phys.* 48:3502-3509.
- Nordal, P.-E., and Kanstad, S. O., 1979, Photothermal radiometry, *Physica Scripta* 20:659-662.
- Nordal, P.-E., and Kanstad, S. O., 1981, Visible-light spectroscopy by photothermal radiometry using an incoherent source, *Appl. Phys. Lett.* 38:486-488.
- O'Hara, E. P., Tom, R., and Moore, T. A., 1981, Absorption of light by pigments in lichens studied by photoacoustic spectroscopy, Technical Digest, Second International Topical Meeting on Photoacoustic Spectroscopy, June 22-25, 1981, Optical Society of America, Washington, D.C. Abs. Tu B29.
- Ort, D. R., and Parson, W. W., 1978, Flash-induced volume changes of bacteriorhodopsin-containing membrane fragments and their relationship to proton movements and absorption transients, *J. Biol. Chem.* 253:6158-6164.
- Ort, D. R., and Parson, W. W., 1979a, The quantum yield of flash-induced proton release by bacteriorhodopsin-containing membrane fragments, *Biophys. J.* 25:341-354.
- Ort, D. R., and Parson, W. W., 1979b, Enthalpy changes during the photochemical cycle of bacteriorhodopsin, *Biophys. J.* 25:355-364.
- Ortner, P. B., and Rosencwaig, A., 1977, Photoacoustic spectroscopic analysis of marine phytoplankton, *Hydrobiologia* 54:3-6.
- Palmer, R. A., Roark, J. C., Robinson, J. C., and Howell, J. L., 1979, Photoacoustic detection of natural circular dichroism in solids, Technical Digest, Topical Meeting on Photoacoustic Spectroscopy, August 1-3, 1979, Optical Society of America, Washington, D.C. Abs. ThA 3-1.
- Pichon, C., LeLiboux, M., Fournier, D., and Boccara, A. C., 1979, Variable-temperature photoacoustic effect: Application to phase transition, *Appl. Phys. Lett.* 35:435-437.
- Pines, E., 1978, A new technique to assess sunscreen effectiveness, *J. Soc. Cosmet. Chem.* 29:559-564.
- Poulet, P., Chambron, J., and Unterreiner, R., 1980, Quantitative photoacoustic spectroscopy applied to thermally thick samples, *J. Appl. Phys.* 51:1738-1742.
- Quimby, R. S., and Yen, W. M., 1979, Three-dimensional heat-flow effects in photoacoustic spectroscopy of solids, *Appl. Phys. Lett.* 35:43-45.
- Quimby, R. S., and Yen, W. M., 1980, Photoacoustic measurement of the ruby quantum efficiency, *J. Appl. Phys.* 51:1780-1782.
- Renard, M., and Delmelle, M., 1980, Quantum efficiency of light-driven proton extrusion in *Halobacterium halobium*, *Biophys. J.* 32:993-1006.
- Renard, M., and Delmelle, M., 1981, The photochemical quantum yield of bacteriorhodopsin in pH independent, *FEBS Lett.* 128:245-248.
- Rockley, M. G., Davis, D. M., and Richardson, H. H., 1980, Fourier transformed infrared photoacoustic spectroscopy of biological materials, *Science* 210:918-920.
- Rosencwaig, A., 1978, Photoacoustic spectroscopy, *Adv. Electr. Electron Phys.* 46:207-311.
- Rosencwaig, A., and Gersho, A., 1976, Theory of photoacoustic effect with solids, *J. Appl. Phys.* 47:64-69.
- Rosencwaig, A., and Pines, E., 1977a, A photoacoustic study of newborn rat stratum corneum, *Biochim. Biophys. Acta* 493:10-23.
- Rosencwaig, A., and Pines, E., 1977b, Stratum corneum studies with photoacoustic spectroscopy, *J. Invest. Dermatol.* 69:296-298.

- Saxe, J. D., Faulkner, T. R., and Richardson, F. S., 1979, photoacoustic detection of circular dichroism, *Chem. Phys. Lett.* 68:71-76.
- Schneider, S., Möller, U., and Coufal, H., 1982, Influence of photoinduced isomerization on the photoacoustic spectra of DODCl, *Appl. Opt.* 21:44-48.
- Smith, K. C., 1977, New topics in photobiology, in: *The Science of Photobiology*, (K. C. Smith, ed.), pp. 397-417, Plenum, N.Y.
- Somoano, R. B., 1978, Photoacoustic spectroscopy of condensed matter, *Angew. Chem. Int. Ed. Engl.* 17:238-245.
- Tilgner, R., 1981, Photoacoustic spectroscopy with light scattering samples, *Appl. Opt.* 20:3780-3786.
- Tom, R. D., O'Hara, E. P., and Benin, D., 1982, A generalized model of photothermal radiometry, *J. Appl. Phys.* 53:5392-5400.
- Yoon, G. J., Lee, T. Y., O'Hara, E. P., Moore, T. A., Yoon, M., and Song, P. S., 1981, The spectroscopy of *Porphyra Sp. in situ*, *Can. J. Spectrosc.* 26:148-157.